UNIVERSITY OF OXFORD

Sir William Dunn School of Pathology

Functions of conserved centriole proteins in African trypanosomes

Nicole Scheumann

Lincoln College

A thesis submitted for the degree of Doctor of Philosophy in the University of Oxford, Hilary Term 2012

ABSTRACT

Centrioles and basal bodies are related nine-fold symmetric microtubule-based eukaryotic organelles central to the formation of cilia/flagella and centrosomes. Understanding of mechanisms of eukaryotic centriole and basal body assembly are mainly based on studies in animal systems.

To understand which centriolar proteins are the universally important ones in the assembly across eukaryotes, a bioinformatic survey presented here investigates the distribution of centriolar and cilia-associated proteins across a diverse range of eukaryotes. This analysis showed also that the basal body function is ancestral to eukaryotes, whereas centrosomal components are specific to Holozoa (which include animals). It also suggested that the ancestor of all eukaryotes possessed a cilium/cilia not only with motility function but also with a sensory role. The most frequently conserved proteins in extant ciliated eukaryotes found in this analysis included SAS-6, SAS-4 and WDR16. To test whether these proteins are also important for basal body assembly in distantly-related species to metazoan and other model organisms where the proteins have been studied to date, the proteins were investigated in *Trypanosoma brucei*. I used a combination of genetic tools and microscopy techniques to demonstrate that both SAS-6 and SAS-4 localise to the assembling pro-basal body, but that only SAS-6 and not SAS-4 is essential for basal body assembly in *T. brucei*. Quantification of SAS-6 demonstrated that the level of the protein at the basal body and pro-basal body is cell-cycle dependent. Analysis of SAS-4 in *T. brucei* showed that the protein localises to several microtubule-organising centres in this species and that it is required for cytokinesis. Furthermore, I showed that WDR16 is a stably integrated component of the transition zone and axoneme but not the basal body. Furthermore, I identified a novel SAS-6 like protein which localises to a position consistent with the basal plate and has the capacity to form into filaments.

This thesis provides new insights into the evolution of centrioles and basal bodies, and into the function of conserved centriole proteins in *T. brucei*, a distantly-related organism to animals.

DECLARATION

No portion of the work referred to in this thesis has been submitted in support of an application for another degree or qualification of this or any other university or other institute of learning.

ACKNOWLEDGEMENTS

First of all I would like to thank my supervisor Prof Keith Gull for his support throughout my DPhil, for providing such a well-organised and stimulating environment for my doctoral studies while also allowing me the freedom to pursue my own scientific interests, and for demanding high-quality science and critical thinking. I am extremely grateful to my co-supervisor Dr Bill Wickstead for giving his time so generously to share his immense knowledge of sciences, for providing continuous support and infective enthusiasm, and for demanding precision.

I am very thankful to all present and past members of the Gull lab for providing invaluable technical and scientific expertise, for sharing their time, reagents and cake, for giving constructive criticism and positive feedback, for generously sharing insights into life, and for being generally very supportive company that made life in the lab very enjoyable; thanks go particularly to Dr Neil Portman, Dr Sylvain Lacomble, Dr Helen Farr, Dr Steve Kelly, Richard Wheeler, Dr Jan-Peter Daniels, Sakura Yamamoto, Helen Banks, Mike Fiebig, Dr Vladimir Varga, Dr Eva Gluenz, Dr Bungo Akiyoshi, and Dr Sue Vaughan. I would like to thank Mike Shaw for his invaluable expertise and support during the electron microscopic work.

Special thanks go to Dr Matthew Hodges for a scientifically fruitful and extremely enjoyable collaboration (Chapter 3). I would like to thank the lab of Prof Naomi Morrissette for the collaboration on the SAS6L protein (Chapter 5). I am also grateful to Dr Monica Bettencourt-Dias and her lab for sharing data and scientific insight with us, and for her warm welcome to Portugal.

I would also like to thank my examiners Prof David Vaux and Dr Paul McKean, and my departmental graduate advisor Prof Jordan Raff for sharing their experience and insight with me, and providing stimulating discussions about my research.

My DPhil research has been facilitated by the E. P. Abraham Trust and the Wellcome Trust. I have been very fortunate to have had the chance to pursue my research in such a friendly and stimulating environment as the Sir William Dunn School of Pathology, and I would like to express my gratitude and sincere appreciation for that.

I am very grateful for having been a part of Lincoln College which with all its students, alumni and staff has been an incredibly inspiring community leaving me with many memorable experiences.

Finally, I am deeply grateful to my mother and my friends for their support on my way.

TABLE OF CONTENT

LIST OF FIGURES AND TABLES

Introduction

Methods

Evolutionary history of the centriole

Characterisation of trypanosomal SAS-6

Characterisation of trypanosomal SAS6L

Characterisation of trypanosomal SAS-4

Characterisation of trypanosomal WDR16

ABBREVIATIONS

BB: basal body
BLAST: basic local alignment search tool
bp: base pair
BSF: bloodstream form
DAPI: 4,6-diamidino-2-phenylinidole
DNA: deoxyribonucleic acid
dNTP: deoxyribonucleoside triphosphate
EDTA: ethylenedinitrilo tetraacetic acid (disodium salt)
EM: electron microscopy
FAZ: flagellum attachment zone
GFP: green fluorescent protein
IFT: intraflagellar transport
K: kinetoplast
LB: Luria broth
MT: microtubule
MTOC: microtubule organising centre
N: nucleus
ORF: open reading frame
pBB: pro-basal body
PBS: phosphate-buffered saline
PCF: procyclic form
PCP: planar cell polarity
PCR: polymerase chain reaction
PFR: paraflagellar rod
PIPES piperazine-N,N-bis (2-ethane sulphonic acid)
RNA:ribonucleic acid
RNAi: RNA interference
SDS-PAGE: sodium dodecyl sulphate-polyacrylamide gel electrophoresis
TEM: transmission electron microscopy
TZ: transition zone
YFP: yellow fluorescent protein
ZPFM: Zimmerman's post fusion medium

INTRODUCTION

1.1 Centrioles & basal bodies

Centrioles and basal bodies are related nine-fold symmetric, eukaryotic organelles central to the formation of cilia/flagella and centrosomes. The canonical structure of centrioles/basal bodies is a cylinder of nine microtubule (MT) triplets. This structure is widely conserved amongst eukaryotes, although exceptions with MT singlets or doublets, or a radial symmetry other than nine-fold exist (Callaini et al., 1997; Perkins et al., 1986; Schrevel and Besse, 1975). Centrioles/basal bodies are ancestral to eukaryotes but have been lost from some lineages, most notably, for example, from higher plants and most fungi.

The scientific interest in centrioles/basal bodies emerges from their involvement in two critical cellular functions: (1) basal bodies nucleate cilia and flagella, which serve key functions in developmental and physiological signalling processes as well as in cell motility. Dysfunction of ciliary signalling can lead to a range of developmental pathologies leading to various severe organ defects (reviewed in Oh and Katsanis, 2012). (2) Centrioles are a core part of the centrosome which is the major MT organising centre. As such it is also involved in the formation of the mitotic spindle and hence central to animal cell division.

1.1.1 The centriole within the centrosome

The centrosome is the major MT organising centre in animal cells, and consists of a centriole pair

involved in the recruitment of the associated pericentriolar material (PCM). The centrosome in animal cells in G1 phase contains one mature mother centriole and one daughter centriole connected via flexible inter-centriolar linker. The mature centriole possesses distal and subdistal appendages, while the daughter centriole is slightly shorter and lacks appendages (reviewed in Bornens, 2012). The PCM contains γ-tubulin-complexes nucleating the majority of the MTs radiating from the centrosome. The composition and amount of PCM is one determining factor of the MT nucleating capacity of the centrosome (reviewed in Bornens, 2012). Additionally, subdistal appendages of the mother centriole are capable of MT nucleation (Piel et al., 2000).

The centrosome is the major MT organising centre in interphase cells and forms the spindle poles in mitosis. As such it is involved in correct spindle orientation and positioning. This is also critical in centrosome-based asymmetric division (Rebollo et al., 2007; Yamashita et al., 2007), which is crucial in embryonic stages for maintenance of stem cell pools and polarised tissue morphogenesis (reviewed in Bornens, 2012).

The centrosome is characteristic for animal cells. Basal bodies in the alga *Chlamydomonas reinhardtii* exhibit behaviour similar to centrioles in mitotic cells, in that the cells disassemble their flagella before mitosis and basal bodies associate with the spindle poles (Coss, 1974). While these basal bodies associated with spindle poles might appear functionally analogous, their composition is unlikely to be similar to metazoan centrosomes as many centrosomal proteins were not identified in this alga (Hodges et al., 2010). Interestingly, centrosomes are absent in the multi-ciliated planarian *Schmidtea mediterranea* (a platyhelminth), which assembles basal bodies but only via an acentriolar pathways (Azimzadeh et al., 2012).

The origin of the centrosome is unclear. One theory suggests that centrosomes evolved early in the lineage of the unikonts or Holozoa (Pickett-Heaps, 1971). It is hypothesised that the association of basal bodies with the spindle poles ensured correct segregation which provided a survival advantage (in form of motility and sensing) to daughter cells. During metazoan evolution basal

bodies and spindle poles became so interlinked that they are now inseparable. Alternatively, basal bodies with involvement in cell-cycle regulation might have accumulated MT-nucleating factors in the course of metazoan evolution, which gradually led to the establishment of centrosomes. The emergence of the centrosome might have contributed to facilitating the complex development of Metazoa.

1.1.2 The basal body in cilium formation

Basal bodies are essential for the formation of cilia and flagella. Like centrioles, canonical basal bodies are built of nine MT triplets symmetrically arranged in a cylinder. They additionally have distal appendages that mediate the attachment of the organelle to membrane. During cilium formation, basal bodies template the structure of the axoneme by extension of the A- and B-tubules from the MT triplets. As cilia have a wide distribution across eukaryotes, while centrosome components are specific to Metazoa, it has been proposed that the nucleation of the cilium is the ancestral function of centrioles/basal bodies (reviewed in Bornens and Azimzadeh, 2007).

A mature centriole and the basal body possess a set of accessory structures. One commonality is the nine-fold symmetric set of distal appendages attached at the distal end of the triplet basal body. These appendages constitute the transitional fibres of the axoneme. Less conserved accessory structures include subdistal appendages and basal feet in vertebrates, kinetodesmal fibres in *Tetrahymena thermophila*, and striated fibres in *Trypanosoma brucei* and *C. reinhardtii* (Dutcher, 2003; Pearson and Winey, 2009). Furthermore, basal bodies frequently have MT systems in their vicinity, such as the specialised MT quartet in *T. brucei*, the rootlet MTs in *C. reinhardtii*, and transverse MTs in *T. thermophila* (reviewed in Hoyer-Fender, 2010).

Although cilia formation itself is conserved across eukaryotes, the conditions under which cilia are formed are diverse: Animal cells form a primary cilium only in non-mitotic cells; in this case the mature centriole transforms into a basal body. During the generation of multi-ciliated epithelia cells, which is specific to animal cells, hundreds of basal bodies assemble simultaneously in G0 phase

(Fig. 1.1). During this, basal body assembly is uncoupled from cell cycle progression. Some protists, such as *T. brucei* or *Paramecium tetraurelia*, possess always at least one flagellum or many hundred cilia respectively. These organisms assemble their flagella/cilia in S and G2 phase and not after mitosis.

Whereas the term cilium was used in the context of the primary cilium or multi-ciliated cells, flagellum was used in a motility context. This strict classification is outdated, and the terms cilium and flagellum are used interchangeably in this thesis.

1.1.3 Centriole & basal body duplication cycle

The centriolar cycle is stringently tied to the cell cycle to ensure centriole duplication once and only once per cell cycle. A mammalian cell in G1 phase possesses one mother centriole with one daughter centriole that was assembled in the previous cell cycle (Fig. 1.1). The two structures are connected by a flexible inter-centriolar linker at their proximal ends. Pro-centriole assembly begins at the transition from G1 to S phase with the formation of the new structure orthogonally onto the wall of the parental centriole. This process continues until the middle of M phase when the pro-centriole/daughter reaches almost the same size as its mother centriole. In anaphase, the tight perpendicular arrangement of mother centriole and pro-centriole/daughter centriole is disengaged by the protease separase (Tsou and Stearns, 2006). However, the daughter centriole remains connected via a flexible inter-centriolar linker which is disconnected only at the beginning of the next M phase to allow the formation of two spindle poles (reviewed in Nigg and Stearns, 2011).

The centriole cycle has been well investigated in mammalian cells. Many but not all features are conserved across eukaryotes. The starting time of basal body assembly in *T. brucei* is similar to mammalian cells (Woodward and Gull, 1990). A trypanosome in G1 phase has a basal body with a pro-basal body. Biogenesis of new pro-basal bodies starts early in S phase (maybe similar to G1/S phase transition in mammalian cells). The bi-flagellated alga *C. reinhardtii* has two pairs of basal

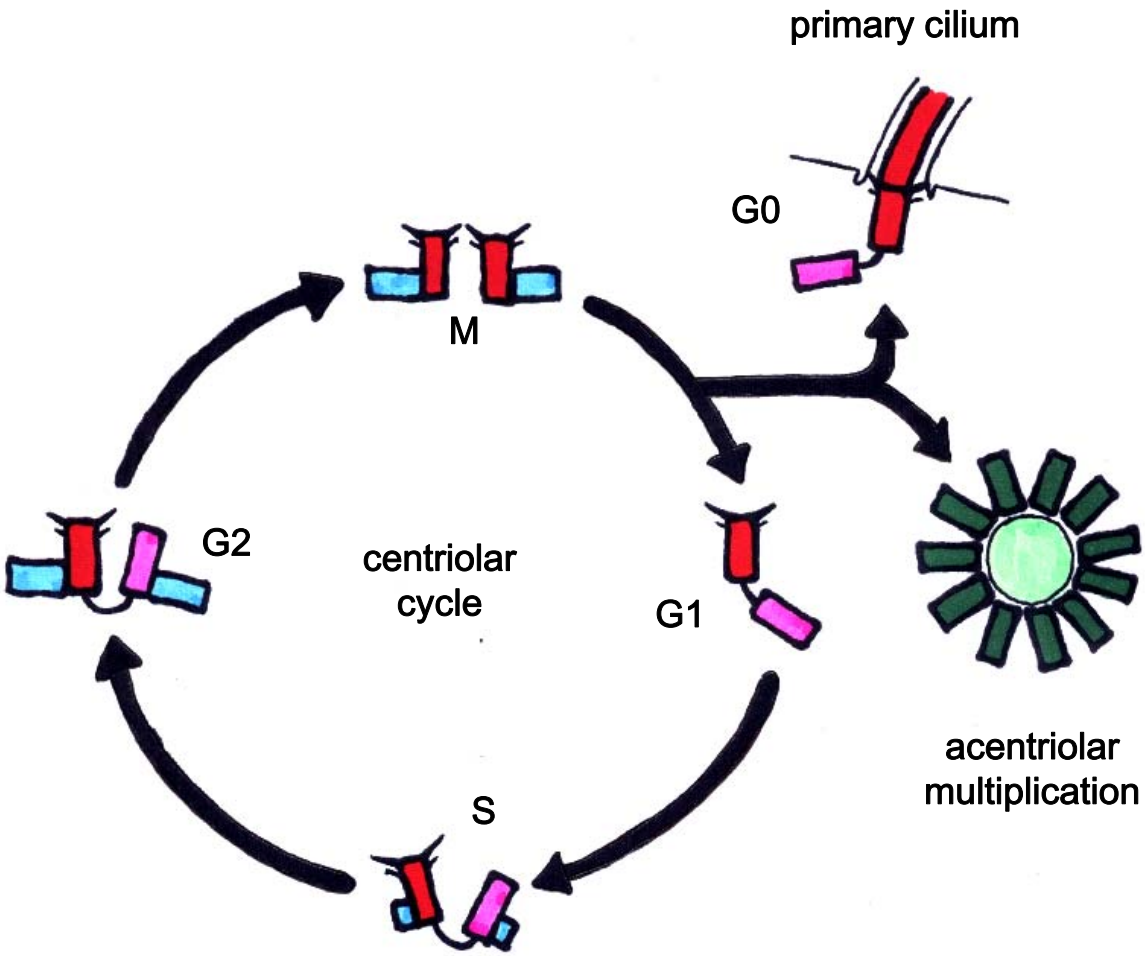

Figure 1.1 **Centriole cycle in mammalian cells.** A non-mitotic cell has one mother centriole and one daughter centriole. Pro-centriole assembly begins at the G1 to S phase transition in the centriolar cycle. Pro-centrioles elongate throughout S until G2 phase. Daughter centrioles remains in a tight perpendicular position with mother structure until metaphase to anaphase transition. After that they remain connected by a flexible inter-centriolar linker. In mammalian cells centrioles need 1.5 cell cycles to mature and acquire appendages; appendages form in M phase. After cytokinesis, daughter cells possess one mature centriole that is capable of nucleating a primary cilium. Cells that differentiate into multi-ciliated cells undergo additional centriole formation via the acentriolar pathway, where hundreds of pro-centrioles can form around dense structures, termed deuterosomes. Mature centriole in red, pro-centriole/daughter in blue, centriole before maturation in pink. Deuterosome in light green. Acentriolarly assembling pro-centrioles in dark green.

bodies which duplicate once per cell cycle. In this alga pro-basal bodies form already in G1 phase and elongate until G2 phase (Dutcher, 2003). The ciliates *T. thermophila* and *P. tetraurelia* possess approximately 750 and 4000 basal bodies respectively. These structures must be duplicated once every cell cycle to maintain a constant number in following generations. Interestingly, assembly dynamics are very different and suggest a loosening of strict control mechanisms. Due to a posterior-anterior gradient of molecules, basal body duplication happens mainly in the middle of the cell but less towards the ends. Furthermore, maturation of newly assembled pro-basal bodies is so rapid that these new structures can give rise to a pro-basal body in the same cell cycle that they themselves were assembled in (Pearson and Winey, 2009).

An obvious difference between distantly-related eukaryotes is the timing of centriole/basal body maturation and consequently cilia formation. While pro-centrioles in mammalian cells pass 1.5 cell cycles before they are capable of cilium formation, pro-basal bodies in ciliates can mature in less than one cell cycle. Pro-basal bodies in *T. brucei* require one full cell cycle for maturation.

1.1.4 Centriole & basal body assembly

The structure of centrioles and basal bodies is highly conserved across eukaryotes. Consistent with this, the molecular compositions and the assembly processes show many similarities (e.g. time point of assembly start, cartwheel formation) but also differences (e.g. time point of maturation, mechanism of initiation of assembly) (reviewed in Carvalho-Santos et al., 2011). While most of our knowledge about the proteins involved in centriole and basal body assembly stems from animal systems, some studies in species distantly-related to Metazoa and bioinformatic studies showed that some major players of centriole assembly and their functions are conserved in a wide range of ciliated eukaryotes.

The major steps of centriole and basal body assembly are: **1) initiation** (by kinase activity), **2) assembly of a cartwheel** or a similar structure that establishes the nine-fold radial symmetry, **3) attachment of centriolar MTs** to the cartwheel, **4) elongation** of the centriolar MTs, and

5) maturation by assembly of appendages (Fig. 1.2).

Despite the complex structure of centrioles and basal bodies, a rather small set of proteins is essential for centriole formation in organisms studied so far. Genome-wide screens in *C. elegans* using RNA interference identified only five proteins that are essential for centriole assembly in the nematode: SPD-2, the kinase ZYG-1, SAS-6, SAS-5, and SAS-4 (Dammermann et al., 2004; Delattre et al., 2006; Kirkham et al., 2003; Leidel et al., 2005; Leidel and Gonczy, 2003; O'Connell et al., 2001; Pelletier et al., 2006). In *D. melanogaster* 18 proteins (out of 13,059 gene analysed) were found to be required for centriole biogenesis (Dobbelaere et al., 2008). These proteins included the kinase SAK, SAS-6, Ana2 (SAS-5 homologue), SAS-4, but not SPD-2. Proteins essential for centriole duplication in *H. sapiens* also include Cep192 (SPD-2 homologue), the kinase PLK4 (SAK homologue), SAS-6, STIL (SAS-5 homologue), CPAP (SAS-4 homologue) (Kleylein-Sohn et al., 2007). Interestingly, only two proteins, namely SAS-6 and SAS-4, are widely conserved amongst ciliated species and have been found to be required for centriole assembly in all model organisms studied so far (Basto et al., 2006; Carvalho-Santos et al., 2010; Culver et al., 2009; Dammermann et al., 2004; Gogendeau et al., 2011; Hodges et al., 2010; Jerka-Dziadosz et al., 2010; Kirkham et al., 2003; Kleylein-Sohn et al., 2007; Leidel et al., 2005; Leidel and Gonczy, 2003; Nakazawa et al., 2007; Rodrigues-Martins et al., 2007a).

1.1.4.1 Initiation of centriole and basal body assembly

- **Molecular mechanisms of assembly initiation in Metazoa**

In animal cells kinase activity is required for the initiation of centriole duplication. The protein kinase **ZYG-1** in *C. elegans* (O'Connell et al., 2001), **SAK** in *D. melanogaster* (Bettencourt-Dias et al., 2005), and **PLK4** in *H. sapiens* (Habedanck et al., 2005) is required for centriole duplication. Overexpression of PLK4 causes the assembly of supernumerary centrioles (Kleylein-Sohn et al., 2007). In *D. melanogaster*, where SAK is normally ubiquitylated for degradation by the SCF/Slimb complex, the depletion of Slimb also results in formation of multiple pro-centrioles per mature

molecules involved:	metazoan	general eukaryotic
① Initiation 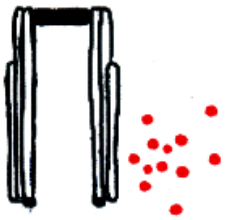	**Kinase:** **PLK-4/SAK, ZYG-1** Phosphatase: PP2A Scaffolding/Matrix: SPD-2/Cep192 Asterless/Cep152	**Not PLK-4/SAK** probably not PLK Kinase? Other enzyme? No SPD-2 or Asterless
② Cartwheel 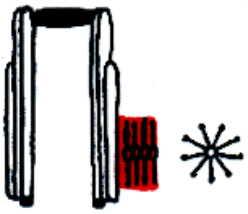	**Cartwheel component:** **SAS-6** Cep135 SAS-5/Ana2/STIL	**Cartwheel component:** **SAS-6/Bld12** Cep135/Bld10
③ MT attachment 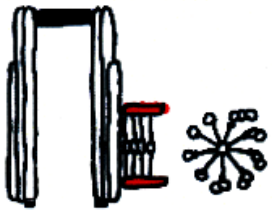	**MT attachment &** **MT nucleation:** **SAS-4/CPAP** **γ-tubulin** δ-tubulin? ε-tubulin?	**MT attachment &** **MT nucleation:** **SAS-4** **γ-tubulin** δ-tubulin ε-tubulin
④ Elongation 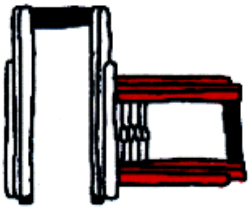	**Elongation promoting:** CPAP & hPOC1 **Elongation inhibiting:** CP110 & OFD1 Kif24/Klp10 Distal proteins: Centrin & hPOC5	POC1 Kinesin-13? Centrin
⑤ Maturation 	Cep164 OFD2	Cep164

Figure 1.2 **Assembly of centrioles and basal body in eukaryotes.** Steps of assembly of a centriole or basal body include 1) initiation, 2) cartwheel formation or symmetry establishment, 3) MT attachment, 4) elongation of the structure, 5) maturation/appendage formation. Carton represents the current understanding of the process in mammalian cells. Proteins are shown for the metazoan pathway, and for a less defined, general eukaryotic pathway.

centriole (Cunha-Ferreira et al., 2009; Rogers et al., 2009). These data demonstrate a role of these kinases in the initiation of centriole assembly.

ZYG-1, SAK and PLK4 seem to fulfil a similar function. While SAK and PLK4 are orthologues, an orthologous relationship to ZYG-1 could not be shown (Carvalho-Santos et al., 2010; Hodges et al., 2010). Regardless of this relationship, in both *C. elegans* and *H. sapiens*, the kinase is required for SAS-6 recruitment to the centriole (Delattre et al., 2006; Kleylein-Sohn et al., 2007; Pelletier et al., 2006). In *C. elegans* SAS-6 is a substrate of ZYG-1 (Kitagawa et al., 2009). A comparable process has not been observed in *H. sapiens*. However, PLK4 phosphorylation activity is essential, as catalytically inactive mutants fail to induce centriole biogenesis (Habedanck et al., 2005). One substrate of PLK4 is GCP6, a subunit of the γ-tubulin ring complex, which is itself required for centriole duplication (Bahtz et al., 2012). FBXW5, a subunit of an E3-ubiquitin ligase complex, is also phosphorylated by PLK4; this phosphorylation inhibits the capacity of the complex to target SAS-6 for degradation early in the cell cycle (Puklowski et al., 2011).

The **protein phosphatase 2A** (**PP2A**) stabilises ZYG-1 and SAK by dephosphorylating residues that in a phosphorylated state target the proteins for degradation (Brownlee et al., 2011; Kitagawa et al., 2011a; Song et al., 2011). PLK4 in human cells undergoes autophosphorylation which targets the protein for degradation by the SCF/betaTrCP complex in interphase (Guderian et al., 2010). However, during mitosis the PLK4 homologue in *D. melanogaster* is stabilised by PP2A which mediates dephosphorylation of the autophosphorylated residues (Brownlee et al., 2011).

The recruitment of ZYG-1 in *C. elegans* and PLK4 in *H. sapiens* to the centrosome and centriole requires the centrosomal protein **SPD-2** and **Cep192** respectively (Delattre et al., 2006; Gomez-Ferreria et al., 2007; Kleylein-Sohn et al., 2007; Pelletier et al., 2006; Zhu et al., 2008). In contrast, SPD-2 in *D. melanogaster* is dispensable for centriole duplication and only required for PCM recruitment, which suggests that SAK recruitment and function is independent of SPD-2 in the fly (Dix and Raff, 2007).

The centrosomal protein **Asterless** in *D. melanogaster* and its orthologue **Cep152** in *H. sapiens* are required for loading SAK and PLK4 respectively onto the centrosome (Cizmecioglu et al., 2010; Dzhindzhev et al., 2010). Therefore, these centrosomal proteins are also essential for centriole replication. No homologue has been identified in *C. elegans*. Super-resolution microscopy has shown that Cep152 forms a discrete ring around the proximal end of parental centriole in human cells (Sir et al., 2011). The N-terminus of Asterless and Cep152 interacts with the cryptic Polo-domain of SAK and PLK4 respectively, while the C-terminus can interact with SAS-4 and CPAP respectively (Cizmecioglu et al., 2010; Dzhindzhev et al., 2010). However, whereas Cep152 is required to hold CPAP in the centrosome in *H. sapiens*, centrosomes lacking Asterless and consequently centrioles still contain SAS-4 in *D. melanogaster* (Dzhindzhev et al., 2010; Gopalakrishnan et al., 2011). Overexpression of Asterless or Cep152 leads to d*e novo* centriole formation in fly embryos, and to centrosome amplification in fly eggs and human cells (Dzhindzhev et al., 2010). Consistent with the role of Asterless/Cep152 in humans and flies, Cep152 in the zebrafish *Danio rerio* was shown to be required for basal body assembly in multi-ciliated cells (Blachon et al., 2008).

- **General mechanisms of assembly initiation across eukaryotes**

In animal cells it has been established that kinase activity is essential for the initiation of centriole duplication. However, PLK4 is specific to the holozoan lineage (Metazoa and choanoflagellates) (Carvalho-Santos et al., 2010; Hodges et al., 2010). The involvement of PLK4 in the initiation might represent an adaptation specific to centriole biogenesis within centrosomes. Since Polo-like kinases appear not to be present in all ciliated eukaryotic species, another kinase or mechanism must initiate basal body duplication in these species (Carvalho-Santos et al., 2010; Hodges et al., 2010). In recent bioinformatic studies, SPD-2/Cep192 and Asterless/Cep152 were not identified in lineages outside of Metazoa (Carvalho-Santos et al., 2010; Hodges et al., 2010). This suggests a low degree of conservation for the mechanism that initiates centriole and basal body duplication

across eukaryotes.

1.1.4.2 Cartwheel - Establishment of the nine-fold symmetry

The first structural step in centriole and basal body assembly is the formation of a structure that establishes the nine-fold symmetry: the cartwheel in most species (Fig. 1.2). The cartwheel, first described by Gibbons and Grimstone (1960), is a conserved structure in the proximal part of the basal body. It consists of a central hub that holds nine spokes evenly spaced radiating outwards. In many eukaryotic species, including many protists and *C. reinhardtii*, the cartwheel is maintained in the mature basal body (Allen, 1969; Dingle and Fulton, 1966; Dippell, 1968; Ringo, 1967). In contrast, in several metazoan species such as *H. sapiens* and the mollusc *Anodonta cataracta* cartwheels are only present in the nascent pro-centriole but lost after centriole maturation (Alvey, 1986; Gibbons, 1961). The cartwheel loss, however, is not a general metazoan feature, as centrioles of *D. melanogaster* maintain a cartwheel structure after maturation (Callaini et al., 1997). The MT singlet centriole of *C. elegans* is very divergent, and exhibits a central tube instead of a cartwheel (Perkins et al., 1986). Evolution of this central tube from the cartwheel, is suggested by the presence of SAS-6 in both structures and the absence of the central tube in other eukaryotic centrioles.

- **Cartwheel assembly in Metazoa**

SAS-6 is essential for centriole duplication in *C. elegans* (Dammermann et al., 2004; Leidel et al., 2005), *D. melanogaster* (Rodrigues-Martins et al., 2007a), and *H. sapiens* (Kleylein-Sohn et al., 2007; Strnad et al., 2007; Vladar and Stearns, 2007). This function is also consistent with the observed centrosome duplication defect in *D. rerio sas-6/cea* embryos (Yabe et al., 2007). In *C. elegans*, SAS-6 is required for the formation of the central tube, a SAS-6 positive structure that is still formed in SAS-4 depleted cells but that fails to assemble in SAS-6 depleted cells (Delattre et al., 2006; Pelletier et al., 2006). Overexpression of SAS-6 in *D. melanogaster* eggs and embryos does not induce overduplication of centrioles (Rodrigues-Martins et al., 2007a). SAS-6 localises to

centriole/basal body in all organisms studies so far. In basal bodies that nucleate axonemes SAS-6 also localises to a more distal site that is consistent with the position of the basal plate (Peel et al., 2007; Rodrigues-Martins et al., 2007a; Vladar and Stearns, 2007).

Our current understanding is that SAS-6 constitutes the central hub and probably parts of the spokes of the cartwheel. This is supported by models based on the crystal structure of an N-terminal portion of SAS-6 from *C. elegans* and *D. rerio* (Kitagawa et al., 2011c; van Breugel et al., 2011). The strongest evidence stems from spontaneous oligomerisation of the N-terminal domain of *D. rerio* SAS-6 into crystals with circular repeats that resembled the central hub of the cartwheel; the assembled structures, however, possessed only an eight-fold symmetry (van Breugel et al., 2011). SAS-6 consists of a globular head domain at the N-terminus, a central coiled coil region and a less defined C-terminus (Kitagawa et al., 2011c; van Breugel et al., 2011). Models predict that SAS-6 proteins form homodimers via the central coiled coil domain, and that nine of these dimers assemble into a ring via hydrophobic interactions between the N-terminal head domains to constitute the central part of the cartwheel (Cottee et al., 2011; Kitagawa et al., 2011c; van Breugel et al., 2011).

SAS-6 recruitment to the centriole depends on the kinases ZYG-1 in *C. elegans*, SAK in *D. melanogaster* and PLK4 in *H. sapiens* (Kleylein-Sohn et al., 2007; Leidel et al., 2005; Peel et al., 2007; Pelletier et al., 2006). In *C. elegans* ZYG-1 phosphorylates SAS-6 in the N-terminal part. This modification is required for the maintenance of SAS-6 at the site of pro-centriole assembly (Kitagawa et al., 2009). Recruitment of SAS-6 to this site requires formation of a complex with SAS-5 (Delattre et al., 2006; Kitagawa et al., 2011a; Leidel et al., 2005; Pelletier et al., 2006).

Cellular levels of SAS-6 in *H. sapiens* oscillate during cell cycle, without significant variation in mRNA levels: the protein is undetectable in G1, levels start increasing at the beginning of S phase throughout G2 phase until the metaphase to anaphase transition in mitosis, when the protein is no longer detectable (Strnad et al., 2007). Vertebrate SAS-6 has a Ken-box at the C-terminal end and

its abrupt clearance is the result of proteasomal degradation mediated by ubiquitin ligation via the anaphase-promoting complex (APC)/Cdh1 (Strnad et al., 2007; van Breugel et al., 2011). This also suggests that the cartwheel in vertebrate centrioles disappears because its key component is degraded. Interestingly, although *C. elegans* lacks an obvious cartwheel, SAS-6 in the nematode shows similar dynamics as its human homologue, in that the centrosomal level decreases by approximately 50% in the second half of mitosis (Dammermann et al., 2008). Another negative regulator of SAS-6 in *H. sapiens* is the SCF/FBXW5 E3-ubiquitin ligase (Puklowski et al., 2011). The level of the FBXW5 subunit is a cell-cycle regulated and peaks at the G1 to S phase transition. However, when PLK4 is active it phosphorylates FBXW5 and hence inhibits its capacity to target SAS-6 for degradation (Puklowski et al., 2011).

As mentioned above, in vertebrates SAS-6 is lost from centrioles during disengagement (Kleylein-Sohn et al., 2007; Strnad et al., 2007). This SAS-6/cartwheel loss is often associated with maturation. However, interestingly, SAS-6 is not lost in multi-ciliated mouse tracheal cells (Vladar and Stearns, 2007). Almost all basal bodies of multi-ciliated cells assemble in G0 phase and do consequently not experience exposure to APC/Cdh1. This raises the question whether the presence of SAS-6 reflects a simple lack of the appropriate degradation machinery or whether it is of functional relevance in these basal bodies.

SAS-5 in *C. elegans*, its homologue in **Ana2** *D. melanogaster*, and its homologue **STIL** in *H. sapiens* are also required for centriole formation (Delattre et al., 2004; Kitagawa et al., 2011b; Stevens et al., 2010a; Tang et al., 2011). In *C. elegans* SAS-6 and SAS-5 are mutually required for localisation to the centriole as they form a complex (Delattre et al., 2006; Leidel et al., 2005; Pelletier et al., 2006). The complex formation between SAS-6 and STIL is controversial in *H. sapiens*, where STIL was reported to fail to localise to the centriole in SAS-6 depleted cells (Tang et al., 2011), but was also described to locate to the centriole in the absence of SAS-6 (Arquint et al., 2012). In *D. melanogaster* overexpression of Ana2 alone has no phenotype, whereas the overexpression of Ana2 with SAS-6 leads to the assembly of structures that resemble

a network of cartwheel hubs (Stevens et al., 2010b). In *C. elegans* the protein phosphatase 2A stabilises SAS-5 within the SAS-5/-6 complex by dephosphorylating a residue that in a phosphorylated state would target SAS-5 for degradation (Kitagawa et al., 2011a; Song et al., 2011).

Bld10p was initially identified in *C. reinhardtii* as cartwheel protein required for basal body assembly (Matsuura et al., 2004). Consistent which this finding, the human orthologue of Bld10p, named **Cep135**, localises to the proximal lumen of the centriole and pro-centriole, and is required for centriole assembly (Kleylein-Sohn et al., 2007). Interestingly, in contrast to SAS-6, Cep135 remains in mature centrioles, suggesting it is not solely a cartwheel component (Kleylein-Sohn et al., 2007). Bld10 is not essential for centriole assembly in *D. melanogaster* as centrioles still assemble in the absence of the protein. However, centrioles and basal bodies are shorter than normal, and the axonemes in spermatids lack the central MT pair (Mottier-Pavie and Megraw, 2009). Whether normal cartwheels assembled in these flies was not shown. No homologue of Cep135 has been identified in *C. elegans* (Carvalho-Santos et al., 2010; Hodges et al., 2010).

Mechanisms of cartwheel assembly outside of animals

As in Metazoa, the assembly of a cartwheel depends on the SAS-6 homologue **Bld12** in *C. reinhardtii*, on **Sas6a** in *T. thermophila* and on **Sas6p** in *P. tetraurelia* which constitute the central part of the cartwheel (Culver et al., 2009; Jerka-Dziadosz et al., 2010; Nakazawa et al., 2007). Interestingly, in the *C. reinhardtii bld12* null mutant basal bodies without cartwheels do assemble in 20% of the cells (Nakazawa et al., 2007). Although these structures have irregular numbers of microtubule triplets it suggests that the cartwheel or at least SAS-6 might not be the sole prerequisite for the assembly of the basal body. Recruitment of SAS-6 to the site of pro-basal body assembly works most likely differently in species outside the metazoan lineage as SAS-5 homologues were only identified in animals (Stevens et al., 2010a).

Bld10p was initially identified in *C. reinhardtii* as cartwheel protein required for basal body

assembly (Matsuura et al., 2004). Interestingly, expression of truncated Bld10p in the *bld10p* null mutant led to the assembly of basal bodies with eight MT triplets and shorter spokes, suggesting that Bld10 might be a spoke component (Hiraki et al., 2007; Matsuura et al., 2004).

1.1.4.3 Assembly of centriolar MTs

After formation of the cartwheel, A-microtubules are attached to the tips of the cartwheel spokes and assemble from minus into plus direction. B-tubules start assembling onto A-tubules even when these are not yet complete in terms of number and length (Guichard et al., 2010). Assembly of B- and C-tubules does not start at the most proximal point but somewhere in the middle onto the A-tubules or B-tubules respectively (Guichard et al., 2010).

- **Molecular mechanisms of microtubule nucleation and attachment in Metazoa**

SAS-4 is essential for centriole duplication in *C. elegans* (Kirkham et al., 2003; Leidel and Gonczy, 2003), *D. melanogaster* (Basto et al., 2006), and *H. sapiens*, where the SAS-4 orthologue is called CPAP or CENPJ (Kleylein-Sohn et al., 2007). CPAP and fly SAS-4 include a PN2-3 domain that interacts with tubulin dimers (Cormier et al., 2009; Hsu et al., 2008; Hung et al., 2004). Tomography of pro-centrioles in *C. elegans* embryos depleted of SAS-4 showed the assembly of the central tube without MTs (Pelletier et al., 2006). This study also described hooks on the central tubes before MT attachment; these hooks were missing in SAS-4 depleted embryos (Pelletier et al., 2006). Thus, SAS-4 has been proposed to be involved in the attachment of MTs to the central tube. As centrioles in *C. elegans* possess only singlet microtubules, it demonstrates involvement of SAS-4 with A-tubule formation. A role in microtubule assembly onto the central tube (or cartwheel) was further supported by the finding that stable integration of SAS-4 into the pro-centriole required γ-tubulin (Dammermann et al., 2008). Electron tomography of human centrioles showed that the A-tubules, but not B- and C-tubules, appear capped at the proximal end, most likely with a γ-tubulin cap (Guichard et al., 2010). Overexpression of CPAP in human cells leads to elongation of the centriolar MTs (Kohlmaier et al., 2009; Schmidt et al., 2009; Tang et al., 2009). Overexpression of

a mutated CPAP incapable of binding tubulin fails to induce MT elongation (Tang et al., 2009). Together, these data support that SAS-4/CPAP has a capacity in the assembly of centriolar MTs.

SAS-4/CPAP dynamics are at least in parts controlled by cell-cycle dependent degradation. In *C. elegans* and *H. sapiens*, SAS-4/CPAP incorporation into the nascent pro-centriole starts in S phase and continues until prophase, before the cytoplasmic SAS-4/CPAP pool is targeted by APC/Cdh1-degradation in late M phase (Dammermann et al., 2008; Tang et al., 2009).

SAS-4/CPAP might have additional roles outside of the centriole. SAS-4 in *D. melanogaster* has also been suggested to act as a platform that tethers other proteins, for example such as Asterless, to the centrosome (Gopalakrishnan et al., 2011). Furthermore, the capability of CPAP to interact with γ-tubulin might also be of relevance in the centriole-independent nucleation of MTs in the centrosome (Dammermann et al., 2008; Hung et al., 2000). CPAP was also reported to localise to the midbody in human cells (Paramasivam et al., 2007), which might also hint towards a broader involvement of the protein with MTs.

Interestingly, in *H. sapiens* CPAP dysfunction has been also associated with microcephaly, a neuro-developmental defect resulting in reduced brain size and retardation (Bond et al., 2005). A lack or mutation of CPAP can cause changes in spindle positioning in neuronal progenitor cells, probably due to an effect of CPAP on size or microtubule-anchoring capacity of centrosomes (Kirkham et al., 2003; Kitagawa et al., 2011b). During the development of the brain it is essential to maintain a pool of neuronal stem cells. This is achieved by asymmetric division with precise spindle positioning (reviewed in Megraw et al., 2011). Premature exhaustion of the pool of neural stem cells leads to reduced brain size. However, it remains to be shown whether the errors in spindle positioning are a secondary defect caused by centriole defects, or whether CPAP/SAS-4 has another capacity that causes the defect directly.

Unsurprisingly, **γ-tubulin** is an essential protein in the formation of the centriolar MTs (Haren et al., 2006; Kleylein-Sohn et al., 2007). The A-tubules possess a γ-tubulin cap early in the assembly

process, whereas B- and C-tubules do not (Guichard et al., 2010). γ-tubulin is also required for the maintenance of SAS-4 at the centriole (Dammermann et al., 2008) and co-immunoprecipitates with CPAP (Hung et al., 2000).

δ- and ε-tubulin have been suggested to be involved in doublet and triplet formation outside Metazoa. However, as *C. elegans* and *D. melanogaster* have no identifiable homologues of these proteins, the roles of δ- and ε-tubulin are not well established in Metazoa. Nevertheless, ε-tubulin is required for centriole duplication in human cells. The protein has a cell-cycle specific localisation to the older centriole that suggests involvement in the maturation process, and immuno-gold labelling showed its localisation to the distal appendages (Chang et al., 2003).

Mechanisms of microtubule nucleation and attachment across eukaryotes

The only study of **SAS-4** outside of animals, in *P. tetraurelia*, showed that simultaneous RNAi-mediated targeting of all three *SAS-4* genes leads to a reduction in the number of basal bodies, suggesting SAS-4 requirement in basal body assembly (Gogendeau et al., 2011).

Unsurprisingly, **γ-tubulin** is also essential for MT formation of basal bodies in eukaryotes outside the Metazoa, as has been demonstrated in *P. tetraurelia* and *T. thermophila* (Ruiz et al., 1999; Shang et al., 2002).

It was proposed that **δ-tubulin** is required for MT triplet formation in centrioles, since the *C. reinhardtii* deletion mutant *uni3-1* possesses basal bodies that have mainly MT doublets (Dutcher and Trabuco, 1998). However, further analysis of the *uni3-1* strain revealed that basal bodies frequently have a subset of MT triplets at the distal end and that some of the associated fibre systems are misplaced or defective which led to the suggestion that δ-tubulin might not be required for the assembly but stable maintenance of C-tubules (O'Toole et al., 2003). Similar to the findings in the alga, knockdown of δ-tubulin in *P. tetraurelia* results in the loss of C-tubules, and occasional loss of B- and A-tubules (Garreau de Loubresse et al., 2001). Basal bodies lacking

varying numbers of C-tubules, or B- and C-tubules were also observed after δ-tubulin depletion in *T. brucei* (Gadelha et al., 2006).

ε-tubulin was suggested to be required for the addition of B- and maybe C-tubules, as the *C. reinhardtii* mutant strain *bld-2* expressing only truncated ε-tubulin has basal bodies with MT singlets (Dutcher et al., 2002; Goodenough and StClair, 1975). However, *C. reinhardtii* carrying null alleles for ε-tubulin are not viable which indicates that the truncated ε-tubulin in the *bld-2* strain might still fulfil a vital capacity (Dutcher et al., 2002). ε-tubulin depletion in *P. tetraurelia* results in basal bodies with aberrant MT numbers - singlets, doublets and triplets (Dupuis-Williams et al., 2002).

1.1.4.4 Distal end formation and centriole elongation control

The pro-centriole has a short length (approximately 70-100 nm) when it starts assembling the B- and the C-tubules (reviewed in Azimzadeh and Marshall, 2010). Pro-centrioles continue to grow in length throughout S, G2 and M phase. As centrioles acquire a consistent length, there must be some kind of length control.

- **Molecular mechanisms of pro-centriole elongation in animals**

CP110 is required for centriole duplication in *H. sapiens* and *D. melanogaster* (Dobbelaere et al., 2008; Kleylein-Sohn et al., 2007). The protein localises to the distal end of centrioles. It has been suggested that the protein forms a cap on the growing tip of centriolar MTs and that tubulin is incorporated into the nascent pro-centriole underneath the cap (Kleylein-Sohn et al., 2007). CP110 interacts with the Kinesin-13 family member **Kif24** in *H. sapiens* and **Klp10A** in *D. melanogaster* (Delgehyr et al., 2012; Kobayashi et al., 2011). Kif24 and Klp10A possess MT depolymerising activity and the interaction with CP110 plays a role in the remodelling of the centriolar MTs (Delgehyr et al., 2012; Kobayashi et al., 2011). Depletion of CP110 or its interaction partners Kif24 or Cep97 leads to in the elongation of centriolar microtubules, and in the case of Kif24 depletion possibly even to ciliogenesis in cycling cells (Kobayashi et al., 2011; Schmidt et al., 2009; Spektor

et al., 2007). Hence, CP110 together with Kif24 and Cep97 have been suggested to be (negative) regulators of the elongation of centrioles and specifically of the centriolar MTs. Consistent with this, the enforced expression of CP110 in quiescent cells inhibits ciliogenesis (Spektor et al., 2007). Interestingly, CP110 is ubiquitylated by SCF/Cyclin F leading to its degradation already in G2 phase (D'Angiolella et al., 2010). The failure of CP110 degradation induces centrosome and mitotic aberrations (D'Angiolella et al., 2010).

CPAP (SAS-4 homologue) is another protein that influences centriole length. Overexpression of the protein in human cells results in the elongation of centriolar MTs, suggesting that CPAP might not or not only play a role in MT attachment to the cartwheel but also in MT elongation or stabilisation (Kohlmaier et al., 2009; Schmidt et al., 2009; Tang et al., 2009). **hPOC1** has also been suggested to be involved in the regulation of centriole length, as overexpression of the protein also leads to elongated centriolar MTs (Keller et al., 2009). **OFD1**, a protein involved in distal appendage formation, was proposed to also play a negative role in centriole length regulation, as OFD1-deficient cells have abnormally elongated mother centrioles (Singla et al., 2010). Collectively, the existent data suggest that CPAP and hPOC1 enhance centriole elongation, whereas CP110 and OFD1 and Kif24/Klp10a are negative regulators of centriole length.

Centrin, a component of the distal end of centrioles, is required for centriole duplication in *H. sapiens* (Paoletti et al., 1996; Salisbury et al., 2002). Its precise role in the centriole assembly process, however, is not clear. **hPOC5** is a centrin-interacting protein which also localises to the distal part of the centriole. Its depletion leads to S phase arrest and to pro-centrioles that retain the short length from early S phase. (Azimzadeh et al., 2009). Whether the short length is a direct consequence of hPOC5 deficiency and induces S phase arrest, or whether hPOC5 absence leads to S phase arrest that consequently prevents pro-centrioles from growing is not clear.

▸ Molecular mechanisms of pro-basal body elongation outside of animals

Centrin is found at the distal end of basal bodies and required for the duplication of the structure in

a wide range of eukaryotes (Geimer and Melkonian, 2005; Koblenz et al., 2003; Ruiz et al., 2005; Stemm-Wolf et al., 2005). Similar to the phenotype observed in human cells, overexpression of **POC1** in *C. reinhardtii* results in elongated basal bodies at the light microscopic level (Keller et al., 2009). Whether these structures represent long basal body MTs or elongated basal bodies is not clear. Immuno-gold electron microscopy has shown that POC1 localises along the triplet MTs, which is in agreement with a possible role in MT elongation (Keller et al., 2009). Interestingly, centriole length is unaffected in POC1-depleted *T. thermophila* cells but basal body defect arises from breaks in the MT blades (Pearson et al., 2009). Together, the data across diverse eukaryotes suggest involvement of POC1 with centriolar/basal body MTs. However, whether it participates directly in MT growth or indirectly via a stabilising function remains to be shown.

Although CP110 homologues cannot be identified outside of Metazoa, homologues of its interaction partner Kif24 (**Kinesin-13A** proteins) are present in a wide range of eukaryotes (Wickstead et al., 2010). Overexpression of Kin13-2 in *Leishmania major* results in shortening of the flagellum (Blaineau et al., 2007). Although Kin13-2 localises to the tip of the growing flagellum in *T. brucei*, neither depletion nor overexpression lead to a significant change in flagellum length (Chan and Ersfeld, 2010; Wickstead et al., 2010). Consistent with a role in MT depolymerisation, depletion of Kinesin-13 in *C. reinhardtii* results in a slower flagellum disassembly rate. However, in contrast, flagellum regrowth was much slower in Kinesin-13 depleted cells after deflagellation, suggesting additionally a role in rapid flagellar assembly (Piao et al., 2009). Collectively, these data propose that Kinesin-13 homologues across ciliated eukaryotes have a function in controlling the flagellum rather than the basal body length. There is, however, the possibility that basal body length control does not require a stringent control mechanism in a pure basal body function outside the centrosomal context

1.1.4.5 Maturation and assembly of distal and subdistal appendages

Distal appendages seem to be required for the ability of a centriole/basal body to dock to the plasma membrane and/or to nucleate a cilium (Graser et al., 2007a; Ishikawa et al., 2005). The

assembly of these appendages is part of the maturation process.

The cell cycle phase when maturation and cilium formation occurs varies between different eukaryotic species: while cilia formation occurs only in differentiated or quiescent cells in Metazoa, it takes place in S and G2 phase in *T. brucei* and ciliates. In *C. reinhardtii*, cilia are lost by resorption or deflagellation before mitosis and are reassembled after several rounds of mitosis have been completed (reviewed in Quarmby and Parker, 2005). This has also implications for the maturation process: whereas metazoan centrioles form appendages only during mitosis in the next cycle and hence need 1.5 cell cycles to mature, basal bodies mature within one cell cycle or less in *T. brucei* and ciliates respectively (Pearson and Winey, 2009; Vorobjev and Chentsov Yu, 1982).

One commonality between mature centrioles/basal bodies of diverse eukaryotic species is the presence of a nine-fold set of distal appendages to form the transitional fibres of the transition zone. The maturation process is often accompanied by the assembly of a variety of accessory structures and/or MT systems that are very divergent between species.

- **Molecular mechanisms of centriole maturation in Metazoa**

Depletion of **Cep164** inhibits ciliogenesis in human cells, and immunogold electron microscopy has shown that the protein localises to the distal appendages (Graser et al., 2007a). **OFD2/Cenexin** is found only at the mature centriole and participates in the formation of distal and subdistal appendages in mammalian cells (Ishikawa et al., 2005; Lange and Gull, 1995). Centrioles deficient of OFD2 fail to attach to the plasma membrane and hence to form cilia (Ishikawa et al., 2005). Additionally, OFD2 is also involved in the assembly of the basal feet at basal bodies in multi-ciliated cells (Kunimoto et al., 2012).

- **General molecular mechanisms of basal body maturation across eukaryotes**

The presence of **Cep164** homologues across a wide range of ciliated species and the identification of TbCep164 in the proteome of *T. brucei* flagella suggest that the protein is involved for the

formation of distal appendage across eukaryotes (Broadhead et al., 2006; Hodges et al., 2010). The appendage protein OFD2 is found in Metazoa but not conserved across eukaryotes.

1.1.5 Temporal & numeral control

Stringent control of the centriole number and time of centriole duplication is essential for maintaining the correct number of this organelle in future generations of cells. Centriole/basal body duplication occurs once and only once per cell cycle in most cells. Exceptions include cells differentiating into multi-ciliated cells or ciliates that have several hundred or thousand basal bodies. Many of the connections between the cell cycle and centriole duplication have been elucidated only in Metazoa or only human cells. The basal body duplication cycle in eukaryotes outside Metazoa is also linked to the cell cycle; however, temporal differences and divergence of cell cycle control mechanism suggest that the connections might be different.

In Metazoa three different types of mechanisms couple centriole biogenesis to the cell-cycle:

Firstly, centriole duplication factors are targeted by cell-cycle-dependent protein degradation. SAK in *D. melanogaster* is ubiquitylated for degradation by the SCF/Slimb complex which is activated at the G1 to S phase transition, and allows kinase activity only during G1 phase and late M phase (Cunha-Ferreira et al., 2009; Rogers et al., 2009). SAS-6 and CPAP in *H. sapiens* are targeted for degradation by APC/Cdh1 starting at the metaphase to anaphase transition until G1 phase (Strnad et al., 2007; Tang et al., 2009). PLK4 inhibits FBXW5, a subunit of an E3-ubiquitin ligase complex, that otherwise would target SAS-6 for degradation early in the cell cycle (Puklowski et al., 2011). CP110 is ubiquitylated by SCF/Cyclin F leading also to degradation (D'Angiolella et al., 2010). Protein degradation is a reliable regulatory mechanism as it ensures irreversibility of the cycle. Additionally, involvement of different cell-cycle-regulated degradation-mediating complexes facilitates the ordered sequence of processes.

Secondly, centriole duplication factors are regulated by cell-cycle-dependent phosphorylation. The

cell-cycle regulator Cdk2 is involved in centriole duplication and phosphorylates CP110, which itself is required for centriole duplication (Chen et al., 2002; Kleylein-Sohn et al., 2007).

Thirdly, centriole duplication employs other central proteins from the cell cycle. Centriole disengagement seems to apply similar mechanisms to sister-chromatid separation. Both events require the cysteine protease separase, which is activated after APC-induced degradation of its inhibitor securin (Tsou and Stearns, 2006). When separase fails to induce centriole disengagement, another cell cycle regulator, PLK1, can complement this function with delay (Tsou et al., 2009). During sister-chromatid separation separase cleaves cohesin (Nasmyth et al., 2000). Surprisingly, cohesin was recently also found at the centriole and identified as the centriole engagement factor that is cleaved by separase (Schockel et al., 2011). Centrioles are also associated with sSgo1, which prevents premature centriole disengagement. This protein is a shorter splice variant of Sgo1, which is a protein that protects centromeric cohesin from premature degradation (Schockel et al., 2011; Wang et al., 2008). The involvement of cohesin and separase in both processes is another strong coordinator between cell cycle and centriole duplication.

Tight cell-cycle connections ensure that centriole biogenesis is temporally well regulated and that centrioles duplicate only once per cell cycle. Experimental overexpression of PLK4 is capable of disturbing this balance and induces aberrant centriole numbers (Kleylein-Sohn et al., 2007).

The numeral control mechanism, that ensures that only one pro-centriole is made per centriole, remains unclear. It seems that the presence of a mother centriole precludes *de novo* synthesis of centrioles in other places in the cell. The mother centriole accumulates essential proteins and is hence the default platform to build a new centriole (Rodrigues-Martins et al., 2007b). Centriole disengagement was suggested as a licensing factor that prevents the assembly of a new pro-centriole before the previously assembled pro-centriole is dissociated (Loncarek et al., 2008; Tsou and Stearns, 2006). However, it is difficult to envision how this mechanism works on a molecular level, and how it ensures that only one and not occasionally two pro-centrioles assemble.

1.1.6 Cilia formation

Motile axonemes across eukaryotes have commonly a 9+2 organisation, meaning 9 outer MT doublets and a central MT pair nucleated at the basal plate. Immotile cilia have generally a 9+0 organisation. However, exceptions include motile 9+0 cilia in the kidney of *D. rerio* and in the node of mouse embryos (Kramer-Zucker et al., 2005; Nonaka et al., 1998). Additional structural differences include the presence of inner and outer dynein arms and radial spokes in a 9+2 axoneme, while these structures are absent in a 9+0 axonemes. The 9+0 organisation is predominately found in primary cilia in Metazoa, but also in distantly-related eukaryotes such as *Leishmania mexicana* amastigotes which have a rudimentary cilium possibly for signalling purposes (reviewed in Ishikawa and Marshall, 2011; Gluenz et al., 2010).

In many cases, the mature centriole needs to migrate close to the cell cortex before a cilium is formed. The trigger and the migration process itself has been suggested to involve proteins known from the planar cell polarity (PCP) pathway (Gray et al., 2009; Park et al., 2008). PCP is conferred by non-canonical Wnt signalling and establishes the orientation of the cell along the plane of the cell tissue (reviewed in Wallingford and Mitchell, 2011). The distal end of the mature centriole/basal body docks usually not directly to the plasma membrane but to a ciliary vesicle in mammalian cells (Sorokin, 1962) or to a pre-existing flagellar pocket in *T. brucei* (Lacomble et al., 2009). This interaction is probably mediated by the distal appendages of the centriole as depletion of appendage proteins leads to problems in organelle attachment and defective ciliogenesis (Dammermann et al., 2009; Graser et al., 2007a; Ishikawa et al., 2005). Parallel to the appendages binding, the MTs doublets extend for a short distance to establish the ciliary necklace region. This region is defined by Y-shaped structures that form a tight connection between the MT doublets and the ciliary membrane (Fig. 1.3). Laurdan staining suggested that this necklace membrane is composed of a denser lipid formation that may form an additional barrier to the ciliary compartment (Vieira et al., 2006). After the interaction between basal body and vesicle is stabilised, the

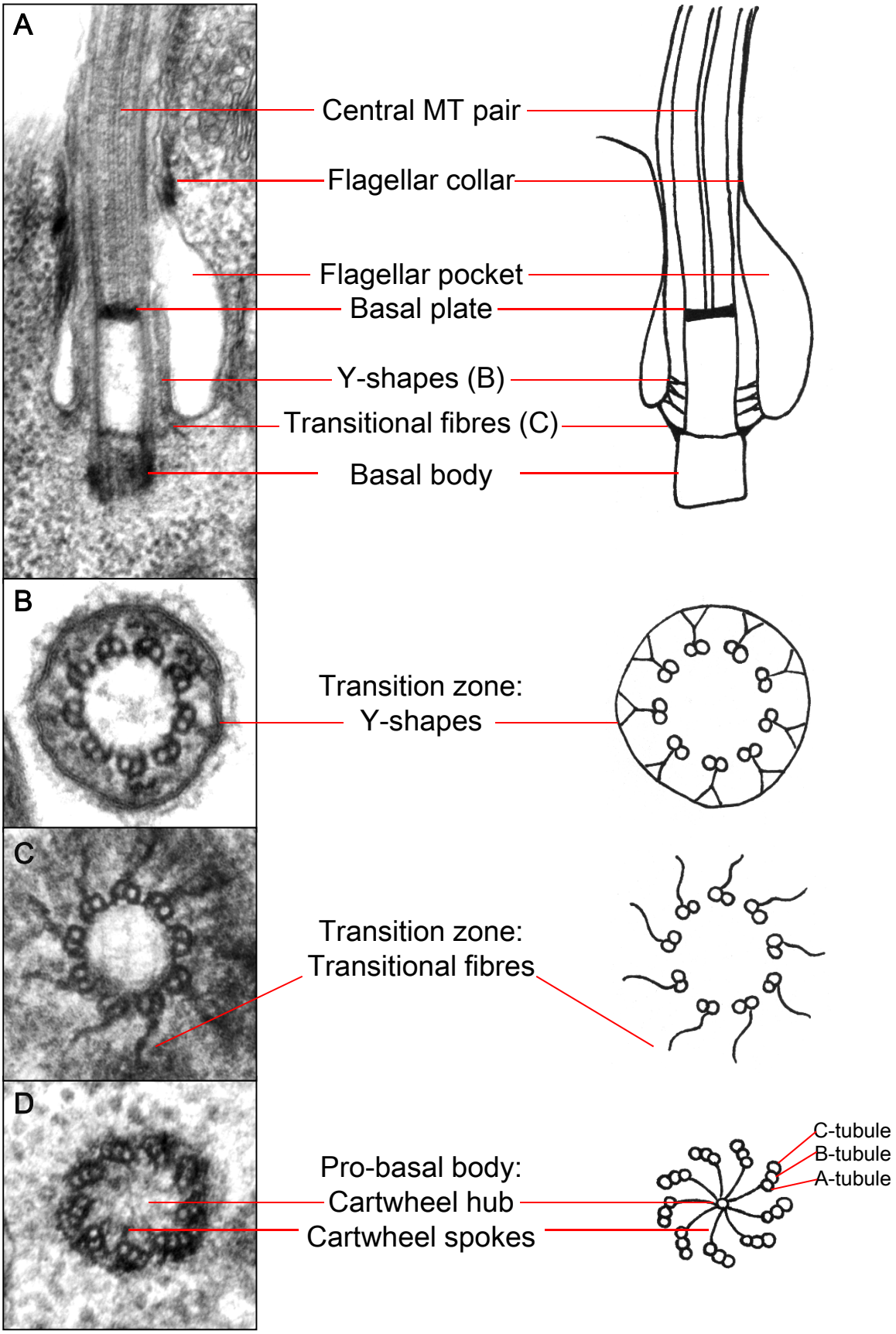

Figure 1.3 **Trypanosome flagellum.** EM images show different parts of the flagellum of *T. brucei* and respective cartons highlight the characteristic features. (A) Longitudinal section of the proximal part of the flagellum. (B,C) Transverse sections of the transition zone with the Y-shaped structures and the transitional fibres, and (D) of the pro-basal body with a cartwheel.

elongation of the axoneme begins. This can be well before the ciliary vesicle fuses with the plasma membrane (Sorokin, 1962). After fusion of the two membranes the cilium extends into the extracellular environment but maintains the ciliary pocket at the base (reviewed in Rohatgi and Snell, 2010). The maintenance of the ciliary pocket requires a collar/ring structure that embraces the bottle neck of the pocket and the cilium. At least in Metazoa this ring is constituted of septin proteins (Hu et al., 2010; Kim et al., 2010); and the presence of homologues across a wide range of eukaryotes (though not trypanosomes) raises the question if this function of septin is conserved.

Axoneme elongation depends in almost all organisms on a process termed intraflagellar transport (IFT). One exception is *Plasmodium falciparum* which assembles axonemes in an IFT-independent matter in the cytoplasm of male gametes, their only ciliated life cycle stage (Briggs et al., 2004a; Sinden et al., 1976).

1.1.7 Ciliary transport

Intraflagellar transport, first described in *C. reinhardtii*, is a bidirectional transport process of multi-protein complexes between cytoplasm and the tip of the flagellum (Kozminski et al., 1993; IFT reviewed in Ishikawa and Marshall, 2011). The machinery contains two motor units, IFT particles and cargo. Anterograde transport from cytoplasm to tip is dependent on motors of the kinesin-2 family, whereas the retrograde transport depends on dynein 2. IFT particles consist of IFT complex A containing six proteins and IFT complex B containing 14 proteins. The majority of the components is conserved in cilia forming species (Avidor-Reiss et al., 2004; Briggs et al., 2004a). The two complexes move together in the cilium and have complementary but also distinct functions. It was suggested that IFT complex B contributes more to anterograde transport as depletion of its components results in short or absent cilia (Huangfu et al., 2003; Pazour et al., 2000). In contrast, the loss of proteins from IFT complex A does not cause defective cilia assembly but large bulges at the end of cilia, a phenotype comparable to dynein 2 mutants (Piperno et al., 1998; Tsao and Gorovsky, 2008). This suggested that IFT complex A is involved in retrograde transport. Cargo of

the IFT machinery includes axonemal and membrane proteins. The proposed site of cargo loading is the transition zone, specifically the transitional fibres (Deane et al., 2001). However, the way the whole machinery works in a coordinated way remains to be understood.

Another complex involved in ciliary transport is the **BBSome**, a biochemical complex of seven BBS proteins (BBS1,2,4,5,7,8,9) (Nachury et al., 2007). The loss or mutation of BBS proteins can cause the ciliopathy Bardet-Biedl Syndrome (BBS), which gave the proteins their name (reviewed in Jin and Nachury, 2009). The BBSome was shown to assemble a coat with structural similarities to clathrin and coat protein 1 (COPI) formations (Jin et al., 2010). The BBSome coat associates with membrane proteins destined for ciliary localisation and transports them in an IFT-dependent manner to the cilium (Blacque et al., 2004; Lechtreck et al., 2009; Ou et al., 2005). Interestingly, loss of BBS7 or BBS8 in *C. elegans* leads to the dissociation of the two IFT complexes from each other (Blacque et al., 2004; Ou et al., 2005). This suggested not only a function in transporting ciliary membrane proteins but also a role in stabilising the IFT machinery. Cargo of the BBSome includes only membrane proteins but no proteins required for axoneme assembly. The BBS complex is already associated with its cargo before arrival at the transition zone; proposed sites of association are the Golgi apparatus and plasma membrane around the base of the cilium (reviewed in Nachury et al., 2010).

1.1.8 Transition zone

The checkpoint for the entrance into the ciliary compartment is most likely at the transition zone. This region is defined proximally by the transitional fibres and distally by the basal plate where the central MT pair is nucleated (Fig. 1.3). Further features of the transition zone are Y-shaped linkers connecting the axonemal outer doublets to the ciliary membrane, and thereby forming the ciliary necklace. This region has been proposed to play an important role in regulating protein access to the cilium. Over the last ten years, several developmental pathologies have been recognised to involve proteins that localise to the transition zone. Mutations or loss of these proteins leads to

dysfunctional cilia resulting in symptomatically-related ciliopathies, such as Meckel-Gruber syndrome (MKS), nephronophthisis (NPHP), Joubert syndrome, BBS and polycystic kidney disease (PKD). Immuno-gold labelling showed localisation of CEP290 (also known as BBS14, MKS4 and NPHP6) to the Y-shaped connectors (Craige et al., 2010). Depletion of the protein results in the loss of these structures and an increase of IFT complex B in the flagellum in *C. reinhardtii*, supporting the idea that Cep290 and the Y-shaped connectors contribute to regulating protein access into the cilium (Craige et al., 2010). Several studies have shown that MKS and NPHP proteins assemble into functional modules involved in connecting the transition zone MTs to the ciliary membrane and in regulating protein trafficking into the cilium (Sang, et al., 2011, Chih et al., 2012; Garcia-Gonzalo et al., 2011; Williams et al., 2011). A large-scale proteomic analysis investigating the interaction partners of ciliopathy-associated proteins in human cells found that NPHP1, NPHP4 and NPHP8 form a functional module at the transition zone (Sang, et al., 2011). NPHP5 and NPHP6 (Cep290) also interact and form a module proximal of NPHP1-4-8 (Sang et al., 2011). These two modules are linked via an interaction with NPHP2/Inversin, a protein which via interaction with AHI1 also links to an MKS protein module (Sang et al., 2011). This MKS module contains MKS1, MKS6 and Tectonic 2, and is associated with Hedgehog signalling (Sang et al., 2011; Chih et al., 2012; Garcia-Gonzalo et al., 2011). The module interacts with B9D1 and B9D2 which form a connection to the ciliary membrane by association with the transmembrane proteins TMEM231 and TMEM17 (Chih et. al., 2012). Knockdown of B9D1, Tectonic1 or 2, or MKS6 results in a lower concentration of some proteins in the ciliary membrane and increased localisation of these proteins to the plasma membrane suggesting that the protein modules function as selective barrier (Chih et al., 2012). Homologous proteins in *C. elegans* form modules with a very similar composition at the transition zone that have been suggested to have an equivalent function (Williams et al., 2011).

As mentioned above, septin proteins form a ring around the ciliary pocket that embraces the bottle neck of the pocket and the cilium (Hu et al., 2010; Kim et al., 2010). Knock down of Septin2 leads

to delocalisation of TMEM231 from the ciliary membrane and loss of B9D1 and MKS6 from the transition zone, demonstrating the requirement of septin for proper localisation of these proteins (Chih et al., 2012).

1.1.9 Ciliary signalling and sensing

Whereas the role of cilia in cell motility has long been appreciated, their central role in signalling was recognised only over the last decade (Huangfu et al., 2003; Nauli et al., 2003; Pazour et al., 2002). As mentioned above a number of developmental ciliopathies are the result of structural cilia defects and/or deregulation of ciliary trafficking of proteins, many of which are components of signalling pathways (reviewed in Berbari et al., 2009).

During embryonic development, cilia are central to signalling and generation of fluid flow involved in the establishment of the left-right asymmetry and correct development of organs (reviewed in Oh and Katsanis, 2012). Amongst other pathways, Hedgehog and Wnt signalling in vertebrates rely hugely on cilia (Corbit et al., 2008; Huangfu et al., 2003). It is hypothesised that cilia serve not only as antenna reaching out into the extracellular space but also to concentrate molecules into a small area to achieve fast and effective responses to signals. Cilia do not only play a role in cellular sensing but also in organismal sensing of the environment: Photons are sensed by modified cilia on photoreceptor cells, odorants by ciliated olfactory neurons, sound waves by mechano-sensitive stereocilia, and flavours by chemo-sensitive cilia (reviewed in Berbari et al., 2009).

1.2 *Trypanosoma brucei*

1.2.1 Sleeping sickness

Trypanosoma brucei, a protozoan parasite, is the causative agent of a disease called trypanosomiasis or sleeping sickness, which is restricted to sub-Saharan Africa. Ten years ago, *T. brucei* was estimated to infect 500,000 people and to kill a fifth of them every year (Welburn and

Odiit, 2002). Efforts to control the disease have resulted in a drop to 7,139 reported cases in 2010 (WHO).

The disease is transmitted by the bite of a *T. brucei*-infected Tsetse fly. In the early phase of the infection, the haemolymphatic stage, the parasite grows in the vascular and lymphatic system. Symptoms include fever, swollen lymph nodes, general weakness and anaemia. In late phase of the disease, the neurological stage, the parasite invades the central nervous system. This has disastrous consequences for the host causing symptoms such as psychiatric, motor and sensory defects, abnormalities in the sleeping pattern including insomnia and extreme lethargy, and eventually seizure or coma. Left untreated the disease is fatal. Current drug regimes have varying degrees of effectiveness and toxicity. However, there is not much hope for improved modern drug therapies or potent vaccine.

1.2.2 Life cycle of *T. brucei*

As with many parasites, *T. brucei* goes through life cycle stages in a mammalian host and an insect host which is accompanied by complexes changes in cell metabolism and cell morphology (Fig. 1.4; Vickerman, 1985).

When a *T. brucei*-infected Tsetse fly takes a blood meal, it transmits metacyclic trypomastigotes into the circulation of the host. These cells differentiate rapidly into long slender bloodstream forms, which use glycolysis to generate energy and multiply as extracellular parasites in the circulation of the host. The bloodstream form is covered by a dense coat of one single type of a glycoprotein also known as a variant surface glycoprotein protein (VSG). As this coat is highly immunogenic it triggers a humoral immune response within a week. The parasite population evades this immune response by antigenic variation. This phenomenon is based on the low stochastic switch of the *VSG* allele in single cells of the population leading to the expression of a different VSG protein (Cross, 1977; Ferrante et al., 1983; McCulloch, 2004). By the time a successful immune response

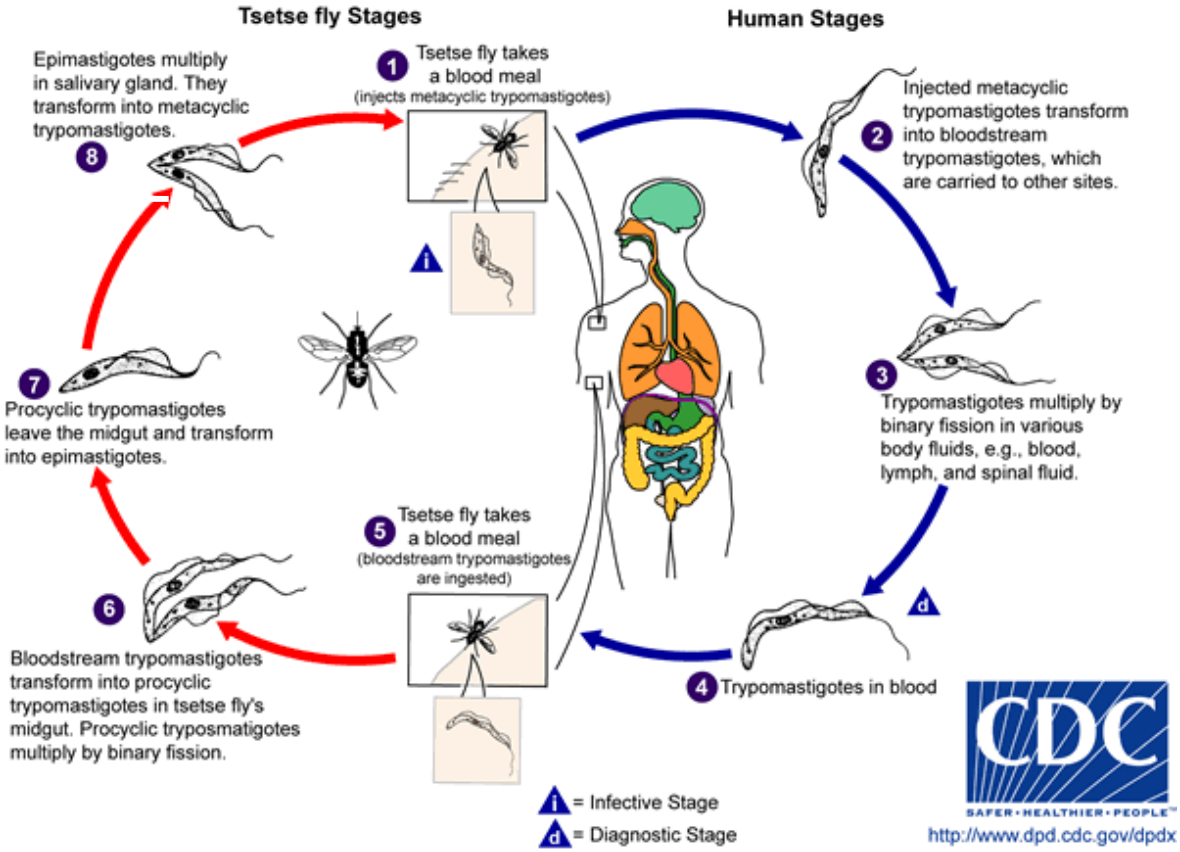

Figure 1.4 ***T. brucei* life cycle.** *T. brucei* goes through life cycle stages in a mammalian host and an insect host. An infected Tsetse fly takes a blood meal and transmits metacyclic trypomastigotes into the circulation of the host, which differentiate into proliferative long slender bloodstream forms. Once a critical density of parasites is reached, some cells differentiate into non-proliferative short stumpy forms pre-adapted for the invasion into the fly. Stumpy forms, taken up by a tsetse fly during a blood meal, differentiate into proliferative procyclic trypomastigotes in the midgut of the fly. After several rounds of multiplication procyclic forms leave the gut and differentiate into epimastigotes. They migrate to the salivary gland where they attach to the epithelium of the gland, multiplicate and give rise to the metacyclic trypomastigote form. This form is the host-infective stage pre-adapted with a VSG coat for successful immune evasion after inoculation into the mammalian host. Source of the image: Centre for Disease Control and Prevention

eliminates the population with the most prevalent VSG, a sub-population masked with an antigenically different VSG grows out. The interplay of antigenic escape and mounting of respective immune responses leads to parasitemia occurring in waves (reviewed in Barry and McCulloch, 2001). Once a critical density of parasites is reached, some cells differentiate into non-proliferative short stumpy forms pre-adapted for the invasion of the environment in the fly. This adaption includes the change of the metabolism from glycolysis to the citric acid cycle with a concomitant elaboration of the mitochondrion structure (reviewed in Matthews, 2005).

When a stumpy form is taken up by a Tsetse fly during a blood meal, the parasite differentiates into proliferative procyclic trypomastigotes in the midgut of the fly. After several rounds of multiplication procyclic forms migrate to the proventriculus and differentiate into non-proliferative mesocyclic forms. These cells undergo one asymmetric division resulting in a larger daughter cell that probably dies and a smaller epimastigote daughter cell that travels to the salivary gland (reviewed in Sharma et al., 2009). There they attach to the epithelium of the gland, divide and give rise to metacyclic trypomastigotes. This form is the host-infective stage pre-adapted with a VSG coat for successful immune evasion after inoculation into the mammalian host. Once a fly is infected is stays infected for the rest of its life.

1.2.3 Cell biology of procyclic *T. brucei*

A non-dividing procyclic cell has one nucleus, one mitochondrion, and one flagellum nucleated by a basal body with a pro-basal body associated (Fig. 1.5 A). Trypanosomes have additionally some specific features such as: subpellicular microtubules array, flagellum attachment zone, specialised MT quartet, flagellar pocket, flagella connector and bilobe structure.

The cell shape of trypanosomes is maintained by an ordered **subpellicular MT array** underneath the plasma membrane (Sherwin et al, 1989; Gull 1999). The array consists of evenly spaced MTs with the minus end polarity to the anterior and the more dynamic plus end to the posterior pole. To

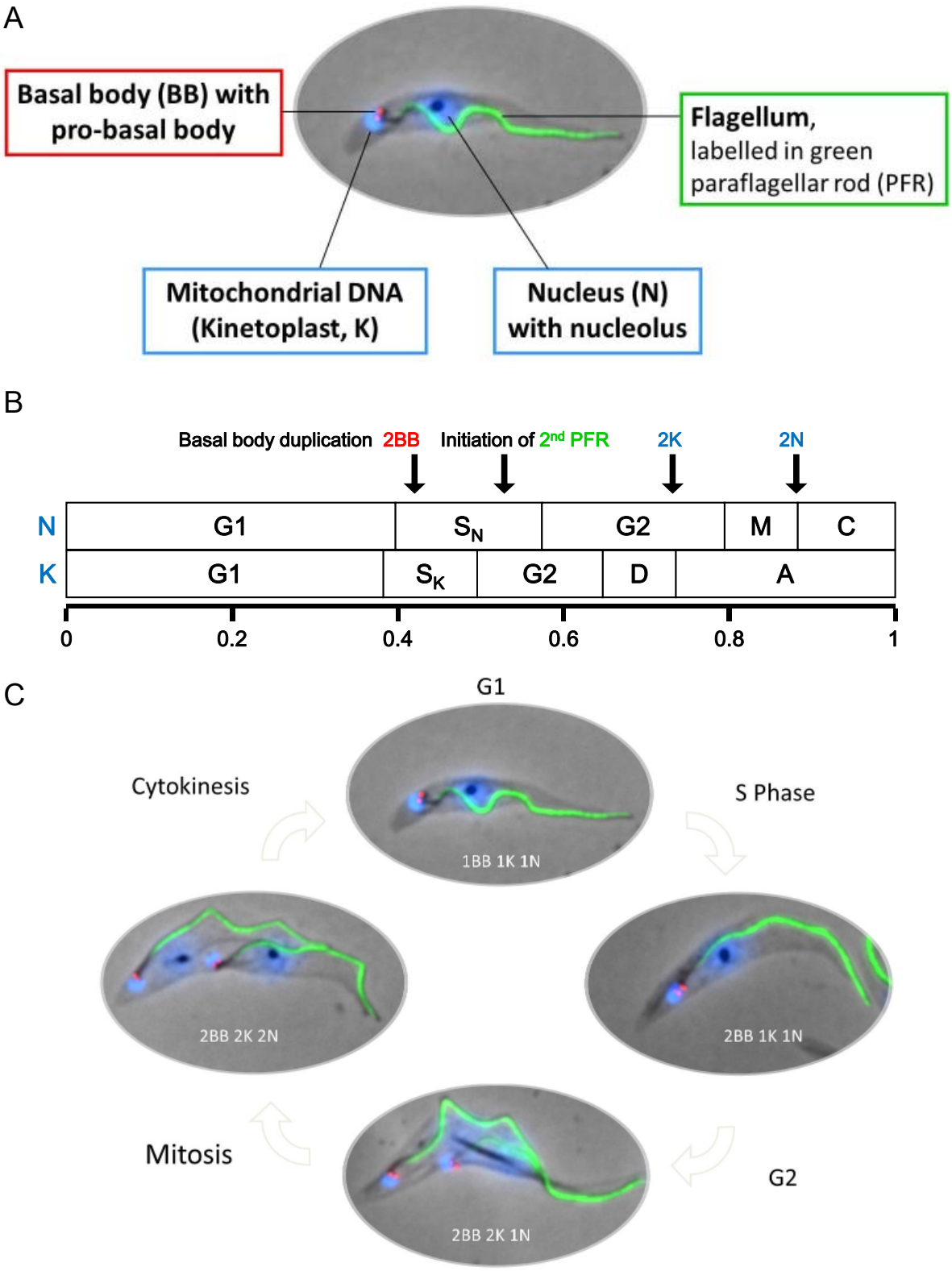

Figure 1.5 **Cell cycle of *T. brucei*** . (A) Cell biology of *T. brucei*. DNA is labelled with DAPI which stains the nucleus (N) and the mitochondrial DNA (Kinetoplast, K). Basal body (BB) with pro-basal body is shown in red. The paraflagellar rod (PFR) of the flagellum is shown in green. (B) Proportions of individual cell cycle events adapted from Woodward et al., 1990. (C) Basal body duplication occurs at the beginning of S phase and leads soon after to the assembly of a new flagellum; new pro-basal bodies assemble in parallel. These events lead from 1BB1K1N to 2BB1K1N cells. Kinetoplast duplication occurs before mitosis, resulting in 2BB2K1N cells. After mitosis cells are described as 2BB2K2N cells, before they split their organelles evenly during cytokinesis, resulting in two 1BB1K1N cells.

facilitate widening of the array while maintaining the even spacing between the MTs, short MTs are intercalated into the array (Sherwin et al, 1989).

The subpellicular MT array is interrupted by the **flagellum attachment zone** (FAZ) which includes the FAZ filament connecting the flagellum to the cell body (Vickerman 1969; Sherwin et al., 1989; Woods et al. 1989), and the **specialised MT quartet** running with anti-parallel polarity to the rest of the subpellicular MT array (Robinson et al. 1995). The MT quartet is nucleated next to the basal body, extends around the flagellar pocket and joins the subpellicular MT array at the beginning of the FAZ.

At the base of the flagellum is a large membrane invagination, called the **flagellar pocket**. This feature is possibly comparable to the smaller ciliary pockets found at base of the majority of cilia (reviewed in Rohatgi and Snell, 2010). The flagellar pocket is the only site of endo- and exocytosis in *T. brucei*, and is tightly sealed by the flagellar collar around the exit of the flagellum from the pocket to the outside. The only connection between the flagellar pocket and the environment is a channel that is associated with the specialised MT quartet (Gadelha et al., 2009).

The distal tip of the new elongating flagellum is connected laterally to the old flagellum via a structure called the **flagella connector** (Briggs et al., 2004b; Moreira-Leite et al., 2001). This structure is mobile and moves along the old flagellum which provides the pathway for the new flagellum along the cell body. An IFT mutant of *T. brucei* has demonstrated that the connector moves also along the old flagellum when the new flagellum is not growing which suggested that at least parts of the motor elements are based in the old flagellum (Davidge et al., 2006).

The **bilobe** was initially defined by light microscopy as a centrin2-containing lobe close to the exit of the flagellum from the pocket (He et al., 2005). Electron microscopic studies showed that the bilobe is a cytoskeletal filament system around the neck of the flagellum, which contains at least the four components MORN1, LRRP1, centrin2 and centrin4 (Fig 1.6; Esson et al., 2012). Both MORN1

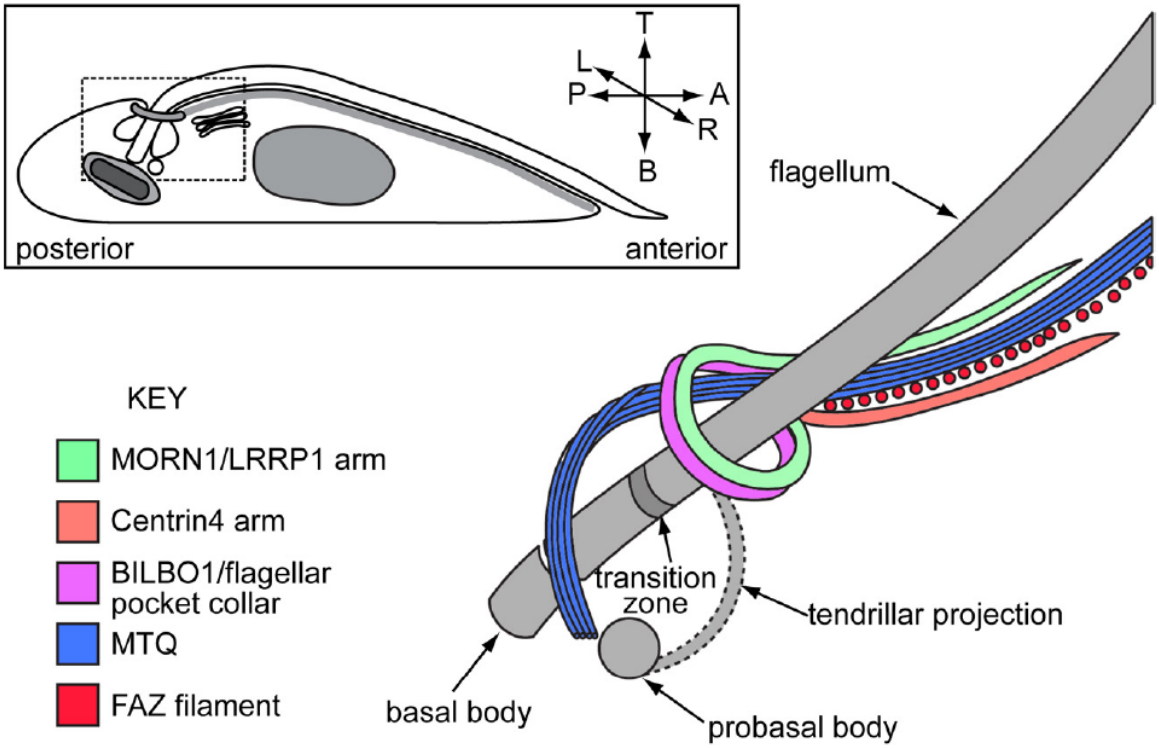

Figure 1.6 **Model of the filament systems around the flagellar pocket in *T. brucei*.** The specialised MT quartet (MTQ, blue) originates between the basal body and the pro-basal body, winds around the flagellar pocket, and runs along the filament of the flagellum attachment zone (FAZ, red). The ring-shaped flagellar collar (pink) forms the distal boundary of the flagellar pocket, the membrane invagination at the proximal end of the flagellum. The flagellar collar contains the protein BILBO1. A MORN1- and LRRP1-containing filament (green) localises in close vicinity to the flagellar collar and extends along the left-hand side of the FAZ. A centrin-contain filament (orange) runs along the FAZ on the right-hand side. The anterior (A) – posterior (P), top (T) – bottom (B), and left (L) - right (R) axes of the cell are shown in the inset. Cartoon from Esson et al., 2012.

and LRRP1 localise in as hook-shape around the exit of the flagellum from the pocket with an extension along the FAZ (Morriswood et al. 2009; Zhou et al. 2010).

The centrin2/4-containing fibre has been implicated in the duplication of the Golgi apparatus, which is positioned adjacent to the fibre (He et al., 2005; Shi et al., 2008). Both structures are duplicated around the time of kinetoplast segregation and stay associated during the rearrangement of organelles. Depletion of centrin2 leads to a defect in Golgi apparatus duplication (He et al., 2005).

1.2.4 Cell cycle of procyclic *T. brucei*

At the beginning of G1 phase, a procyclic trypanosome has one nucleus, one kinetoplast, and one flagellum nucleated by a basal body with a pro-basal body associated. The first cytoskeletal event of cell division is the maturation of the pro-basal body into the second basal body (Sherwin and Gull, 1989). This happens early in the S phase of kinetoplast and nucleus (Fig. 1.5 B) (Woodward and Gull, 1990). The new basal body docks to the membrane of the flagellar pocket of the old flagellum, starts elongating into the pocket and attaches its distal tip via the flagella connector to the lateral aspect of the old flagellum. Parallel to these processes, assembly of new pro-basal bodies begins. Flagellum elongation is accompanied by the movement of the new assembling flagellum from the anterior side to the posterior of the old flagellum (Lacomble et al., 2010). While the new flagellum grows it remains attached to the plasma membrane via a newly assembling FAZ, and to the old flagellum which serves as a structural railing for elongation (Briggs et al., 2004b; Moreira-Leite et al., 2001). The flagella connector keeps moving along the old flagellum until it reaches a “stop point” (after approximately 60% of flagellum growth; Davidge et al., 2006). While the flagella connector does not go beyond this point and fixes the distal tip of the new flagellum to this site, flagellum growth continues. This has been suggested to create pushing forces at the proximal end of the structure. These forces translocate the new basal body further to the posterior side and the old basal body closer to the nucleus, which leads to the segregation of the replicated mitochondrial DNA (Davidge et al., 2006). Flagellum growth occurs from S to M phase (Fig. 1.5 C).

After segregation of the kinetoplast, nuclear mitosis occurs. During mitosis the basal body of the old flagellum moves to a position between the two nuclei. Cytokinesis is initiated at a site close to the distal tip of the new flagellum. Cleavage furrow ingression starts between the two flagella/FAZs from the anterior side and continues towards the posterior. This cytokinesis process requires the concomitant formation and rearrangements of subpellicular MT array. Cytokinesis is terminated at the posterior end of the cells and results in two daughter cell with one nucleus, one kinetoplast and one flagellum each (Woodward and Gull, 1990).

Interestingly, cytokinesis in *T. brucei* can be completed independently of successful mitosis (Ploubidou et al., 1999). If flagellum duplication occurs but mitosis fails, cells frequently undergo cytokinesis regardless of the lack of the second nucleus, resulting in daughter cells with 1K0N and 1K1N, or in 1K0N and 1K2N.

The cell cycle in *T. brucei* is, like in mammalian cells and yeast, regulated by cyclins, cyclin-dependent kinases (CDKs) and CDK inhibitors. However, several trypanosome orthologues of key players are functionally divergent or absent, and checkpoints control applies different mechanisms. To date ten cyclins and eleven CDKs have been identified in *T. brucei* (Hammarton, 2007). This high number for a single cell organism indicates a complex cell cycle regulation with life stage specific differences of cell cycle regulation (reviewed in McKean, 2003). However, much about the interplay between specific cyclins and CDKs, and their connection to basal body duplication remains to be elucidated. Cytokinesis in *T. brucei* is morphologically very different to mammalian cytokinesis. PLK has been suggested to participate in the initiation of cytokinesis as its depletion ablates cytokinesis while mitosis and flagellum duplication continue several rounds (Kumar and Wang, 2006). However, no further proteins involved in this process have been identified to date.

1.2.5 Basal body cycle of procyclic *T. brucei*

The mammalian centriole cycle shows many similarities to the trypanosome basal body cycle (Woodward and Gull, 1990). At the beginning of the G1 phase, *T. brucei* has one basal body with a

full-length flagellum and one pro-basal body. This pro-basal body matures in late G1 phase. At G1 to S phase transition, the second basal body docks to the flagellar pocket and starts the formation of a second flagellum. Flagellum elongation is accompanied by an ordered movement of the new basal body from the anterior side of the cell around the old basal body to the posterior side (Lacomble et al., 2010). Parallel to the beginning of the formation of the second flagellum, biogenesis of two pro-basal bodies begins on the anterior side of the basal bodies. Assembly of one pro-basal body occurs also perpendicularly onto the wall of the basal body. Once the pro-basal body is near-full length it dissociates from the basal body wall and performs an ordered sequence of movements until it is parallel to the basal body (Lacomble et al., 2010). In contrast to the flexible inter-centriolar linker observed between centriole and pro-centriole in mammalian cells, no such inter-basal body connection has been observed after the disengagement of basal body and pro-basal body.

1.3.6 *T. brucei* as a model organism for studying basal body assembly

T. brucei can serve as a valuable model organism for basal body biology as it provides several advantages to other systems. In trypanosomes basal bodies act solely in flagellum formation and do not, as in metazoa, additionally participate in the organisation of spindle poles. This simplifies the functional analysis of basal body proteins, since mitosis is not disturbed by basal body defects and observation of basal body/flagellum phenotypes is more accessible. Basal body duplication in *T. brucei* occurs with the typical number and temporal control, comparable to canonical centriole duplication in Metazoa. *T. brucei* offers additionally spatial control with consistent positioning of the new basal body posterior of the old one, which readily allows identification of the more recently assembled basal body (Lacomble et al., 2010; Sherwin and Gull, 1989).

Another benefit of *T. brucei* are convenient reverse genetics with established systems for inducible RNA interference and gene expression. Straightforward endogenous loci tagging, achieved by homologous recombination highly favoured over non-homologous end-joining, allows expression

levels of tagged protein comparable to the native protein.

1.4 Aims

The aim of this work is to increase the knowledge about centriole and basal body evolution. Particularly, I aim to understand which centriolar proteins are the universally important ones in centriole and basal body assembly across eukaryotes. To address this, a bioinformatic survey investigates the distribution of centriolar proteins across a diverse range of eukaryotes, to ask whether proteins exist that are conserved in all ciliated species and absent from non-ciliated species (Chapter 3).

Mechanisms of eukaryotic centriole assembly are mainly based on studies in metazoan cells and need to be evaluated by comparison to the basal body assembly in evolutionary distantly-related eukaryotes in order to distinguish general eukaryotic mechanisms from centrosome-specific adaptations. To test whether centriolar proteins identified in a wide range of ciliated species also have a conserved function in basal body assembly across eukaryotes, the proteins are investigated in *T. brucei*. To this purpose, the conserved proteins, including SAS-6, SAS-4 and WDR16, are analysed using a combination of genetic tools and microscopy techniques (Chapter 4, 6, 7). Furthermore, after identification of a new protein family with similarity to SAS-6 and an evolutionary distribution pattern with cilia-fingerprint, the function of this novel protein (SAS6L) is investigated in the basal body/flagellum of *T. brucei* (Chapter 5). The focus of the studies of these conserved proteins is to provide insight into the commonalties of the eukaryotic concept of centrioles/basal bodies assembly and composition.

METHODS

2.1 Cell culture

2.1.1 Culture of trypanosomes

Trypanosoma brucei brucei procyclic forms (PCF) were cultured at 28°C in SDM-79 medium supplemented with 10% foetal bovine serum [Gibco] (Brun and Jenni, 1977). Bloodstream forms (BSF) were cultured in HMI-9 medium supplemented with 15% foetal bovine serum in vented-cap flasks at 37°C in 5% CO_2 (Hirumi and Hirumi, 1989). Cells were diluted as necessary to maintain mid log phase growth (PCF: $1x10^5$ - $2x10^7$ cells ml^{-1}, BSF: $1x10^3$ to $1x10^6$ cells ml^{-1}). Cell density was determined using a Casy-counter [Schärfe systems GmbH]. PCF were frozen in a freezing medium containing 7.5% Glycerol and 92.5% PCF culture medium. BSF were frozen in a freezing medium containing 10% Glycerol and 90% BSF culture medium.

RNA interference and ectopic gene expression systems were induced by the addition of doxycycline to the medium to a final concentration of 1μg ml^{-1}. The medium of cell lines with selective markers was supplemented with the appropriate drug. Final concentration for PCF: 1μg ml^{-1} Puromycin, 10 μg ml^{-1} Blasticidin, 5 μg ml^{-1} Phleomycin, 20 μg ml^{-1} Hygromycin, 10 μg ml^{-1} Neomycin. Final concentration for BSF: 0.1 μg ml^{-1} Puromycin, 5 μg ml^{-1} Blasticidin.

Parental cell lines used: in Chapter 4-7: PCF SiMPs (Lister-427 expressing T7 RNA polymerase and tetracycline repressor); in Chapter 5: PCF SMOX P9 (TREU-927 expressing T7-RNA

polymerase and tetracycline repressor (Poon et al., 2012)); in Chapter 7: BSF S16 (Lister-427 expressing T7 RNA polymerase and tetracycline repressor).

2.1.2 Transfection of trypanosomes

10 μg plasmid DNA was linearised by restriction digest with NotI. DNA was precipitated by addition of two volumes 100% Ethanol to one volume digest reaction mix, incubation on ice for 15 min, followed by centrifugation at 14,000x*g* for 15 min. The DNA pellet was wash with 70% Ethanol, air-tried and resuspended in 10 μl Zimmermann's Post Fusion Medium (ZPFM: 132 mM NaCl; 8 mM KCl; 8 mM Na_2HPO_4; 1.5 mM $Mg(CH_3COO)_2$; 0.09 mM $Ca(CH_3COO)_2$; pH 7.0).

2.5 x 10^7 PCFs were centrifuged at 500x*g* for 10 min, washed with 10 ml ZPFM, resuspended in 300 μl ZPFM and transferred into a 4mm electroporation cuvette. 10 μg linearised DNA were added and PCFs were electroporated twice applying each time three consecutive 100 μs square pulses at 1.7 kV at 200 ms intervals [Electro Square Porator ECM830, BTX]. Cells were transferred into 8 ml warm culture medium and incubated overnight at 28°C. After 24h cells were diluted 1:2 into flasks for the generation of transfected populations, and 1:20 and 1:200 into 96-well plates for the generation of clones. The appropriate selection drug was added to the final concentration stated above.

For transfection of BSFs, 1 x 10^7 cells were centrifuged at 800x*g* for 10 min, washed in warm ZPFM with 50 mM glucose, resuspended and transferred into the electroporation cuvette. 10 μg linearised DNA were added and BSFs were electroporated once applying three 100 μs square pulses at 1.7 kV at 200 ms intervals. Cells were transferred into 25 ml warm culture medium and incubated overnight before the appropriate selection drug was added.

2.2 Molecular Biology

2.2.1 Integration site check

Cells were boiled in alkaline solution (50mM NaOH, 2 mM EDTA) for 10 min at 95°C. The mix was neutralised by the addition of 450 mM Tris HCl (pH 6.8) to a final concentration of 75 mM, placed on ice and stored at - 20°C

Genomic DNA was tested for the correct integration of the targeting cassette (for 5' modifications) into the endogenous locus by two PCR reactions (together in one tube or in two separate tubes). The first PCR tested the presence of the wild-type allele using a forward primer binding ~250 bp upstream and a reverse primer binding ~250 bp downstream of the start codon of the target gene, generating a product of ~500 bp if a wild-type allele was present. The second PCR tested the presence of a *YFP* gene upstream of the target gene using a forward primer binding ~100 bp before the 3' end of YFP gene and the same reverse primer as in the first reaction, generating a ~350 product if the modified allele is present.

2.2.2 DNA constructs

In this thesis three types of expression strategies were used.

For RNA interference, a fragment encoding a short hairpin against the target gene was inserted between the HindIII site and the BamHI site in the pDEX477-Y2 vector (Fig. 2.1).

The short hairpin was generated by two PCR reactions. The first PCR amplified 250-300 bp of the target ORF with a forward primer containing a HindIII and a reverse primer containing an EcoRI site (Primers Table 2.1). The second PCR amplified the same fragment plus ~50 bp at the 3' end using a forward primer containing a BamHI site and a reverse primer containing an EcoRI site. Connection of these two fragments via the EcoRI sites generated a fragment encoding a hairpin

against the target gene.

For ectopic expression of N-terminally tagged protein, the full-length ORF was inserted in frame with the Ty-YFP reading frame between the XbaI site and the BamHI site into the pDEX477-Y2 vector (Primers Table 2.1; Fig. 2.1).

For the expression of an N-terminally tagged fusion protein from the endogenous locus of a gene, a 200-250 bp fragment starting from the start codon of the gene was amplified using a forward primer with a XbaI site and a reverse primer with a NotI site (Primers Table 2.1). A 200-250 bp fragment of the 5' intergenic region directly upstream of the gene was amplified using a forward primer containing a NotI site and a reverse primer containing a BamHI site. The two fragment where inserted into pEnT6P-Ty-YFP-Ty or pEnT6B-Ty-YFP-Ty (with puromycin or blasticidin resistance gene respectively) between the XbaI and the BamHI sites (Fig. 1.2) (Kelly et al., 2007).

The cloning strategy to construct plasmid for the expression of C-terminally tagged fusion protein from the endogenous locus was analogous. The 3' intergenic fragment behind the stop codon and the 3' end of the gene (without the stop codon) were amplified and inserted between the HindIII and SpeI sites into pEnT6P-Ty-YFP-Ty or pEnT6B-Ty-YFP-Ty.

pEnT6B-Ty-GFP-WDR16 was received from Helen Farr (Gull lab). pEnT5-Ty-YFP-PLK was received from Bungo Akiyoshi (Gull lab). pLEW-SAS6L-MH-TAP-YFP was received from Naomi Morrissette's lab.

To generate constructs for the expression of red fluorescent versions of target proteins, pDEX477-Y2 and pEnT6B-Ty-YFP-Ty were modified by excision of the YFP gene and insertion of the mCherry gene.

2.2.3 Polymerase chain reaction

A PCR reaction in 50 μl volume contained 0.2 mM each dATP, dCTP, dGTP, dTTP, 10 μM of

forward and reverse primer (Table 1.1), ~100 ng genomic DNA, 1 U Phusion DNA Polymerase [New England Biolabs] in appropriate buffer conditions. A thermo-cycle protocol starts with 2 min at 95°C, followed by 35 cycles containing 3 steps: 25 s at 95°C, 25 s at 57±2°C, 60 s (per 1000 bp) at 72°C, and finished with 5 min at 72°C. The PCR product was analysed using agarose gel electrophoresis.

Table 2.1 Primers.

Function	Name	Sequence
endogenous SAS-6 locus	TbSas6(S,Xba)	gctctagaATGAGTCGTAGCGTAGACAC
	TbSas6(AS,Not)	attgcggccgcGTGACAGTCCATTACTGCC
	5i_Sas6(S,Not)	attgcggccgcTGAAATATAGTTTTGCCACAACC
	5i_Sas6(AS,Bam)	caggatccGTGCTTATTTGACTAAATGACAC
endogenous SAS6L locus	TbSSL1_gene_S_NotI	gttgcggccgcAAAGAACCCCAACGCTTTTT
	TbSSL1_gene_AS_SpeI	gtctactagtTCGCGTTTTTCCAAGTGTG
	3intergSSL1_S_HindIII	gttaagcttGAGTGCAAATTCTTCAGTGCG
	3intergSSL1_AS_NotI	gttgcggccgcCGACATTAGCTCCGGTTTCT
endogenous SAS-4 locus	TbSas4(S,Xba)	gctctagaATGGCAGAGGTGAAGCTTCC
	TbSas4(AS,Not)	attgcggccgCATATCATTGGCTATTGCTTCG
	5i_Sas4(S,Not)	attgcggccgCTGGACTGTTTGATTGTTCG
	5i_Sas4(AS,Bam)	caggatCCGCTATTCTTACTATTATTAACG
shSAS-6	shTbSas6(S,Hind)	cagtaagcttAAGAGAAAAGGAACATAAGATGC
	shTbSas6a(AS,Eco)	cagtgaattCAGTGGAAGATGATAACTCACC
	shTbSas6(S,Bam)	cagtggatccAAGAGAAAAGGAACATAAGATGC
	shTbSas6b(AS,Eco)	cagtgaatTCTGTTTTCTCCAACTGATCTC
shSAS-4	shTbSas4(S,Hind)	cagtaagcttCAGCATTAGAACGTGGTGAG
	shTbSas4a(AS,Eco)	cagtgaaTTCCTCCTCCTCTTTAGCAC
	shTbSas4(S,Bam)	cagtggatcCAGCATTAGAACGTGGTGAG
	shTbSas4b(AS,Eco)	cagtgaattCTTTCCTCCTCTTCATGGGC
shWDR16	shWDR16_S_Hind	cagtaagcttCATCACCTCCGTTGTTGTG
	shWDR16a_AS_Eco	cagtgaattcGAAAGTAATGCCACTTCAC
	shWDR16_S_Bam	cagtggatccATCACCTCCGTTGTTGTG
	shWDR16b_AS_Eco	cagtgaattcAAATTCCCGTAACAGAGCCT
SAS-6 ectopic expression	TbSAS-6_S_XbaI	gctatctagaATGAGTCGTA GCGTAGAC
	TbSAS-6_AS_BglII	gctaagatctTTAGAAGTATGAGCTCCTC
SAS-4 ectopic expression	TbSAS-4_S_XbaI	gctatctagaATGGCAGAGG TGAAGCTTC
	TbSAS-4_AS_BamHI	gctaggatccTCAACTTTCGTCAGGGAA
screening of genomic DNA	FP sequencing primer S	Cacatggtcctgctggagttc
screening for WDR16 allele	WDR16_5intergenic_S	CCCATTCGGTTCCTTCTC
	WDR16_gene_AS	CCTGAAATCCTGGGTGAG

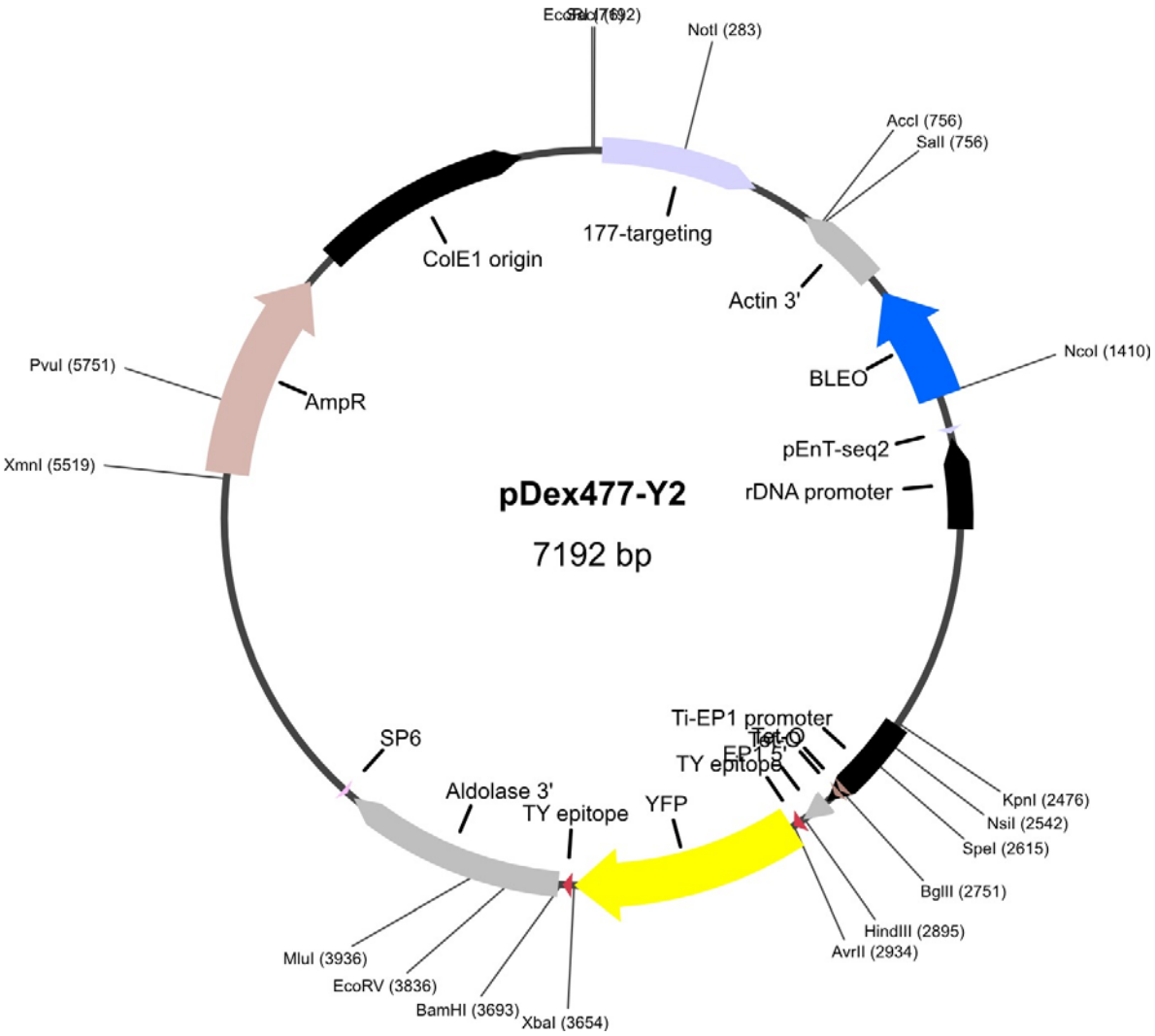

Figure 1.1 **pDEX477-Y2 for ectopic expression of tagged protein and short hairpin against target proteins.** For RNAi a fragment encoding a short hairpin against the target gene is inserted between the HindIII and the BamHI site. For ectopic protein expression (overexpression) full-length OFR is inserted in frame with the Ty-YFP reading frame between the XbaI and the BamHI site.
http://www.wicksteadlab.co.uk/vectors.shtml

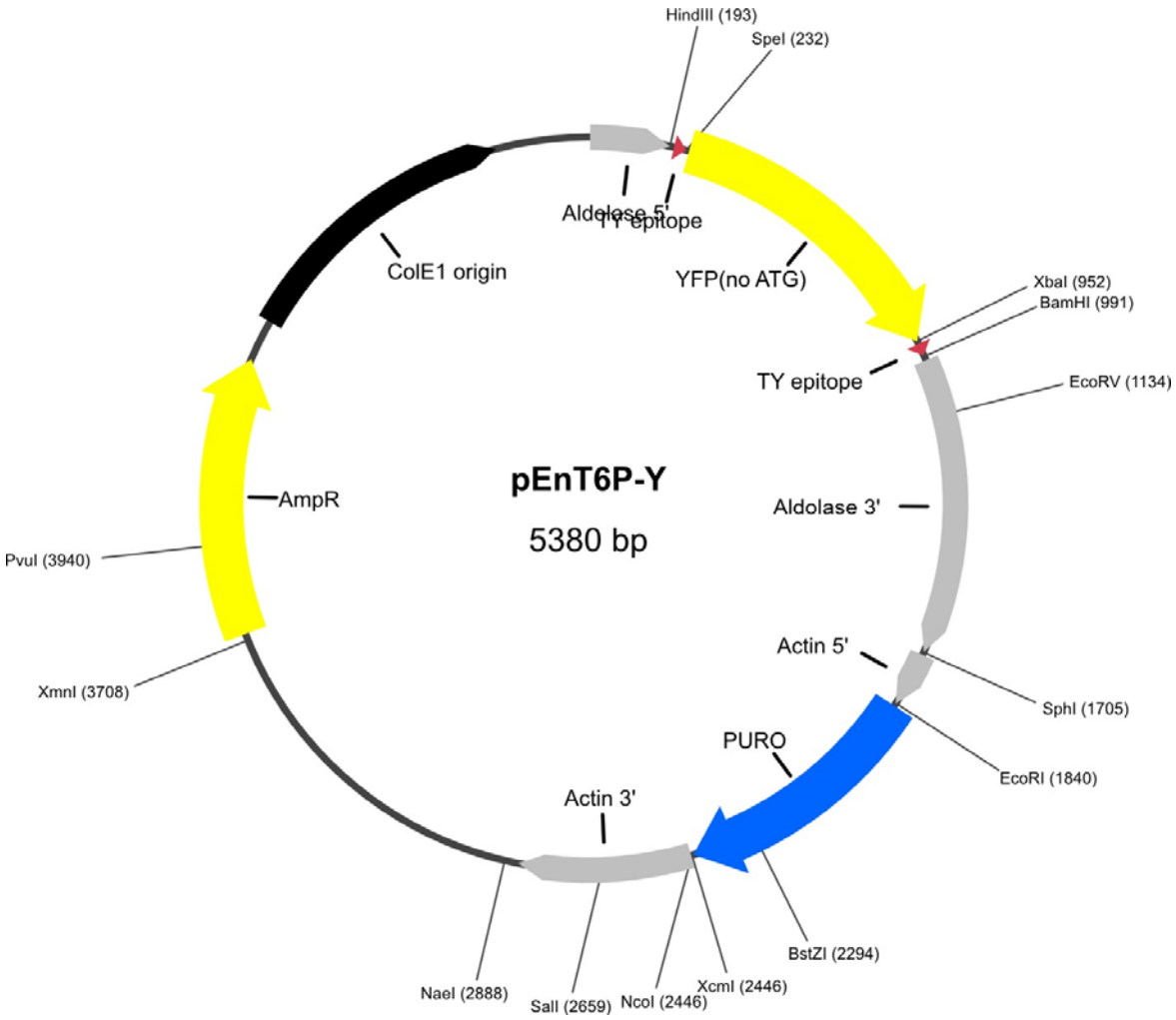

Figure 1.2 **pEnT6P-Ty-YFP-Ty**. Plasmid for the expression of N- or C-terminally tagged target protein from its endogenous locus (Kelly et al., 2007). To modify alleles at the 5' side, targeting cassette is inserted between the XbaI and the BamHI sites. The targeting cassette is constructed of a 200-250 bp fragment from the start of the gene with XbaI and NotI site, and a 200-250 bp fragment of the end of the 5' intergenic region with a NotI site and a BamHI site. The vector has a puromycin resistance gene. Vector was linearised with NotI for transfection.
Vector map from http://www.wicksteadlab.co.uk/vectors.shtml

2.2.4 Agarose gel electrophoresis

DNA samples were separated in gels containing 0.8-1.5% Agarose/TAE (40 mM Tris, 20 mM acetic acid, 10 mM EDTA) and 0.2 μg ml^{-1} ethidium bromide, applying 100 V.

2.2.5 Generation of plasmids

Purified PCR products and vector DNA were digested with restriction endonucleases [Roche] according to the manufacturer's specifications. The vector was dephosphorylated by the addition of Alkaline Phosphatase [Roche] and incubated for 30 min at 37°C. Digestion products were separated by agarose gel electrophoresis. Appropriate DNA bands were cut out of the gel and purified by a gel extraction kit according to the instructions of the manufacturer [QIAGEN]. For ligation of three DNA fragments, 100 ng vector backbone was mix with the two inserts in a molecular ratio of 1:5:5. Ligation was performed with T4 DNA Ligase under the specified buffer condition overnight at 4°C.

2.2.6 Transformation of bacteria

Chemocompetent XL1-blue *Escherichia coli* [Stratagene] were incubated on ice with 5 μl ligation mix or 10 ng plasmid DNA for 20 min. Cells were heat-shocked at 42°C for 45 s and placed on ice for 2 min. Cells were plated on LB agar plates supplement with 100 μg ml^{-1} ampicillin and incubated overnight at 37°C. Bacterial colonies were transferred into 2 ml LB medium [Sigma] for screening of plasmid DNA or as starter culture for larger LB volumes. Bacterial cultures were grown in sterilised conical flasks at 37°C shaking at 200 rpm min^{-1}.

2.2.7 Preparation of Plasmid DNA

Plasmid DNA was isolated from 1 ml bacterial culture using a silica column [QIAprep Spin Miniprep kit, QIAGEN] or from 100 ml culture using an anion exchange column [HiSpeed Plasmid Midi Kit, QIAGEN] according to the manufacturer's specifications.

2.3 Protein Biochemistry

2.3.1 Preparation of cell extracts

Trypanosomes were centrifuged at 500x*g* for 10 min, washed in PBS and again centrifuged. Cell pellet was resuspended in hot Laemmli buffer (2% SDS, 10% glycerol, 50 mM Tris HCl (pH 6.8), 0.002% bromophenol blue, 400 mM β-mercaptoethanol) to a final concentration of $2.5x10^5$ cells μl^{-1}. Samples were incubated for 5 min at 95°C and stored at -20°C.

2.3.2 SDS electrophoresis

Protein samples (0.5-$1x10^7$ cells) were run in Bis-Tris gels [Criterion XT, Biorad] in MOPS running buffer [Biorad] at a constant power of 6W per gel for approximately 1h. Apparent molecular weight was indicated by Precision Plus Protein marker [Biorad].

To visualise proteins, gels were stained with Brilliant Blue R [Sigma] for 15 min and treated with destain solution (50% methanol, 40% distilled H2O, 10% acetic acid) for 30 min.

2.3.3 Western blot

Protein was transferred onto a nitrocellulose membrane [Whatman] by semi-try blotting using transfer buffer (25 mM Tris, 192 mM glycine, 0.01% SDS, 20% methanol) applying a constant current of 1 mA cm^{-2} of gel for 90 min. Transferred protein was visualised by staining of the membrane with PonceauS [Sigma]. Membrane was blocked with 5% milk in TBST (140 mM NaCl, 10 mM Tris HCl pH 7.4, 0.05% Tween-20) for 30 min, incubated with primary antibody (1:500 anti-GFP [Roche, 11814460001]; 1:100 BB2 antibody recognising the Ty epitope (Bastin et al., 1996); 1:5000 L8C4 (Kohl et al., 1999); 1:100 Y/L12 (Kilmartin et al., 1982)) in 1% milk in TBST for 45 min, washed 3 times for 5 min in TBST, incubated with 1:20,000 horseradish peroxidise-conjugated secondary antibody [Sigma, A9044] in 1% milk in TBST for 45 min, and washed 3 times for 5 min in TBST. Membrane was treated with enhanced chemiluminescence reagent ECL [Elmer-Perkins]

and exposed to photosensitive film which was developed in a Kodak M35-M X-OMAT.

2.3.4 Dot blot

1 μl of protein sample ($2.5x10^5$ cells) was put on a nitrocellulose membrane [Whatman] and left drying. The membrane was blocked and incubated with antibodies according to the same procedure found above for Western blot membranes.

2.4 Microscopy

2.4.1 Whole cell and cytoskeleton preparation for light microscopy

Cells were washed in PBS and resuspended to a final density of $5x10^6$ - $1x10^7$ cells ml^{-1}. Cells were settled onto a glass slide (glutaraldehyde-derivatised slide for BSF) for 5-10 min until an appropriate density was reached. Cells were either fixed with 1% formaldehyde for 5 min, or permabilised with 1% Nonidet P-40 in PEME (100 mM PIPES, 2 mM EGTA, 0.1 mM EDTA, 1 mM $MgSO_4$, pH 6.9) twice for 2 min to make cytoskeleton preparations. If depolymerisation of the subpellicular MT array was required, cytoskeleton preparations were additionally treated with 65 mM $CaCl_2$ in 100 mM PIPES twice for 2 min. All cell preparations were exposed to ice-cold methanol for 30 min to fix/permabilise, and rehydrated for 5 min in PBS. Cells were either immunolabelled or directly prepared for microscopy of native fluorescence of proteins tagged with fluorescent proteins. For immunolabelling cells were incubated with primary antibody in a humid chamber for 45 min, washed 3 times with PBS for 5 minutes, incubated with the secondary antibody for 45 min and washed 3 times with PBS. Preparations were mounted in DAPI (4,6-diamidino-2-phenylindole)-containing DABCO medium (1% 1,4-diazabicyclo [2.2.2]octane, 90% glycerol, 50 mM sodium phosphate pH 8.0, 200 ng ml^{-1} DAPI). Cells were examined and images were acquired on a Leica DM5500B microscope with a 100x, 1.4 N/A oil immersion lens, and a CCD camera. Image acquisition was controlled by Leica software and images were

processed with ImageJ.

Primary antibodies:

Name	Target	Type	Dilution	Reference
BBA4	proximal BB	mouse IgM	1:50	(Woodward et al., 1995)
20H5	centrin1,2	mouse IgG	1:200	Millipore 04-1624
LAZ1	δ-tubulin	mouse IgG	neat (in 1% milk)	(Gadelha et al., 2006)
YL1/2	tyrosinated α-tubulin	rat IgG	1:200	(Kilmartin et al., 1982)
TAT1	α-tubulin	mouse IgG	1:50	(Woods et al., 1989)
L8C4	PFR2	mouse IgG	1:50	(Kohl et al., 1999)
L3B2	FAZ	mouse IgG	1:50	(Kohl et al., 1999)

Secondary antibodies [Jackson Immunno Research]

Name	Dilution	Number
Anti-mouse IgM, TRITC	1:200	115-025-075
Anti-mouse IgG, Cy5	1:200	115-175-164
Anti-mouse (cross-absorbed to rat), Cy5	1:200	112-025-167
Anti-rat (cross-absorbed to mouse), TRITC	1:200	115-175-166

2.4.2 Chemical fixation for Transmission Electron Microscopy (TEM)

Cells were fixed in suspension by the addition of glutaraldehyde to a final concentration of 2.5%. Cells were centrifuged at 500x*g* for 10 min and resuspended in fixation mix (2% glutaraldehyde, 2% formaldehyde, 0.1% picric acid in 100 mM phosphate buffer, pH 7.0). Cells were centrifuged and incubated with fresh fixation mix for 2h at 4°C. After washing with 200mM phosphate buffer, cells were post-fixed with 1% osmium in 100 mM phosphate buffer for 1 h at 4°C. After 5 washes in distilled H_2O, cell were en bloc stained with 2% aqueous uranyl acetate for 2h at 4°C in the dark. Samples were washed in distilled H_2O, and dehydrated through a series of incubation steps with 30%, 50%, 70% and 90% acetone for 15 min each followed by 3 incubations with 100% acetone for 30min each. Samples were transferred into propylene oxide (PO) and embedded into polyepoxide resin by a series of progressive infiltration steps (2:1 PO:epoxy for 1h, 1:1 PO:epoxy,

1:2 PO:epoxy, and 100% epoxy overnight). Fresh epoxy was added and polymerised overnight at 60°C. Sections of nominal 80nm thickness were cut from the hardened block using a diatome diamond knife on an Ultracut E ultramicrotome [Reichert-Jung], and collected onto copper grids [Agar]. Sections were stained with aqueous uranly acetate and Renyold's lead citrate. Sections were examined using a FEI Tecnai-F12 electron microscope [FEI Company Ltd.] operating at 80 kV.

2.4.3 Wholemount cytoskeletons

Cells were washed in PBS and resuspended in PBS to a final density of $1x10^7$ cells ml^{-1}. In the following steps the solutions were placed as 20 μl drops on parafilm and grids put floating onto the drops with forceps. Cells were settled onto formvar-coated, glow discharged EM Nickel grids approximately 5 min until an appropriate density was reached. Cells were washed twice in PBS, treated twice with 1% Nonidet P-40 in PEME twice for 2 min each, washed 5 times in PEME, fixed with 2.5% glutaraldehyde for 10 min, washed 5 times in distilled water and negatively stained by 1% goldthioglucose. Samples were examined using a FEI Tecnai-F12 electron microscope [FEI Company Ltd.] operating at 80 kV.

2.4.4 Correlative microscopy

Cells were washed in PBS and resuspended in PBS to a final density of $1x10^7$ cells ml^{-1}. In the following steps the solutions were placed as 20 μl drops on parafilm and grids put floating onto the drops with forceps. Cells were settled onto formvar-coated, glow discharged EM marked Nickel grids approximately 5 min until an appropriate density was reached. Cells were washed twice in PBS, treated twice with 1% Nonidet P-40/Igepal in PEME for 2 min each (followed by 2 times 65 mM $CaCl_2$ in 100 mM PIPES for 2 min if depolymerisation of the subpellicular MT array was required), washed 5 times in PEME, fixed with 2.5% glutaraldehyde for 10 min, and blocked with 1% Glycine in PEME. Grids were transferred onto as glass slide with printed slots that formed basins for the grid. A coverglass was placed on top of the slide and fixed with nail varnish at the

corners. Fluorescence was examined using a Leica DM5500B microscope. Images were acquired and their position was marked on a map of the marked grid. The coverglass was carefully removed. Grids were washed 5 times in distilled water and negatively stained by 1% goldthioglucose. Samples were examined using a FEI Tecnai-F12 electron microscope. Cytoskeletons for which a fluorescence image had been taken were found using the map of the marked grid.

2.5 Bioinformatics

For the bioinformatic analysis of the distribution of centriolar and ciliopathy-associated proteins in Chapter 3, 56 proteins were selected. A list of the selected proteins with information about their function and references is given in Table 3.1, Chapter 3. The protein sequences were used to search the predicted proteomes of 45 eukaryotic species for which complete or near-complete genome sequences were available (Table 2.2). These species were chosen to represent a wide evolutionary spread across eukaryotes and included ciliated and non-ciliated species.

During the initial work, we found that reciprocal best BLAST approaches were generally too conservative for the identification of orthologues in distantly-related species, whereas simple BLAST searches (Altschul et al., 1990) were too noisy and unable to distinguish between paralogues. To circumvent these issues, we used a method based on clustering of proteins by BLASTp score, previously established by Wickstead and Gull (2007).

Using a human query sequence (except for *C. elegans* ZYG-1) we first generated a “seed” group by reciprocal best BLASTp with an e-value threshold of $<10^{-5}$ against the 45 genomes. This “seed” was then used in a BLASTp search with an e-value cut off $<10^{-2}$, which resulted in a generous set of similar, but not necessarily orthologous, sequences. This generous set was then formed into clusters using a distance matrix derived from BLASTp-scores, as described by Wickstead and Gull (2007). The orthologous cluster which included the query sequence was selected manually (Table 3.2 IDs of proteins in orthologous clusters). In the case of ambiguous clustering, Bayesian and

Maximum Likelihood phylogenetic inference was applied. For that, protein sequences were aligned using MAFFT adopting the E-INS-i strategy (Katoh et al., 2005; Katoh et al., 2002). Aligned sequences were trimmed to remove poorly aligned positions. MrBayes v3.1.2 (Ronquist and Huelsenbeck, 2003) was used to infer the Bayesian phylogeny. The Whelan and Goldman (WAG) substitution matrices (Whelan and Goldman, 2001) were used with four discrete categories of gamma-distribution substitution rate. For Markov chains were run for 250 000 generations from a random start tree with a temperature of 0.2. Tree likelihoods appeared to reach stationary phase at around 60 000 generations, and the remaining 190 000 generations were used to build the consensus tree.

Tree of SAS-4 and SAS-6 proteins with a fixed topology, based on species relationships in an existing model, were produced through setting the proposal probability of all topology moves to zero. Maximum likelihood bootstrap values were generated using PHYMLv2.4.4 (WAG matrix with four discrete categories of gamma-distribution substitution rates, 100 replicates, and alpha parameter-estimation for each replicate). Bootstrap values give a conservative estimate of the confidence of the monophyly of a particular group (groups with >90% bootstrap support were believed to be well supported, those with >70% bootstrap support to have some support).

Table 2.2 Source and version of the genomes used in the analysis.

Species	Source	Version	Web reference
Apis mellifera	beebase	v2 (prerelease)	racerx00.tamu.edu
Arabidopsis thaliana	TAIR	TAIR7	www.arabidopsis.org/
Aspergillus nidulans	Broad Institute	v1.0	www.broad.mit.edu/annotation/fgi/
Aureococcus anophagefferens	JGI	v1.0	www.jgi.doe.gov/
Batrachochytrium dendrobatidis	Broad Institute	v1.0	www.broad.mit.edu/annotation/fgi/

Caenorhabdatis elegans	WormBase	WS170	www.wormbase.org/
Capitella sp.	JGI	v1.0	www.jgi.doe.gov/
Chlamydomonas reinhardtii	JGI	v3.1	www.jgi.doe.gov/
Ciona intestinalis	JGI	v2.0	www.jgi.doe.gov/
Cryptosporidium parvum	CryptoDB	v3.4	www.cryptodb.org/
Cyanidioschyzon merolae	C.merolae genome project	v1	merolae.biol.s.u-tokyo.ac.jp/
Danio rerio	VEGA	May 2007	vega.sanger.ac.uk/
Dictyostelium discoideum	dictyBase	05-20-2007	dictybase.org/
Drosophila melanogaster	ENSEMBL	BDGP4.3, 44.43b	www.ebi.ac.uk/ensembl/
Encephalitozoon cuniculi	NCBI	1	www.ncbi.nlm.nih.gov
Entamoeba histolytica	geneDB	17102005	www.genedb.org/
Gallus gallus	ENSEMBL	WASHUC2, 44.2b	www.ebi.ac.uk/ensembl/
Giardia lamblia	GiardiaDB	v1.0	www.giardiadb.org/
Homo sapiens	VEGA	Jun-07	vega.sanger.ac.uk/
Leishmania major	geneDB	v5.2	www.genedb.org/
Lottia gigantea	JGI	v1.0	www.jgi.doe.gov/
Monosiga brevicollis	JGI	v1.0	www.jgi.doe.gov/
Naegleria gruberi	JGI	v1.0	www.jgi.doe.gov/
Nematostella vectensis	JGI	v1.0	www.jgi.doe.gov/
Neurospora crassa	Broad Institute	v7.0	www.broad.mit.edu/annotation/fgi/
Oryza sativa	TIGR	v5.0	www.tigr.org/tdb/e2k1/osa1/
Ostreococcus tauri	JGI	v2.0	www.jgi.doe.gov/
Paramecium tetraurelia	ParameciumDB	v1.04	paramecium.cgm.cnrs-gif.fr/
Phaeodactylum tricornutum	JGI	v2.0	www.jgi.doe.gov/
Physcomitrella patens	JGI	v1.1	www.jgi.doe.gov/
Phytophthora sojae	JGI	v1.1	www.jgi.doe.gov/
Plasmodium falciparum	PlasmoDB	v5.2	www.plasmodb.org/
Populus trichocarpa	JGI	v1.1	www.jgi.doe.gov/
Rhizopus oryzae	Broad Institute	v3.0	www.broad.mit.edu/annotation/fgi/
Saccharomyces cerevisiae	Saccharomyces genome DB	20070713	www.yeastgenome.org/
Schistosoma mansoni	geneDB	v4.0	www.genedb.org/
Schizosaccharomyces pombe	Sanger	v19	www.sanger.ac.uk/Projects/S_pombe
Strongylocentrotus purpuratus	Baylor College of Medicine	Spur_2.1, v4	www.hgsc.bcm.tmc.edu/
Takifugu rubripes	ENSEMBL	Assembly4, 44.4e	www.ebi.ac.uk/ensembl/
Tetrahymena thermophila	TIGR	10/24/2006	www.tigr.org/tdb/e2k1/tta1/
Thalassiosira pseudonana	JGI	v3.0	www.jgi.doe.gov/
Theileria annulata	GeneDB	v4	www.genedb.org/
Toxoplasma gondii	ToxoDB	v4.1	www.toxodb.org/
Trichomonas vaginalis	TIGR	20050331	www.tigr.org/tdb/e2k1/tvg/
Trichoplax adhaerens	JGI	v1.0	www.jgi.doe.gov/
Trypanosoma brucei	geneDB	v4	www.genedb.org/
Ustilago maydis	Broad Institute	v1.0	www.broad.mit.edu/annotation/fgi/

EVOLUTIONARY HISTORY OF THE CENTRIOLE

The work presented in Chapter 3 is the joint work of myself, my co-supervisor Bill Wickstead and another graduate student Matthew Hodges. The work was published in a research paper titled "Reconstructing the evolutionary history of the centriole from protein components" in the *Journal of Cell Science* (123:1407-1413) in 2010 with three joint first authors who were Matthew Hodges, Nicole Scheumann and Bill Wickstead. All three authors were involved in the design, execution and analysis of the work and co-wrote the paper. The major part of this paper is presented here in my thesis in rewritten form.

3.1 Preface

Centrioles are highly conserved organelles fulfilling two important cellular functions: nucleation of cilia (basal body function) and organisation of pericentriolar material (centrosome function). While the experimental data on individual centriolar, centrosomal and basal body proteins derived from different species, life-cycle stages and cell types have rapidly increased over the last decade, the involvement of these proteins in the common eukaryotic mechanism underlying centriole/basal body duplication or function are usually not known. Additionally to these proteins, several genes

products have been implicated in basal body or ciliary function by their association with human pathologies caused by defective cilia, collectively termed ciliopathies (reviewed in Badano et al., 2006).

Our aim was to provide an analysis of the distribution of proteins known either for localisation to the centriole, basal body and/or centrosome, or for involvement in ciliopathies. From the distribution pattern across eukaryotes we infer the participation of individual proteins in the general eukaryotic mechanisms, and the components and functions in the last common ancestor of all eukaryotes.

3.2 Approach to analyse the phylogenetic distribution of centriolar and ciliopathy-associated proteins

We hypothesised that proteins which have a centriolar or ciliary function are present in cilia-forming species and lost from non-ciliated species. Therefore, we analysed the phylogenetic presence and absence of 56 selected proteins in 45 eukaryotic species and compared the protein distribution pattern to the cilia biology of the species. 53 proteins were selected on the basis of either their localisation to the centriole/basal body and/or centrosome, or their association with ciliopathies (Table 3.1). As controls three proteins involved with general MT dynamics and hence expected to have a wider eukaryotic distribution were included (XMAP215, EB1 and γ-tubulin).

45 species with complete or near-complete genome sequences with predicted proteomes distributed across the six groups of eukaryotes (Plantae, Excavata, Chromalveolata, Holozoa, Fungi and Amoebozoa) were selected for the analysis of protein distribution. Selection was based on providing a wide evolutionary spread and a meaningful combination of species forming cilia at some point of their life cycle and species that do not (Table 2.2).

During the initial work, we found that reciprocal best BLAST approaches were generally too conservative in the identification of orthologues, whereas simple BLAST searches (Altschul et al.,

1990) were too noisy and unable to discriminate between paralogues. To circumvent these issues, we applied a method based on clustering of proteins by BLASTp score (Wickstead and Gull, 2007), with support from phylogenetic inference where necessary, as outlined in Methods (Chapter 2).

3.3 Validation of our bioinformatic approach

To test the validity of our approach, homologues of the three proteins γ-tubulin, XMAP215, and EB1 associated with a general microtubule function were searched across the 45 predicted proteomes. As expected, γ-tubulin was present in all species and could be distinguished from homologues of other tubulin families (Fig. 3.1). While EB1 and XMAP215 were also found to be widely conserved (Fig. 3.2); the previously described absence of EB1 in *Leishmania major* (Berriman et al., 2005) and of XMAP215 in some chromalveolatan species (Devaux et al., 2007) was confirmed with our approach.

To validate the hypothesis that proteins which have a centriolar or ciliary function should be identified in cilia-forming species but not in non-ciliated species, δ- and ε-tubulin were searched as proof-of-concept examples. These two tubulins were previously shown to have a crucial centriolar role in *Chlamydomonas reinhardtii*, *Trypanosoma brucei*, *Paramecium tetraurelia* and *Homo sapiens* (Chang and Stearns, 2000; Dupuis-Williams et al., 2002; Dutcher and Trabuco, 1998; Gadelha et al., 2006). δ- and ε-tubulin are known to be present in ciliated species except *Drosophila melanogaster* and *Caenorhabditis elegans* (Chang and Stearns, 2000), both of which form cilia but have unusual centrioles (Callaini et al., 1997; Perkins et al., 1986). Using our approach we found δ-tubulin homologues in 25 species, and ε-tubulin homologues in 26 out of 29 ciliated species and no homologues in non-ciliated species (Fig. 3.2). Consistent with previous findings (Chang and Stearns, 2000), our approach did not identify homologues in *C. elegans* and *D. melanogaster*. No δ-tubulin and ε-tubulin homologues were detected in the ciliated diatom *Thalassiosira pseudonana*. Although it is unknown whether *T. pseudonana* has atypical centrioles,

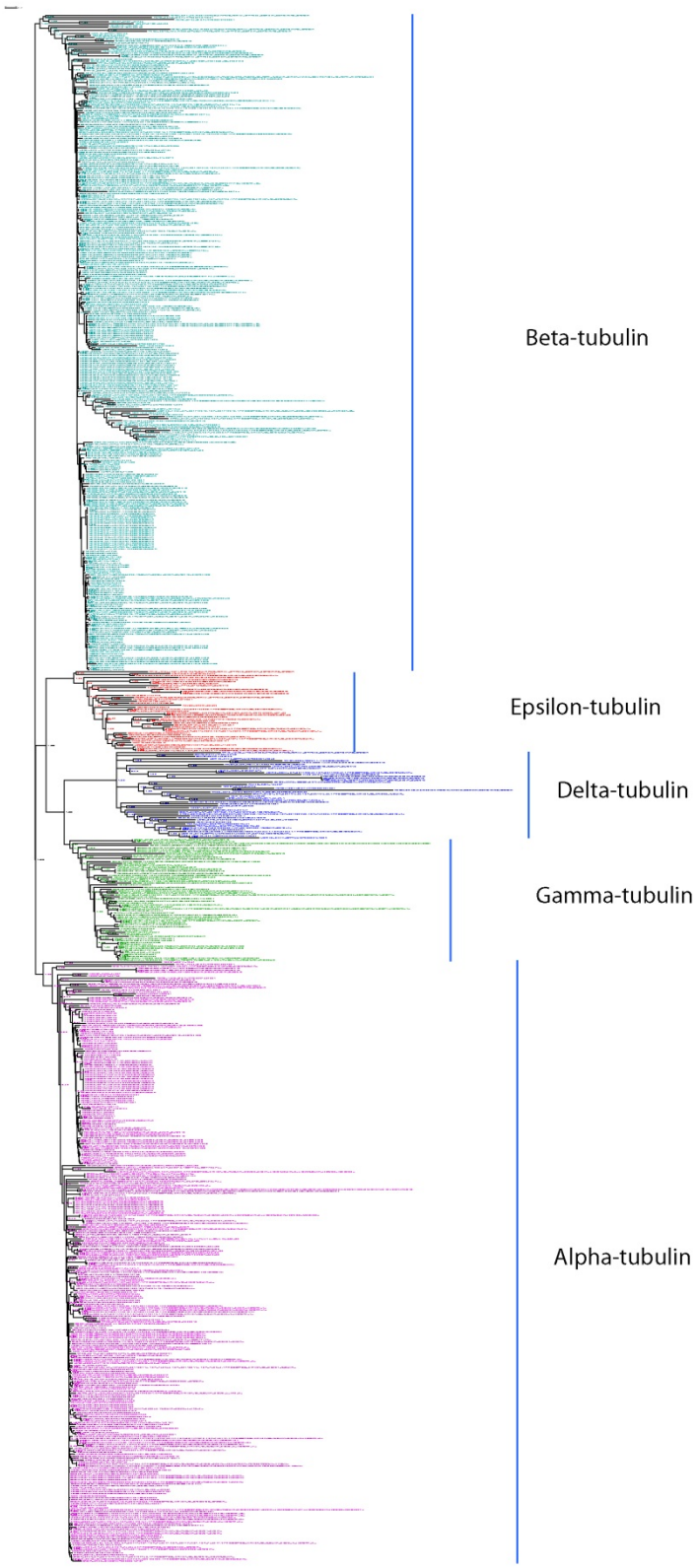

Figure 3.1 **Tubulin phylogeny.** Overview of a BLASTp cluster of the tubulin family generated demonstrating that related proteins, in this can the different tubulin paralogues α-, β- δ-, ε-, and γ-tubulin, can be distinguished by the cluster methodology. (Protein IDs are not intended to be legible).

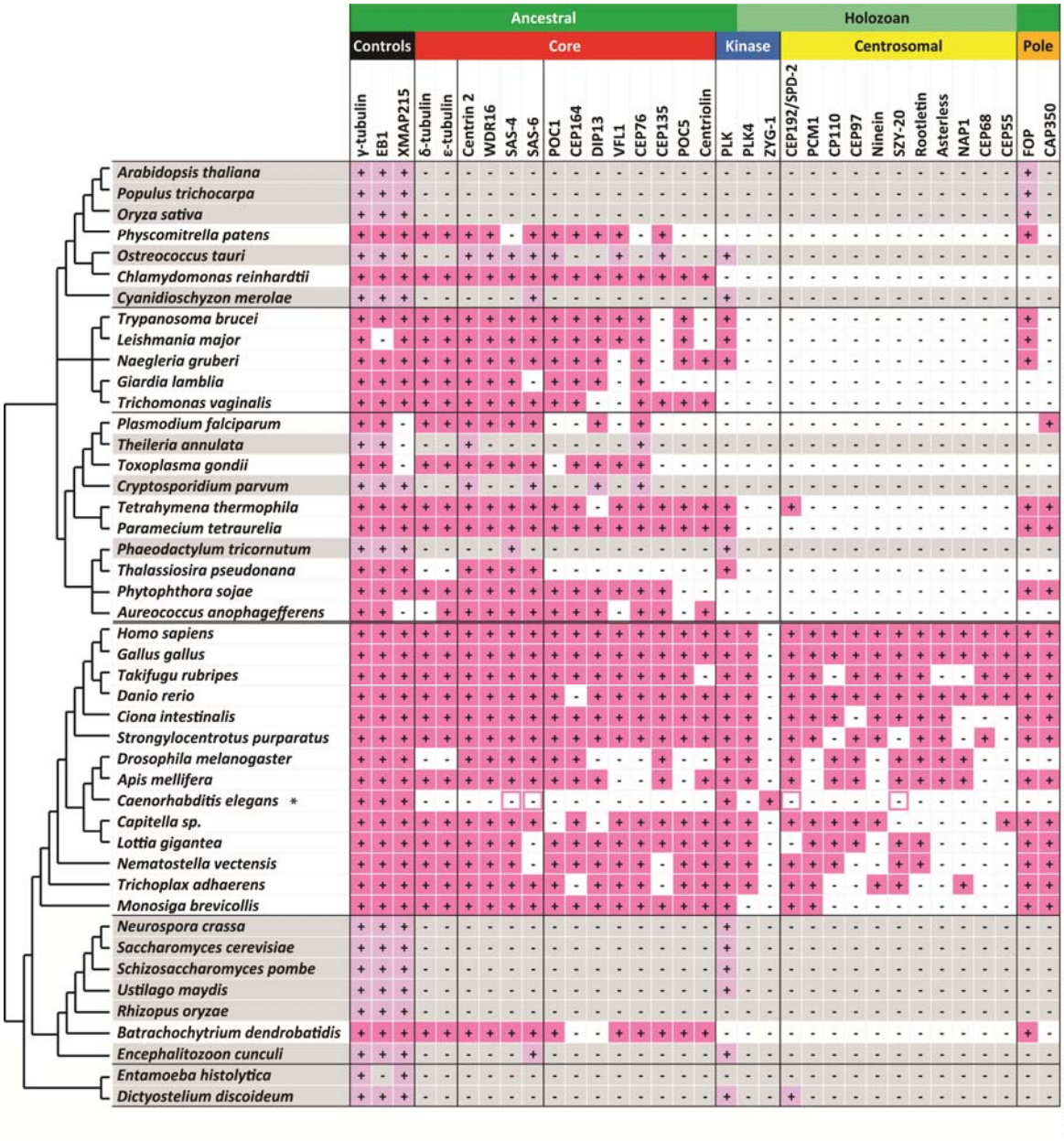

Figure 3.2 **Distribution of centriolar/centrosomal proteins across eukaryotes.** Protein homologues were identified in 45 eukaryotic genomes, including 29 ciliated species and 16 non-ciliated species (grey). Presence of homologue(s) is indicated by +. “Core” proteins are conserved ancestral centriolar proteins. “Centrosomal” proteins are associated with centrosomal functions. “Pole” proteins might have fulfilled a function in the ancestral spindle pole. “Controls” are proteins that are associated with general microtubule dynamics. “Ancestral” proteins are present across extant eukaryotes. “Holozoan” proteins have a restricted presence in Holozoa (Metazoa and *M. brevicollis*). Asterisk indicates sequence drift of core and centrosomal proteins in *C. elegans*; divergent homologues known in the literature but not identified by our approach are highlighted with a pink border.

other centric diatoms produce basal bodies with MT doublets instead of triplets (Jensen et al., 2003). The absence of an identifiable δ-tubulin in the stramenopile alga *Aureococcus anophagefferens* is either a reflection of the biology of the species or an artefact of the incomplete status of the assembled proteome. Nevertheless, the phylogenetic pattern of δ-tubulin and ε-tubulin suggest an association with a canonical MT triplet assembly pathway for the centriole, as also supported from the functional data on these proteins. Furthermore, the joint absence or presence might indicate that the two proteins act as a functional module.

The two test runs confirmed that our approach can identify homologous sequences in multiple organisms, and that our assumption that proteins important in centriolar functions can be identified in ciliated species but not in non-ciliated species is applicable.

3.4 Ancestral centriolar core proteins

The ultrastructure of centrioles/basal bodies is widely conserved across eukaryotes (reviewed in Beisson and Wright, 2003). To determine whether this structural conservation is reflected in the molecular composition, we analysed the phylogenetic distribution of centriolar proteins. Our analysis identified a core set of 14 centriolar proteins which are present in at least four of the five major eukaryotic groups that contain ciliated representatives in our analysis (Fig. 3.2). Given our current understanding of eukaryotic evolution the most parsimonious explanation for this pattern is that these 14 centriolar proteins were present in the ancestor of all extant eukaryotes (cenancestor). However, no single protein of the set is present in all species that possess centrioles/basal bodies. In extant organisms, the composition of the core set varies between species, implying a surprising plasticity in the composition of centrioles/basal bodies.

The most ubiquitously distributed centriolar core set proteins in ciliated species were centrin 2, WDR16, SAS-4 and SAS-6; they were more frequently associated with ciliated species than ε-tubulin homologues (Fig. 3.2). SAS-4 has been suggested to be involved in the attachment of

microtubules to the central tube of pro-centrioles in *C. elegans* (Pelletier et al., 2006) and in the elongation of centriolar microtubules in human cells (Kohlmaier et al., 2009; Schmidt et al., 2009; Tang et al., 2009). SAS-6 constitutes the central hub and possibly parts of the spokes of the cartwheel at the proximal end of pro-centrioles and basal bodies (Kilburn et al., 2007; Kitagawa et al., 2011c; Nakazawa et al., 2007; Rodrigues-Martins et al., 2007a; van Breugel et al., 2011). Centrin 2 is a well established centriolar protein which is essential for centriole/basal body duplication in a wide range of eukaryotes (Geimer and Melkonian, 2005; Koblenz et al., 2003; Salisbury et al., 2002). While the wider centrin family participates in multiple cellular functions and is found in non-ciliated species, there is a clade termed CrCen-type/centrin 2 with a distribution restricted to ciliated organisms (Bornens and Azimzadeh, 2007). In contrast, WDR16 is a protein of unknown function associated with hydrocephalus in the zebrafish *Danio rerio* (Hirschner et al., 2007) and had a described localisation to the basal body, pro-basal body, and the axoneme of *T. brucei* (H. Farr and K. Gull, unpublished). Based on the observed distribution pattern, it is likely that WDR16 also plays a key role in centriolar or ciliary function.

The centriolar core set also includes a number of proteins which are less frequently present in extant eukaryotes (Fig. 3.2) but are also involved in a centriolar function, such as POC1 (Keller et al., 2009; Kilburn et al., 2007), Cep164 (Kilburn et al., 2007), Vfl1 (Silflow et al., 2001), Cep76 (Tsang et al., 2009), Bld10 (Matsuura et al., 2004), and POC5 (Azimzadeh et al., 2009). However, the absence of identifiable homologues of these proteins in multiple species suggests that the requirement for the function of the protein may have been lost or replaced.

The phylogenetic distribution of the 14 core set proteins indicates that the composition of centrioles/basal bodies varies across eukaryotes. Consistent with the unusual ultrastructure of centrioles in *C. elegans*, none of the 14 core set proteins could be identified by our analysis. However, SAS-4 and SAS-6 homologues are present in the nematode, but are more divergent (Fig. 3.3) (Dammermann et al., 2004; Kirkham et al., 2003; Leidel et al., 2005; Leidel and Gonczy,

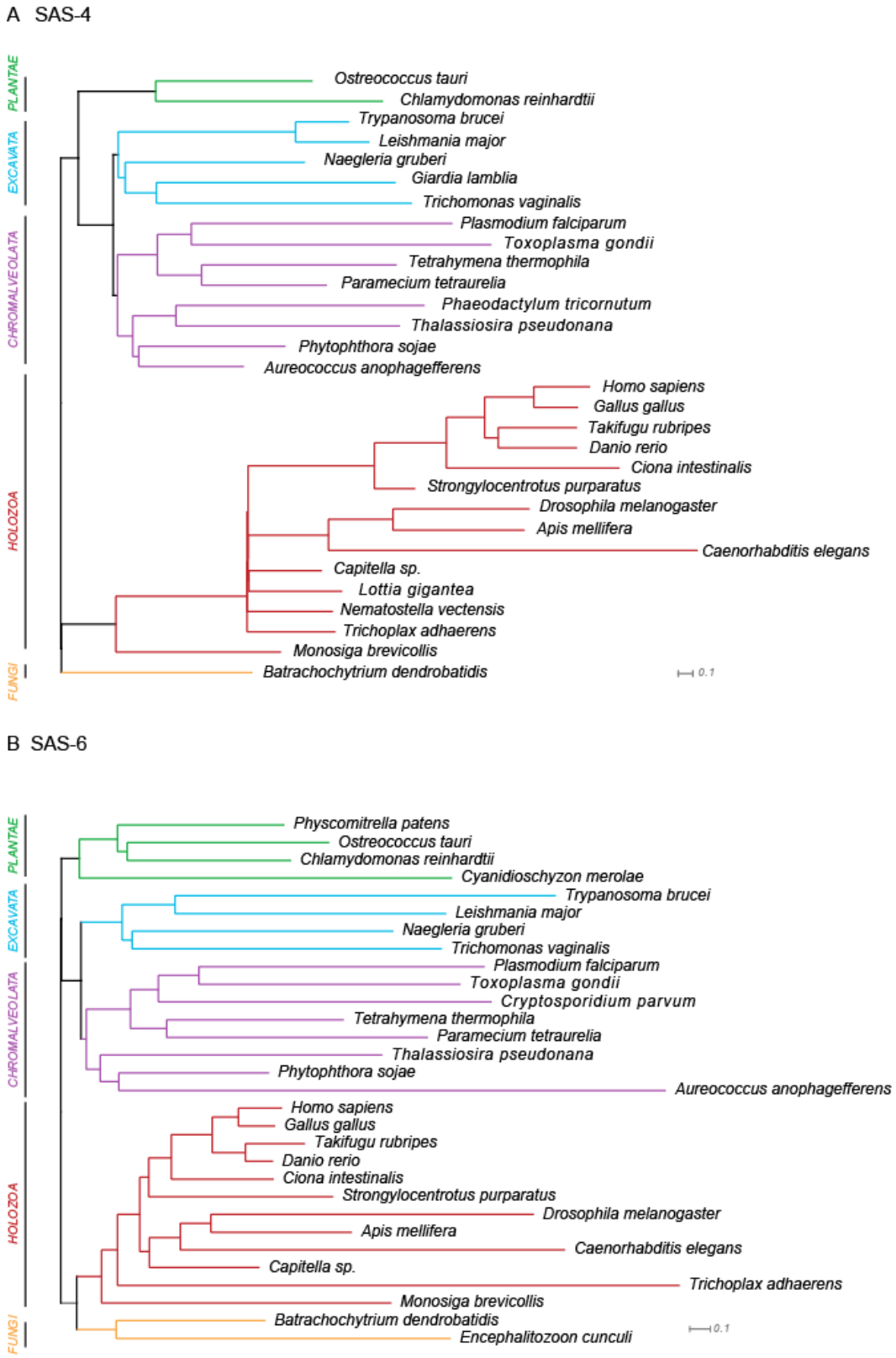

Figure 3.3 **Constrained phylogeny of SAS-4 and SAS-6 proteins.** Bayesian trees with fixed topology, that represents the current understanding of eukaryotic evolution, were produced for identified (A) SAS-4 and (B) SAS-6 homologues including SAS-4 and SAS-6 of *C. elegans* known from the literature. It highlights that SAS-4 of *C. elegans,* and SAS-6 of *C. elegans* and *D. melanogaster* are more divergent compared to its eukaryotic homologues.

2003). The diatom, *T. pseudonana*, possesses only the four most ubiquitous centriolar core set proteins centrin, WDR16, SAS-4 and SAS-6. This, together with the absence of δ- and ε-tubulin, suggests that the diatom basal body has a divergent molecular composition.

Interestingly, in the green algae *Ostreococcus tauri*, which has been previously described as aflagellate (Henderson et al., 2007), we show that seven of the 14 core set proteins are present. In addition, *O. tauri* has been shown to possess inner arm dyneins (Wickstead and Gull, 2007). This strongly suggests that *O. tauri* forms centrioles and possibly cilia at some point in its life-cycle.

3.5 Origin and diversification of kinases associated with centriole duplication

Kinase activity is critical for the regulation of centriole duplication in Metazoa. The kinases ZYG-1 in *C. elegans*, SAK in *D. melanogaster*, and PLK4 in *H. sapiens* are required for centriole duplication (Bettencourt-Dias et al., 2005; Habedanck et al., 2005; O'Connell et al., 2001). The phosphorylation activity of PLK4 is essential as catalytically inactive mutants fail to induce centriole biogenesis (Habedanck et al., 2005). It was proposed that PLK4, SAK and ZYG-1 are orthologous (Bettencourt-Dias et al., 2005).

To address the distribution and relationships between the centriole-associated kinases, the phylogeny of all Polo-like kinases, plus SAK and ZYG-1 homologues was analysed (Fig. 3.4). This identified a well-supported Polo-like kinase clan in the majority of organisms in our analysis. The *PLK* gene was duplicated near the root of animals has duplicated, as shown by the presence of PLK1-4. The PLK4 clade forms a clear subgroup, and includes human PLK4 and SAK showing that the two kinases are as proposed orthologous. However, we find no evidence to support the grouping of PLK4/SAK with ZYG-1 (Fig. 3.4). As ZYG-1 cannot be placed in any kinase family, it is unclear if ZYG-1 evolved from PLK4 or if it is a different kinase that has replaced PLK4 function.

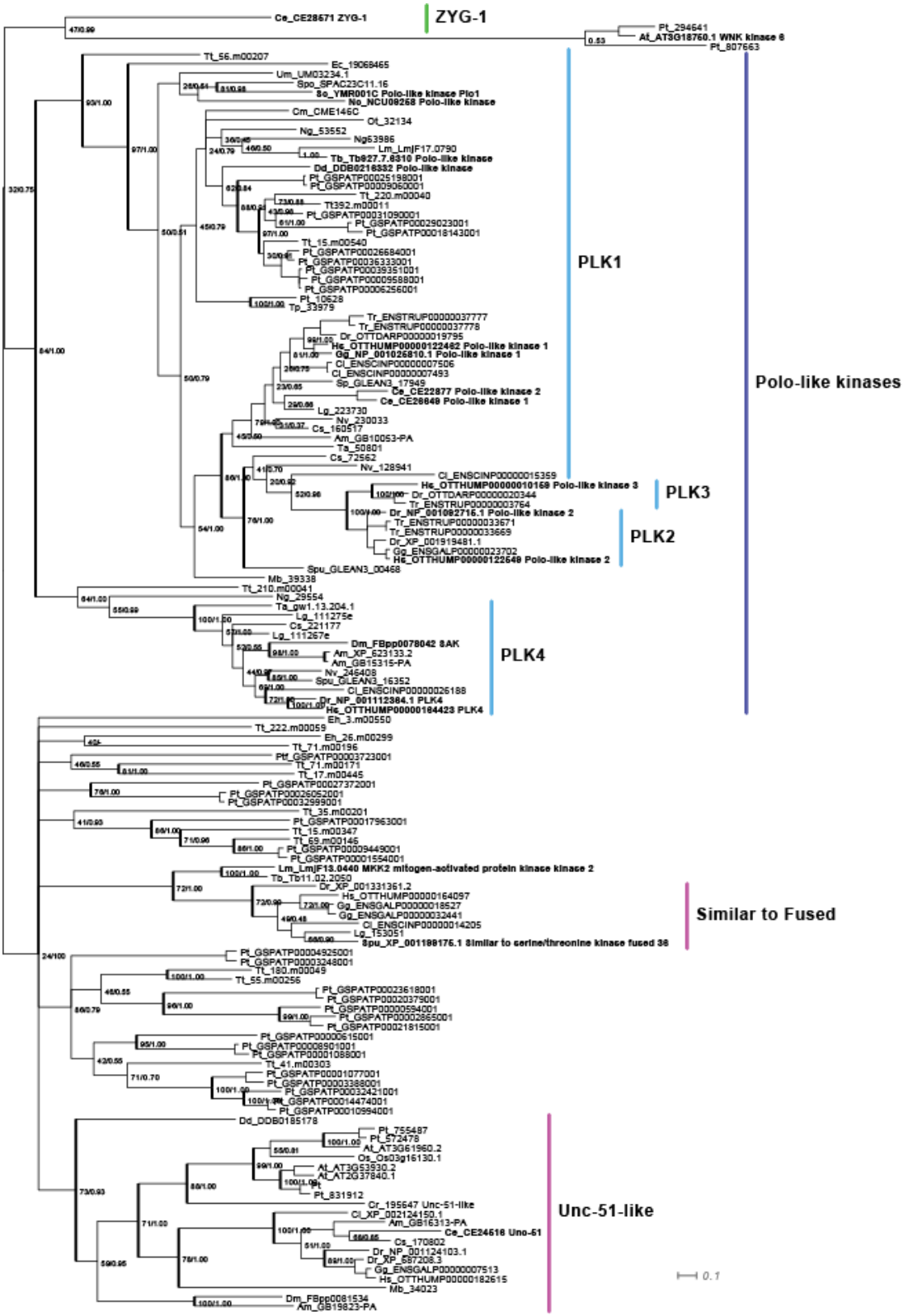

Figure 3.4 **PLK superfamily.** Maximum likelihood and Bayesian trees were produced for several kinase families including PLKs with PLK4, and ZYG-1. Topology support for nodes is indicated (maximum likelihood bootstrap values/posterior probability). Bootstrap values give a conservative estimate of the confidence that a particular group of sequences are monophyletic. It shows that ZYG-1 is not part of the PLK family but that it has an orphan position.

The PLK4 clade forms a clear subgroup containing only metazoan homologues, suggesting that centriole duplication within the centrosome is initiated differently than the duplication of basal bodies in ciliated species outside the Metazoa. The presence of PLK in all six supergroups shows that the cenancestor of eukaryotes possessed PLK wherein it may or may not have had a role that included initiation of centriole/basal body duplication. However, we found that neither PLK nor ZYG-1 were identified in nine of the 29 analysed ciliated species suggesting either that centriolar duplication does not require kinase activity in these species, or that other kinases fulfil that role.

3.6 Basal body function is ancestral, but centrosomal proteins are not

Our analysis identified proteins found only in Holozoa (represented by Metazoa and *Monosiga brevicollis* Fig. 3.2). These proteins are associated mainly with centrosomal functions or have been localised to the pericentriolar material. The observation of this restricted phylogenetic distribution raises the question whether the centrosome is a Holozoa-specific adaptation, or whether centrosomal proteins have diverged to such a high degree outside of the Holozoa that they are not identifiable. Only two, of the 13 centrosome-associated components searched, namely FOP and CAP350, had detectable homologues outside of the Holozoa (Fig. 3.2). However, the distribution pattern of these two components does not correlate well with ciliated-organisms, which would be expected if these proteins are involved in a general eukaryotic centrosome function. This indicates that the animal centrosome is constructed from mainly holozoan-specific components.

In *C. elegans*, which as previously mentioned has an unusual centriolar structure, no homologues of the centrosomal proteins were detected, although it has a centrosome. Since SPD-2 and SZY-20 were originally identified in *C. elegans* (Kemp et al., 2004; Pelletier et al., 2006; Song et al., 2008), these centrosomal proteins are present but diverged to a high degree which makes them non-identifiable in our approach. This is in line, with the divergence of the centriolar core set proteins SAS-4 and SAS-6. The divergence of both centriolar and centrosomal proteins in *C. elegans*

indicates that either the constraints on the protein's sequence during evolution are independently lower than in other species, or more likely that the centrosomal and centriolar proteins interact and hence co-evolved.

Our data provide phylogenetic support for the hypothesis that the basal body function of the centriole was present in the cenancestor of the eukaryotes (Cavalier-Smith, 1987), and that the centrosomal function is a tightly co-evolving holozoan addition.

3.7 Sensory function of the cenancestor's cilium

Defects in centrioles and cilia are emerging as the cause for numerous human disorders (for review see Badano et al., 2006). To assess whether ciliopathy-associated proteins have a role conserved across ciliated eukaryotes we investigated their phylogenetic distribution.

Bardet-Biedl Syndrome (BBS) is a pathology that is linked to defects in cilia (reviewed in Blacque and Leroux, 2006). Mutations in *BBS1* to *BBS14* have been linked to the disorder. BBS1, 2, 4, 5, 7, 8, and 9 together acts as a coat complex (termed BBSome) that via association with IFT delivers membrane proteins to the ciliary membrane (Jin et al., 2010; Lechtreck et al., 2009; Nachury et al., 2007). The phylogenetic distribution, presence or absence of the seven components generally as a group, reinforces that the BBSome has a modular nature across eukaryotes (Fig. 3.5). Our analysis also supports that the BBSome is cenancestral to eukaryotes. Moreover, the two BBSome components BBS5 and BBS8 are more frequently conserved than the other members. While most components of the BBSome are lost in individual species, BBS5 and BBS8 are never lost when the rest of the BBSome is present in that species (Fig. 3.5). BBS5 and BBS8 are present in *Giardia lamblia* and BBS5 in *Toxoplasma gondii*, even though the rest of the complex could not be identified. Together these observations suggest that BBS5 and BBS8 have a central role in the function of the complex. Furthermore, we find that BBS3, an ARF-like GTPase, though not a

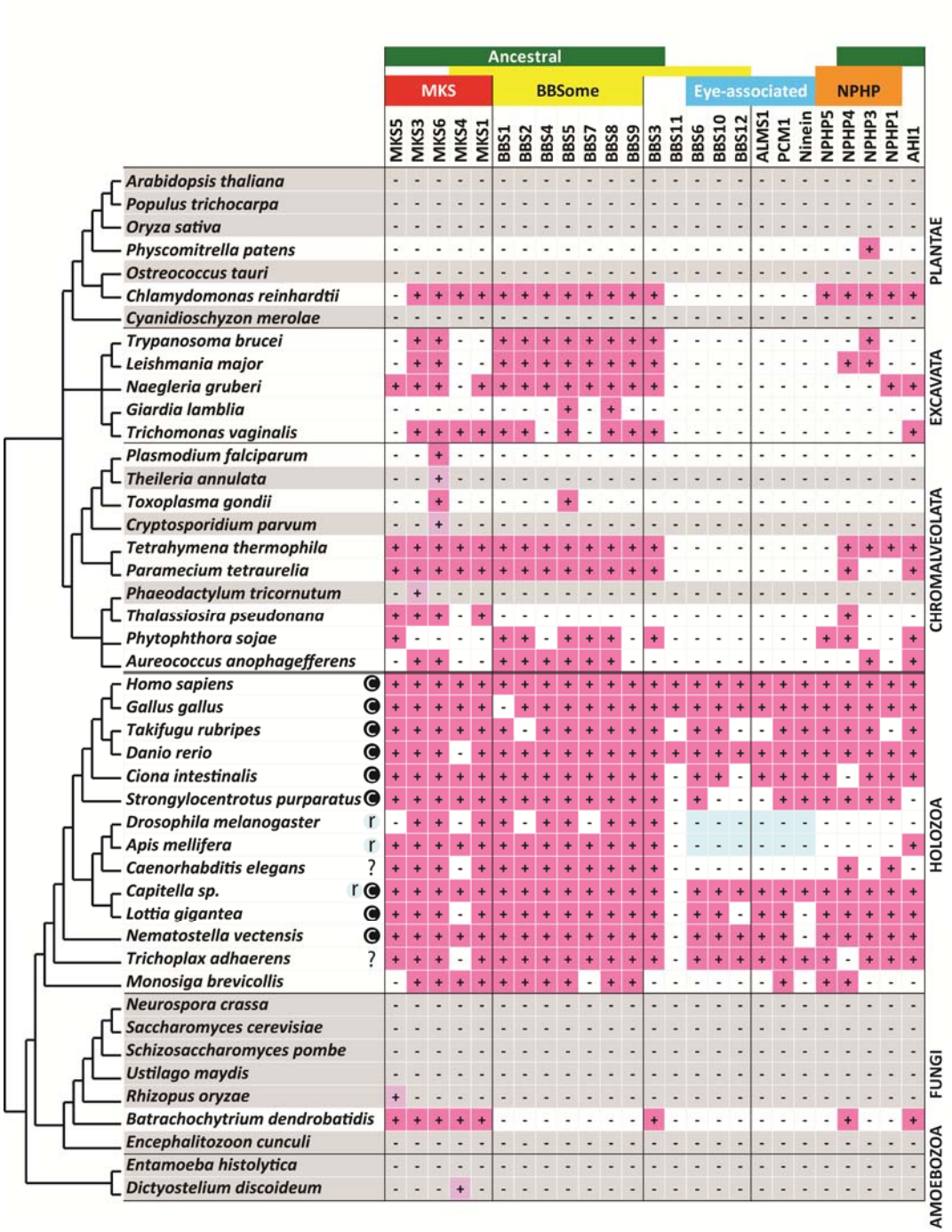

Figure 3.5 **Distribution of ciliopathy-associated proteins across eukaryotes.** Protein homologues were identified in 45 eukaryotic genomes, including 29 ciliated species and 16 non-ciliated species (grey). Presence of homologue(s) is indicated by +. The proteins are grouped according to the ciliopathy or/and ciliary photoreceptor association: MKS = Meckel-Gruber Syndrome; BBS = Bardet-Biedl Syndrome; NPHP = Nephronophthisis, "Eye-associated" proteins show a distribution that correlates with ciliary "c" photoreceptor (light blue shade = exclusive presence of rhabdomeric "r" photoreceptor).

member of the biochemical BBSome complex, and BBS13 (also known as MKS1), display a similar pattern as the BBSome suggesting a functional link. In contrast to the ancestral BBSome, BBS6 and BBS10-12 appear to be an addition specific to animals.

Interestingly, we found that the BBSome is completely absent from the four ciliated species *Physcomitrella patens*, *Plasmodium falciparum*, *T. pseudonana* and *Batrachochytrium dendrobatidis*. These species only produce motile cilia in their gametes (Armbrust, 1990; Berger et al., 2005; Merchant et al., 2007; Sinden et al., 1978). Thus, we predicted that the BBSome is not required in gametes or for motility, but instead is involved with the sensory role of cilia. This is also supported by the conservation of the BBSome in *C. elegans*, which produces only sensory cilia. As some BBSome proteins are known to be transported by intraflagellar transport (IFT) (Blacque et al., 2004) we analysed whether the absence of the BBSome in the four ciliated species corresponds with the absence of IFT proteins IFT88 and IFT172 (data not shown). However, of these four species only *P. falciparum* does not contain these proteins. As previously mentioned, the phylogenetic distribution of the centriolar core set proteins supports the hypothesis that the cenancestor of the eukaryotes possessed a cilium. Together these observations provide molecular evidence, that the cenancestral cilium did not only serve motility but performed also a sensory function.

Meckel-Gruber Syndrome (MKS) is another important ciliopathy characterised by mutations in MKS1, 3, 4, 5 and 6 causing a variety of severe malformations (see Badano et al., 2006). Our data show that MKS proteins are cenancestral to eukaryotes with their phylogenetic distribution correlating with the presence of cilia. MKS proteins have been shown to have a role in connecting the transition zone and the ciliary membrane to establish a “ciliary gate” controlling the access of molecules to the cilium (Craige et al., 2010; Garcia-Gonzalo et al., 2011; Williams et al., 2011). Noteworthy, BBSome and MKS proteins have distinct, albeit overlapping, phylogenetic distribution patterns (for example, *B. dendrobatidis* and *T. pseudonana* contain MKS but no BBS proteins).

This observation indicates that the BBSome and MKS proteins can function independently.

3.8 Summary

Our study provides molecular evidence that basal body function is ancestral, whereas centrosome components are specific to the Holozoa. Hence, our bioinformatic analysis suggests that the cenancestor of eukaryotes possessed a basal body with no association to the centrosome. This cenancestor possessed 14 centriolar proteins still present in extant ciliated eukaryotes, Polo-like-kinase, and BBS and MKS proteins. The BBSome is absent from organisms that produce cilia only for motility, which suggests a role for the BBS complex in the sensory function of cilia. Since the cenancestor possessed the BBSome complex, we predict that is used cilia not only for motility but also for sensory functions.

We define a set of 14 centriolar proteins that is still present in the centrioles of most extant ciliated eukaryotes. The most frequently present proteins of this set are centrin 2, WDR16, SAS-4, and SAS-6. Interestingly, the morphology of the centriole seems surprisingly insensitive to multiple losses from the centriolar set. Major changes in the ultrastructure of the centriole occur only when the majority of the set is lost or highly divergent, as demonstrated in the unusual centrioles of *C. elegans*. Similarly, PLK4/SAK kinases that are essential for the initiation of centriole assembly in most metazoa, or any member of the PLK family are not ubiquitously conserved.

3.9 Information about input proteins

Table 3.1 List of proteins used in the bioinformatic survey including localisation and function.

Protein	Localisation	Additional information	References
ALMS1	Centrosome, basal body	Mutated in Alström Syndrome, ciliary protein	(Hearn et al., 2005; Knorz et al., 2010; Purvis et al., 2010)

Protein	Localisation	Additional information	References
Asterless/ Cep152	Centrosome, ring-shape around the proximal end of parental centriole	Found in the human centrosome proteome; required to load PLK4 onto and to hold CPAP in the centrosome in *H. sapiens*; required for centriole duplication also in *Drosophila* as it loads SAK onto the centrosome; overexpression leads to de novo centriole formation in fly embryos and centrosome amplification in fly eggs and human cells	(Andersen et al., 2003; Blachon et al., 2008; Cizmecioglu et al., 2010; Dobbelaere et al., 2008; Dzhindzhev et al., 2010; Gopalakrishnan et al., 2011; Sir et al., 2011; Varmark et al., 2007)
BBS1		Mutated in Bardet-Biedl Syndrome; component of the biochemical complex BBSome which is important for ciliogenesis; BBSome forms a coat complex that sorts membrane proteins to primary cilia; mouse model with $BBS1^{M309R/M309R}$ (most common mutation in humans) has elongated cilia with swollen distal ends; found in a complex with BBS4,5,7 and 8 in *Chlamydomonas* flagella fractions	(Davis et al., 2007; Jin et al., 2010; Lechtreck et al., 2009; Nachury et al., 2007)
BBS2	Base of cilia	Mutated in Bardet-Biedl Syndrome; component of the BBSome; not required for global ciliogenesis but BBS2-/- mice have cilia with swollen distal ends	(Jin et al., 2010; Nachury et al., 2007; Shah et al., 2008)
BBS3		Mutated in Bardet-Biedl Syndrome; ADP ribosylation factor(ARF)-like small GTPase; not part of the BBSome, but interacts with the complex; interdependence between BBS3 and BBSome for ciliary localisation; expressed in ciliated neurons in *C. elegans*; BBS3 interact with membrane	(Fan et al., 2004; Zhang et al., 2011)
BBS4	Base of cilia; dotted along cilium	Mutated in Bardet-Biedl Syndrome; component of the BBSome; BBS4-/- mouse model shows BBS4 is not required for global ciliogenesis but spermatozoa ciliogenesis; BBS-4 interacts with PCM1	(Jin et al., 2010; Lechtreck et al., 2009; Mykytyn et al., 2004; Nachury et al., 2007)
BBS5		Mutated in Bardet-Biedl Syndrome; component of the BBSome; BBS5 has 2 PH domains which interact with Phosphatidylinositol 3-phosphate	(Jin et al., 2010; Nachury et al., 2007)
BBS6	Base of cilia (ring-shape), midbody	Mutated in Bardet-Biedl Syndrome; Type II Chaperonin-like protein that participates together with BBS10 and BBS12 in the assembly of the BBSome complex	(Kim et al., 2005; Seo et al., 2010; Stoetzel et al., 2007)
BBS7	Base of cilia; centrosome, basal body	Mutated in Bardet-Biedl Syndrome; component of the BBSome; BBS7 and BBS8 undergo IFT and are involved in stabilising IFT particle in *C. elegans*; BBS7 interacts with a Polycomb protein and has a direct role in transcription regulation	(Blacque et al., 2004; Gascue et al., 2012; Jin et al., 2010; Nachury et al., 2007; Ou et al., 2005)

Protein	Localisation	Additional information	References
BBS8	Base of cilia	Mutated in Bardet-Biedl Syndrome; component of the biochemical complex BBSome which is important for ciliogenesis; BBSome forms a coat complex that sorts membrane proteins to primary cilia; BBS7 and BBS8 undergo IFT and are involved in stabilising IFT particle in *C. elegans*; loss of BBS8 perturbs olfactory function in a mouse model	(Blacque et al., 2004; Jin et al., 2010; Nachury et al., 2007; Ou et al., 2005; Tadenev et al., 2011)
BBS9		Mutated in Bardet-Biedl Syndrome; component of the BBSome which is important for ciliogenesis; BBS9 interacts with BBS8,5,4,2 and 1	(Jin et al., 2010; Nachury et al., 2007)
BBS10	Base of cilia	Mutated in Bardet-Biedl Syndrome; involved in transient ciliogenesis in adipocytes; Type II Chaperonin-like protein that participates together with BBS6 and BBS12 in the assembly of the BBSome complex	(Marion et al., 2009; Seo et al., 2010; Stoetzel et al., 2007)
BBS11		Also known as TRIM32; E3 ubiquitin ligase; mutated in Bardet-Biedl Syndrome; depending on mutation causes either muscular dystrophy or BBS	(Chiang et al., 2006; Locke et al., 2009)
BBS12	Base of cilia	Mutated in Bardet-Biedl Syndrome; involved in transient ciliogenesis in adipocytes; Type II Chaperonin-like protein that participates together with BBS6 and BBS10 in the assembly of the BBSome complex	(Marion et al., 2009; Seo et al., 2010; Stoetzel et al., 2007)
BBS13/ MKS1	Transition zone	Mutated in Bardet-Biedl Syndrome and Meckel-Gruber Syndrome; depletion results in block of centriole migration to apical membrane; interacts with MKS3; part of a transition zone complex that regulates mammalian ciliogenesis and ciliary membrane composition	(Cui et al., 2011; Dawe et al., 2007; Garcia-Gonzalo et al., 2011)
BBS14/ MKS4/ Cep290/ NPHP6	Centrosome, transition zone, centriolar satellites	Mutated in Bardet-Biedl Syndrome, Meckel-Gruber Syndrome, Joubert Syndrome, and Nephronophthisis/Senoir-Loken Syndrome; positive regulator of ciliogenesis; Cep290 depletion prevents ciliogenesis; interacts with RPGR and important in photoreceptor cilium formation; part of a transition zone complex that regulates mammalian ciliogenesis and ciliary membrane composition; connects flagellar transition zone microtubules to the membrane and regulates flagellar protein content	(Chang et al, 2006; Sayer et al., 2006; McEwen et al., 2007; Tsang et al., 2008; Kim et al., 2008; Murga-Zamalloa et al., 2011; Garcia-Gonzalo et al., 2011; Craige et al., 2010; Betleja et al., 2010}

Protein	Localisation	Additional information	References
CAP350	Centrosome	Human centrosome proteome; MT anchoring centrosome with FOP and EB1 and Ninein, p150glued; FOP is required for CAP350 localisation to the mitotic spindle; MT stabilising role in centrioles	(Andersen et al., 2003; Le Clech, 2008; Yan et al., 2006)
Centrin	Centriole (distal end)	Required for centriole duplication in humans, Chlamydomonas, *Tetrahymena*; often multiple paralogues per species involved into many cellular processes	(Koblenz et al., 2003; Salisbury et al., 2002; Stemm-Wolf et al., 2005)
Centriolin	Centriole (subdistal appendages), midbody	Depletion and overexpression cause cytokinesis failure; anchoring of Exocyst and SNARE complexes at the midbody, required for secretory-vesicle-mediated abscission	(Gromley et al., 2003; Gromley et al., 2005)
Cep55	Centrosome, midbody	Found in the human centrosome proteome; recruitment of ESCRT-III/ALIX to the midbody; Cep55 recruitment to the midbody is negatively regulated by PLK1; Cep55 participates in abcission	(Andersen et al., 2003; Bastos and Barr, 2010; Carlton et al., 2008; Morita et al., 2007)
Cep68	Centrosome	Found in the human centrosome proteome; centrosome cohesion	(Andersen et al., 2003; Graser et al., 2007b)
Cep76	Centriole (mature and pro-centriole)	Found in the human centrosome proteome; in *T. brucei* flagella proteome; interacts with CP110; depletion of Cep76 results in accumulation of centriolar intermediates (in some human cell lines); overexpression does not affects normal centriole duplication	(Andersen et al., 2003; Broadhead et al., 2006; Tsang et al., 2009)
Cep97	Centrosome	Found in the human centrosome proteome; CP110 and Cep97 suppress cilia assembly; Cep97 recruits CP110 to the centrosome, and vice versa; Cep97 interacts with Kif24 that is involved in remodelling microtubules and ciliogenesis	(Andersen et al., 2003; Kobayashi et al., 2011; Spektor et al., 2007)
Cep135/ BLD10	Centriole (cartwheel)	Found in the human centrosome proteome; Chlamydomonas CEP135/BLD10 null mutant has no basal bodies but is viable; expression of truncated CEP135/BLD10 results in shorter cartwheel spokes (reduced centriole diameter with less MT triplets); depletion of CEP135/BLD10 in Drosophila induces shorter basal bodies leading to immotile sperm but not disturbed sensory function; CEP135/BLD10 interacts with C-NAP1 which is involved in linking the disengaged centrioles until centrosome splitting	(Andersen et al., 2003; Hiraki et al., 2007; Kim et al., 2008; Matsuura et al., 2004; Mottier-Pavie and Megraw, 2009)

Protein	Localisation	Additional information	References
Cep164	Centriole (mature, distal appendages, ring-shape)	Found in the human centrosome proteome; essential for primary cilia formation; not essential for centriole duplication in human cells	(Graser et al., 2007a; Otto et al., 2002)
Cep192/ SPD-2	Centrosome	Found in the human centrosome proteome; recruitment of PCM to the centriole; in *C. elegans* embryos: essential for centriole duplication; in *Drosophila*: not required for somatic centriole duplication, indispensible for centriole duplication in the egg after fertilisation; centrosomal accumulation partially dependent on Aurora-A and Dynein, and co-dependent on SPD-5; SPD-2 required for ZYG-1 recruitment to the centrosome; overexpression results in multiple extra-centrosomal foci of γ-tubulin and pericentrin which supports an early role of Cep192 in centrosome assembly	(Delattre et al., 2006; Dix and Raff, 2007; Gomez-Ferreria et al., 2007; Joukov et al., 2010; Kleylein-Sohn et al., 2007; Otto et al., 2002; Pelletier et al., 2006; Zhu et al., 2008)
CP110	Centriole (distal end), not at basal body	Regulator of cilia formation (together with CEP97); in human cells: essential for centrosome duplication; substrate for Cdk2; abundance is cell-cycle regulated (has protein degradation motif); depletion results in centriole elongation (no homogenous extension of the centriole, but elongated centrioles have frayed ends); CP110 interacts with the kinesin Kif24 in human cells and with Klp10A in *Drosophila* to inhibit remodelling of microtubules and ciliogenesis; CP110 degradation is mediated by SCF/CyclinF	(Chen et al., 2002; D'Angiolella et al., 2010; Delgehyr et al., 2005; Kobayashi et al., 2011; Schmidt et al., 2009; Spektor et al., 2007; Tsang et al., 2008)
DIP13	Centriole, basal body, axoneme	In *Chlamydomonas*: depletion results in growth reduction, multi-nucleated, multi-flagellated cells; Dip13 assembles into fibril-like structure in *T. brucei*	(Pfannenschmid et al., 2003; Price et al., 2012)
EB1	MTs, centrosome, along the spindle	Associated with MT plus ends (growing ends); tubulin sheet closure (zipper)	(Sandblad et al., 2006; Vitre et al., 2008)
FOP	Centrosome	Human centrosome proteome; MT anchoring at centrosome with CAP350 and EB1; FOP interacts with CAP350 and this interaction is required for FOP's centrosomal localisation; interacts with EB1, localisation to plus-end due to this interaction	(Andersen et al., 2003; Yan et al., 2006)

Protein	Localisation	Additional information	References
MKS3	Primary cilium and plasma membrane	Mutated in Meckel-Gruber Syndrome; interacts with MKS1; Depletion results in block of centriole migration to apical membrane; required for photoreceptor intraciliary transport; part of a basal body/transition zone membrane assembly with ciliary gate function during ciliogenesis	(Collin et al., 2012; Dawe et al., 2007; Williams et al., 2011)
MKS5/ RPGRIP1 L	Centrosome, basal body, cilium	Mutated in Meckel-Gruber Syndrome and Joubert Syndrome; interact with NPHP4; required for ciliogenesis and chemosensation in *C. elegans*; part of a basal body/transition zone membrane assembly with ciliary gate function during ciliogenesis	(Arts et al., 2007; Delous et al., 2007; Liu et al., 2011; Williams et al., 2011)
MKS6/ CC2D2A	Centrosome, base of cilium	Mutated in Meckel-Gruber Syndrome and Joubert Syndrome; interacts with CEP290; part of a basal body/transition zone membrane assembly with ciliary gate function during ciliogenesis	(Chih et al., 2012; Garcia-Gonzalo et al., 2011; Gorden et al., 2008; Williams et al., 2011)
C-NAP1/ Cep250	Centrosome	Found in the human centrosome proteome; involved in centriole coupling/linkage after disengagement; phosphorylated and displaced from centrosomes by the Nek2A kinase	(Andersen et al., 2003; Kim et al., 2008; Mardin et al., 2011; Mardin et al., 2010; Mayor et al., 2002; Smith et al., 2011)
Ninein	Centrosome, around mother centriole appendages	Centrosomal MT anchoring; non-nucleating MT minus-end stabilising; interacts with γ-tubulin; role in organising centrosomal proteins; role in asymmetric cell division via MT anchoring	(Delgehyr et al., 2005; Ibi et al., 2011; Mogensen et al., 2000; Ou et al., 2002; Wang et al., 2009)
NPHP1	Base of cilia	Mutated in Nephronopthisis/Senoir-Loken Syndrome; interacts with signalling molecules involved in cell-adhesion and actin cytoskeleton organisation	(Fliegauf et al., 2006; Omran, 2010; Otto et al., 2002; Sang et al., 2011)
NPHP3	cilium	Mutated in Nephronopthisis/Senoir-Loken Syndrome; myristoylation targets NPHP3 to the primary cilium;	(Nakata et al., 2012; Olbrich et al., 2003; Omran, 2010; Wright et al., 2011)
NPHP4	Primary cilium, base of cilium	Mutated in Nephronopthisis/Senoir-Loken Syndrome; NPHP1,4 and 8 form a functional module; negative regulator of the Hippo pathway; required for normal photoreceptor maintance	(Habbig et al., 2011; Omran, 2010; Otto et al., 2002; Sang et al., 2011; Won et al., 2011)
NPHP5	Primary cilium connecting cilia of photoreceptors, primary cilia of renal epithelial cells	Mutated in Nephronopthisis/Senoir-Loken Syndrome; interacts with RPGR; NPHP5 and 6 form a functional module;	(Omran, 2010; Otto et al., 2005; Sang et al., 2011; Zhao and Malicki, 2011)

Protein	Localisation	Additional information	References
PCM1	Pericentriolar satellites, site of ciliogenesis	Depletion results in reduced levels of centrin, pericentrin and ninein at centrosome, and disrupted centrosomal MT organisation; involved in MT- and dynactin-dependent recruitment of proteins to the centrosome; interacts with BBS4; involved in ciliogenesis in a huntingtin-HAP1-PCM1 pathway and this pathway is altered in Huntington disease	(Dammermann and Merdes, 2002; Keryer et al., 2011; Kubo et al., 1999; Li and Li, 2012; Nachury et al., 2007)
PLK		Polo-like kinases; cell-cycle regulated kinase family	(Archambault and Glover, 2009)
PLK4	Centrosome	Member of the polo-like kinase family; required for centriole duplication in *Drosophila* and humans; PLK4 phosphorylates GCP6, a subunit of the γ-tubulin ring complex, and FBXW5, a subunit of an E3-ubiquitin ligase complex; undergoes autophosphorylation which during interphase targets it for degradation by SCF/betaTrCP; during mitosis stabilised by PP2A mediating dephosphorylation of the autophosphorylated residues	(Bahtz et al., 2012; Bettencourt-Dias et al., 2005; Brownlee et al., 2011; Guderian et al., 2010; Habedanck et al., 2005; Kleylein-Sohn et al., 2007; Puklowski et al., 2011)
POC1	Centriole (proximal end), fiber systems	Identified in *Chlamydomonas* centriole proteome and Tetrahymena basal body proteome; depletion in *Drosophila* is lethal; depletion in *Chlamydomonas* impairs centriole duplication and overexpression results in elongated centrioles	(Dietzl et al., 2007; Keller et al., 2009; Keller et al., 2005; Kilburn et al., 2007; Pearson et al., 2009)
POC5	Centriole (distal end)	Identified in Chlamydomonas centriole proteome; centrin-interacting protein; depletion results in growth defect	(Azimzadeh et al., 2009; Keller et al., 2005)
Rootletin	Centrosome, rootlets	Interacts with C-NAP1; linker is phosphorylated and displaced from centrosomes by the Nek2A kinase	(Mardin et al., 2011; Mardin et al., 2010; Yang et al., 2006)
SAS-4/ CPAP	Centriole (mature and pro-centriole)	Essential for centriole duplication in *C. elegans*, *Drosophila*, and humans; required for basal body assembly in *Paramecium*; involved in attachment of microtubules to the central tube/centriole in *C. elegans*; MT-interacting domain; quantity of SAS-4 affects the length of the centriolar MTs; cell-cycle dependent degradation mediated by APC/Cdh1; acts as a platform that tethers other proteins such as Asterless to the centrosome in *D. melanogaster*; CPAP dysfunction is associated with microcephaly	(Basto et al., 2006; Bond et al., 2005; Dammermann et al., 2008; Gogendeau et al., 2011; Gopalakrishnan et al., 2011; Hsu et al., 2008; Hung et al., 2004; Kirkham et al., 2003; Kleylein-Sohn et al., 2007; Kohlmaier et al., 2009; Leidel and Gonczy, 2003; Pelletier et al., 2006; Schmidt et al., 2009; Tang et al., 2009)

Protein	Localisation	Additional information	References
SAS-6/ BLD12	Centriole (cartwheel)	Essential for centriole duplication in *C. elegans*, *Drosophila*, humans, *Chlamydomonas*, zebrafish, *Tetrahymena*; acts early during centriole biogenesis, either as component (hub) of the cartwheel or another proximal structure in *C. elegans*; cell-cycle dependent degradation mediated by APC/Cdh1; spontaneous polymerisation of N-terminal SAS-6 protein fragements into circular structures and models based on the crystal structure of N-terminal part of SAS-6 from *C. elegans* and also *D. rerio* suggest that SAS-6 constitues the central hub of the cartwheel and possibly parts of the spokes; In *C. elegans* SAS-6 is phosphorylated by ZYG-1 which is a required for the maintenance of SAS-6 at the site of pro-centriole assembly	(Culver et al., 2009; Dammermann et al., 2004; Delattre et al., 2006; Kitagawa et al., 2009; Kitagawa et al., 2011c; Kleylein-Sohn et al., 2007; Leidel et al., 2005; Nakazawa et al., 2007; Peel et al., 2007; Pelletier et al., 2006; Rodrigues-Martins et al., 2007a; Strnad et al., 2007; van Breugel et al., 2011; Vladar and Stearns, 2007; Yabe et al., 2007)
SZY-20	Centrosome	Suppressor of *C. elegans* zyg-1 phenotype; negative regulator of centriole duplication	(Song et al., 2008)
VFL1	Basal body (mature and pro-basal body)	*Chlamydomonas* mutant: variable flagella length; rotational asymmetric localisation of VFL1 mostly to triplet 1 (or 2) which is the site of pro-basal body assembly	(Adams et al., 1985; Silflow et al., 2001)
WDR16	Transition zone axoneme, previously thought basal body	Identified in *T. brucei* flagella proteome, highly conserved across ciliated species; high levels in testis and cilia-bearing ependymal cells of the brain; depletion of WDR16 in *Danio rerio* causes severe hydrocephalus	(Broadhead et al., 2006; Hirschner et al., 2007; Silva et al., 2005); Thesis of Helen Farr; this thesis Chapter 5
XMAP215	Microtubles (preferentially plus ends), centrosome	Control of MT dynamics; MT polymerase	(Brouhard et al., 2008; Popov et al., 2001)
ZYG-1	Centrosome	Kinase, required for daughter centriole formation in C. elegans; requires SPD-2 for its centrosomal recruitment; upstream of SAS-6/SAS-5 and SAS-4 in the centriolar pathway; In *C. elegans* ZYG-1 phosphorylates SAS-6 in the N-terminal part, which is a required for the maintenance of SAS-6 at the site of pro-centriole assembly	(Delattre et al., 2006; Kitagawa et al., 2009; O'Connell et al., 2001; Pelletier et al., 2006)
γ-tubulin	Centrosome, MT nucleation sites	MT nucleation	(Oakley and Oakley, 1989; Raynaud-Messina and Merdes, 2007)

Protein	Localisation	Additional information	References
δ-tubulin	Centrosome	In *Chlamydomonas*: uni3-1 strain has centrioles with mainly MT doublets, but also MT triplets, misplaced fibre systems; in human:, δ-tubulin localises to the centrosome, presumably between the centrioles, interacts with γ-tubulin; in *T. brucei*: depletion causes basal bodies with some MT doublets	(Chang and Stearns, 2000; Dutcher and Trabuco, 1998; Gadelha et al., 2006; Kato et al., 2004; O'Toole et al., 2003; Smrzka et al., 2000)
ε-tubulin	Centriole (distal appendages)	In *Chlamydomonas*: bld-2 strain has centrioles with MT singlets, null alleles for ε-tubulin not viable; in *Paramecium*: depletion results in basal bodies with aberrant MT numbers; in human: stronger association with the older centriole, localisation to the distal appendages (EM), required for centriole duplication	(Chang et al., 2003; Chang and Stearns, 2000; Dupuis-Williams et al., 2002; Dutcher et al., 2002; Goodenough and StClair, 1975)

CHARACTERISATION OF TRYPANOSOMAL SAS-6

4.1 Preface

In Chapter 3, the centriolar protein SAS-6 was identified as part of a core set of proteins that is conserved in cilia-producing species but not in species without cilia. Thus, the evolutionary pattern already suggests that SAS-6 is generally important in eukaryotic centrioles/basal bodies or cilia. SAS-6 was initially identified in two independent RNAi screens for cell division defects in *Caenorhabditis elegans* embryos (Dammermann et al., 2004; Leidel et al., 2005). The protein was investigated in several animal species, where centrioles participate not only in their ancestral function of cilia formation but also in the organisation of the centrosome. The studies of SAS-6 in animals focused on the centriole in the centrosomal context and suggested that SAS-6 is involved in an early step in centriole assembly (Kleylein-Sohn et al., 2007; Peel et al., 2007; Pelletier et al., 2006; Rodrigues-Martins et al., 2007a; Strnad et al., 2007; Vladar and Stearns, 2007). Experiments in *Chlamydomonas reinhardtii* showed that the protein is part of the cartwheel based on immunogold-labelling, and the absence of this structure in a *SAS-6* null mutant (Nakazawa et al., 2007). Polymerisation of fragments of the N-terminal part of SAS-6 into a ring, and models based on the recently identified crystal structure of the N-terminus of SAS-6 proteins suggest that SAS-6

forms the central hub and possibly the spokes of the cartwheel (Kitagawa et al., 2011c; van Breugel et al., 2011). For a complete introduction to SAS-6 see Chapter 1.

My aim in this chapter is to study the role of SAS-6 in the model organism *Trypanosoma brucei* where centrioles are involved only in their ancestral function as basal bodies in flagellum formation but not in centrosome and spindle pole organisation. This allows studying the role of SAS-6 in flagellum formation without the disturbance of mitosis defects. Electron tomography studies of the basal body in *T. brucei* elucidated the spatial events of the organelle's duplication in much detail making trypanosomes an ideal model to study basal body proteins and effects of their absence (Lacomble et al., 2009; Lacomble et al., 2010). This work also provides the first evidence for SAS-6 function in a eukaryotic lineage that is very anciently diverged from those in which this protein has been studied to date.

4.2 Bioinformatic analysis of *T. brucei* SAS-6

The *T. brucei* orthologue of SAS-6 is encoded by Tb 09.211.1930. It is predicted to be a 726 amino acid protein with a molecular weight of 81.4kDa and an isoelectric point of pH 7.2. Alignment with previously described SAS-6 proteins from *C. elegans*, *Drosophila melanogaster, Homo sapiens* and *C. reinhardtii* showed most identity and similarity in the N-terminus, which includes the previously annotated 53 aa long PISA motif (= Present in SAS-6, Fig. 4.1 A; (Leidel et al., 2005)). All SAS-6 proteins possessed a predicted Pfam B domain (Pfam-B_2528) towards the N-terminus, central coiled-coil domains and an undefined C-terminus (Fig. 4.1 B).

4.3 Trypanosomal SAS-6 localises to the basal body and the pro-basal body throughout the cell cycle

To study SAS-6 in trypanosomes, I generated a procyclic form cell line that expressed *T. brucei*

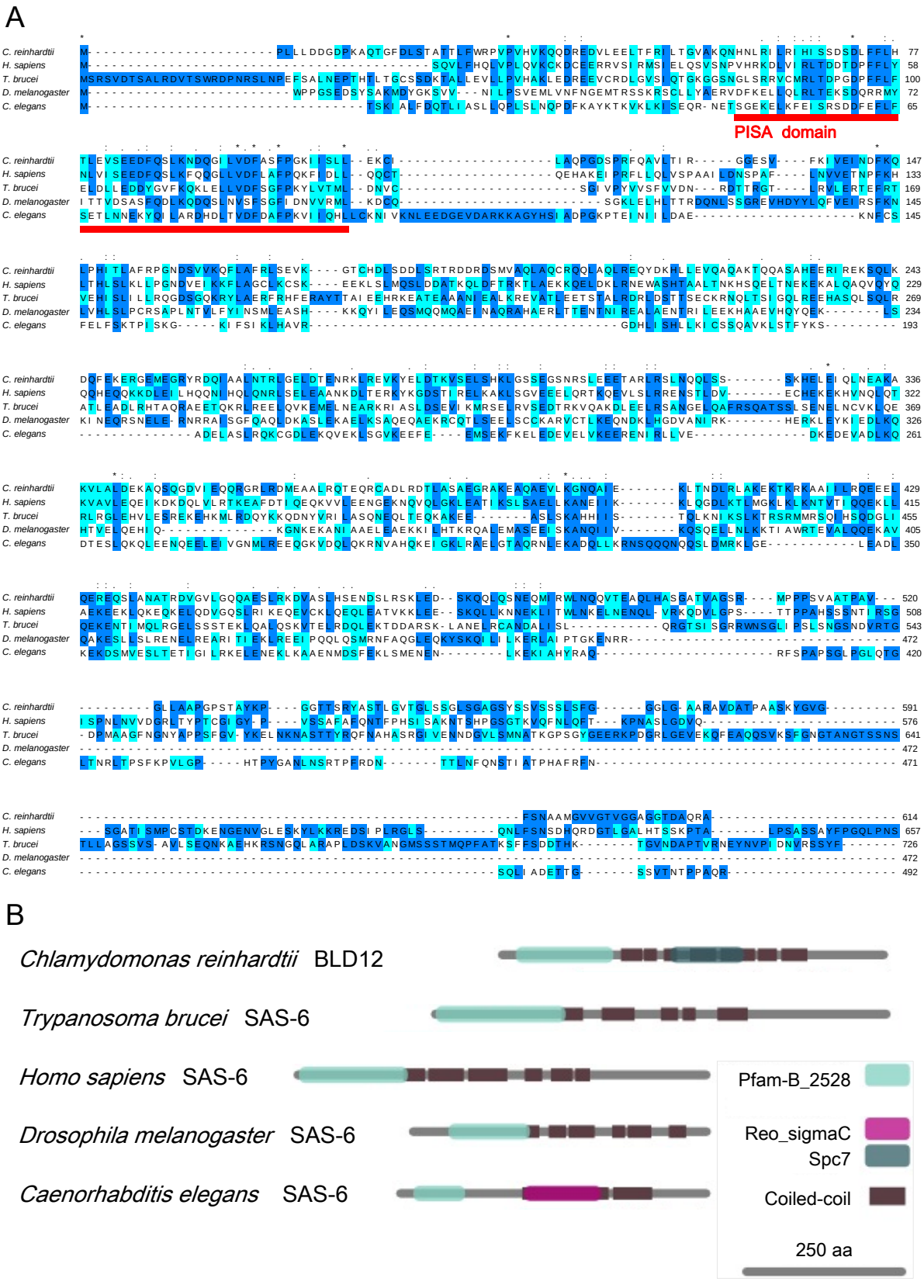

Figure 4.1 **Bioinformatic analysis of *T. brucei* SAS-6.** (A) Amino acid alignment of *T. brucei* SAS-6 with SAS-6 protein sequences of other eukaryotes. Alignment was generated with MAFFT version 6 E-INS-I (http://mafft.cbrc.jp/alignment/server/). The Pisa domain is highlighted underneath the sequence in red. Amino acids are shown with blue backgorund when they are identical to the majority consensus, and in cyan when they are similar. (B) Pfam domains of SAS-6 from *T. brucei* and other eukaryotes showing that all proteins have an N-terminal Pfam-B_2528 domain, coiled-coils domain in the middle and a less conserved C-terminus.

SAS-6 with an N-terminal Ty-YFP tag (Y-SAS-6) from the endogenous *SAS-6* locus. To examine the localisation of Y-SAS-6, cells were fixed, labelled with anti-PFR2 antibody (L8C4; (Kohl et al., 1999)) and DAPI for better visualisation of the flagellum, nucleus and kinetoplast. Analysis by fluorescence microscopy showed that Y-SAS-6 localised to a position consistent with both the basal body and the pro-basal body throughout the cell cycle (Fig. 4.2 A). A proportion of cells with 1 kinetoplast and 1 nucleus (1K1N) possessed two Y-SAS-6 dots distal to the kinetoplast which are consistent with the position of the basal body and pro-basal body in a G1 phase cell (Woodward and Gull, 1990). The remaining proportion of 1K1N cells had four Y-SAS-6 dots most likely representing two basal bodies with associated pro-basal body after the duplication of the structure which happens in the third quarter of the 1K1N stage (Woodward and Gull, 1990). 2K1N and 2K2N cells continued to possess two pairs of YFP dots in the proximity of the kinetoplasts. This pattern throughout the cell cycle is consistent with a basal bodies and pro-basal body localisation.

To confirm the localisation of Y-SAS-6, cells were immunolabelled with the basal body markers BBA4 and YL1/2. BBA4 antibody is specific to an unknown antigen at the proximal end of the basal body (Woodward et al., 1995), and its labelling was found proximal to Y-SAS-6 (Fig. 4.2 B). The YL1/2 antibody recognises tyrosinated α-tubulin which locates at the posterior end of the subpellicular MT cytoskeleton and around the distal appendages of the basal body (Kilmartin et al., 1982; Stephan et al., 2007). YL1/2 labelling was found distal to Y-SAS-6. The fluorescent signal of Y-SAS-6 at the basal body had a consistently sized, dot-like shape compared to the larger YL1/2 labelling. This indicated that Y-SAS-6 localisation was spatially more restricted and probably in the basal body rather than around it.

4.4 Tagged SAS-6 is able to complement loss of wild type protein

In order to test whether tagged SAS-6 is functional, I generated a cell line in which both endogenous *SAS-6* alleles were modified to express Y-SAS-6. SAS-6 is an essential protein

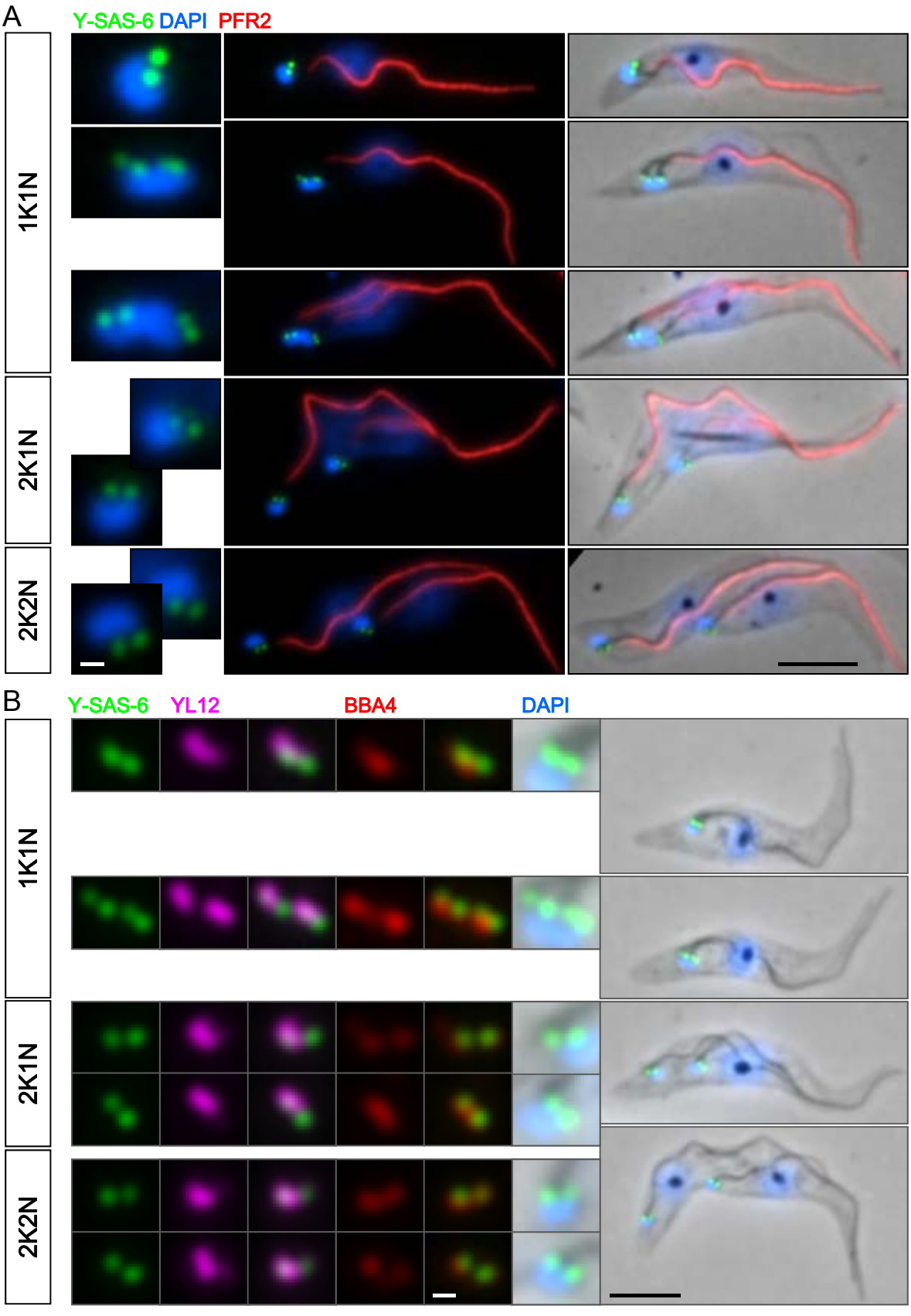

Figure 4.2 **Localisation of Y-SAS-6 throughout the cell cycle: Y-SAS-6 localises to the basal body and the pro-basal body.** *T. brucei* SAS-6 N-terminally tagged with Ty-YFP (Y-SAS-6, green) was expressed from an endogenous *SAS-6* locus in procyclic form *T. brucei*. Cells were detergent-extracted, fixed in methanol and immunolabelled. DNA was labelled with DAPI (blue). Insets show basal bodies. White scale bars: 500μm. Black scale bars: 5μm. (A) Immunolabelling: L8C4 (anti-PFR2, red). (B) Immunolabelling of basal body markers with YL1/2 (magenta) and BBA4 (red).

(ablation of SAS-6 is lethal, as shown in section 4.6), so if cells survive with only tagged SAS-6, then the tagged protein must complement loss.

Integration of the *Y::SAS-6* constructs and presence of the wild type locus was checked by PCR on genomic DNA. This verified that *Y::SAS-6/Y::SAS-6* cells possessed only modified and no wild type alleles of *SAS-6* (Fig. 4.3 A). Western blot analysis of whole cell extracts antibodies directed against the tag demonstrated that the *Y::SAS-6/Y::SAS-6* cells expressed a higher amount of the tagged protein compared to the single *Y::SAS-6* allele cells (Fig. 4.3 B). *Y::SAS-6/Y::SAS-6* cells also had a significantly higher YFP fluorescence signal at the basal body and pro-basal body ($p = 5e-16$), suggesting that additional SAS-6 binding sites have been occupied by tagged protein (Fig. 4.3 C). Cells expressing Y-SAS-6 from both endogenous loci were morphologically indistinguishable from wild type or single *Y-SAS-6* locus cells (Fig. 4.3 D). The doubling time of *Y::SAS-6/Y::SAS-6* cells was 10h compared to only 8.5h of wild-type and single *Y::SAS-6* allele cells (Wilcoxon test, $p=0.03$) (Fig. 4.3 D). Despite the significant difference in the growth rate, the results showed that Y-SAS-6 is functional and can complement the essential roles of wild type SAS-6.

4.5 The amount of SAS-6 at the basal body varies throughout cell cycle

The cell cycle dependent changes of the amount of SAS-6 at the pro-centriole were studied in centrosomes in *C. elegans* embryos and human cell lines (Dammermann et al., 2008; Strnad et al., 2007). However, whether SAS-6 shows the same dynamics in a basal body and pro-basal body context is unknown.

In order to address this question, *Y::SAS-6/Y::SAS-6* cells were fixed, immunolabelled and analysed by fluorescence microscopy. Using the number of basal bodies, kinetoplasts and nuclei the individual cells were categorised according to cell cycle stage into: 1BB1K1N, 2BB1K1N,

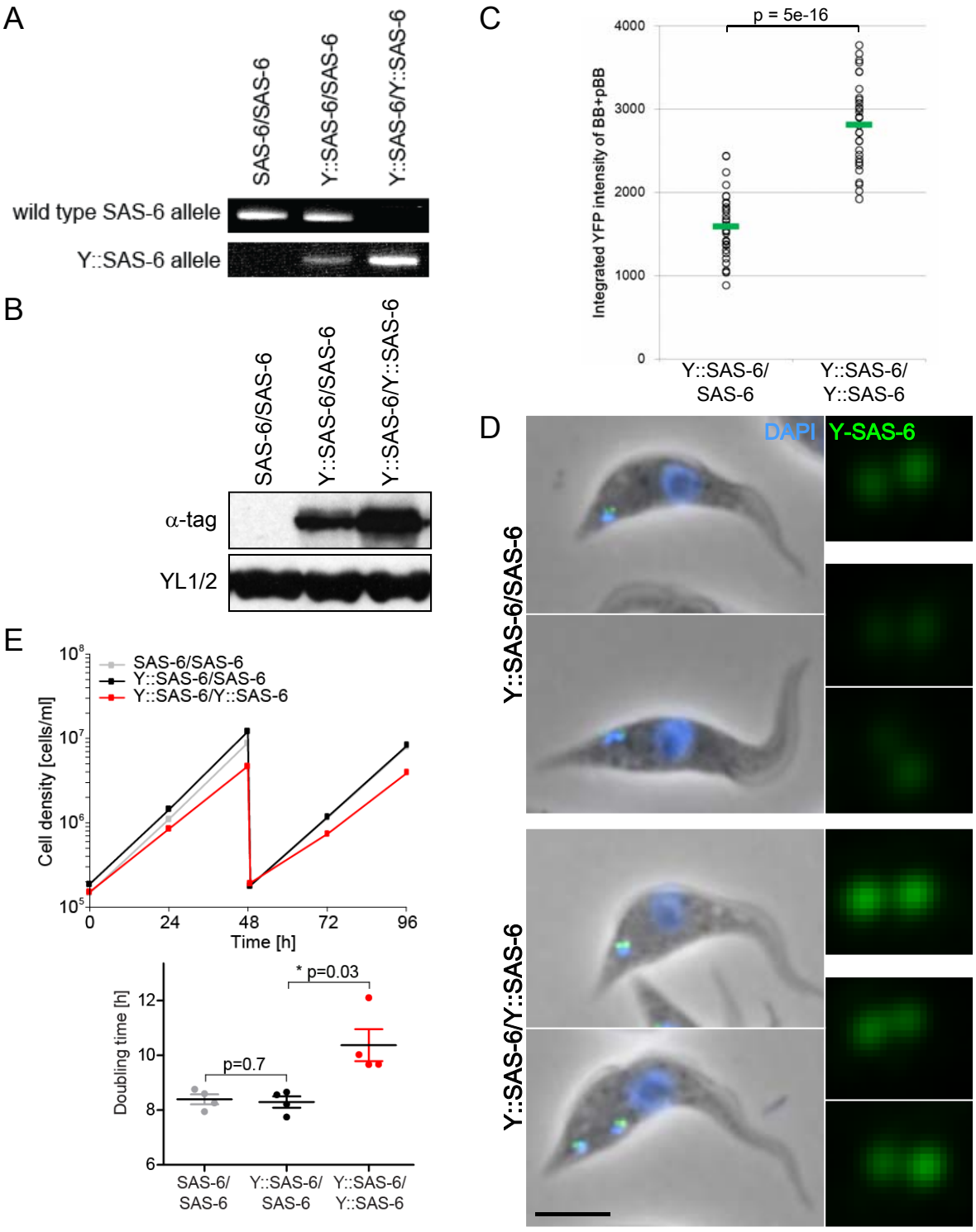

Figure 4.3 **Analysis of the functionality of Y-SAS-6.** In *Y::SAS-6/SAS-6* cells one endogenous SAS-6 allele and in *Y::SAS-6/Y::SAS-6* cells both endogenous SAS-6 alleles were modified to express Y-SAS-6 which in the later abolished expression of wild type SAS-6. (A) Examination of genomic DNA of cells given above image for wild type and modified SAS-6 loci. The PCR confirmed that *Y::SAS-6/Y::SAS-6* has no wild type allele left. (B) Immunoblot analysis of cells given above image with anti-tag antibodies (anti-GFP, anti-Ty) showing that *Y::SAS-6/Y::SAS-6* has a higher amount of Y-SAS-6. (C) Quantification of native YFP fluorescence intensity of BB+pBB of *Y::SAS-6/SAS-6* and *Y::SAS-6/Y::SAS-6* cells confirmed that the latter were brighter. Green bar = average. (D) Microscopy showed that *Y::SAS-6/Y::SAS-6* cells looked morphologically normal and that their BB and pBB appear brighter. Insets show Y-SAS-6 (green) in the BB area. DNA was labelled with DAPI (blue). Scale bar: 5μm. (E) Population growth was measured every 24h over 96h and cultures were diluted every 48h. Doubling time of *Y::SAS-6/Y::SAS-6* was slower but cells were viable.

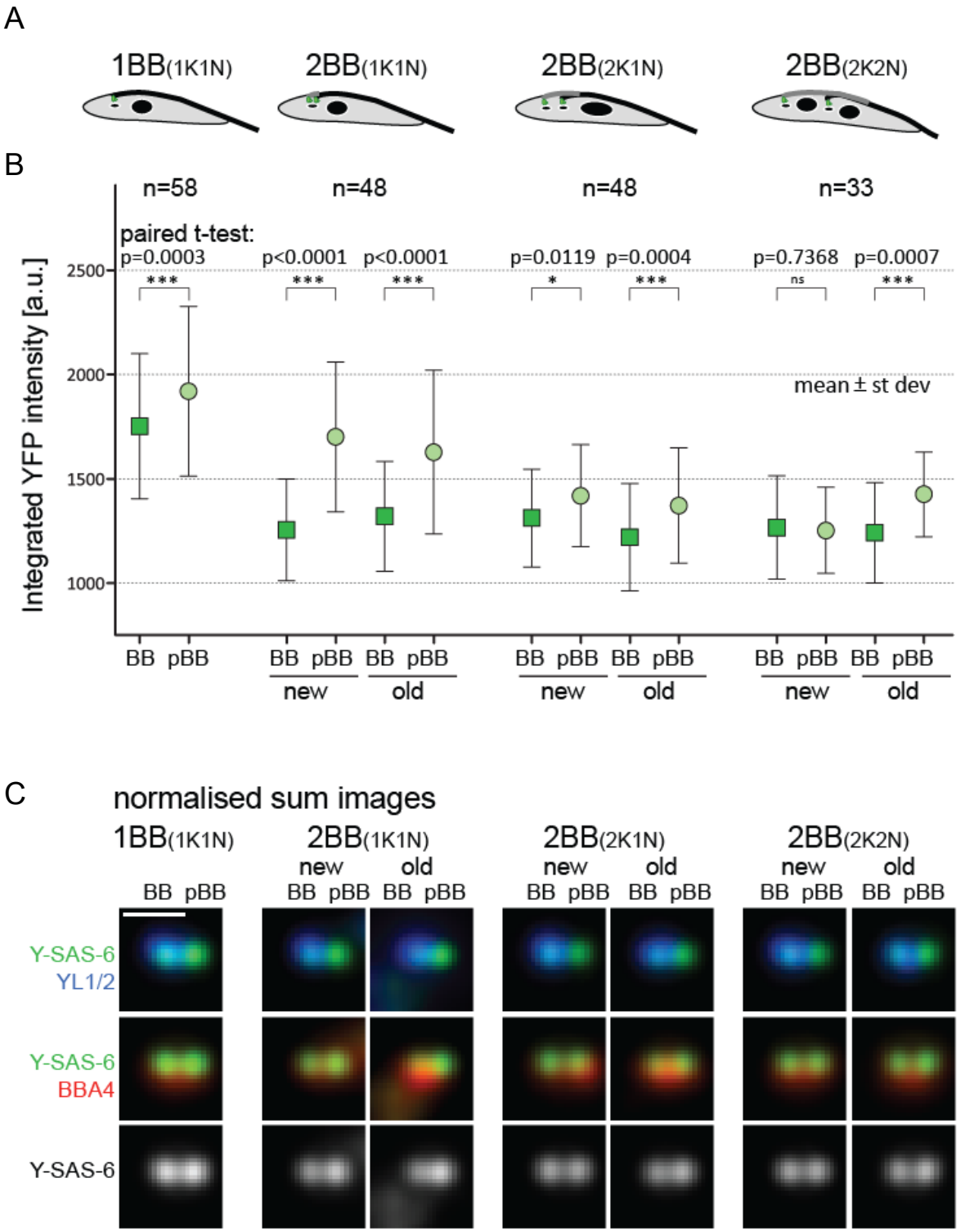

Figure 4.4 **The amount of Y::SAS-6 at the basal body and pro-basal body varies throughout the cell cycle.** *Y::SAS-6/Y::SAS-6* cells were detergent-extracted, fixed in methanol and immunolabelled. Images were taken and processed with equal settings. Cells were categorised by cell cycle stage. (A) Schematic overview of cell cycle categories according to number of basal bodies (BB), kinetoplasts (K) and nuclei (N). (B) Graph showing mean intensity of YFP fluorescence (in arbitrary units with standard deviation) at the basal body and the pro-basal body for each cell cycle stage. (C) Images of basal bodies and pro-basal bodies were aligned with BB in the centre and pBB to its right, summed up and normalised according to number of input images. Basal bodies were distinguished of pro-basal bodies by the presence of YL1/2 (blue). Scale bar 1um

2BB2K2N, and 2BB2K2N (Fig. 4.4 A). Identification of the basal body (versus pro-basal body) was confirmed by the presence of YL1/2 labelling, which is found only at the mature structure as part of the distal appendages. Basal bodies of the old versus new flagellum were distinguished by their anterior or posterior position within the cell respectively. The native YFP intensity of basal body and pro-basal body was measured individually by summing up the brightness of all pixels in equally sized regions of interest around the organelles.

The quantification of the YFP signals showed that basal bodies and pro-basal bodies in 1BB1K1N cells showed the highest amount of Y-SAS-6 (Fig. 4.4 B). Interestingly, in the next stage in 2BB1K1N cells, directly after the pro-basal body of the previous stage had matured into a basal body and assembly of two new pro-basal bodies had started, the high Y-SAS-6 amount remained with the pro-basal bodies but not with the basal bodies. Later in the cell cycle, in 2BB2K1N and in 2BB2K2N cells, the amount of Y-SAS-6 at the pro-basal body decreased to the level found at basal bodies. The amount of Y-SAS-6 found at the basal body of the old flagellum compared to that at the new flagellum basal body was similar. The different levels of Y-SAS-6 between the cell cycle stages were also observed by visual comparison of the normalised sum images (Fig. 4.4 C).

This analysis showed that the amount of Y-SAS-6 at the basal body and pro-basal body of *T. brucei* changes during the cell cycle and that a higher amount of Y-SAS-6 seems linked to pro-basal body assembly. These dynamics are similar with the ones at the pro-centriole in *C. elegans* where the onset of SAS-6 increase is in S Phase and SAS-6 decrease occurs in mitotic prophase (Dammermann et al., 2008).

4.6 Higher Y-SAS-6 amount coincidences with strong anti-δ-tubulin

1BB1K1N cells did not only exhibit the highest amount of Y-SAS-6, but also a wide spread of measured intensities at the basal bodies and pro-basal bodies. This raised the question whether additional events in this stage occur which are not taken into account by the #BB#K#N

categorisation. To further investigate the 1BB1K1N stage I used LAZ1, a monoclonal antibody specific to *T. brucei* δ-tubulin (Gadelha et al., 2006). LAZ1 marks two dots next to the basal bodies in 2BB1K1N cells and essentially disappears in 2BB2K1N cells, which suggests labelling of assembling pro-basal bodies in a distinct cell cycle dependent manner (personal communication with Paul McKean).

Interestingly, immunolabelling of *Y::SAS-6/Y::SAS-6* cells with LAZ1, revealed that already a proportion of the 1BB1K1N cells displayed LAZ1 labelling colocalising with the two Y-SAS-6 dots (Fig. 4.5 A). As expected, in the next stage (2BB1K1N), the LAZ1 signal remained associated only with the pro-basal bodies but not the basal bodies. LAZ1 labelling largely decreased in 2BB2K1N cells and completely disappeared in 2BB2K2N cells. Considering the association of the LAZ1 signal solely with the pro-basal bodies in 2BB1K1N cells, the onset of LAZ1 labelling in 1BB1K1N cells indicated that the recruitment of δ-tubulin to the site of new pro-basal body assembly preceded the segregation of pro-basal body assembled in the previous cell cycle from the basal body.

Quantification of fluorescence intensity of LAZ1 labelling and Y-SAS-6 revealed that higher quantities of Y-SAS-6 in 1BB1K1N cells coincidences with a strong labelling of δ-tubulin (Fig. 4.5 B). These similar dynamics, together with the association of these signals with the pro-basal body in 2BB1K1N cells, support the idea, that both the presence of δ-tubulin and high levels of SAS-6 mark pro-basal body assembly.

4.7 SAS-6 is essential

To assess the function of SAS-6, I generated an inducible RNAi cell line encoding a short hairpin against *SAS-6* (sh*SAS-6*) in a *Y::SAS-6/Y::SAS-6* background. Western Blot analysis of doxycycline-induced cells using anti-tag antibodies confirmed that the short hairpin construct is

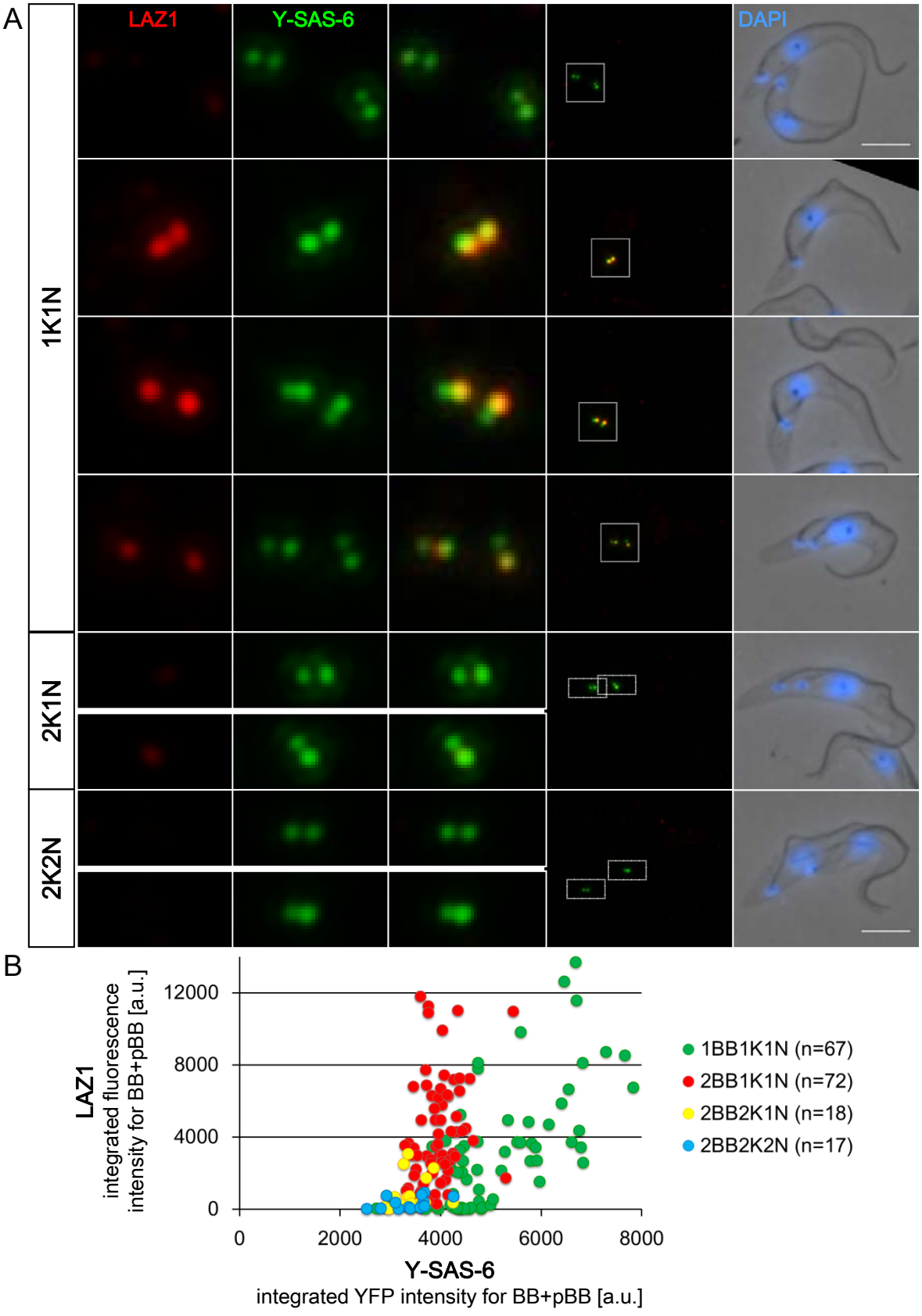

Figure 4.5 **Higher amount of Y-SAS-6 coincides with strong δ-tubulin labelling at the basal body and pro-basal body.** (A) *Y::SAS-6/Y::SAS-6* cells were detergent-extracted, fixed in methanol and immunolabelled with LAZ1 (anti-δ-tubulin, red). Insets show BB and pBB. DNA was labelled with DAPI (blue). Scale bar: 5μm. (B) Integrated fluorescence intensity of Y-SAS-6 for individual BB+pBB pairs was measured and plotted against the measured LAZ1 labelling intensity. The increase of Y-SAS-6 correlates with the appearance of LAZ1 labelling.

effective in reducing the amount of Y-SAS-6 in cells to below detectable levels by 36h post induction (Fig. 4.6 A). However, the amount of Y-SAS-6 in non-induced cells is also much lower than in the parental cell line. This could be the result of leakiness in the expression of sh*SAS-6* in non-induced cells. Induction of SAS-6 RNAi resulted in a strong growth defect after 24h (Fig. 4.6 B). Microscopic examination showed a homogenous Y-SAS-6 ablation across the population and the accumulation of aberrant multinucleated cells which suggests defective cell division in the absence of SAS-6 (Fig. 4.6 C).

4.8 Depletion of SAS-6 leads to a failure in kinetoplast segregation and flagellum assembly

In order to analyse the phenotype associated with SAS-6 depletion, shSAS-6 cells were prepared for fluorescence microscopy. Counts of kinetoplasts and nuclei showed the accumulation of aberrant multinucleated cells across the population over time (Fig. 4.7 A). The ratio of the number of nuclei to the number of kinetoplasts is 0.85 in a healthy population (Woodward and Gull, 1990). This ratio increased to 5 in cells 72h post induction (n=50 per time point), indicating a failure in kinetoplast duplication (Fig. 4.7 B).

48h after SAS-6 RNAi induction ~50% of the cells were multinucleated and possessed one large kinetoplast and one full-length flagellum (Fig. 4.7 C). The most likely explanation for the high number of nuclei per cell is failure of cytokinesis while mitosis continued. The large appearance of the kinetoplast was most likely generated by multiple rounds of replication of mitochondrial DNA without kinetoplast segregation.

After RNAi indication all cells have at least still one full-length flagellum. Apart from that, SAS-6 depleted cells frequently possessed a second short flagellum which got thinner towards the distal end and that had its tip disconnected from the old flagellum (Fig. 4.8 A).

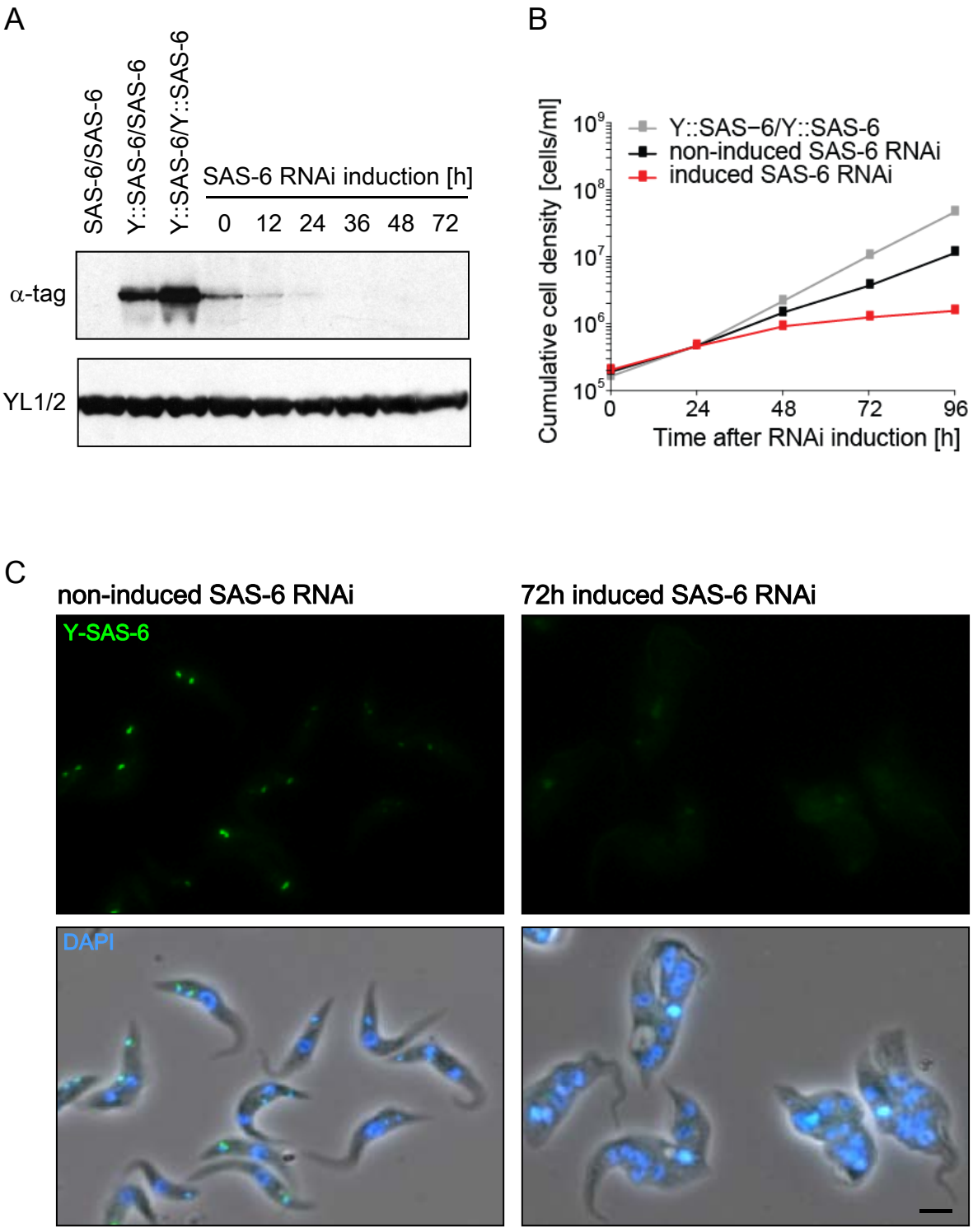

Figure 4.6 **Depletion of SAS-6 results in a lethal growth defect.** (A) Immunoblot analysis of cells given above image with anti-tag antibodies (anti-GFP, anti-Ty) showing the depletion of Y-SAS-6 after induction of RNAi against SAS-6, but also the leakiness of the inducible RNAi construct before induction. (B) Population growth measured every 24h over 96h with cultures diluted every 48h showed that the ablation of SAS-6 resulted in a dramatic reduction in cell duplication. (C) Fluorescence microscopy analysis of non-induced and 72h induced SAS-6 RNAi cells confirmed the depletion of Y-SAS-6 and revealed the aberrant morphology of cells post SAS-6 RNAi induction. DNA was labelled with DAPI (blue). Scale bar: 5μm.

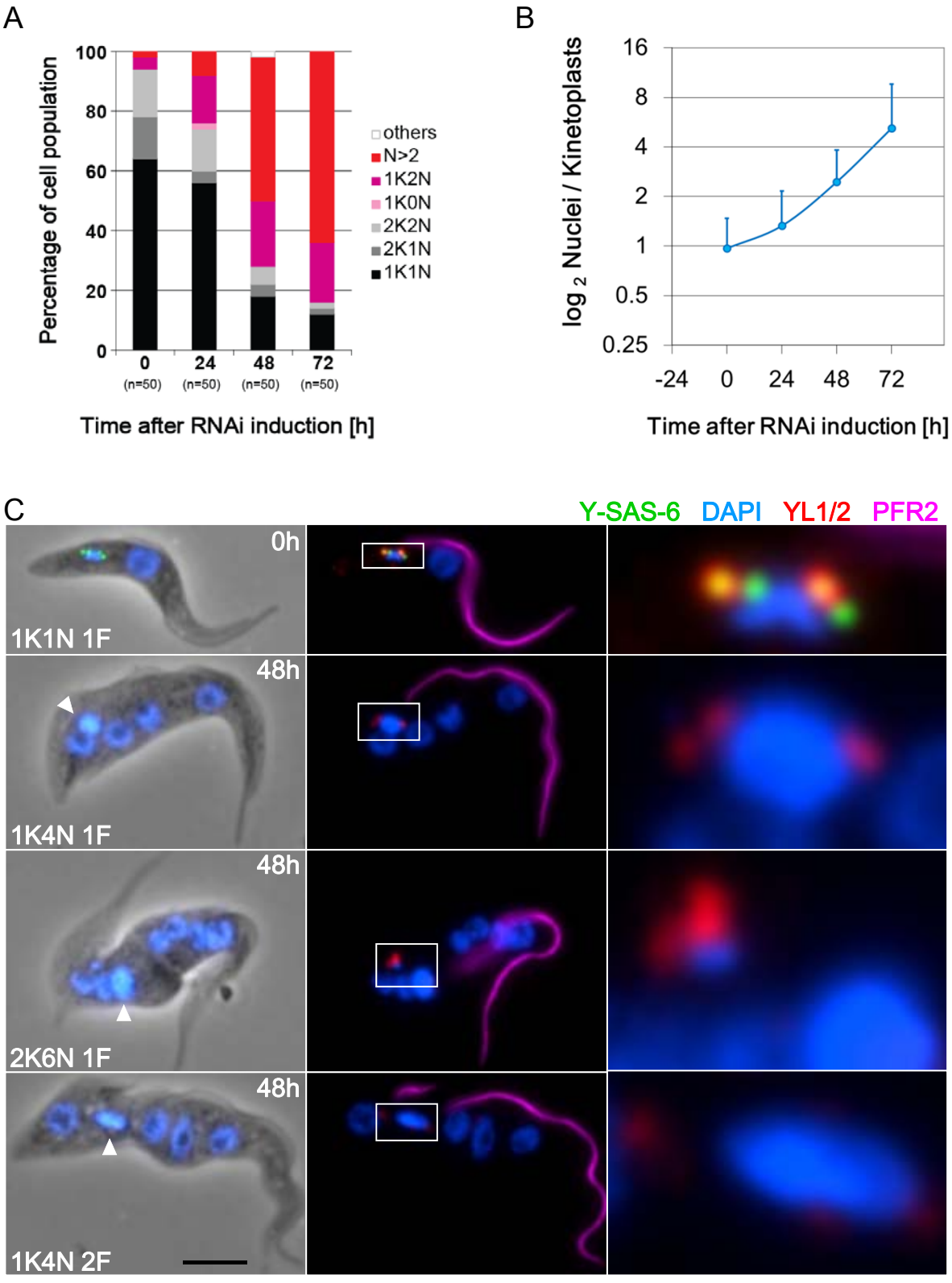

Figure 4.7 **Depletion of SAS-6 leads to multinucleated cells with defective kinetoplast segregation.** (A) Kinetoplast and nucleus counts at several time points after SAS-6 RNAi induction demonstrating an increase of abnormal cell cycle stages (redish colours). (B) Ratio of the number of nuclei to number of kinetoplasts suggesting defective kinetoplast segregation in cells post SAS-6 RNAi induction. N=50/time point. Error bars: standard deviation. (C) Immunolabelling of whole cell preparations of non-induced and 48h induced SAS-6 RNAi cells with YL1/2 (anti-tyrosinated α-tubulin, red) and L8C4 (anti-PFR2, magenta), and fluorescence microscopy showed the accumulation of multinucleated cells with an oversized kinetoplast (arrow head) post SAS-6 RNAi induction. DNA was labelled with DAPI (blue). Scale bar: 5μm.

A

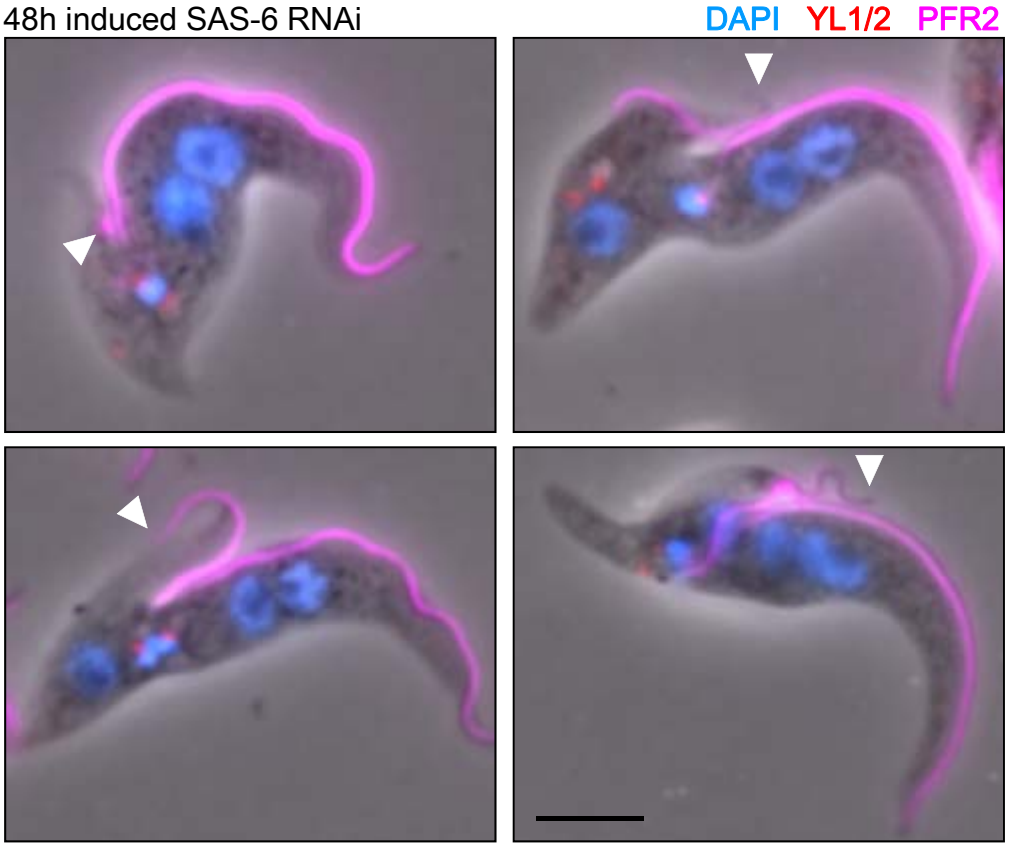

B

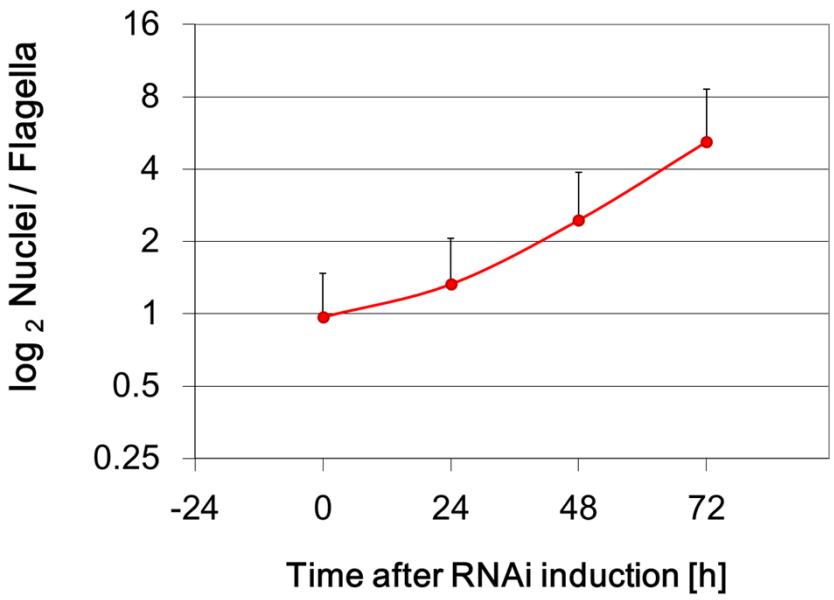

Figure 4.8 **Depletion of SAS-6 leads to aberrant cells with defective flagellum assembly.** (A) Immunolabelling of whole cell preparations of 48h induced SAS-6 RNAi cells with YL1/2 (anti-tyrosinated α-tubulin, red) and L8C4 (anti-PFR2, magenta), and fluorescence microscopy showed that the aberrant SAS-6 depleted cells had only one complete flagellum and sometimes a short, detached flagellum that got thinner towards the end indicating failed flagellum assembly (arrow heads). Scale bar 5μm. (B) Ratio of the number of nuclei to number of flagella suggesting defective flagellum formation in cells post SAS-6 RNAi induction. N=50/time point. Error bars: standard deviation.

The ratio of the number of nuclei to the number of flagella is 0.75 in a healthy population (Woodward and Gull, 1990). This ratio increased to 4.5 in cells 72h post RNAi induction (n=50 per time point) which indicated disrupted flagellum biogenesis (Fig. 4.8 B).

4.9 SAS-6 depleted cells can have a basal body with a reduced number of MT triplets

The failures in flagellum formation and kinetoplast segregation in SAS-6 depleted cells raised the question whether these defects had independent causes, or if they were linked by basal body dysfunction leading to both defects as a secondary effect.

In order to address the question of a basal body defect, thin section electron microscopy was used. Investigation on the ultrastructural level revealed basal bodies and pro-basal bodies with different morphologies. 36% of the basal bodies and pro-basal bodies in cells 36h post SAS-6 RNAi induction possessed a reduced number of microtubule triplets (Fig. 4.9). Reduced numbers of MT doublets were also observed in transition zones and axonemes suggesting that these aberrant basal bodies were still capable of supporting the nucleation of more distal structures. The same defects in basal bodies and distal structures could also be observed, though less frequently, in non-induced cells, which is not surprising considering the reduced amount of Y-SAS-6 in these cells (Fig. 4.6 A).

4.10 Incomplete basal bodies are competent to support flagellum assembly

In order to confirm that a basal body with a reduced number of MTs can nucleate a transition zone and an axoneme, and to investigate whether these abnormal structures template a pro-basal body,

A

	# MT triplets or duplets	9	8	7	6	5	< 5
Basal bodies and pro-basal bodies	example image	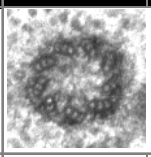	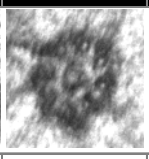	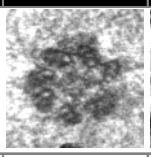	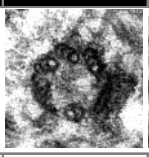	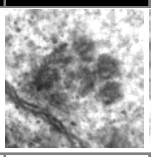	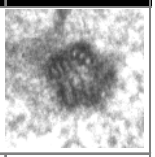
	non-induced n = 50	**46**	**3**	**1**	0	0	0
	SAS-6 RNAi 36h induced n = 50	**32**	**9**	**5**	**1**	**1**	**2**
	χ^2	p = 3E-13					
Transition zones	example image	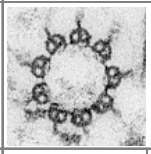	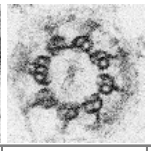	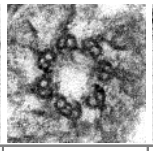	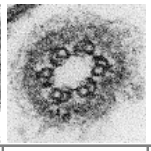		
	non-induced n = 50	**47**	**2**	**1**	0	0	0
	SAS-6 RNAi 36h induced n = 50	**42**	**4**	**3**	**1**	0	0
	χ^2	p = 0.003					
Axonemes	example image	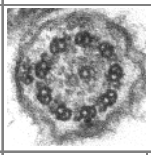	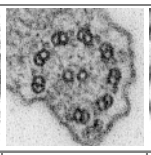	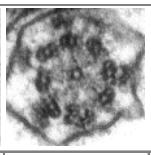			
	non-induced n = 50	**48**	**2**	0	0	0	0
	SAS-6 RNAi 36h induced n = 50	**45**	**4**	**1**	0	0	0
	χ^2	p = 0.03					

B

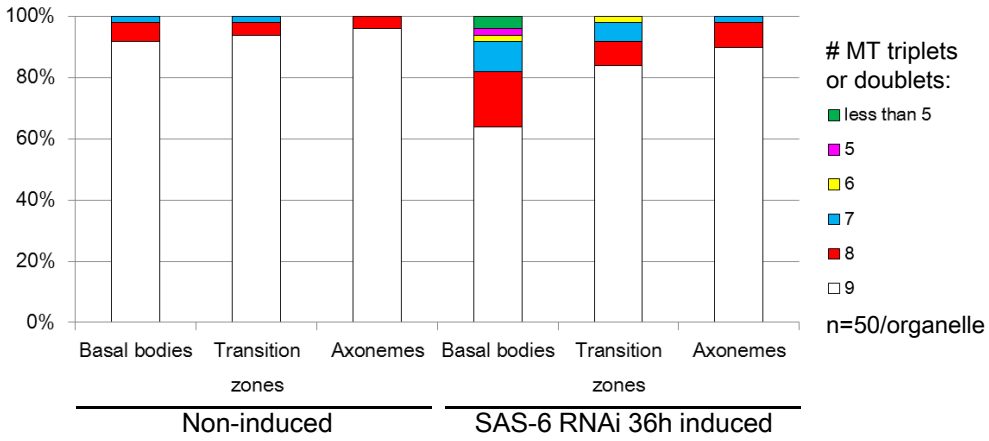

Figure 4.9 **SAS-6 ablation results in a reduced number of microtubule triplets in basal bodies.** (A) Counts of the number of MT triplets in basal bodies and the number of MT doublets in transition zones and axonemes of non-induced and 36h induced SAS-6 RNAi cells. Counts were done on TEM thin sections and an example image is shown for each phenotype for each organelle. (B) Graph with observed frequencies of the phenotypes for basal bodies, transition zones and axonemes.

serial thin sections were analysed by TEM. Figure 4.10 shows basal bodies with eight and seven microtubule triplets that supported the formation of a transition zone with the respective number of MT doublets. The structures progressed by entering into the flagellar pocket and forming an axoneme (Fig. 4.10 C). Figure 4.11 displays a transition zone with six MT doublets developing into an axoneme that had a flagellar collar indicating that it exited the pocket. Remarkably, even a basal body with only five microtubules was still able to form transition zone microtubules (Fig. 4.12 A). Although this transition zone lacked full-length transitional fibres it showed recruitment of vesicular material.

However, the axonemes extending from basal bodies with a reduced number of MT triplets lacked usually one or both of the central MTs (Fig. 4.12 B). This lack might be caused by the reduced interior axonemal space due to the lower number of MT doublets that compose the axonemal cylinder. As a consequence of this the MT pair itself might not fit in anymore or the dimensions of other supporting protein components such as radial spoke were not that adaptable to fit to the reduced space. The only observation of an axoneme with a complete set of a central MT pair was in axonemes with 8 MT doublets with the connection between each other broken leading to a normal sized axoneme diameter (Fig 4.9 A).

No pro-basal body was observed in any of the serial sections of basal bodies with a reduced number of MT triplets (Fig. 4.12 B). This suggests that either basal bodies with a reduced amount of MT triplets can not template a new pro-basal body, or there is a problem with pro-basal body assembly in general.

Normal basal bodies possessed a ring-shaped density in the centre with diameter of approximately 50-70 nm (Fig. 4.10 A ii). This ring density is different from the small cartwheel hub with a diameter of 25 nm (for comparison Fig. 4.9 A: image of a basal body with nine MTs has a small pinhole cartwheel). I will refer to this as the central ring density. Interestingly, the incomplete basal bodies possessed a central ring density (Fig. 4.10 B iii,iv,C vi,vii, 4.12 A ii-iv, 4.9 A). Incomplete

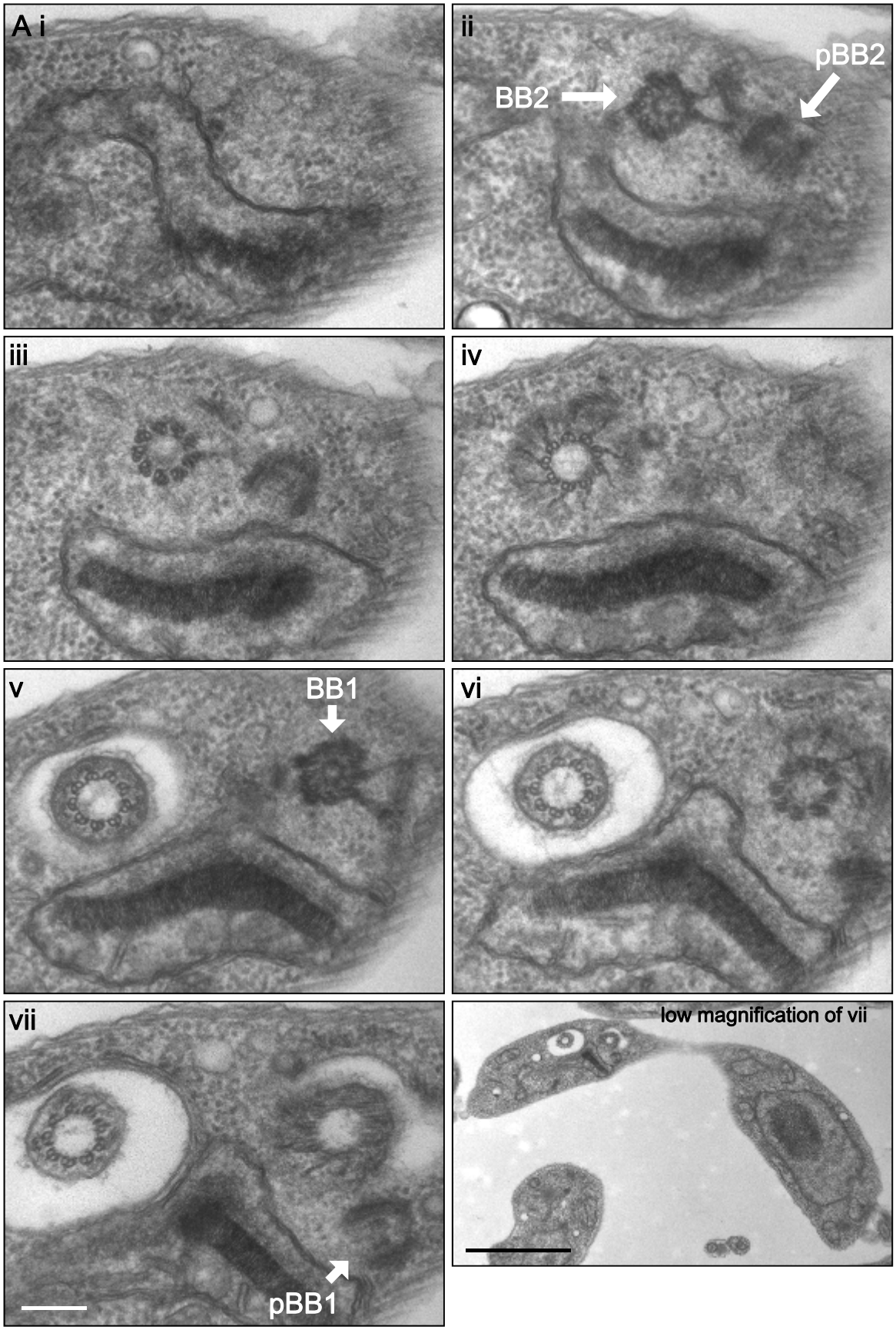

Figure 4.10 **Basal bodies with a reduced number of microtubule triplets still form a transition zone.** (A) Serial transverse TEM sections of the basal body area of a non-induced cell showing a normal basal body with nine MT triplets (and a central ring density that has a larger diameter than the cartwheel hub). BB1 = basal body of the old flagellum. BB2 = basal body of the new flagellum. Scale bars: 200nm (white), 2μm (black). Next pages: BB with (B) 8MTs and (C) 7MTs.

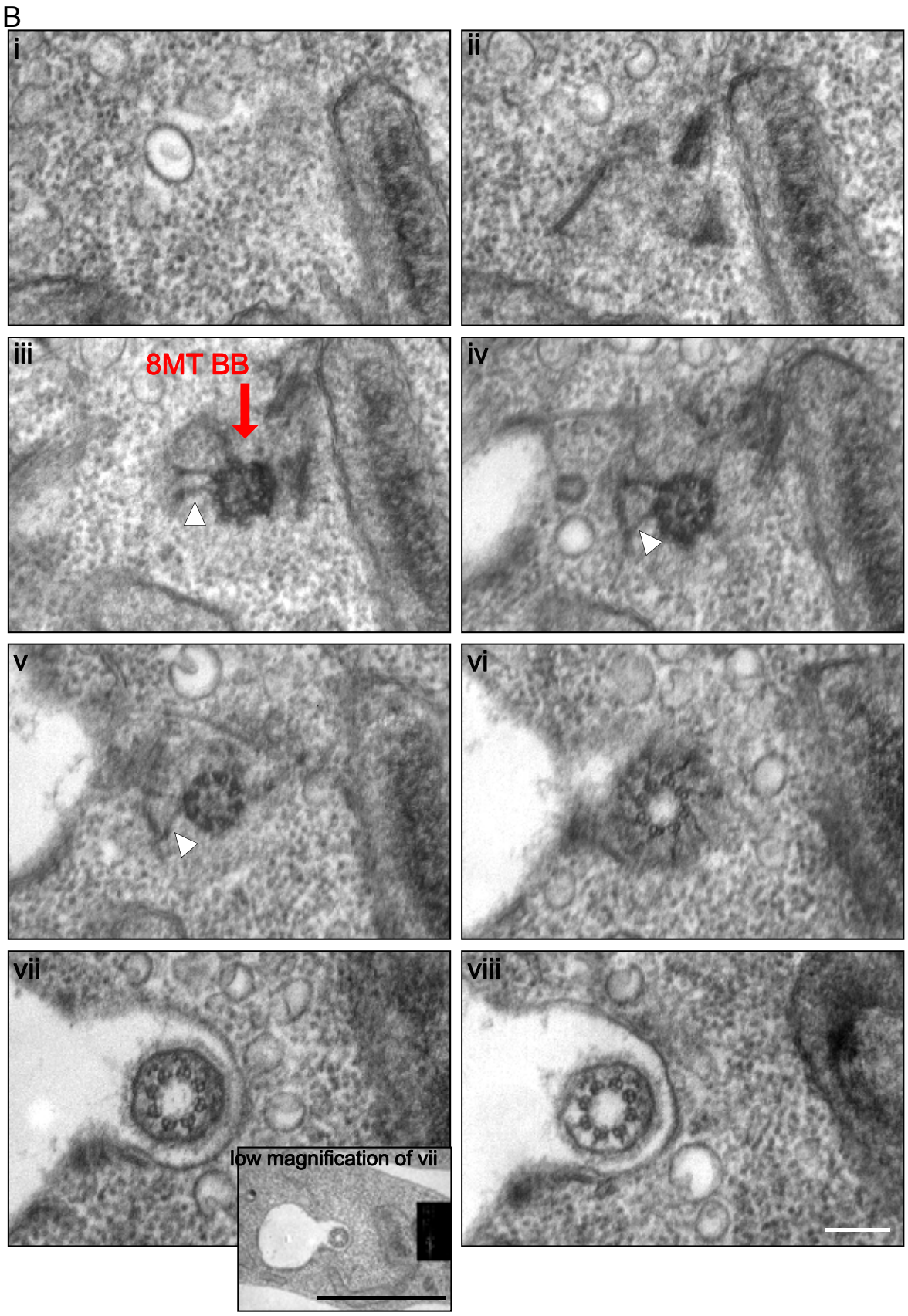

Continuation of Figure 4.10 **Basal bodies with a reduced number of microtubule triplets still form a transition zone.** (B) Serial transverse TEM sections of the basal body area of a 36h induced SAS-6 RNAi cell with a basal body which had only eight MT triplets. It still had a central ring density and continued to form a transition zone. The basal body possessed striated fibres (white arrow head in 3,4,5) but lacked a new pro-basal body. Scale bars: 200nm (white), 2μm (black). Next page: (C) BB with 7MTs.

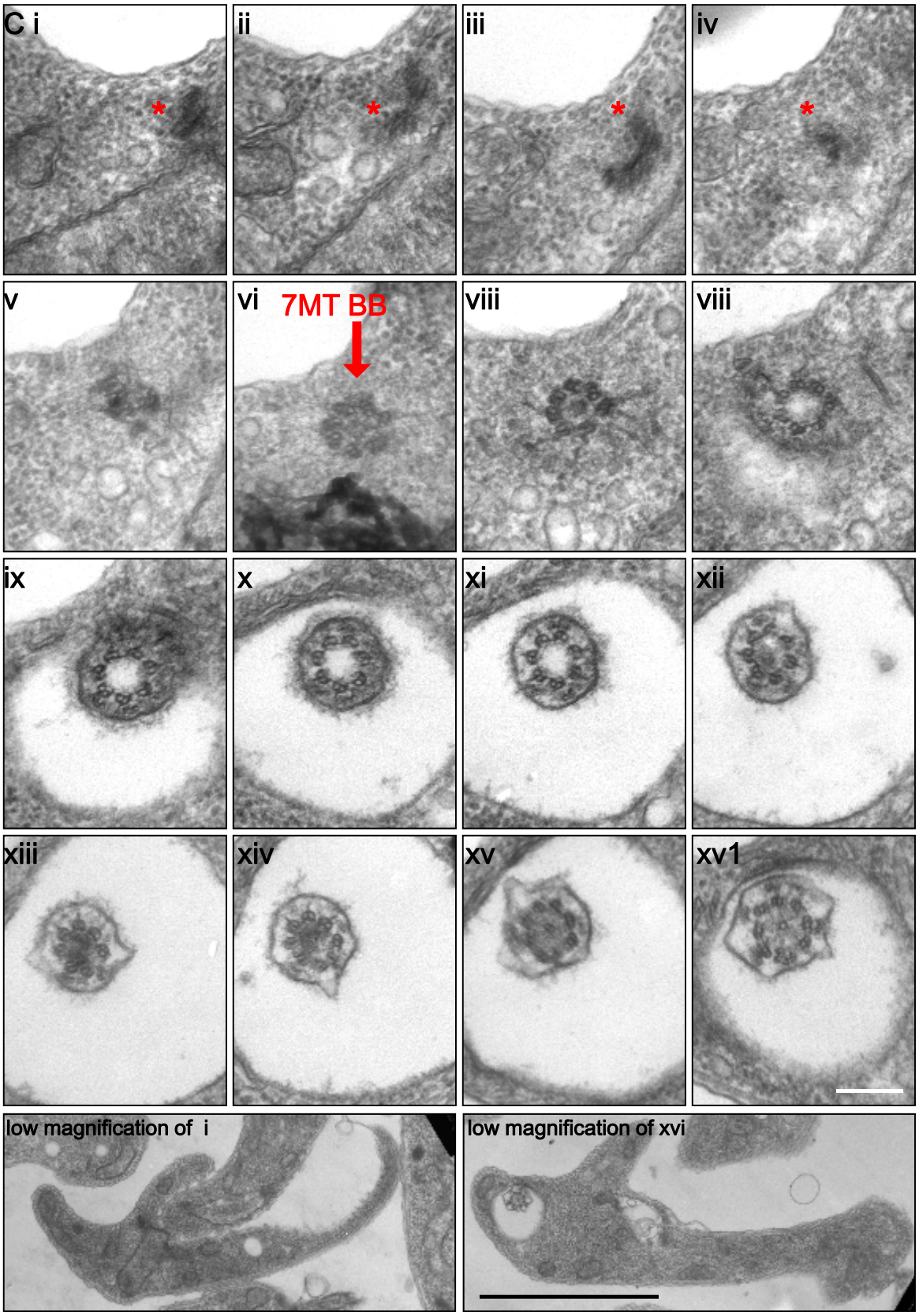

Continuation of Figure 4.10 **Basal bodies with a reduced number of microtubule triplets still form a transition zone.** (C) Serial transverse TEM sections of the basal body area of a 36h induced SAS-6 RNAi cell with a basal body which had only seven MT triplets. It still had a central ring density, and it continued to form a transition zone and an axoneme. The axoneme had only one central MT (section 16). The basal body had no pro-basal body and no striated fibres. There was some dense material (asterisk in sections 1-4) which might indicate a failed attempt of pBB formation. Scale bars: 200nm (white), 2μm (black).

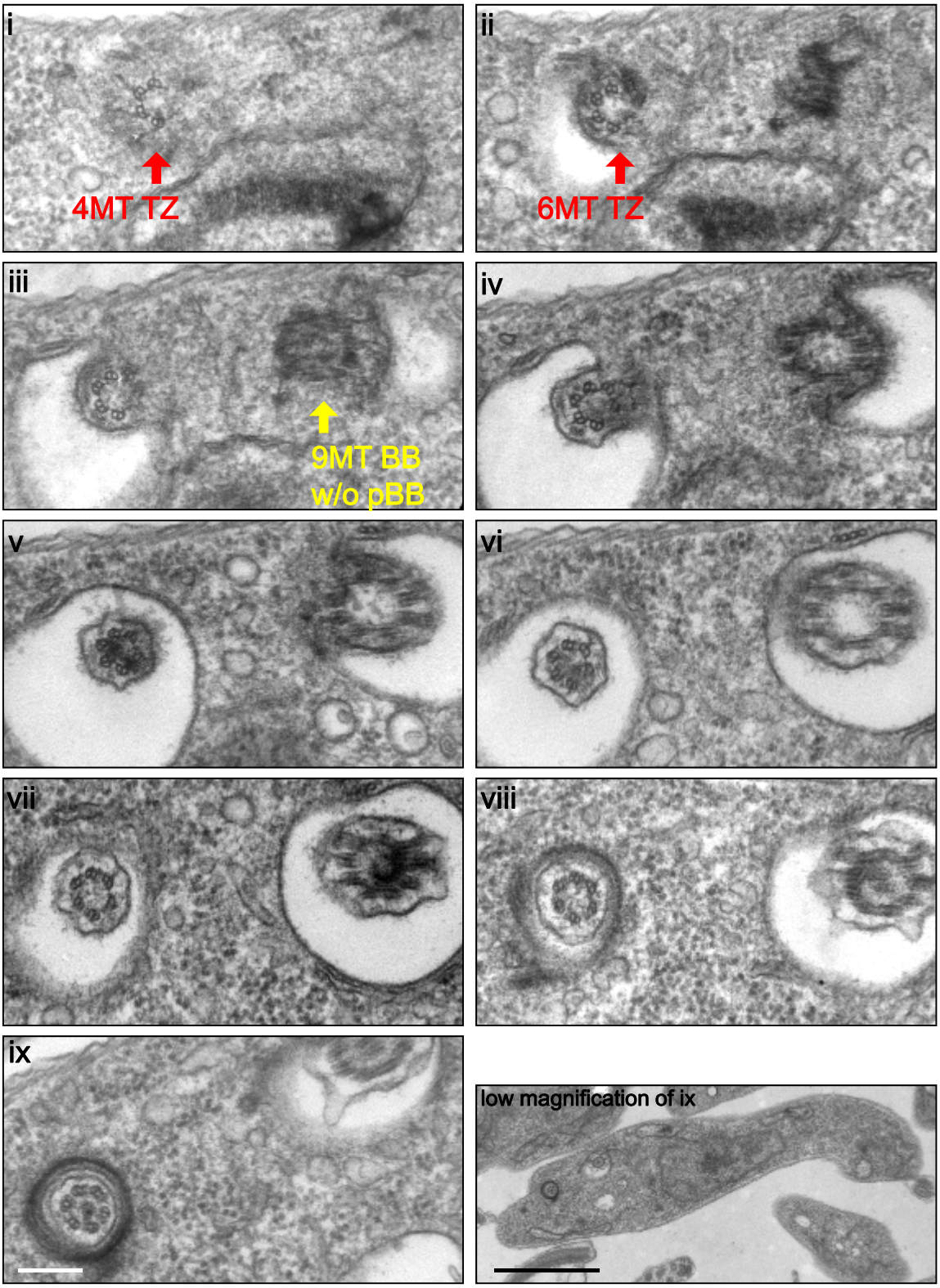

Figure 4.11 **Transition zone with only six microtubule doublets still progresses into an axoneme.** Serial transverse TEM sections of the transition zone area of a 36h induced SAS-6 RNAi cell with a transition zone with four and then six MT doublets which continued to form an axoneme. The axoneme lacks the central MT pair. While the doublets were arranged as a half circle towards the proximal end they were organised into a circle in the pocket. The cell also showed a basal body with 9MT triplets that lacked a pro-basal body. Scale bars: 200nm (white), 2μm (black).

A

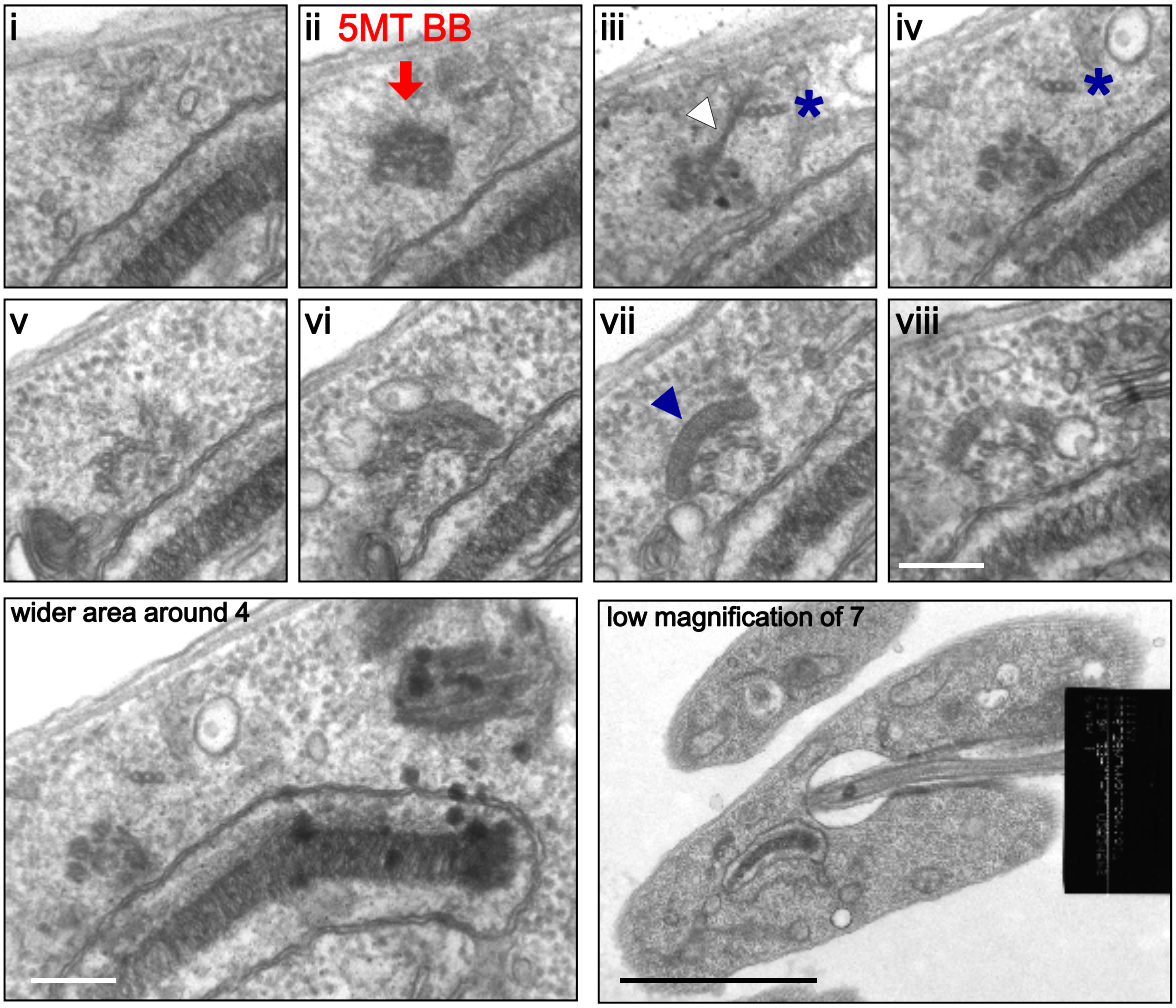

B

Serial Nr	Symmetry (# MT doublets/ triplets)	BB: central ring (bigger than cartwheel hub)	TZ MTs	Radial fibres	Flagellar pocket	Axoneme: extented MT doublets	Axoneme: central MT pair	pBB	Striated fibres	4 MTs
7 **Fig. 4.12 A**	5	✔	✔	✘	?	?	?	✘	✔	✔
6 (TZ) **Fig. 4.11**	6	?	✔	✔	✔	✔	✘	?	?	?
12 **Fig. 4.10 C**	7	✔	✔	✔	✔	✔	1 central MT	✘	✘	✘
2c		✔	✔	✔	✔	✔	?	✘	✘	✘
2a (TZ)		?	✔	✔	✔	✔	✘	?	?	?
1 **Fig. 4.10 B**	8	✔	✔	✔	✔	✔	?	(✘)	✔	✔

Figure 4.12 **Incomplete basal bodies are competent to support flagellum elongation.** (A) Serial TEM sections of the basal body area of a 36h induced SAS-6 RNAi cell with a basal body which had only five MT triplets. The triplets were arranged in a half circle which had a central ring density and striated fibres (white arrow head in 3) to the 4MTs (blue asterisk in 3,4). The triplets extended to form transition zone doublets but no extended radial fibres were detected. Transition zone MTs did not penetrate into the pocket but recruited material that looked like vesicles or membrane material (blue arrow head in 7). Scale bars: 200nm (white), 2μm (black). (B) Overview of features observed in six transverse serial sections of basal bodies and transition zones with reduced number of MT triplets and doublets (see Fig. 4.10, 4.11).

basal bodies were still capable of forming striated fibres (Fig. 4.12 A, 4.10 B).

These data show that despite their incomplete state in terms the number of MT triplets, the basal bodies still supported many steps of early flagellum assembly.

4.11 Analysis of the components of SAS-6 depleted basal bodies

After ablation of SAS-6 no cell with YFP dots could be detected, which means that basal bodies built before RNAi induction lost their YFP-SAS-6 (Fig. 4.6 C, 4.7 A). This suggested that the old basal bodies existed without SAS-6. It raised the question whether other known basal body markers were retained in the absence of normal SAS-6 levels. LAZ1 immunolabelling of cytoskeleton preparations of SAS-6 RNAi cells showed that 36h post RNAi induction delta-tubulin is still at the basal body and/or at the pro-basal body despite the absence of detectable Y-SAS-6 (Fig. 4.13 A). As LAZ1 marks assembling pro-basal bodies, this labelling in SAS-6 depleted cells might represent unfinished pro-basal bodies. However, it is unclear whether Y-SAS-6 was present or absent at the time of δ-tubulin recruitment.

BBA4 immunolabelling demonstrated that 12h after RNAi induction the intensity of the BBA4 signal remained unchanged despite a reduced amount of Y-SAS-6 at the basal body. However, 36h after induction in the absence of detectable Y-SAS-6 the intensity of BBA4 labelling was decreased but still present (Fig. 4.13 B,C).

4.12 Absence of pro-basal bodies in SAS-6 depleted cells

As shown above, basal bodies with a reduced number of MT triplets had no pro-basal body associated. In order to investigate whether this is specific to aberrant basal bodies or whether the lack of a pro-basal body is a more general phenomenon, I analyse transverse serial sections of

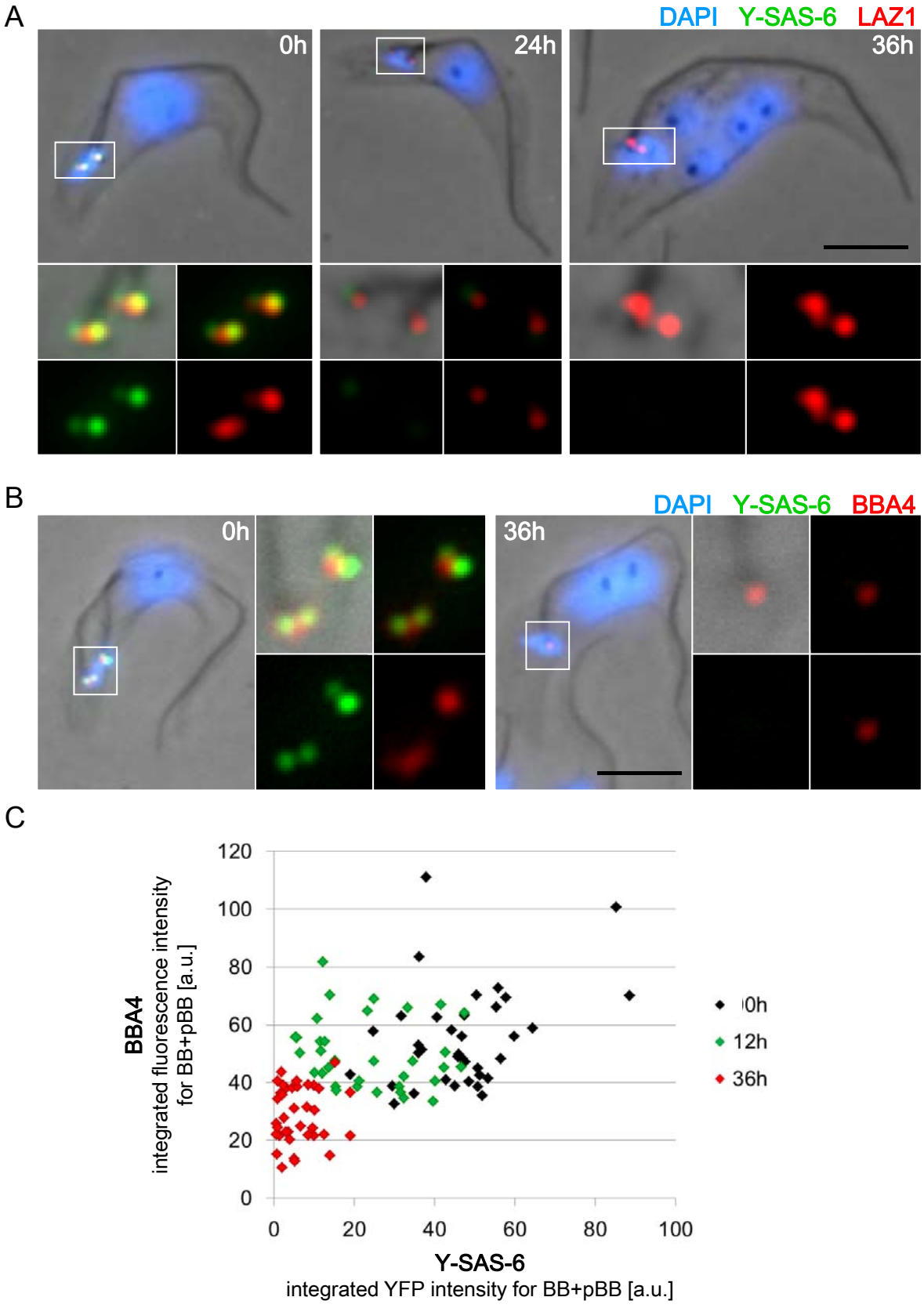

Figure 4.13 **Analysis of the components of SAS-6 depleted basal bodies.** (A,B) Immunolabelling of cytoskeleton preparations of non-induced and induced SAS-6 RNAi cells with (A) LAZ1 (anti-δ-tubulin, red) and (B) BBA4 (red). DNA was labelled with DAPI (blue). Scale bar: 5μm. (C) Quantification of the fluorescence intensity of Y-SAS-6 and BBA4 labelling at BB+pBB at different time points after SAS-6 RNAi induction.

basal bodies with nine MT triplets of 36h induced SAS-6 RNAi cells. Pro-basal bodies were completely absent from four out of seven analysed basal bodies with nine MT triplets (Fig. 4.11(iii)). This finding demonstrated that the abnormal structure with reduced number of MT triplets and smaller diameter alone could not account for the lack of a pro-basal body but that there was another reason leading to the deficiency.

To quantify the frequency of the absence of pro-basal bodies across the population, I applied an EM technique by which the crude structure of the pro-basal body is detectable while the whole cell cytoskeleton with nucleus is also observed. Cytoskeleton preparations of detergent-extracted cells were mounted on formvar-coated grid, negatively stained with goldthioglucose and viewed by TEM. In non-induced cells, 83% (n=42) of all basal bodies were accompanied by a clearly identifiable pro-basal body (Fig. 4.14 A,B). The remaining 17% did not reveal a clear pro-basal body. Pro-basal body absence could be due to: covering by other cellular structures (such as the axoneme), early time point in its assembly process, or true absence caused by leakiness of the RNAi construct. In contrast, 36h post induction 69% (n=77) of the basal bodies had no visible pro-basal body, with the remaining 31% possessing some material near the basal body which could not be identified as a bone fide pro-basal body.

The absence of pro-basal bodies observed after SAS-6 depletion could have resulted from at least two different scenarios. Firstly, if SAS-6 is involved in the maintenance of pro-basal body stability, then the lack of SAS-6 could have caused unstable pro-basal bodies that disintegrated. Assembly of new pro-basal bodies would have failed because of lacking integrity. Secondly, if SAS-6 is important in an early step during the assembly process, then the lack of the protein would cause that no new pro-basal bodies are assembled. However, pro-basal bodies built before SAS-6 depletion could have still matured and become a basal body that formed a flagellum. The current understanding of the role of SAS-6 as a cartwheel component in other organisms would favour the support of the second scenario (Nakazawa et al., 2007; van Breugel et al., 2011).

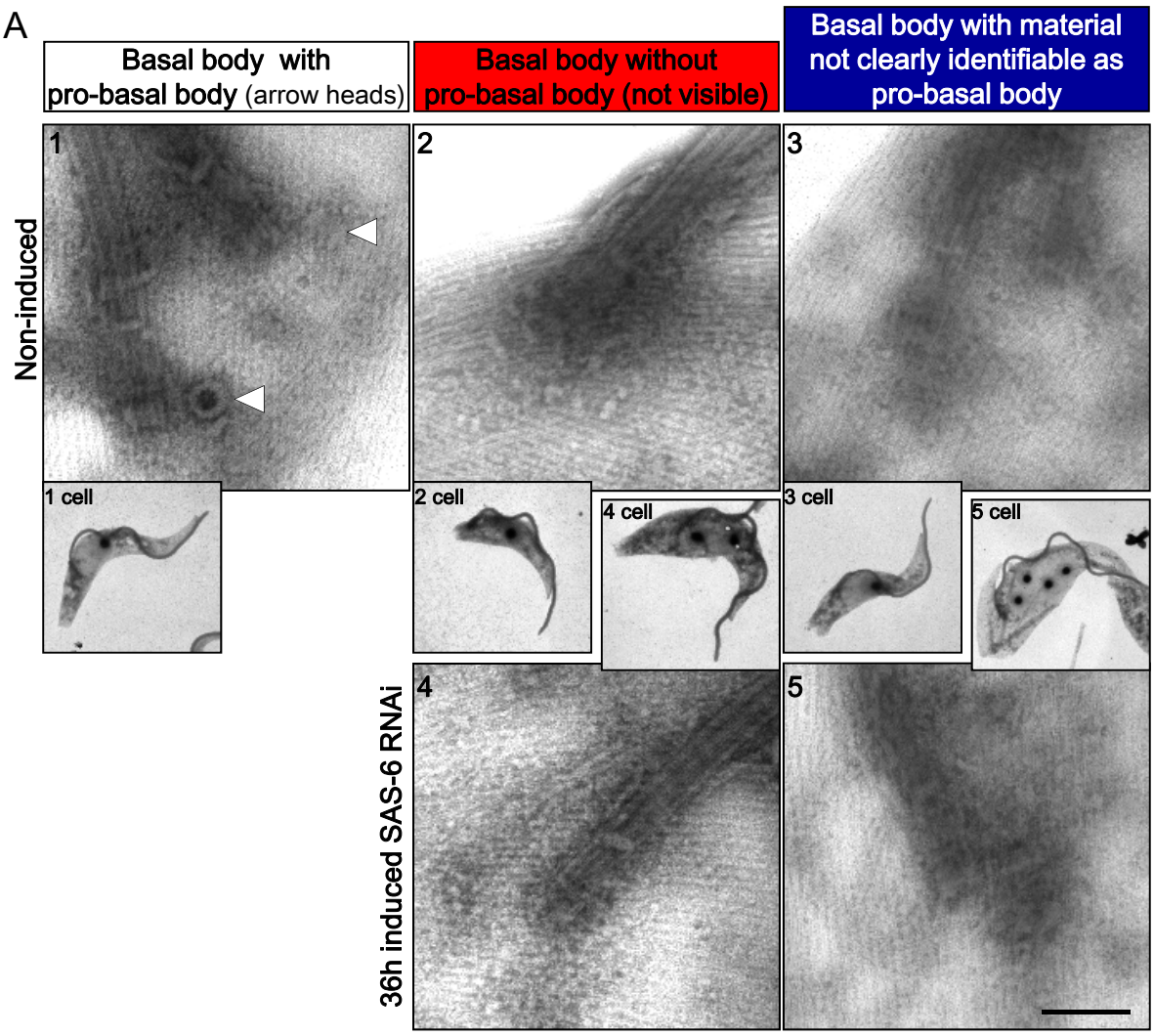

B

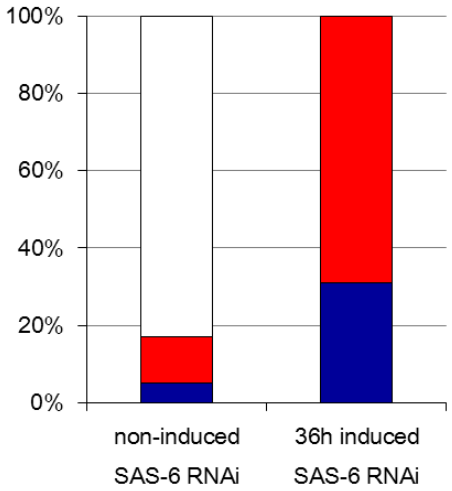

	non-induced n = 42	36h induced n = 77
Basal body with pro-basal body	83%	0%
Basal body without pro-basal body (no visible pro-basal body)	12%	69%
Basal body with material not clearly identifiable as pro-basal body	5%	31%

Figure 4.14 **Basal bodies in SAS-6 depleted cells lack a proper pro-basal body.** (A) TEM images of basal bodies of negatively stained whole-mount cytoskeletons of non-induced and 36h induced SAS-6 RNAi cells were categorised according to presence, absence/undetectability or uncertain identification of the associated pro-basal body. The inset shows the cell cytoskeleton of the respective basal body regions. Scale bar: 500nm. (B) Counts and graph of the observed frequency of the three scenarios showing the decrease in basal bodies with pro-basal bodies and the increase of basal bodies without pro-basal body or unidentifiable material post SAS-6 RNAi induction.

In order to investigate whether in the absence of SAS-6 pro-basal body material was still recruited to the usual site of pro-basal body assembly close to or onto the basal body wall, I analysed serial longitudinal thin sections of the organelles by TEM. In twelve sets of longitudinal serial sections of non-induced cells all basal bodies displayed a pro-basal body always detectable within the two consecutive sections of the basal body centre section (Fig. 4.15 A,B). In seven sets of longitudinal serial sections of basal bodies of induced SAS-6 RNAi cells six lacked a pro-basal body (Fig. 4.15 C,D). Material at the basal body wall that looked like assembling pro-basal bodies could not be detected. Some dense material at the basal body was observed both in non-induced and induced cells, and most likely represents striated fibres which were seen in transverse sections of basal bodies without pro-basal body (Fig. 4.10 B, 4.11, 4.12 A). The lack of any pro-basal body material is in agreement with the current model of SAS-6 being the earliest structural component in the assembly (Pelletier et al., 2006).

4.13 Overexpression of SAS-6 does not lead to general basal body overduplication

To address whether SAS-6 can act as initiator of pro-basal body assembly, I tested if higher amounts of SAS-6 lead to basal body overduplication in *T. brucei*. A cell line with inducible Ty-mCherry-SAS-6 (mC-SAS-6) expression in a *Y::SAS-6/Y::SAS-6* background was generated. This cell line allowed: the observation of SAS-6 made due to induction, the unambiguous identification of individual cells overexpressing SAS-6, and the detection of all SAS-6 in a cell. Western Blot analysis of whole cell extracts using anti-tag antibody confirmed that induction of mC-SAS-6 led to a higher amount of SAS-6 in the cells (Fig. 4.16 A). However, fluorescence microscopy showed heterogeneity across the population with only 50% of the cells expressing mC-SAS-6 (Fig. 4.16 B). Overexpression of SAS-6 over five days did not cause a change in the population growth rate (Fig. 4.16 C).

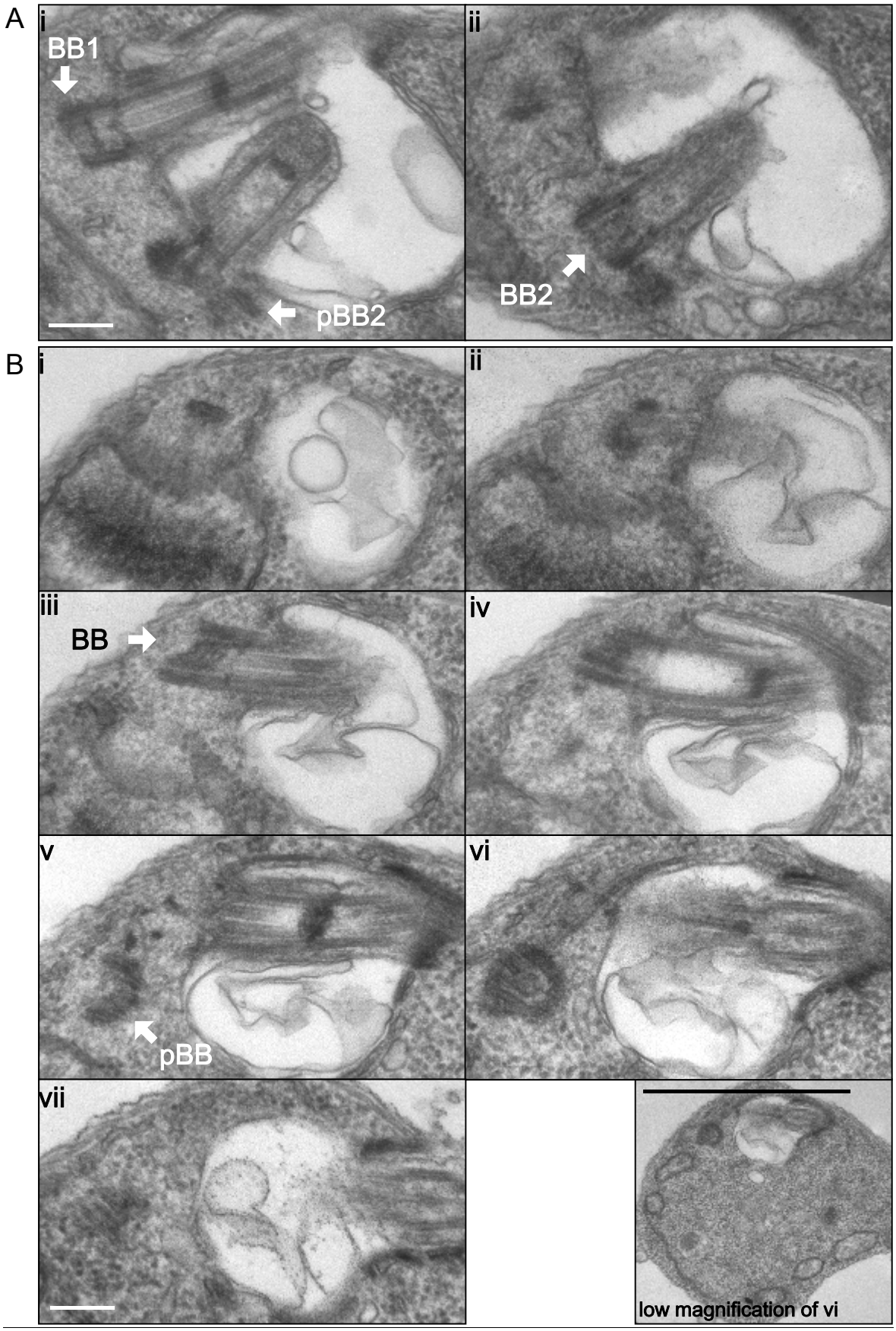

Figure 4.15 **No indication of pBB assembly at the usual site of pBB assembly next to the BB in SAS-6 depleted cells.** (A,B) Serial longitudinal sections of the BB area of non-induced cells. (A) Early after BB duplication demonstrating that new pBB was already detectable at that time point. (B) Example of a BB in the same position as the following examples. pBB was always visible within two sections of BB. Scale bars: 200nm (white), 2μm (black). Next pages: (C,D) Induced SAS-6 RNAi.

C

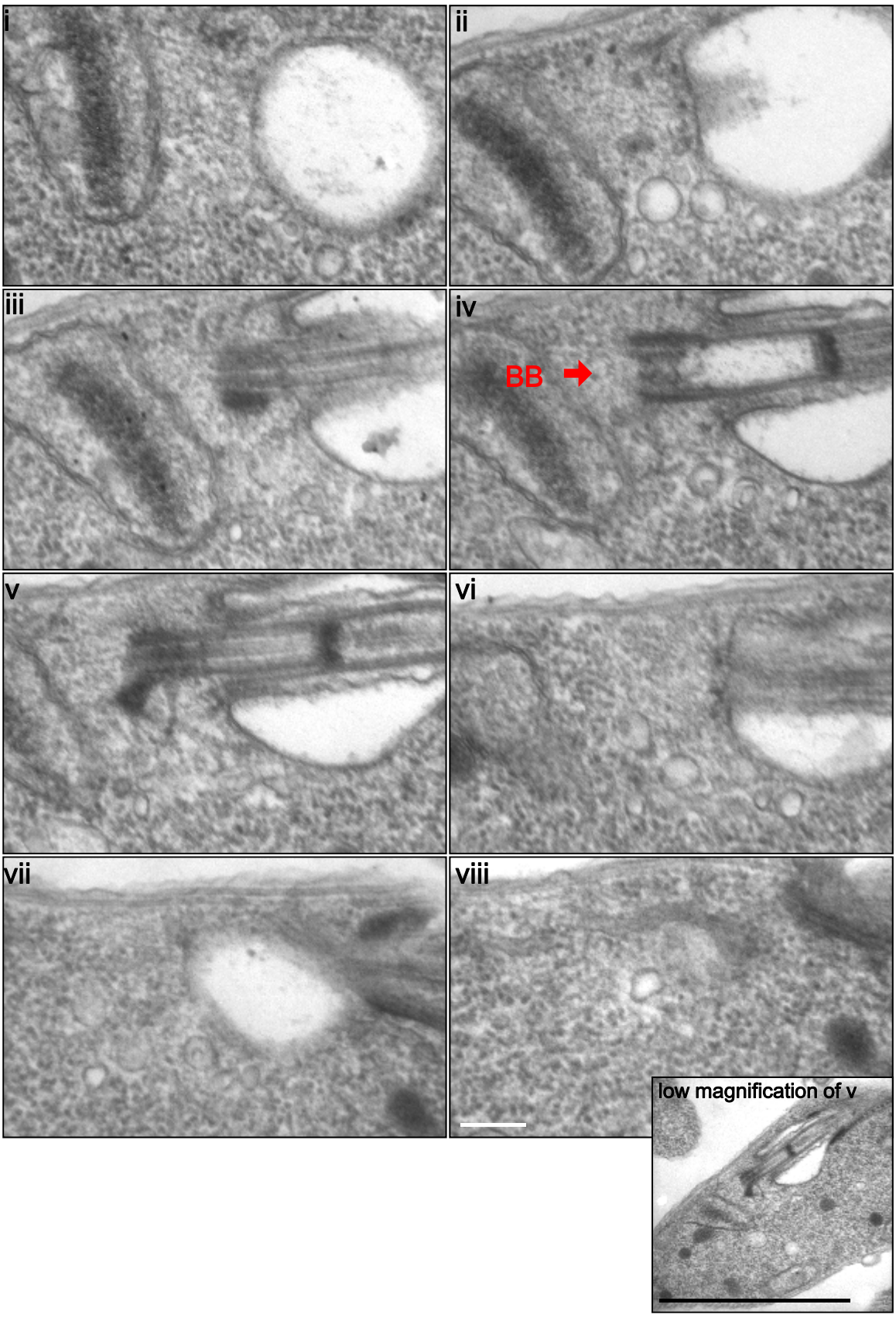

Continuation of Figure 4.15 **No indication of pBB assembly at the usual site of pBB assembly next to the BB in SAS-6 depleted cells.** (C) Serial longitudinal TEM sections of the basal body area of a 36h induced SAS-6 RNAi cells showing that no pro-basal body was detectable near the basal body. Scale bars: 200nm (white), 2μm (black). Next pages: (D) Induced SAS-6 RNAi.

D

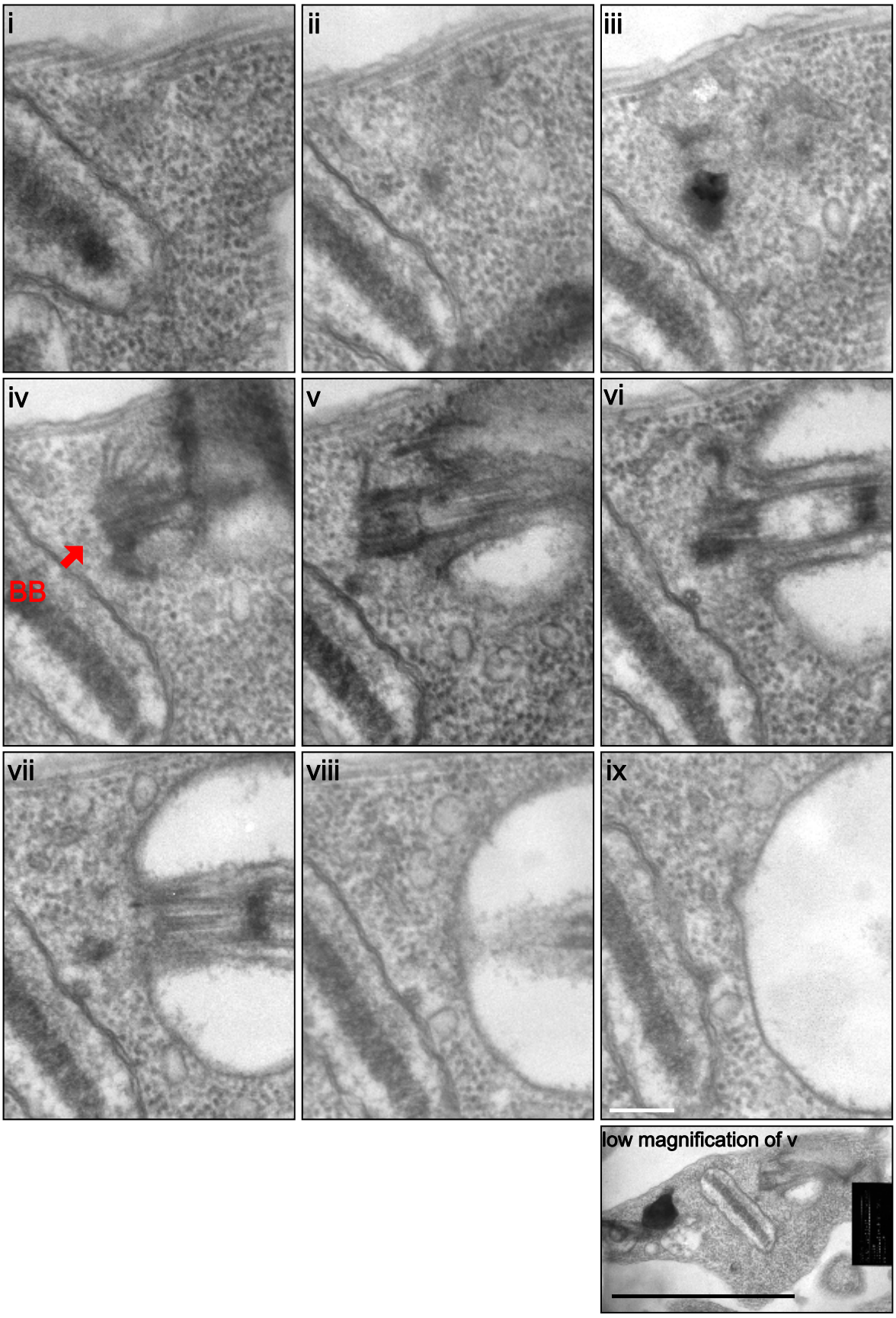

Continuation of Figure 4.15 **No indication of pBB assembly at the usual site of pBB assembly next to the BB in SAS-6 depleted cells.** (D) Serial longitudinal TEM sections of the basal body area of a 36h induced SAS-6 RNAi cells showing that no pro-basal body was detectable near the basal body. Scale bars: 200nm (white), 2μm (black).

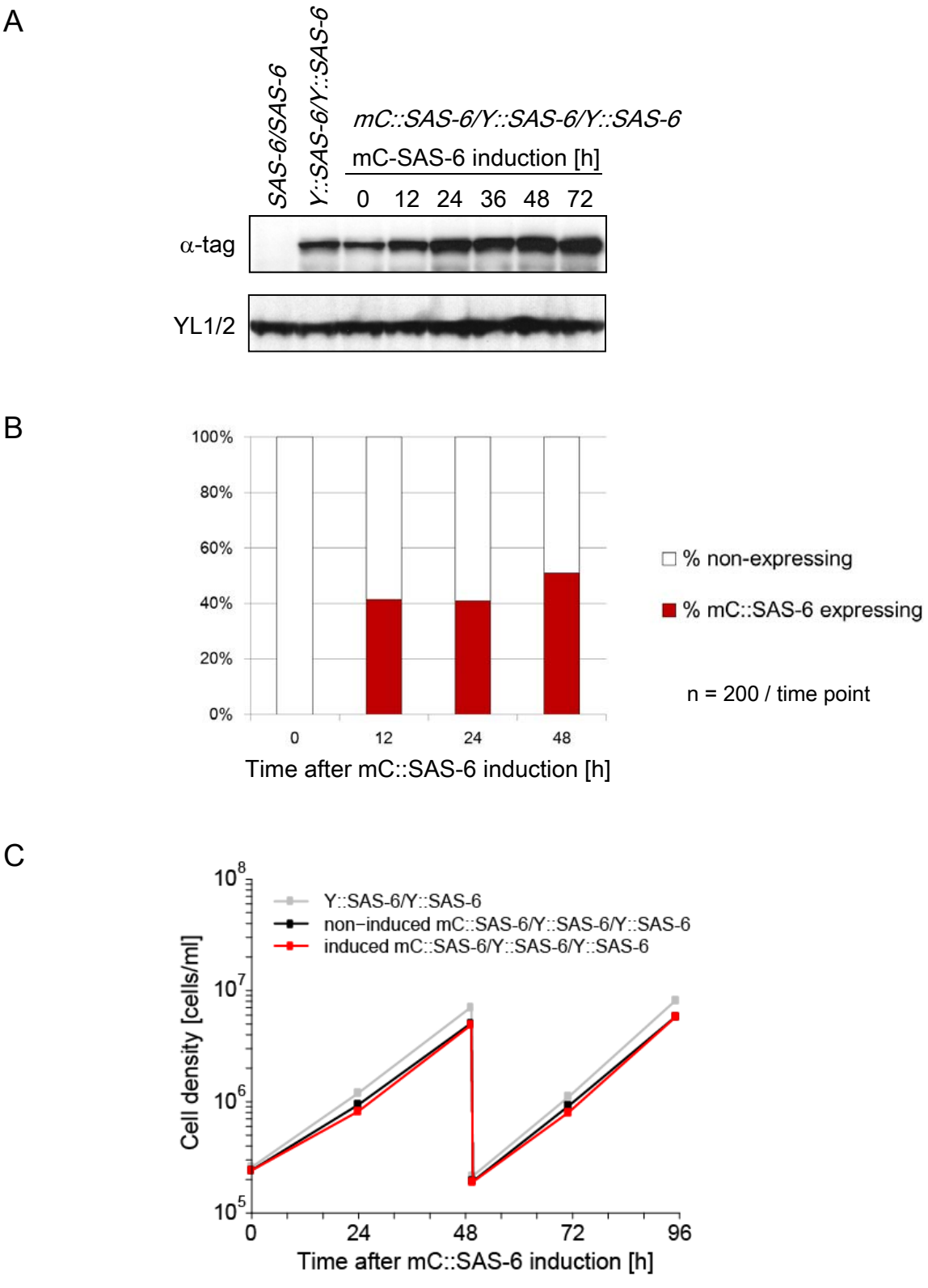

Figure 4.16 **Overexpression of SAS-6 does not cause a change in the population growth rate.** (A) Immunoblot analysis of cells given above image with anti-tag antibodies (anti-GFP, anti-Ty) showing that *mC::SAS-6/Y::SAS-6/Y::SAS-6* cells express more SAS-6 after induction. Loading control: YL1/2. (B) Observed frequency of mC-SAS-6 expression in induced *mC::SAS-6/Y::SAS-6/Y::SAS-6* cells demonstrating heterogeneity in mC-SAS-6 expression in the population and that only 40-50% of the cells overexpress SAS-6. (C) Population growth measured every 24h over 96h with dilution every 48h showed that SAS-6 overexpression did not cause a change in the population growth rate.

Examination of cells overexpressing SAS-6 by fluorescence microscopy showed that cells with a high level of mC-SAS-6 had commonly a normal morphology with only few cells being aberrant (Fig. 4.17 A). Counts of kinetoplasts, nuclei, basal bodies and flagella showed that 48h post induction of mC-SAS-6 expression the number of abnormal cells increased by 15% across the whole population (n=200) and by 25% in the cells overexpressing SAS-6 (n=98; Fig. 4.17 B). However, these defective cells lacked a uniform phenotype and the ratios of the numbers of different organelles remained unchanged during SAS-6 overexpression (Fig. 4.17 C) which did not give any insight into a cause of the abnormalities.

Most importantly, overexpression of SAS-6 did not lead to a general overduplication of basal bodies (Fig. 4.18). Only 5% of the cells in the population showed an over-representation of basal bodies correlated to their number of nuclei.

4.14 SAS-6 is not a stable basal body component but dynamic

Above I showed Y-SAS-6 localisation to the basal body and the pro-basal body throughout the cell cycle. Although the level of Y-SAS-6 varied depending on the cell cycle stage, the structures showed a base-level Y-SAS-6 signal which was also maintained in cytoskeleton preparations. It was surprising to find that in a population of induced SAS-6 RNAi cells basal bodies built before RNAi induction lacked Y-SAS-6 (Fig. 4.6 C, 4.7 A). This indicated that Y-SAS-6 was not stably integrated into the structure but dynamic. Furthermore, during early time points after RNAi induction Y-SAS-6 was reduced at a similar dynamic from old and new basal bodies compared to pro-basal bodies (Fig. 4.19 A).

To further test the idea that SAS-6 is dynamic, I induced expression of mC-SAS-6 in *Y::SAS-6/Y::SAS-6* cells for only 3h and analysed mC-SAS-6 localisation. As a normal cell cycle in these cells takes 10h (Fig. 4.16 C), all cells had at least one basal body that was built before

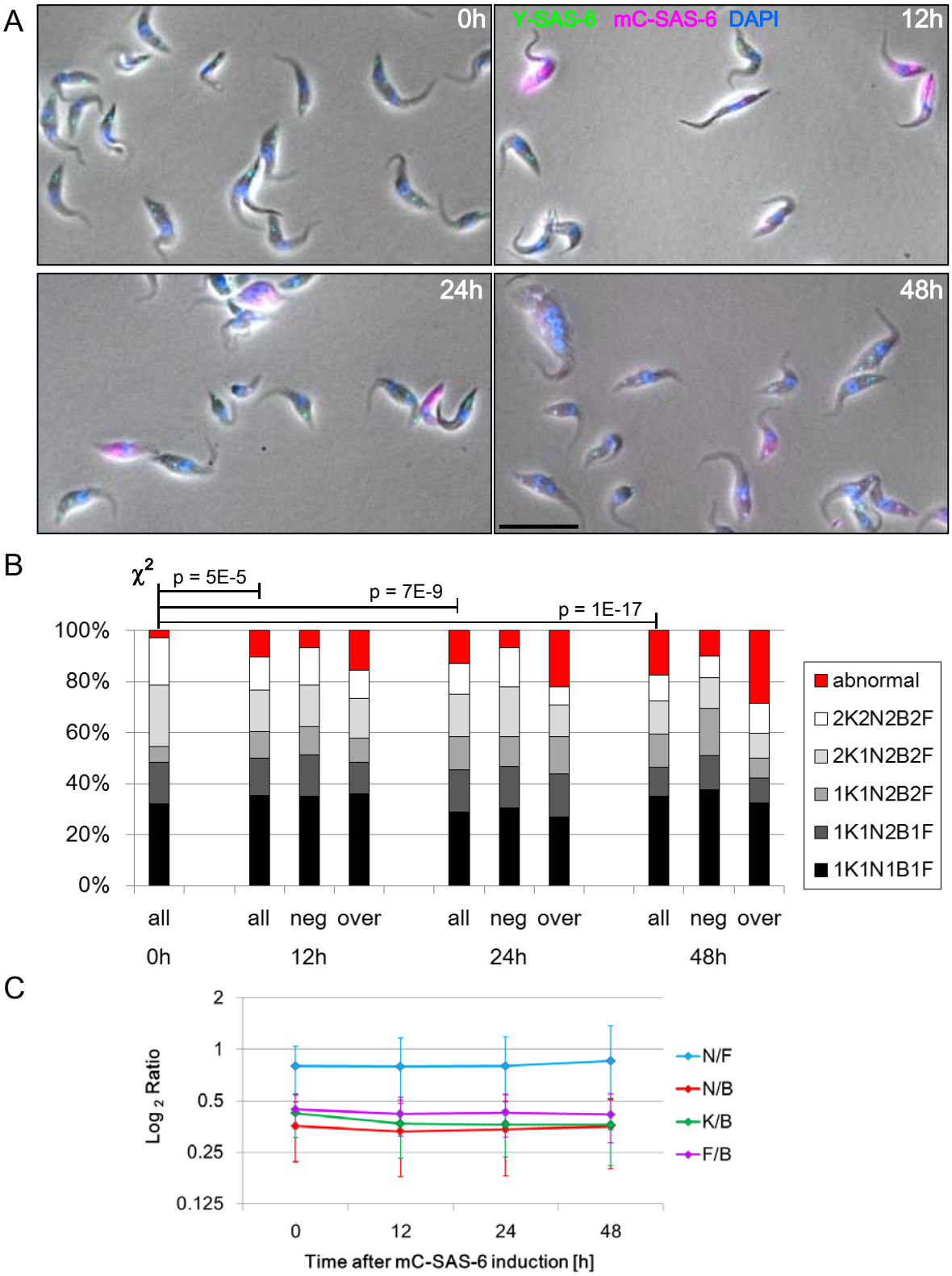

Figure 4.17 **Overexpression of SAS-6 leads to abnormalities in a proportion of the cell population.** (A) Overview images of non-induced and induced expression of mC-SAS-6 in *mC::SAS-6/Y::SAS-6/Y::SAS-6* cells. Scale bar: 20μm. (B) Counts of kinetoplasts (=K), nuclei (=N), basal bodies (=B) and flagella (=F) for the whole population (=all) which where then separated according to presence (=over) or absence (=neg) of mC-SAS-6 expression. N = 200 counts for all, split between negative cells (12h: 117cells, 24h: 118cells, 48h: 98cells) and overexpressing cells (12h: 83cells, 24h: 82cells, 48h: 102cells). (C) Graph displays ratios of the number of the in (B) counted cell organelles (average of single cell ratios of all cells with standard deviation), which did not reveal a change after induction of SAS-6 overexpression.

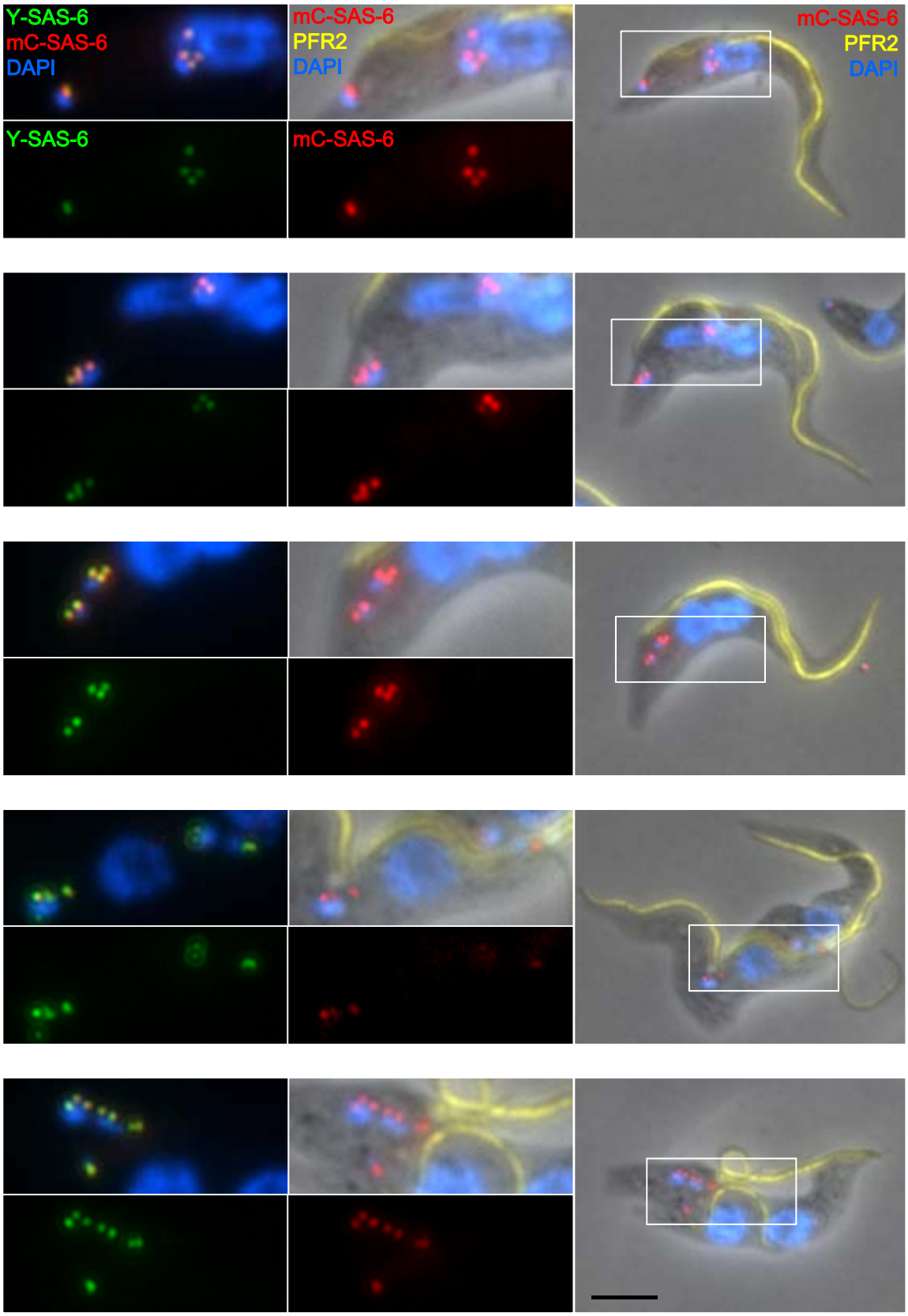

Figure 4.18 **SAS-6 overexpression does not lead to a general basal body overduplication: Only a small percentage (5%) of cells showed an overduplication of basal bodies 48h after induction of SAS-6 overexpression**. Fluorescence microscopy images of whole cell preparations of 48h induced mC::SAS-6/Y::SAS-6/Y::SAS-6 cells immunolabelled with L8C4 (anti-PFR2, yellow). Insets show basal body area. DNA was labelled with DAPI (blue). Green=Y-SAS-6. Red=mC-SAS-6. Scale bar: 5μm.

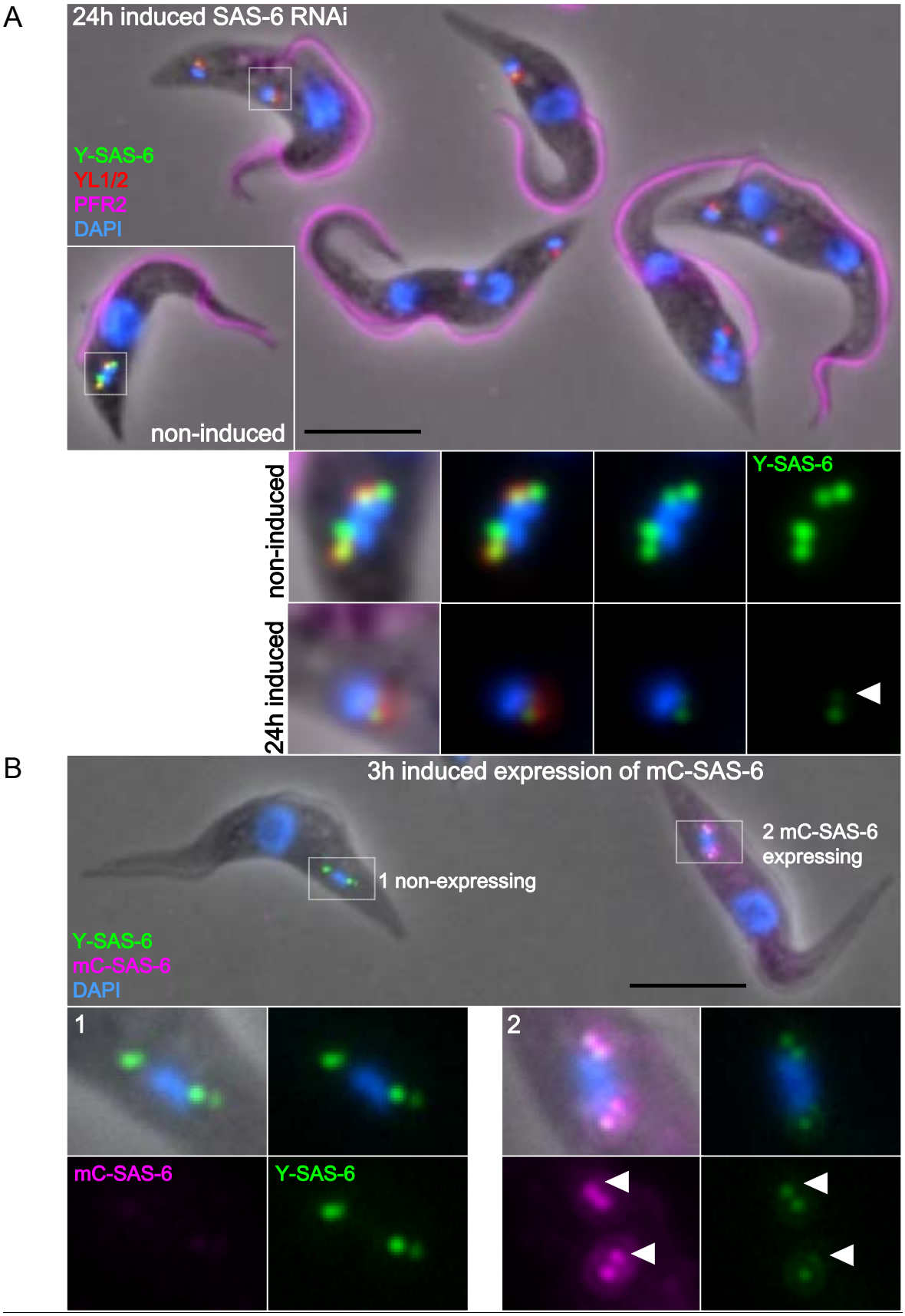

Figure 4.19 **SAS-6 at the basal body is dynamic.** (A) Native YFP fluorescence showed that after SAS-6 RNAi induction Y-SAS-6 is reduced at the newly assembled pBB but also at the old BB (arrow head). (B) 3h mC-SAS-6 induction showed that mC-SAS-6 associates not only with newly assembled pBB but also with old BBs built before induction (arrow heads). Displacement of Y-SAS-6 is observed at mC-SAS-6 positive BBs and pBBs (lower Y-SAS-6 intensity of 2 compared to 1). (A,B) Insets show indicated area. Scale bar: 5μm.

mC-SAS-6 induction. Nevertheless, in cells expressing mC-SAS-6 all basal bodies and pro-basal bodies were mC-SAS-6 positive (Fig. 4.19 B). Additionally, I also observed that mC-SAS-6 positive basal bodies had a lower amount of Y-SAS-6 compared to structures from the same stage without mC-SAS-6. This demonstrated that a proportion of Y-SAS-6 had been displaced from these basal bodies.

These four observations suggest that SAS-6 is not a stably integrated component of the basal body but that it is dynamic. Together with the EM data of SAS-6 depleted cells which showed that old basal bodies are morphologically normal, this also implies that SAS-6 is not required for the maintenance of the basal body.

4.15 Summary

Here, I characterised the SAS-6 orthologue in *Trypanosoma brucei*. I showed that tagged SAS-6 localises to the basal body and the pro-basal body, and that this tag does not impede with the functionality of the protein. The amount of SAS-6 at the basal body and pro-basal body is cell-cycle dependent, with the highest amount residing at assembling pro-basal bodies. Moreover, I demonstrated that SAS-6 is not stably integrated into the basal body but that it is in dynamic exchange probably with a cytoplasmic pool. SAS-6 in *T. brucei* is essential for basal body assembly. Thin section electron microscopy revealed both ultrastructural defects of basal bodies and a complete lack of pro-basal bodies in the absence of SAS-6. Furthermore, ectopic overexpression of the protein does not induce a general basal body overduplication.

CHARACTERISATION OF TRYPANOSOMAL SAS6L

5.1 Preface

During the survey for SAS-6 proteins in the bioinformatic analysis of centriole components in Chapter 3, another *Trypanosoma brucei* protein with similarity to SAS-6 was identified. SAS-6 is well investigated in a range of eukaryotes, but no related proteins have been mentioned in the literature. Since the protein encoded by Tb927.10.7920 had similarity to *T. brucei* SAS-6 (encoded by Tb09.211.1930) we named it SAS-6 like protein, SAS6L. The aim of this part of my thesis was to characterise SAS6L in *T. brucei* and compare its function to SAS-6. The bioinformatic analysis in this chapter was done by Bill Wickstead and the work concerning SAS6L in *Toxoplasma gondii* by collaborators in the Morrissette lab.

5.2 SAS6L and the N-terminus of SAS-6 share a conserved sequence

The similarity between SAS6L and SAS-6 in *T. brucei* was found in the N-terminal region of SAS-6 containing the conserved Pfam-B domain Pfam-B_2528. Similarity searches for proteins containing Pfam-B_2528 in the predicted proteomes of 43 diverse eukaryotes identified SAS-6 and SAS6L

homologues in other species showing that the existence of SAS6L proteins was not only specific to *T. brucei*. Phylogenetic analysis based on the conserved domain sequence of the identified SAS-6 and SAS6L proteins demonstrated the existence of two distinct subfamilies (Fig. 5.1). A typical SAS-6 protein was composed of the N-terminal Pfam-B_2528, followed by coiled-coil regions and an undefined C-terminus. In contrast, SAS6L proteins consisted mainly of the defining Pfam-B_2528 domain and were with ~250 amino acids much shorter. SAS-6 and SAS6L proteins share a conserved sequence of ~200 amino acids which includes the “PISA” motif identified as a part of the SAS-6 head domain (Leidel et al., 2005; van Breugel et al., 2011) (Fig. 5.2).

Threading of SAS6L proteins suggested that they may acquire structures similar to those of the N-terminal part of SAS-6 proteins (Fig. 5.3).

5.3 SAS6L is specific to species that form cilia except Holozoa

SAS6L proteins were identified in four of the six eukaryotic “supergroups”: Archaeplastida, Fungi, Excavata and Chromalveolata. With the exception of Holozoa, the presence of SAS6L in species correlates largely with the presence of SAS-6 and the capability of cilia formation (Fig. 5.4). Interestingly, SAS6L could not be identified in animals or their close relatives, such as the choanoflagellate *Monosiga brevicollis* (collectively known as the Holozoa). The identification of SAS6L in the fungus *Batrachochytrium dendrobatidis*, suggests that the protein was present at the root of the unikonts and that the lack of identifiable SAS6L orthologues in animals represents a specific loss near the root of the Holozoa. The existence of SAS6L and SAS-6 in unikonts and all supergroups included in the bikonts (meaning in every lineage branching from the last common ancestor of all eukaryotes) suggested that the split of the SAS-6 and SAS6L subfamilies pre-dates the split of the supergroups and that the last common ancestor of all eukaryotes possessed a SAS6L protein.

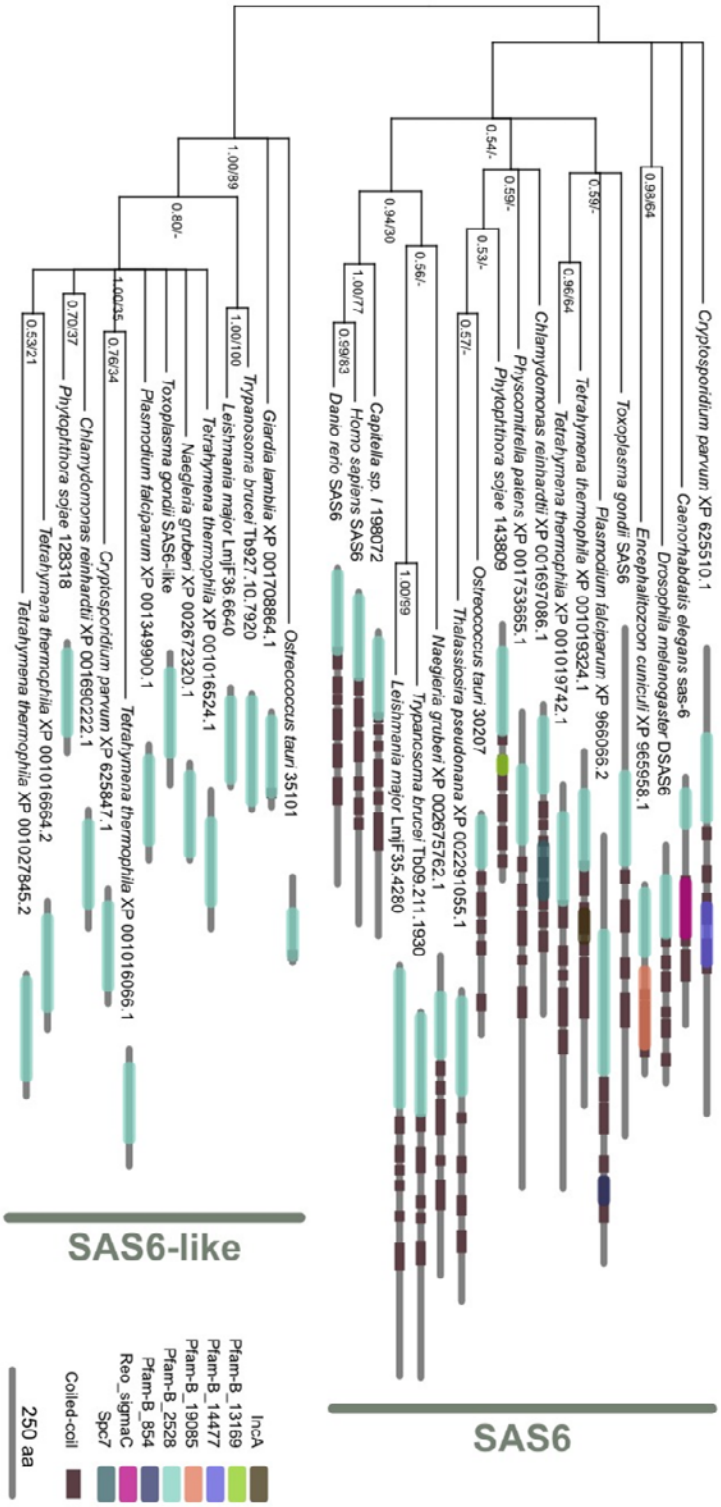

Figure 5.1 **SAS-6 and SAS6L proteins form two distinct subfamilies.** The hidden Markov model defining Pfam-B_2528 was used to survey the predicted proteomes of 43 diverse eukaryotes (HMMER3.0; hmmer.janelia.org). 69 proteins containing the domain (e-value < 0.001) were extracted, trimmed to the conserved domain and aligned by MAFFT v6.811b adopting the E-INS-I strategy. Bayesian phylogenies were inferred from four runs of the metropolis-coupled Markov chain Monte Carlo method implemented in the program MrBayes3.1.2. Maximum likelihood support for the inferred topology was generated from 100 bootstraps replicates of the data using PhyML3.0. Analysis was done by Bill Wickstead.

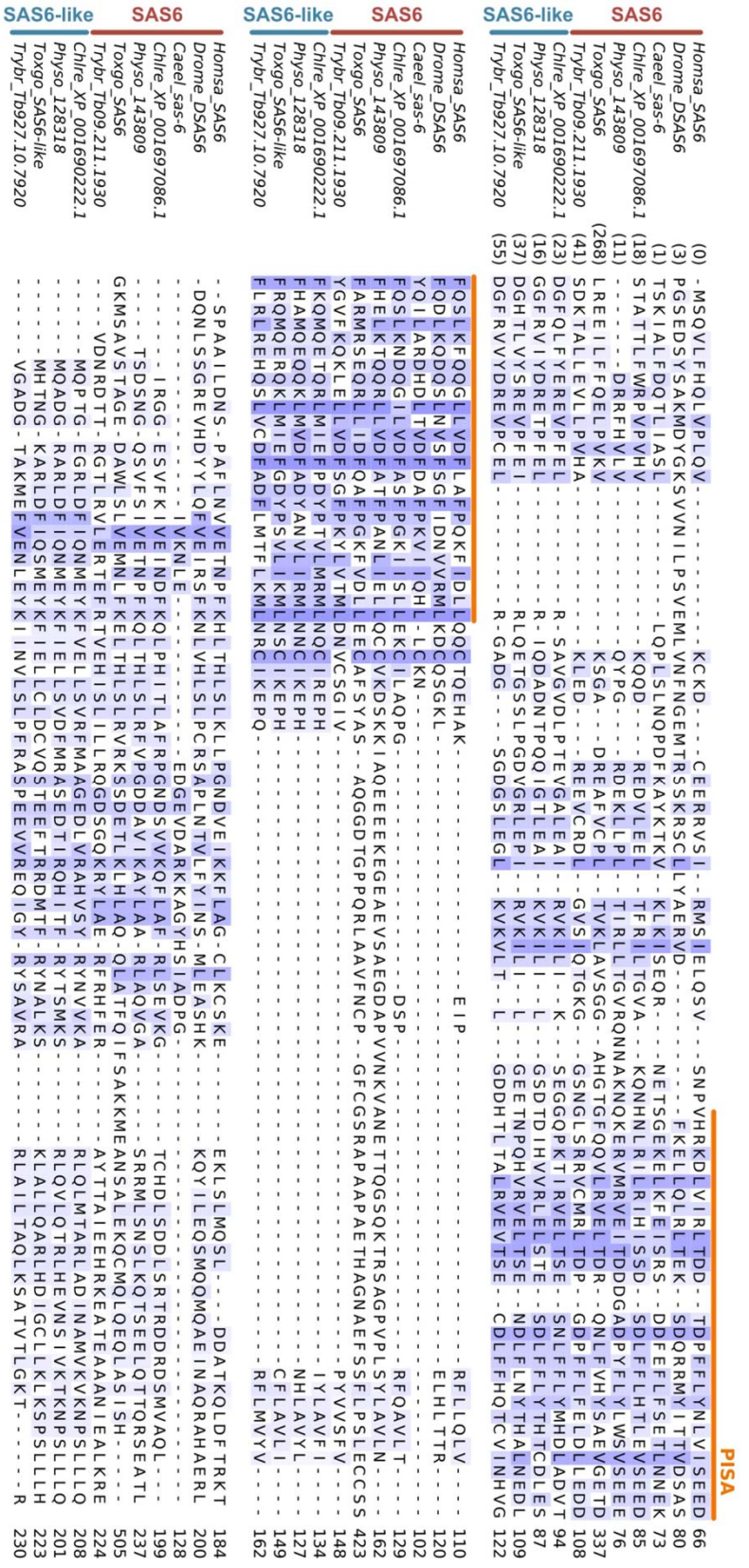

Figure 5.2 **SAS6L and the N-terminus of SAS-6 share a conserved sequence.** Conserved sequence of SAS-6 and SAS6L proteins of diverse eukaryotes aligned by MAFFT v6.811b adopting the E-INS-I strategy. Pisa domain is highlighted in orange above the sequence. Homsa = *Homo sapiens*. Drome = *Drosophila melanogaster*. Caeel = *Caenorhabditis elegans*. Chlre = *Chlamydomonas reinhardtii*. Physo = *Phytophthora sojae*. Toxgo = *Toxoplasma gondii*. Trybr = *Trypanosma brucei*. Analysis was done by Bill Wickstead.

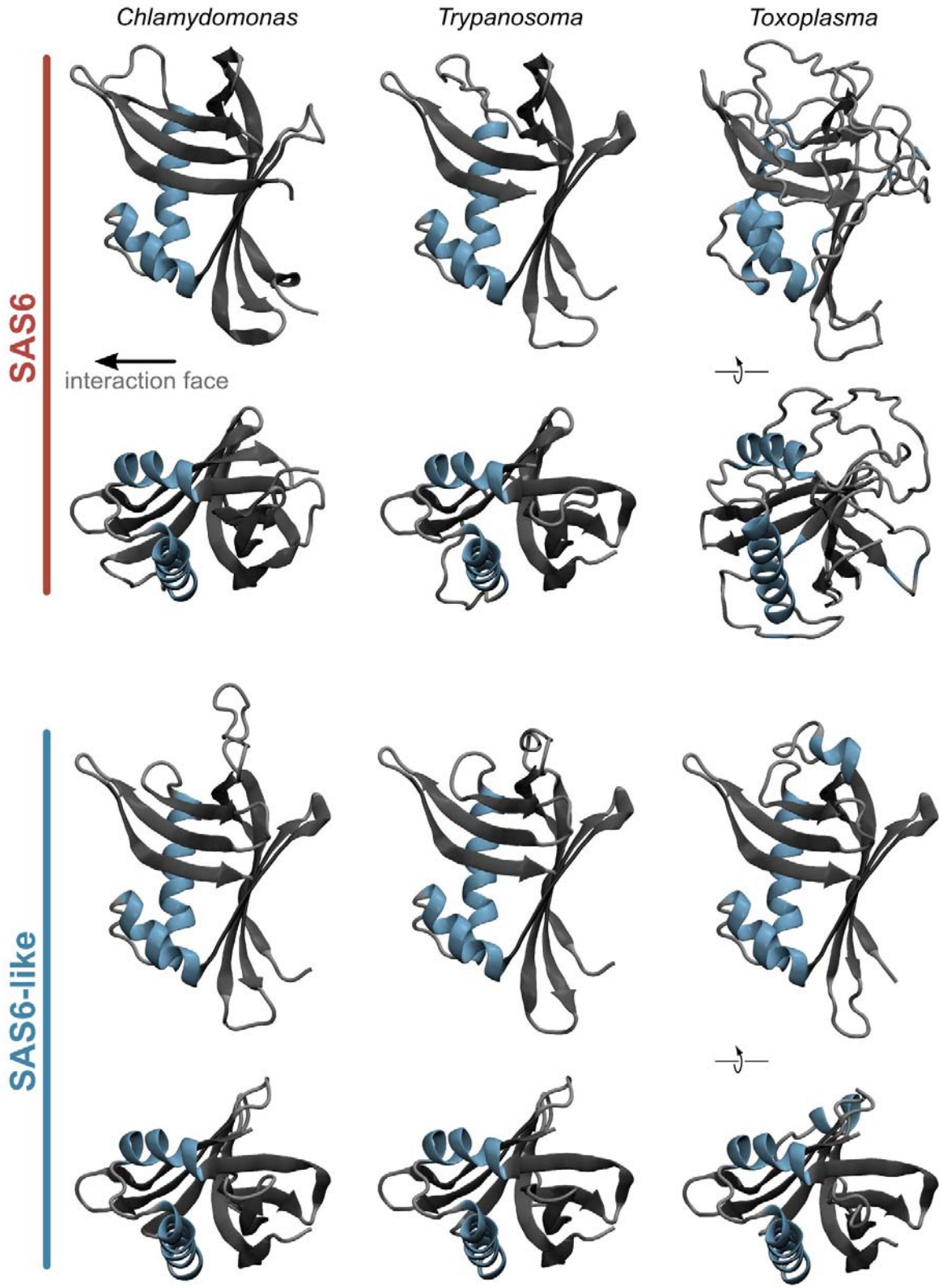

Figure 5.3 **The structure of SAS6L is predicted to be similar to the structure of the N-terminus of SAS-6.** Homology modelling suggested that SAS6L proteins can adopt structures very similar to those seen for the N-terminus of SAS-6. Analysis was done by Bill Wickstead.

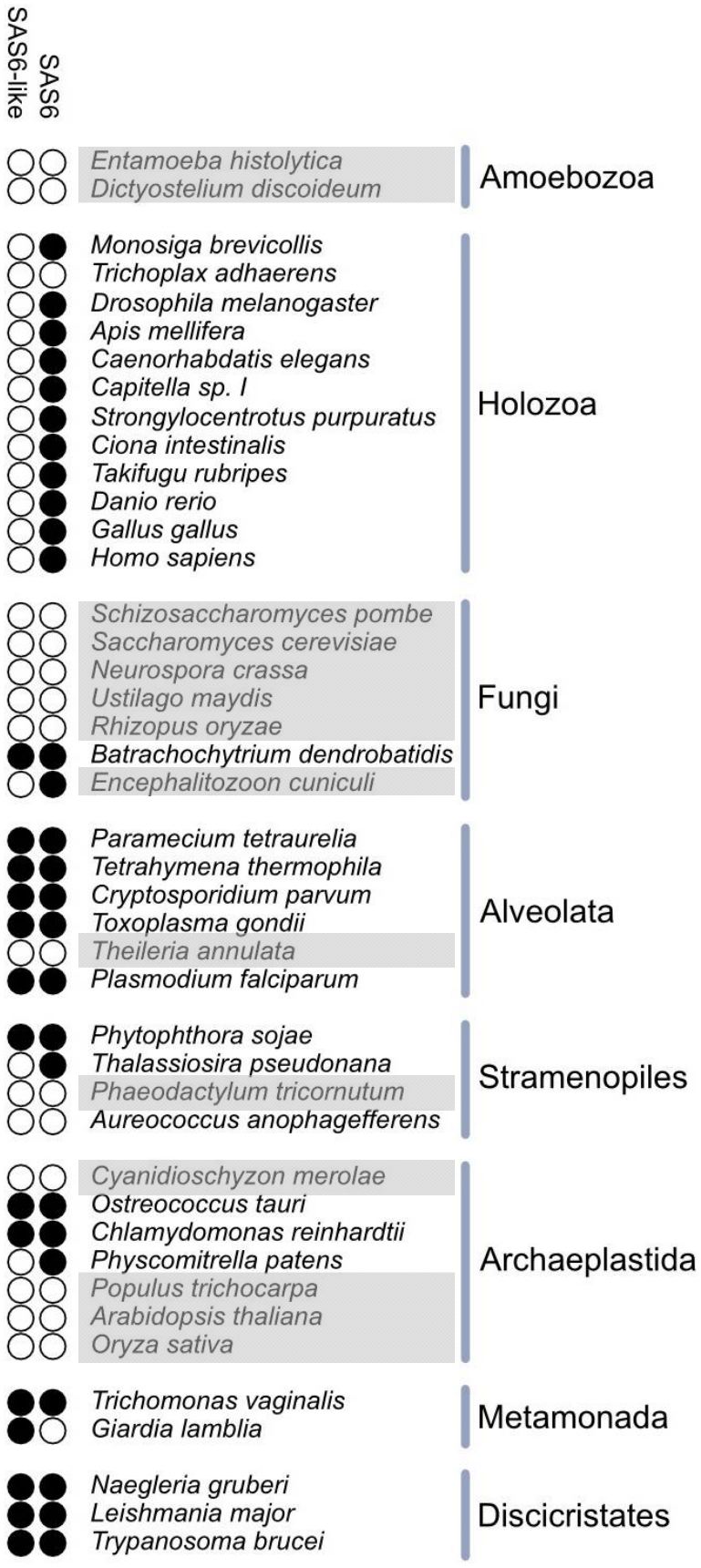

Figure 5.4 **SAS6L is specific to species that form cilia but it was lost from Holozoa.** The predicted proteomes of 43 eukaryotic species were surveyed for homologues of SAS-6 and SAS6L using the hidden Markov model defining Pfam-B_2528. Black circle indicates presence of the protein. White circle indicates absence/undetectablity. Grey background for non-ciliated species. Analysis was done by Bill Wickstead.

5.4 SAS6L-Y localises to the basal plate and around the exit of the flagellum from the pocket

SAS6L in *T. brucei* is encoded by Tb927.10.7920. It is predicted to be a 230 amino acid protein with a molecular weight of 26kDa and an isoelectric point of pH 5.4, which is smaller and more acidic than SAS-6. In order to study the protein, I generated a procyclic form cell line expressing *T. brucei* SAS6L with a C-terminal YFP-Ty tag (SAS6L-Y) from an endogenous *SAS6L* locus. Additionally, another cell line was generated which expressed *T. brucei* SAS6L with a C-terminal Myc-His-YFP-TAP tag (SAS6L-Y-TAP) after induction with doxycycline from an ectopic locus.

Examination of preparations of cells expressing SAS6L-Y from the endogenous locus revealed the localisation of the protein to three sites: (1) to the beginning of the axoneme (distal of the basal body) as a prominent dot, (2) to the pro-basal body depending on the cell cycle stage, and (3) to the exit of the flagellum from the pocket as a weaker signal in shape of a half-ring with an extension directed towards the anterior end of the cell (Fig. 5.5).

(1) Localisation to the basal plate

To determine the site of the prominent SAS6L-Y dot, cells were immunolabelled with the basal body markers BBA4 and YL1/2. The BBA4 antibody labels an unknown antigen at the proximal end of the basal body (Woodward et al., 1995). The YL1/2 antibody recognises tyrosinated α-tubulin which locates at the posterior end of the subpellicular MT cytoskeleton and around the distal appendages of the basal body (Kilmartin et al., 1982; Stephan et al., 2007). The labelling of both antibodies was proximal of the SAS6L-Y-TAP signal (Fig. 5.6 A,B). The SAS6L-Y dot was also distal to Ty-mCherry-WDR16, which localises to the transition zone (see Chapter 7 about WDR16, Fig. 5.5). The distance between the prominent SAS6L dot and YL1/2 labelling measured 520 $\pm$ 34nm (Fig. 5.6 C). This localisation is consistent with the position of the basal plate.

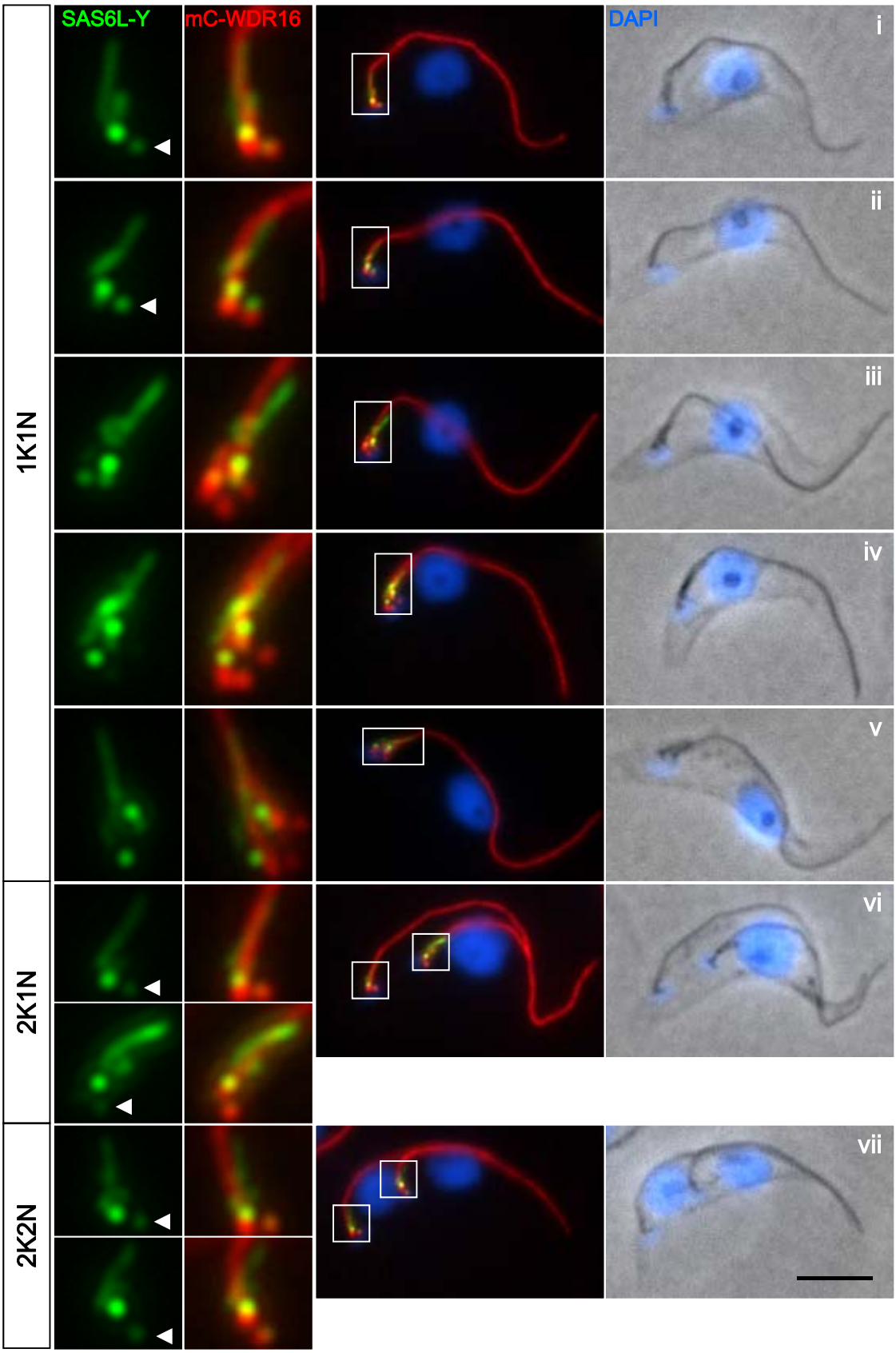

Figure 5.5 **Overview over localisation of SAS6L-Y throughout the cell cycle: SAS6L-Y localises distal to the BB as a prominent dot, to the pBB before BB duplication** (white arrow head) **and to a site around the flagellar collar.** *T. brucei* SAS6L C-terminally tagged with YFP-Ty (SAS6L-Y, green) was expressed from an endogenous *SAS-6* locus in procyclic form cells which additionally expressed Ty-mCherry-WDR16 as marker for the axoneme, BB and pBB. Cells were detergent-extracted and fixed in methanol. DNA was labelled with DAPI (blue). Scale bar: 5μm.

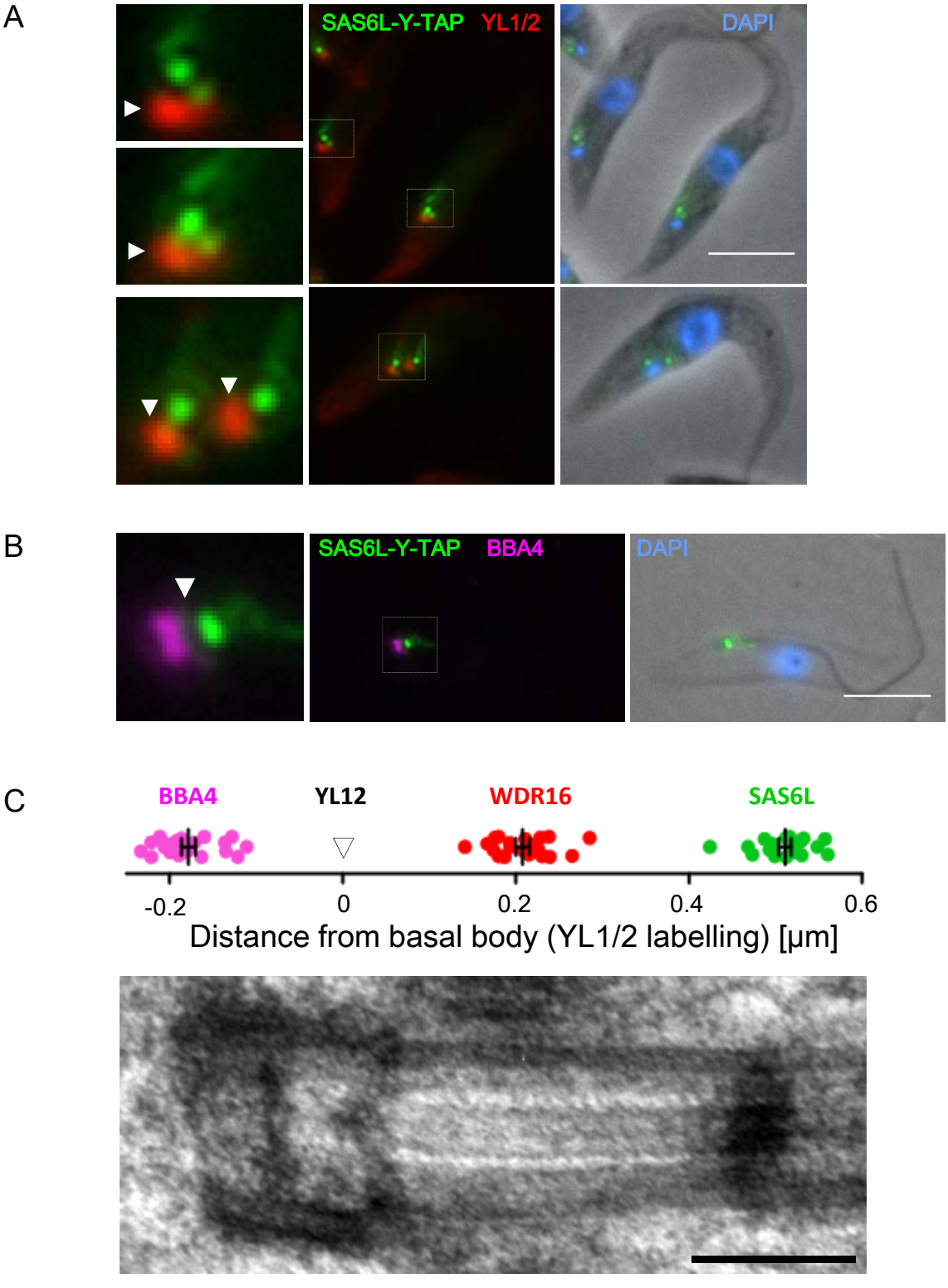

Figure 5.6 **SAS6L-Y localises to the basal plate.** (A) Whole cell preparation of cells expressing SAS6L-Y-TAP (green) 16h post induction was immunolabelled with YL12 (red). (B) Cytoskeleton preparation of cells expressing SAS6L-Y-TAP (green) 16h post induction was immunolabelled with BBA4. (A,B) DNA was labelled with DAPI (blue). Insets show basal body area. White arrow head points towards the BB (= site of YL1/2 labelling, reference point for measurements). White scale bar: 5µm. (C) Distance measurements in relation to YL1/2, a basal body marker labelling the appendages. This showed that SAS6L localises to a site consistent with the axonemal basal plate. TEM image of a longitudinal flagellum section. Length of BB ~200nm. Length of TZ ~500nm. Black scale bar: 200 nm.

(2) Localisation at the pro-basal body

SAS6L-Y localised to the pro-basal body late during its assembly process. The SAS6L-Y signal at this site gradually established in 2K1N and 2K2N cells (Fig. 5.5 vi,viii), and was strongest in 1K1N cells before basal body duplication (Fig. 5.5 i,ii). The appearance of the SAS6L-Y signal around the pro-basal body might reflect the accumulation of new material required late in basal body assembly or maturation.

(3) Localisation around the exit of the flagellum from the pocket

The SAS6L-Y signal around the exit of the flagellum from the pocket was present throughout the cell cycle. The shape of the YFP fluorescence as half-ring and its position suggested that SAS6L-Y localises around the collar of the flagellar pocket (Fig. 5.5). The extension of the half-ring followed the flagellum attachment zone (FAZ) closely, and is most likely in the cell body and not the flagellum (Fig. 5.7 A,B, 5.5). However, it was unclear what this signal could represent on a structural level.

To investigate SAS6L at this site, I tested whether it colocalises with centrin and SAS-4, two proteins known as basal body components with additional localisation sites in the area around the flagellum exit from the pocket. Centrin2 localises above the Golgi apparatus and marks a phenomenon called the bilobe (Esson et al., 2012; He et al., 2005). Immunolabelling of SAS6L-Y-TAP expressing cells with 20H5, an anti-centrin antibody, showed that the two proteins did not colocalise but that SAS6L-Y-TAP was in close proximity above the centrin2 labelling (Fig. 5.8 A,B).

SAS-4 is another basal body protein that was observed in that area during the formation of the new axoneme (see Chapter 6 about SAS-4). Fluorescence microscopy analysis of cells expressing SAS6L-Y-TAP and Ty-mCherry-SAS-4 showed that the localisation of the two proteins was distinct but in close proximity (Fig. 5.8 C).

A

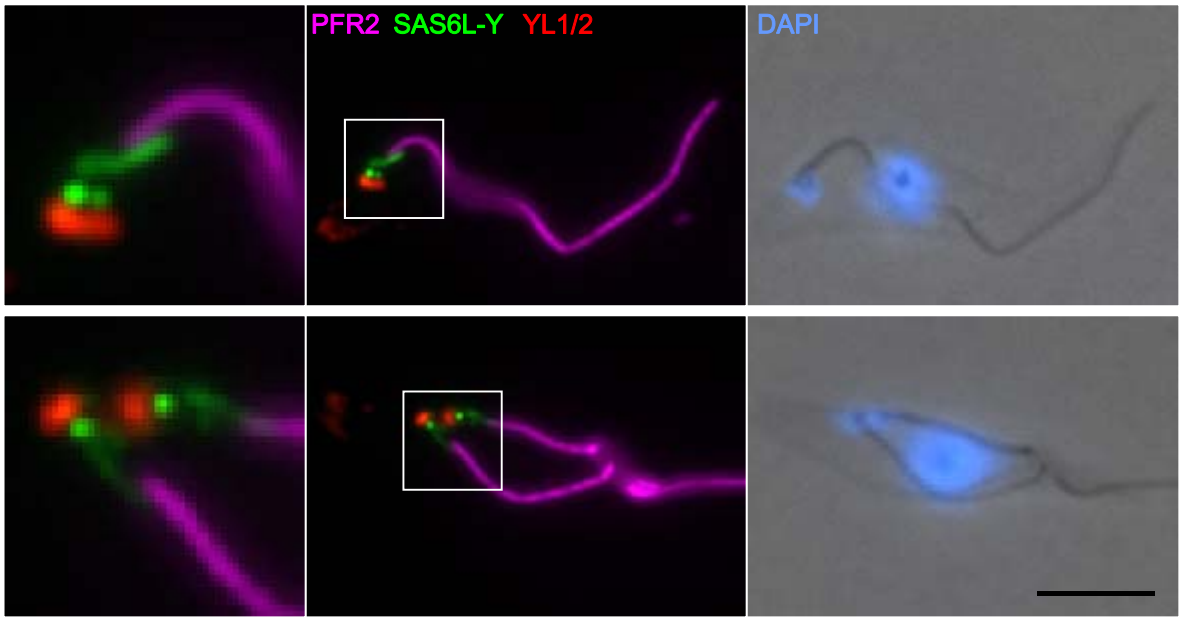

B

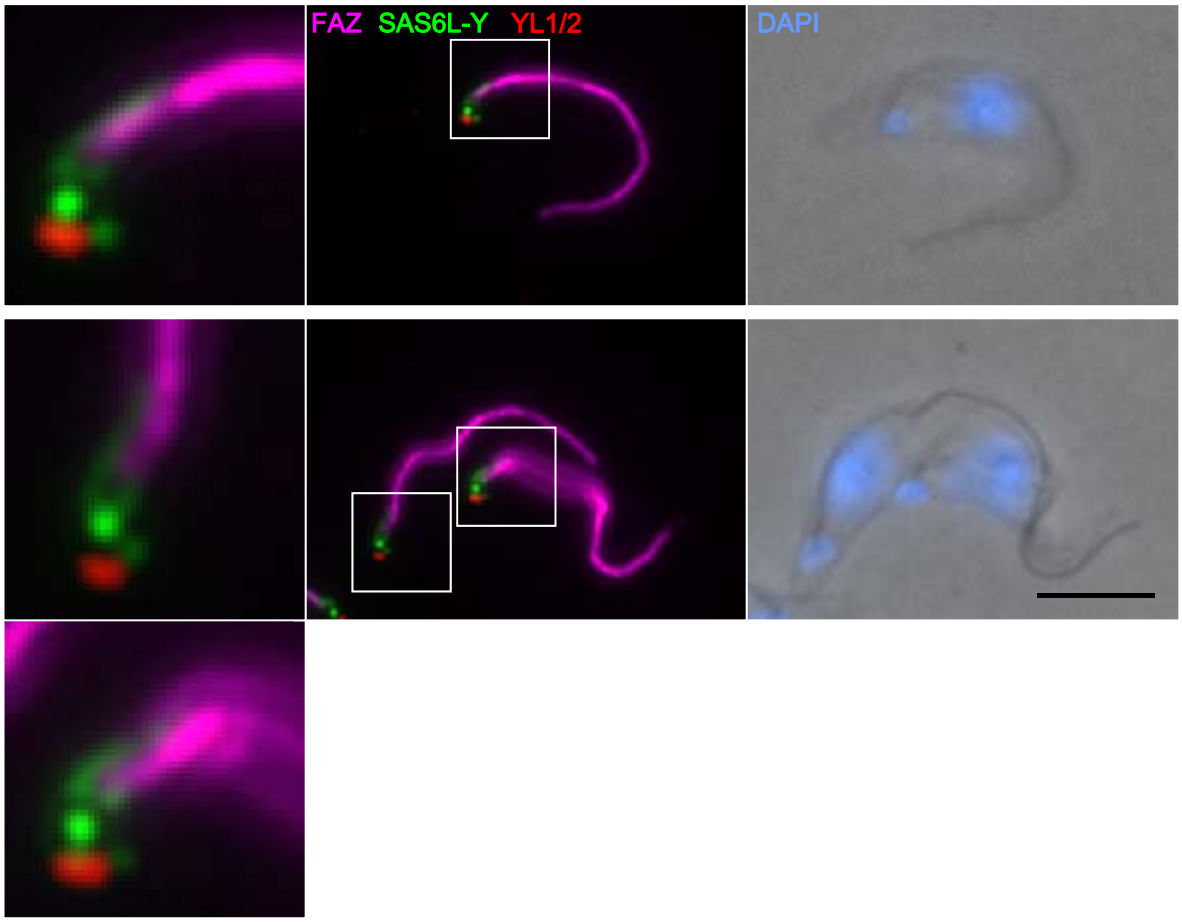

Figure 5.7 **The SAS6L-Y extension follows the course of the FAZ.** Cytoskeleton preparation of cells expressing SAS6L-Y (green) was immunolabelled with YL1/2 (anti-tyrosinated α-tubulin, red) and (A) L8C4 (anti-PFR2, magenta) or (B) L3B2 (anti-FAZ, magenta). DNA was labelled with DAPI (blue). Insets show the area around the exit of the flagellum from the pocket. Scale bar: 5μm.

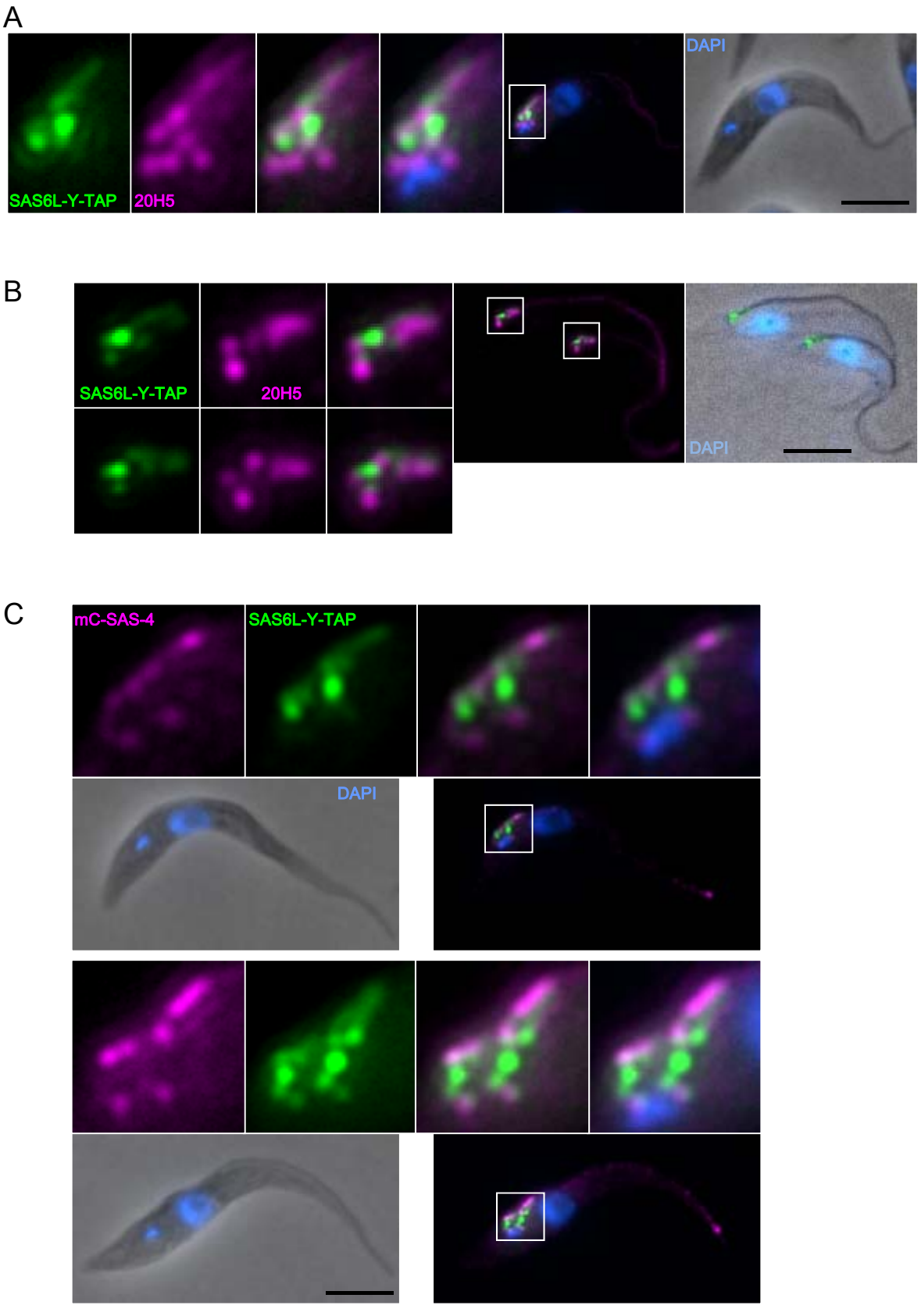

Figure 5.8 **The SAS6L localisation around the flagellum exit from the pocket is distinct from the bilobe and from the SAS-4 localisation.** (A) Whole cell and (B) cytoskeleton preparations of cells expressing SAS6L-Y-TAP (green) 16h post induction were immunolabelled with 20H5 (anti-centrin1/2, bilobe, magenta). (C) Whole cell preparation of cells expressing SAS6L-Y-TAP (green) 16h post induction and Ty-mCherry-SAS-4 (magenta). DNA was labelled with DAPI (blue). Insets show the area around the flagellum exit from the pocket. Scale bar: 5μm.

5.5 Overexpression of SAS6L results in the formation of SAS6L-Y-TAP filaments

In order to analyse the function of SAS6L, a cell line overexpressing SAS6L with a C-terminal Myc-His-YFP-TAP tag was generated (as mentioned above). Western blot analysis of whole cell extracts using anti-GFP antibodies confirmed the expression of SAS6L-Y-TAP after induction with doxycycline (Fig. 5.9 A). Localisation of SAS6L-Y-TAP 16h after induction is consistent with that observed for SAS6L-Y expressed from an endogenous *SAS6L* locus. However, longer induction of SAS6L-Y-TAP resulted in formation of fluorescent filaments in 22% of the population after 24h, 27% after 36h, and 36% after 48h (n=200 per time point, Fig. 5.9 B). Cell morphology appeared normal despite filament formation. Counts of cell numbers over 5 days did not reveal an effect of SAS6L-Y-TAP over-expression and filament formation on the growth rate of the population (Fig. 5.9 C).

5.6 SAS6L-Y-TAP filaments originate from the region of the flagellar collar

SAS6L-Y-TAP filaments showed a wide variety of shapes. To investigate the nucleation site and the path of the filaments, filament forming cells 36h after induction were examined by fluorescence microscopy.

The nucleation site of the filaments was in the vicinity to the proximal end of the flagellum (Fig. 5.10). As some filament forming cells showed the distinct basal plate dot separate from the filament, the nucleation site was most likely from the region of the flagellar collar rather than the

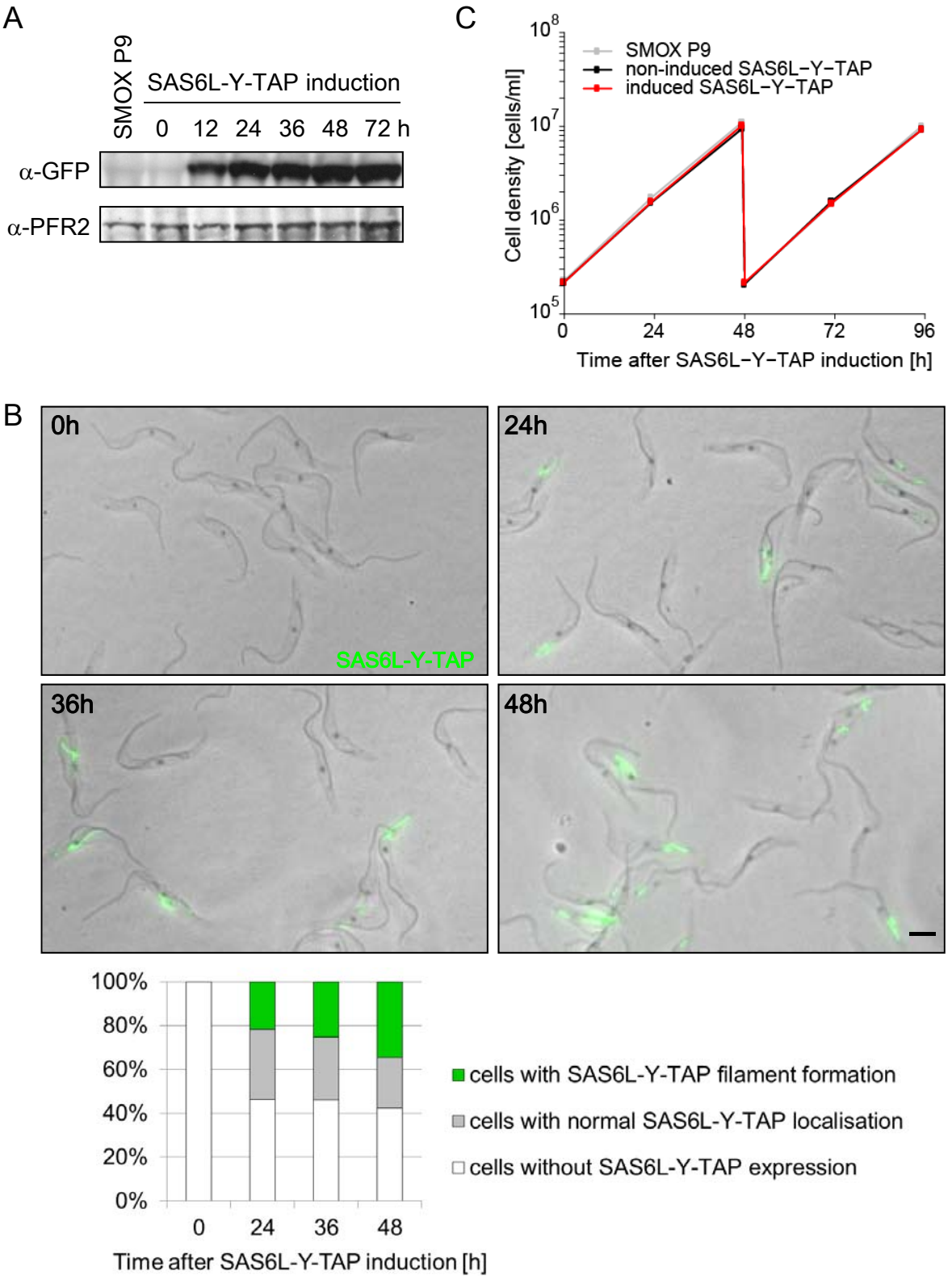

Figure 5.9 **Overexpression of SAS6L-Y-TAP.** (A) Immunoblot analysis of cells given above image with anti-GFP antibody showing that the cells expressed SAS6L-Y-TAP after induction with Doxycycline and that amount of the protein increased over time. Loading control: L8C4 (anti-PFR2). (B) Fluorescence microscopy analysis at different time points after SAS6L-Y-TAP induction showing the formation of fluorescent filaments in some cells. Scale bar: 5μm. Graph shows percentage of cells with and without SAS6L-Y-TAP expression, and frequency of filament formation. (C) Population growth measured every 24h over 96h with dilution every 48h showed that SAS6L over-expression and filament formaiton did not cause a change in the population growth rate.

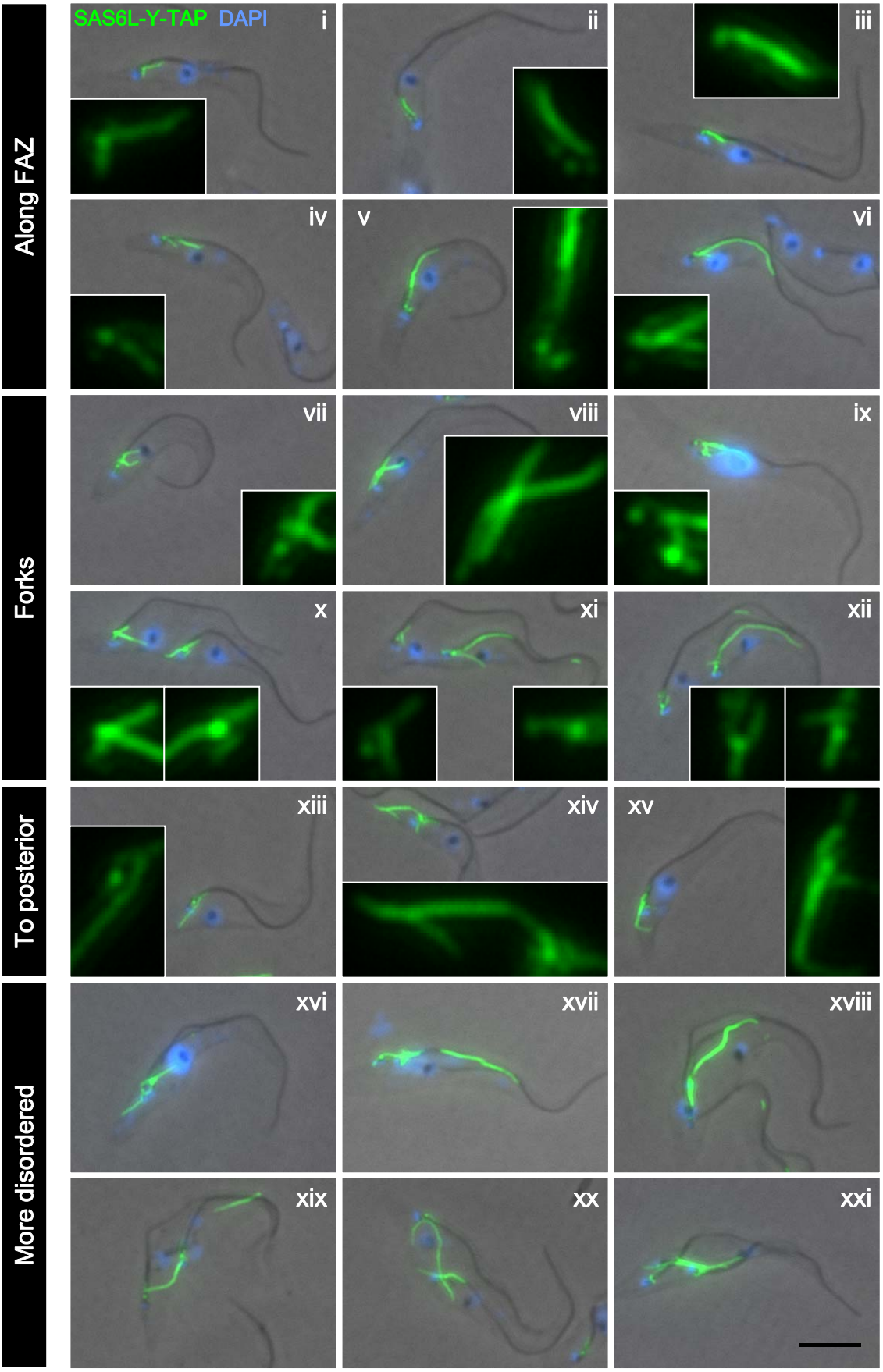

Figure 5.10 **Overview of SAS6L-Y-TAP filament formation.** Cytoskeleton preparation of cells 36h after SAS6L-Y-TAP (green) induction. DNA was labelled with DAPI (blue). Examples showing the variety of shapes of SAS6L-Y-TAP filaments and sites in the cell. Insets show filaments of the respective cell. Scale bar: 5μm.

basal plate area (Fig. 5.10 i-v). This is further supported by the assumption that SAS6L at the basal plate is inside the axoneme whereas the filaments were in the cell body. SAS6L-Y-TAP filaments were also detected in other places in the cell, for example at the anterior tip of the cell body or somewhere along the FAZ (Fig. 5.10 xi,xii,xviii). These fragments might, however, have broken off the initial filament, rather than having been nucleated at these sites.

Filament progression could be typically detected along the FAZ towards the anterior direction (Fig. 5.10 i-vi). Forking of filaments with one part of the structure not running along the FAZ was another frequent phenomenon (Fig. 5.10 vii-xii). Filaments going from the vicinity of the proximal end of the flagellum towards the posterior direction of the cell (Fig. 5.10 xiii-xv), and filaments following different, more complex patterns were also observed (Fig. 5.10 xvi-xxi). Most likely, these structures had experienced a longer period of filament growth starting in previous cell generations.

5.7 SAS6L-Y-TAP filaments are not microtubule-based

To test whether the SAS6L-Y-TAP filaments were microtubules decorated with the SAS6L protein, I used an established method to depolymerise subpellicular microtubules. Cytoskeleton preparations of detergent-extracted cells were treated with calcium ions at a concentration that destabilised subpellicular MTs but not axonemal MTs. SAS6L-Y-TAP filaments were resistant to calcium extraction suggesting a composition distinct from microtubules (Fig. 5.11 A). However, since the protocol depolymerised only subpellicular but not the axonemal microtubules, the possibility remained that the filaments represent a more stable version of microtubules or that SAS6L-Y-TAP is MT-stabilising. Immunolabelling of calcium-treated cytoskeleton preparations with TAT1 (anti-α-tubulin antibody) confirmed that SAS6L-Y-TAP filaments did not contain α-tubulin (Fig. 5.11 B).

The filaments neither contained SAS-4 nor induce its localisation next to the filaments

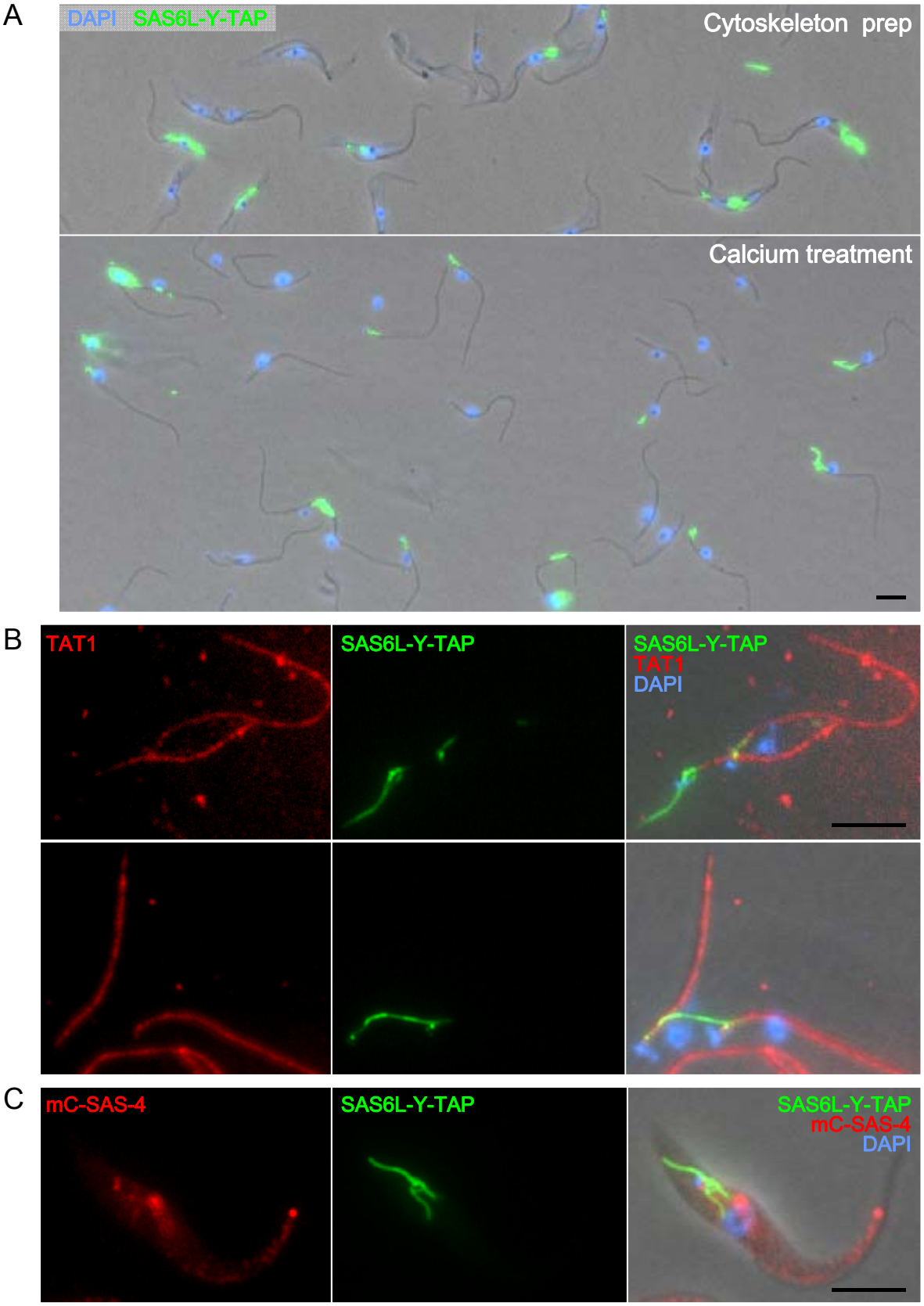

Figure 5.11 **SAS6L-Y-TAP filaments are not microtubule-based.** (A) Cells 36h after SAS6L-Y-TAP (green) induction were detergent-extracted (cytoskeleton prep) and treated with calcium, showing that the SAS6L-Y-TAP filaments are calcium-resistant. (B) Calcium-treated cytoskeleton preparation immunolabelled with TAT1 (anti-α-tubulin, red) showing that SAS6L-Y-TAP filaments do not contain tubulin. (C) Whole cell preparation of cells expressing SAS6L-Y-TAP (green) and Ty-mCherry-SAS-4 (red) demonstrating that filaments do neither contain SAS-4 nor induced its accumulation around it. DNA was labelled with DAPI (blue). Scale bar: 5μm.

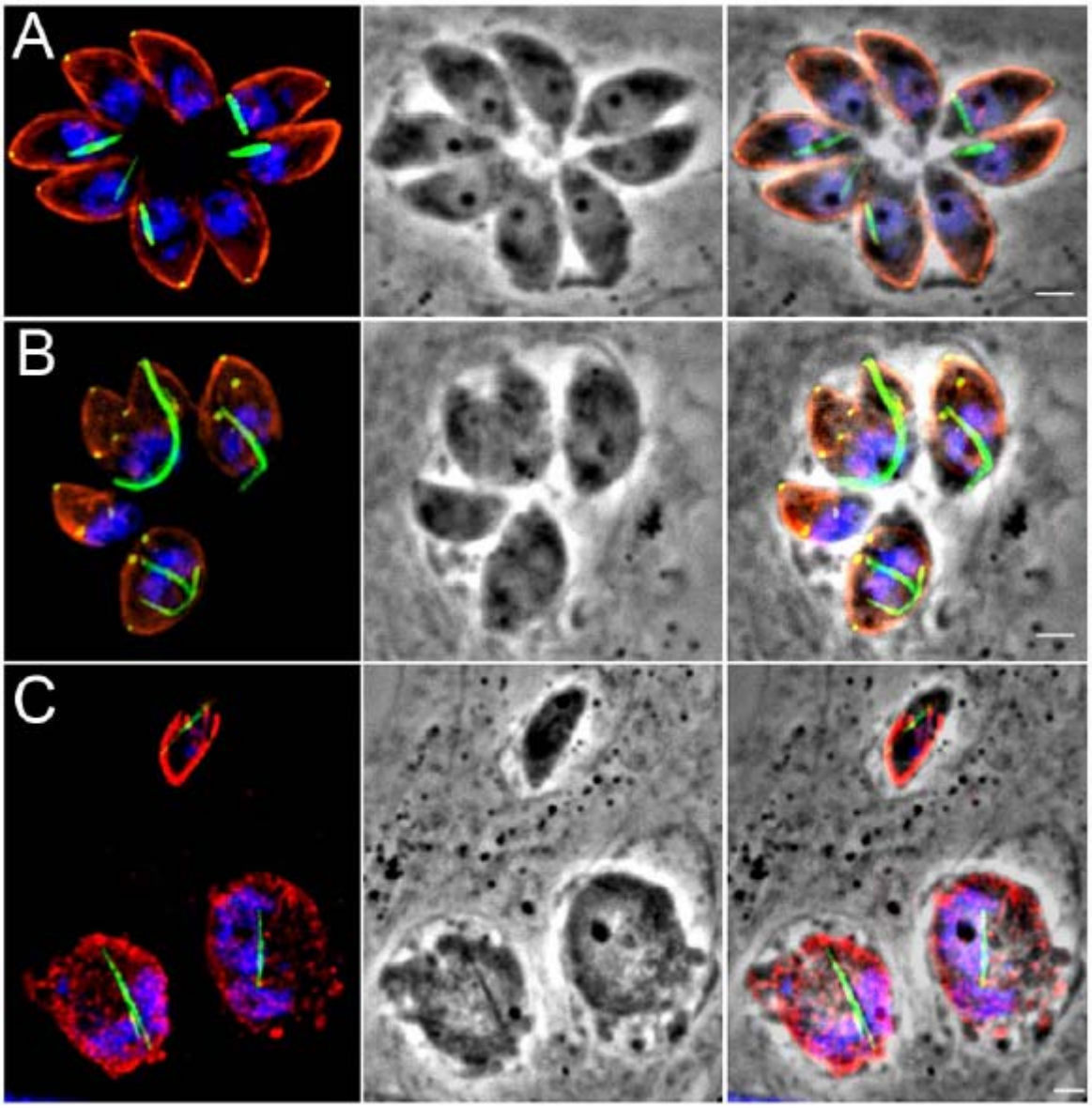

Figure 5.12 **The ectopic expression of TgSAS6L-YFP leads to the formation of filaments in *Toxoplasma gondii*.** Ectopic expression of TgSAS6L-YFP under the control of an α1-tubulin promoter led to the formation of TgSAS6L-YFP filaments. Tubulin (red), TgSAS6L-YFP (green) and DNA (blue). (A) A subset of intracellular Toxoplasma tachyzoites possessed TgSAS6L-YFP filaments in the cytoplasm. (B) Cytoplasmic filaments seemed to interfere with completion of cytokinesis in some parasites. (C) After treatment of the parasites with oryzalin, which depolymerises microtubules, TgSAS6L-YFP filaments were still present. Scale bars: 2 µm.
These experiments were performed by our colaborators Jessica Cruz de Leon and Naomi S. Morrissette at the University of California, Irvine.

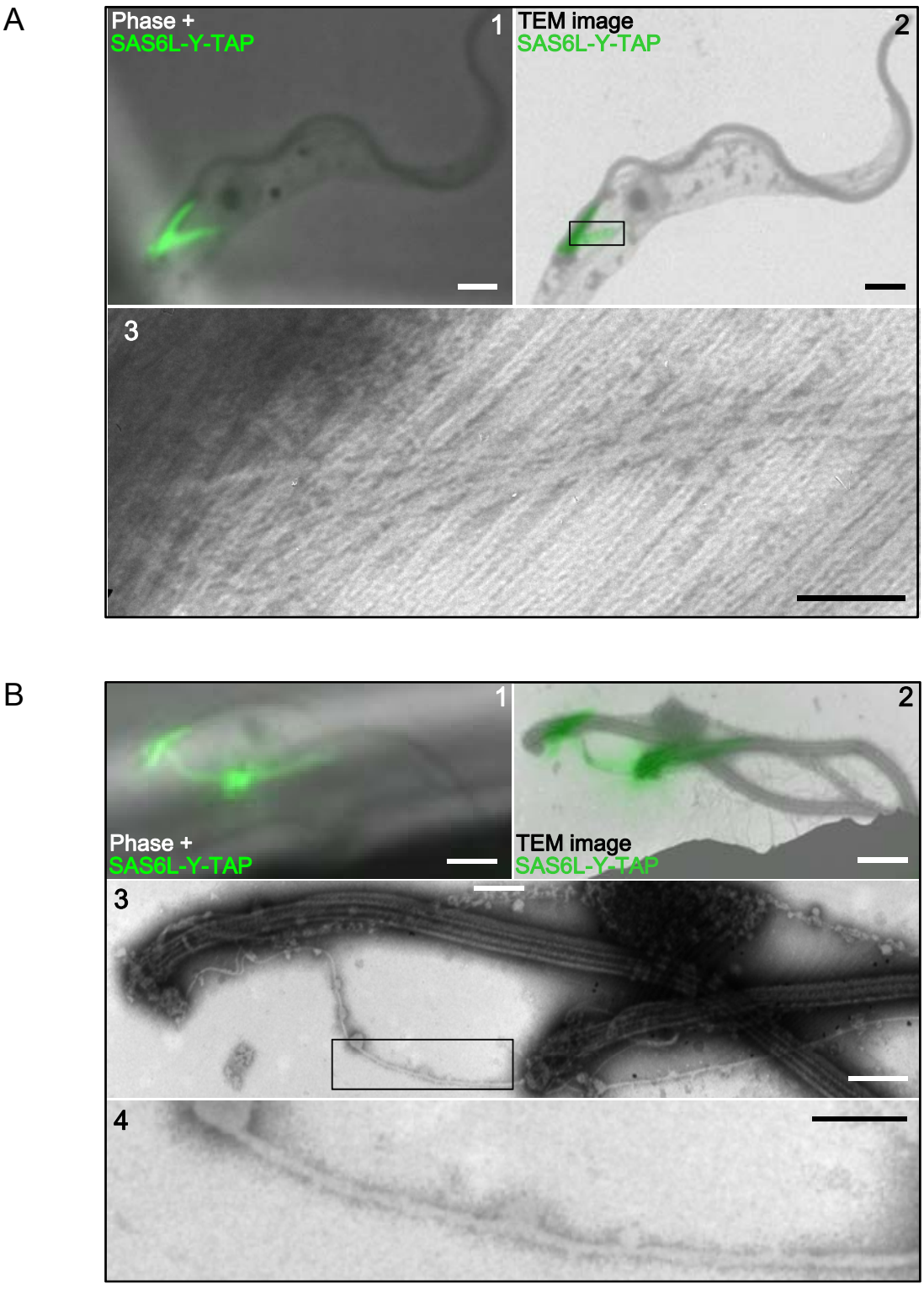

Figure 5.13 **Ultrastructure of the SAS6L-Y-TAP filaments.** Correlative microscopy of SAS6L-Y-TAP filaments with fluorescence and electron microscopy. (A) The same cell cytoskeleton is shown by phase with epifluorescence in (A1) and by TEM with YFP signal overlaid (A2). This allows the unambiguous identification of the SAS6L-Y-TAP filaments (A3). Scale bars: 2µm (A1,2), 200nm (A3). (B) The same SAS6L-Y-TAP filament in calcium-treated cytoskeleton preparation by phase with epifluorescence in (B1) and by TEM with YFP signal overlaid (B2). Scale bars: 2µm (B1,2), 500nm (B3), 200nm (B4).

(Fig. 5.11 C). The same was the case for centrin-1 and -2 (data not shown).

Our collaborators, J. Cruz de Leon and N. Morrissette, showed that ectopic expression of *Toxoplasma gondii* SAS6L with the C-terminus fused to YFP resulted also in the formation of filaments in the parasite (Fig. 5.12).

5.8 Ultrastructure of SAS6L-Y-TAP filaments

In order to confidently identify SAS6L-Y-TAP filaments and investigate their ultrastructure, I developed a microscopy approach that correlated the native YFP signal to the TEM image of the same cell. Cytoskeleton preparations of detergent-extracted cells were mounted onto formvar-coated marked grids, and analysed by fluorescence microscopy followed by TEM. This showed that SAS6L-Y-TAP filaments had a distinct appearance from microtubules. Whereas microtubules were hollow with a white border, the filaments did not look hollow and not as rigorously straight (Fig. 5.13 A). It also showed that a single YFP line could represent several filaments.

To see the ultrastructure of the filaments more clearly, the subpellicular microtubules were depolymerised by treatment with calcium ions. This revealed SAS6L-Y-TAP filaments with a twisted/helical appearance and an approximate width of ~20-25nm (Fig. 5.13 B). This size is similar to the diameter of ring polymers formed by N-terminal fragments of SAS-6 and to the predicted dimensions for the hub of the cartwheel in models based on the crystal structure of SAS-6 (Kitagawa et al., 2011c; van Breugel et al., 2011).

5.9 Summary

Here I describe a novel family of proteins with similarity to the N-terminal proportion of SAS-6. The SAS6L family was shown to be most likely ancestral to all eukaryotes but lost near the root of

Holozoa. I showed localisation of YFP-tagged SAS6L to a position consistent with the basal plate and around the exit of the flagellum from the pocket in *T. brucei*. Ectopic overexpression of the protein led to the formation of long cytoplasmic filaments that most likely originated from the latter localisation site.

CHARACTERISATION OF TRYPANOSOMAL SAS-4

6.1 Preface

In Chapter 3, the centriolar protein SAS-4 was identified as part of a core set of proteins that is conserved in the majority of cilia-producing species but not in species without cilia. This conservation pattern suggested that SAS-4 is important in the centriole assembly pathway across eukaryotes. Like SAS-6, SAS-4 was initially identified in two independent RNAi screens for cell division defects in *Caenorhabditis elegans* embryos (Kirkham et al., 2003; Leidel and Gonczy, 2003). SAS-4 is essential for centriole and/or basal body assembly in all species studied to-date, which include *C. elegans*, *Drosophila melanogaster*, *Homo sapiens* and *Paramecium tetraurelia* (Basto et al., 2006; Gogendeau et al., 2011; Kirkham et al., 2003; Kleylein-Sohn et al., 2007; Leidel and Gonczy, 2003). EM tomography of centrioles in *C. elegans* suggested that the protein is required for the attachment of microtubules to the central tube, a centriole part which is still assembled in SAS-4 depleted cells (Pelletier et al., 2006). Overexpression of CPAP, the human SAS-4 homologue, leads to elongated centriolar microtubules (Kohlmaier et al., 2009; Schmidt et al., 2009; Tang et al., 2009). During the assembly of basal bodies of *P. tetraurelia* SAS-4 is also required, though the exact stage is unclear. In this species, however, SAS-4 overexpression leads

to supernumerary germinative disks instead of elongated MTs (Gogendeau et al., 2011). For a complete introduction to SAS-4 see Chapter 1.

Despite the presence of SAS-4 in diverse eukaryotes, the protein has been studied mainly in animals with the exception of one study in *P. tetraurelia* (Gogendeau et al., 2011). My aim in this chapter is to study the role of SAS-4 in the protozoan *T. brucei*, which is distantly-related to either animals or ciliates, and where basal bodies serve the purpose of flagellum nucleation throughout the cell cycle and never participate in centrosome or spindle pole organisation. This allows studying the protein's role in the basal body without being disturbed by mitosis defects.

6.2 Bioinformatic analysis of *T. brucei* SAS-4

In the bioinformatic study of centriole components in Chapter 3, two predicted proteins in *T. brucei*, Tb11.02.0810 and Tb11.02.3880, were found to be similar to SAS-4 proteins in other organisms. Alignment of the sequences of the two predicted *T. brucei* proteins with those of other SAS-4 homologues of other eukaryotes showed that the most sequence conservation in SAS-4 proteins was found in the C-terminal part which includes the Tcp10 domain (Islam et al., 1993). The sequence of Tb11.02.0810, but not of Tb11.02.3880, aligned well with the region comprising the Tcp10 domain and displayed conservation in the majority of the residues conserved in eukaryotic SAS-4 proteins (Fig. 6.1 A). Analysis of the protein domain architecture showed that SAS-4 proteins (with the exception of the divergent SAS-4 of *C. elegans)* possessed a C-terminal Tcp10 domain, as did Tb11.02.0810 but not Tb11.02.3880 (Fig. 6.1 B). However, Tb11.02.0810 lacked the Pfam-B_19564 domain, a predicted domain with unknown function, which is present in other SAS-4 proteins. Whether the lack of this domain has any functional implications for Tb11.02.0810 is not known. Another difference is that Tb11.02.0810, like the predicted SAS-4 in *C. reinhardtii*, possessed a Pfam-B_244 domain, which was not detected in SAS-4 in unikonts. The function of this domain or the consequence of its presence is not known either. Collectively, these data

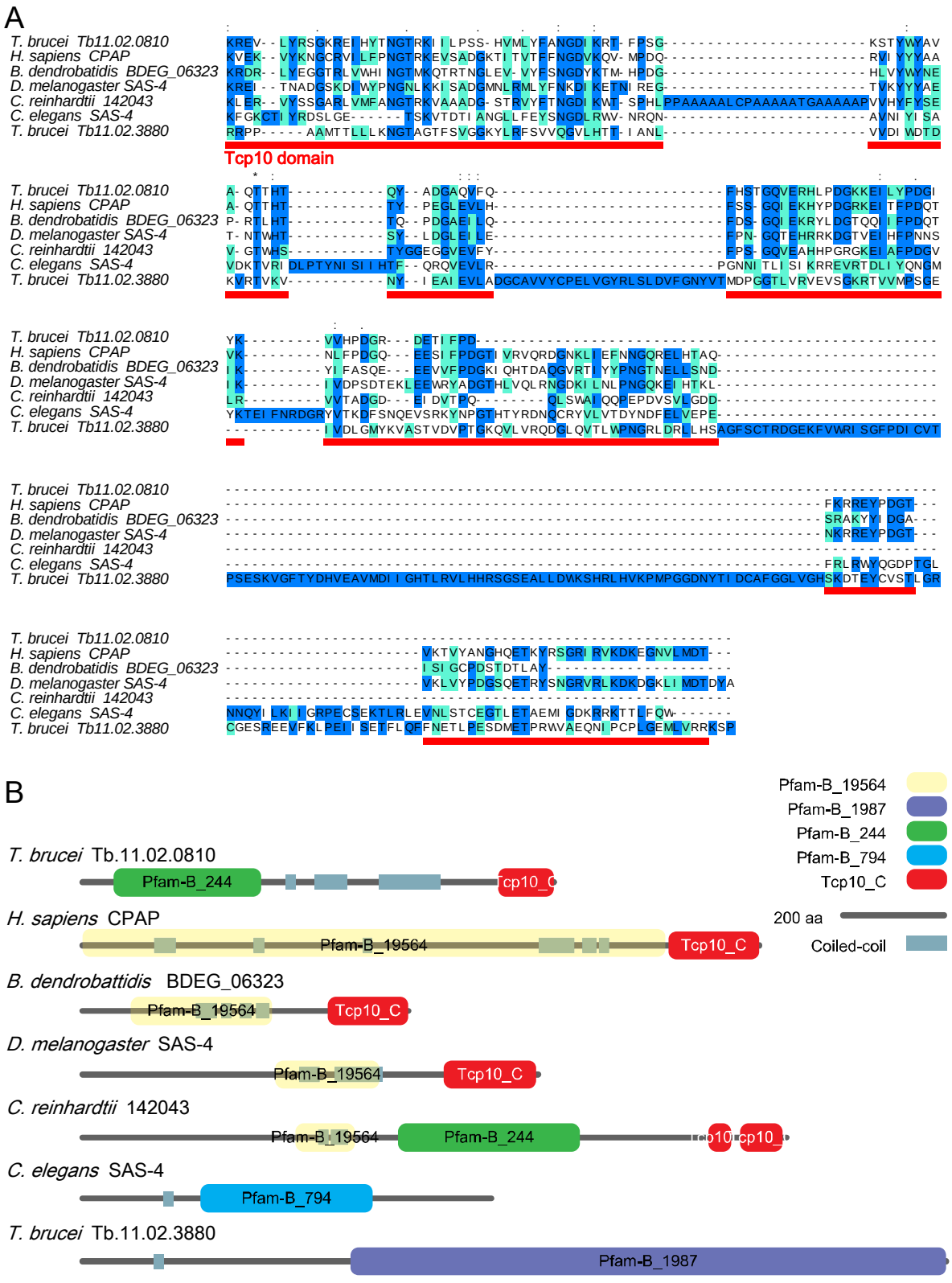

Figure 6.1 **Tb11.02.0810 encodes a SAS-4 protein, but Tb11.02.3880 does not.** (A) Amino acid alignment of two *T. brucei* proteins with SAS-4 protein sequences of other eukaryotes was generated with MAFFT version 6 E-INS-I (http://mafft.cbrc.jp/alignment/server/). Shown here is the C-terminal part of the alignment which exhibited the highest conservation among SAS-4 proteins and included the Tcp10 domain (highlighted underneath the sequence in red). Tb11.02.0810 showed conservation in the Tcp10 domain, whereas Tb11.02.3880 did not. Amino acids are shown with blue backgorund when they are identical to the majority consensus, and in cyan when they are similar. (B) Pfam domain architecture of the two *T. brucei* proteins and SAS-4 of other eukaryotes. SAS-4 proteins (except the divergent SAS-4 of *C. elegans*) have a C-terminal Tcp10 domain.

support that Tb11.02.0810 encodes a SAS-4 orthologue, but Tb11.02.3880 does not. Although Tb11.02.3880 is similar to SAS-4 homologues of other species it possesses a different domain architecture.

6.3 Trypanosomal SAS-4 localises to multiple sites

To study SAS-4 in trypanosomes, I generated a procyclic form cell line that expressed *T. brucei* SAS-4 with an N-terminal Ty-YFP tag (Y-SAS-4) from the endogenous *SAS-4* locus. Analysis by fluorescence microscopy showed that Y-SAS-4 localised to multiple sites in trypanosomes: (1) to a position consistent with the basal body region, (2) to the anterior tip of the cell, and (3) to a site close to the exit of the flagellum from the pocket (Fig. 6.2).

(1) More Y-SAS-4 localises to the pro-basal body than to the basal body

To investigate the YFP signal in the basal body region, cells were immunolabelled with a marker for mature basal bodies, YL1/2. The YL1/2 antibody recognises tyrosinated α-tubulin which locates at the posterior end of the subpellicular MT cytoskeleton and around the distal appendages of the basal body (Kilmartin et al., 1982; Stephan et al., 2007). While only a faint YFP signal co-localised with the YL1/2 labelling, an intense YFP signal was observed as a dot next to the basal body marker (Fig. 6.3). This intense Y-SAS-4 signal was consistent with the position of the pro-basal body.

(2) Y-SAS-4 localises to the anterior end of the cell and to the site where the new anterior end forms

Throughout the cell cycle, a strong YFP signal could be observed at the anterior end of the cell body both in whole cell as well as in cytoskeleton preparations (Fig. 6.2, 6.3). In 2K1N and 2K2N cells, Y-SAS-4 accumulated additionally at a site close to the end of the new flagellum (Fig. 6.4 A).

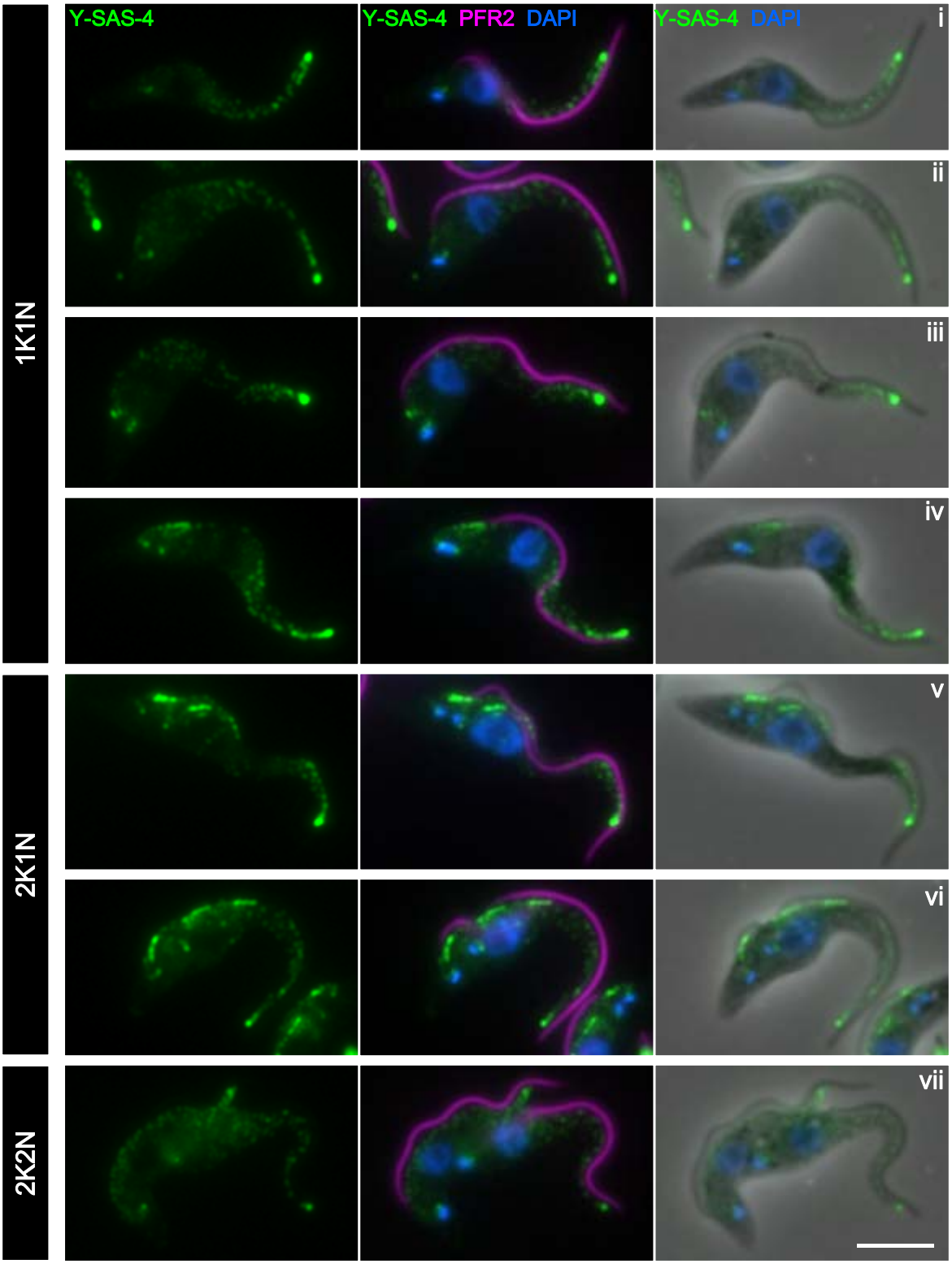

Figure 6.2 **Y-SAS-4 localises to multiple sites in trypanosomes: (1) distal to the kinetoplast, (2) to the anterior tip of the cell body, and (3) to a site close to the exit of the flagellum from the pocket.** *T. brucei* SAS-4 N-terminally tagged with Ty-YFP (Y-SAS-4, green) was expressed from the endogenous *SAS-4* locus in procyclic forms. Cells were fixed with formaldehyde and labelled with L8C4 (anti-PFR2, magenta). DNA was labelled with DAPI (blue). Scale bar: 5μm.

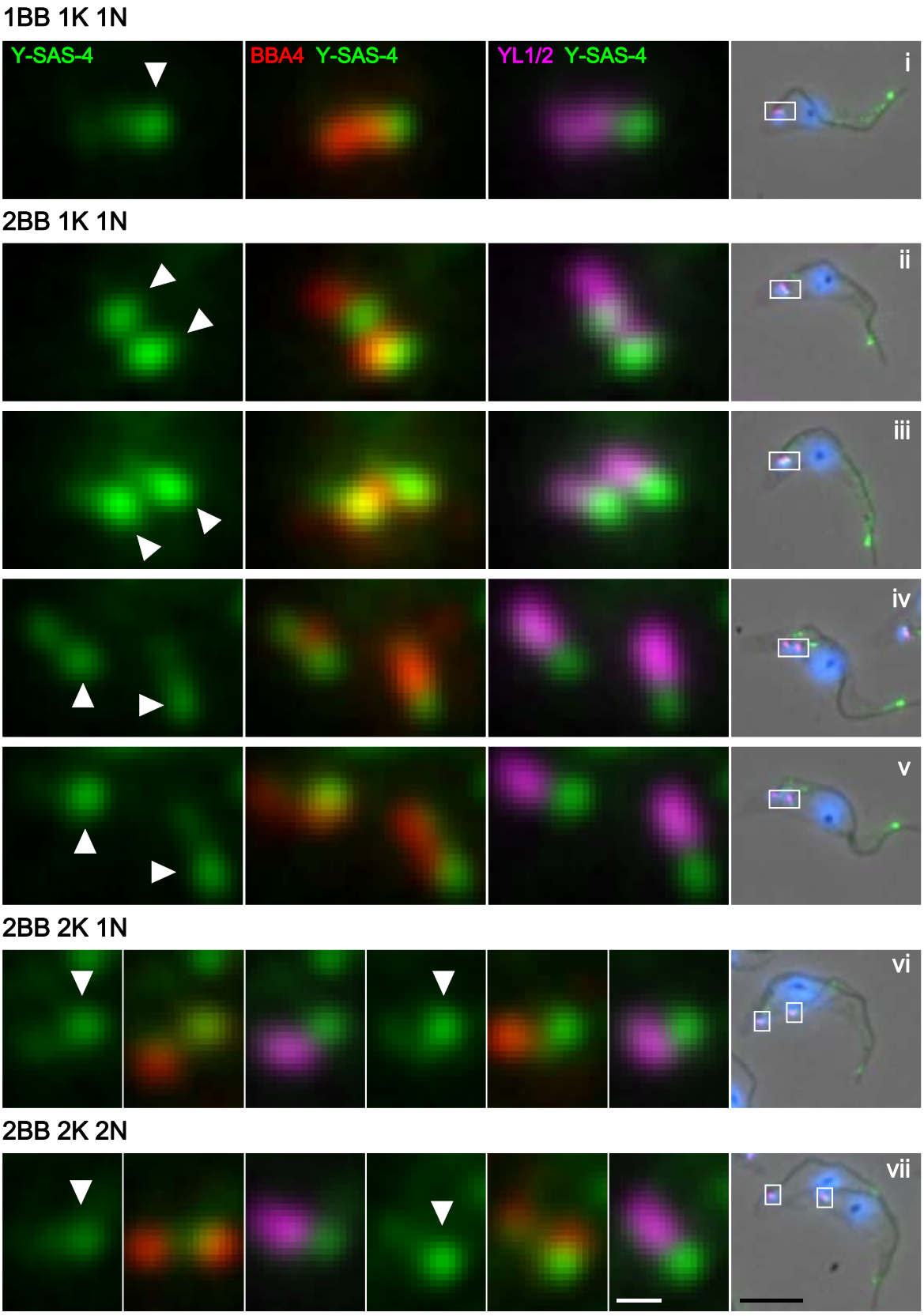

Figure 6.3 **More Y-SAS-4 localises to the pro-basal-body than to the basal body.** Cells expressing Y-SAS-4 (green) were detergent-extracted, fixed in methanol and immunolabelled with YL1/2 (magenta) and BBA4 (red). DNA was labelled with DAPI (blue). Insets show basal body area. White arrow heads point towards pro-basal body. White scale bar: 500nm. Black scale bar: 5μm.

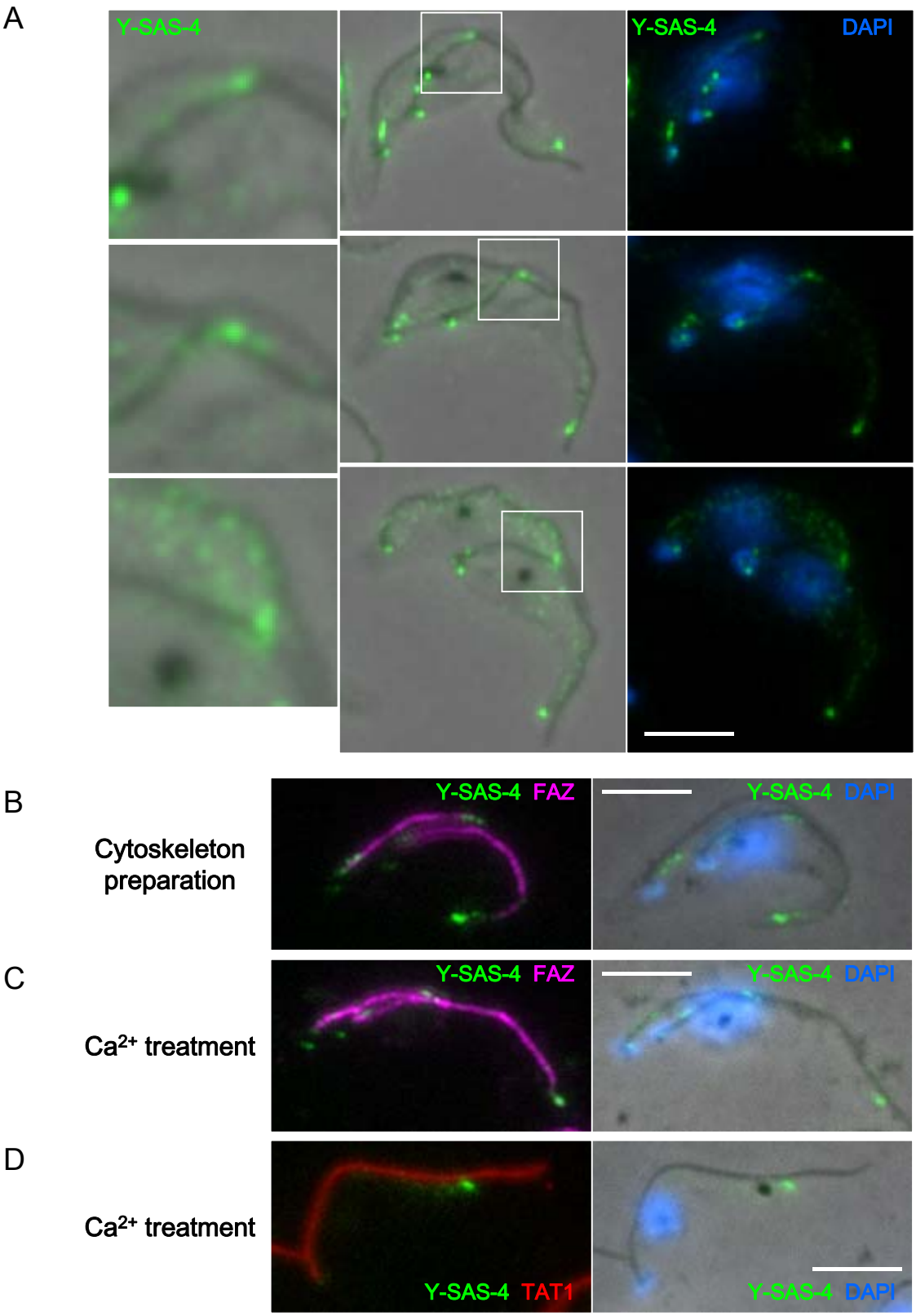

Figure 6.4. **Y-SAS-4 is associated with both the tip of the old and of the new flagellum attachment zone (FAZ).** (A) Cytoskeleton preparation of cells expressing Y-SAS-4 (green) showing the accumulation of Y-SAS-4 at the site where a new anterior cell end is formed (insets). (B-D) Cytoskeleton preparation (B) or cytoskeleton preparation additionally treated with calcium ions (C,D) were immunolabelled with L3B2 (anti-FAZ, magenta) or with TAT1 (anti-α-tubulin, red). Cell preparations were made at the same time and YFP signal was processed in the same way. This showed that Y-SAS-4 localised to the end of both the old and new FAZ and that the YFP signal is retained in the absence of subpellicular MTs. DNA was labelled with DAPI (blue). Scale bars: 5μm.

This is the site where the formation of the new anterior end of the posterior daughter cell is expected to occur. To validate the SAS-4 localisation to the new anterior end, immunolabelling with L3B2, an antibody recognising a protein of the flagellum attachment zone (FAZ; Kohl et al., 1999), was performed. Y-SAS-4 localised to the distal tip of the new FAZ in 2K1N and 2K2N cells (Fig 6.4 B). In these cell cycle stages the FAZ had grown close to full length and marked the site of the new anterior end.

In *T. brucei* the subpellicular cytoskeleton has a polarity with the microtubule minus ends towards the anterior end of the cell, with the exception of the four specialised microtubules which have the opposite polarity. This and the data about the MT interacting capacity of metazoan SAS-4 homologues (Cormier et al., 2009; Hsu et al., 2008; Hung et al., 2004) raised the question whether SAS-4 is associated with MT minus ends at the anterior end of the cell. Interestingly, Y-SAS-4 also showed a weak punctuated signal towards the anterior end (Fig. 6.4 A). To test whether the SAS-4 signal remained present when the subpellicular MT corset was depolymerised, cytoskeleton preparation were treated with calcium ions. Interestingly, Y-SAS-4 was still detected after removal of the subpellicular microtubules (Fig. 6.4 C,D). This observation could have several explanations: i) Y-SAS-4 was not associated with MTs, ii) Y-SAS-4 was associated with the MTs but stabilised by another protein which kept it attached to the slide even after MT depolymerisation, or iii) Y-SAS-4 itself stuck to the glass slide despite MT removal.

(3) Y-SAS-4 localises near the exit of both flagella from the pocket during the assembly of the new flagellum

During the formation of a new flagellum, Y-SAS-4 could be observed near the exit of the flagellum from the pocket (Fig. 6.2). This Y-SAS-4 signal appeared in 1K1N cells after basal body duplication and extended along the beginning of both the old and new FAZ. The YFP at this site was essentially absent in 2K2N cells.

Y-SAS-4 localisation near the exit of the flagellum from the pocket was reminiscent of the bilobe

signal, which was initially defined by the labelling of 20H5, an anti-centrin antibody (He et al., 2005). Recent work has shown that this signal is from a short filament in that area (Esson et al., 2012). To test whether Y-SAS-4 localised to the bilobe, immunolabelling with 20H5 was performed. This showed that the Y-SAS-4 localisation pattern is distinct from the bilobe signal despite partial overlap (Fig. 6.5). Whereas 20H5 labelling was at a fixed localisation at the beginning of the FAZ, Y-SAS-4 seemed more dynamic, moving distal to the 20H5 signal along the FAZ.

Another protein that is observed near the bilobe is Polo-like Kinase (PLK, de Graffenried et al., 2008), which phosphorylates the bilobe component centrin-2 (Yu et al., 2012). Kinase activity is critical for the activity of several centriole components in other eukaryotes. The function of the human SAS-4 homologue CPAP for example is dependent on phosphorylation by PLK2 (Chang et al., 2010). This raised the questions whether SAS-4 function in trypanosomes depends on PLK, the only PLK in *T. brucei* (Graham et al., 1998; Hodges et al., 2010), and whether the two proteins co-localise. To address the latter question, Ty-YFP-PLK (Y-PLK) and Ty-mCherry-SAS-4 (mC-SAS-4) were co-expressed and localisation was analysed by fluorescence microscopy. The localisation pattern of Y-PLK and mC-SAS-4 was distinct despite partial overlap (Fig. 6.6). In 1K1N cells after BB duplication, Y-PLK appeared and localised to the collar region (Fig. 6.6 iii,iv). Y-PLK was detected at the tip of the newly forming FAZ after the synthesis of the new flagellum had started. In contrast, mC-SAS-4 localised towards the proximal end of the FAZ (Fig. 6.6 iv-vi). Interestingly, Y-PLK also localised to the flagellum connector (Fig. 6.6 iv-vi, a PLK localisation site previously not described. In contrast to earlier cell cycle stages, in 2K2N cells Y-PLK was no longer detectable at the distal end of the FAZ, and mC-SAS-4 located to this site (Fig. 6.6 vii).

6.4 SAS-4 is essential

To investigate the function of SAS-4, I generated a cell line with inducible RNA interference against *SAS-4* in a *Y::SAS-4/Y::SAS-4* background. Western blot analysis of doxycycline-induced cells

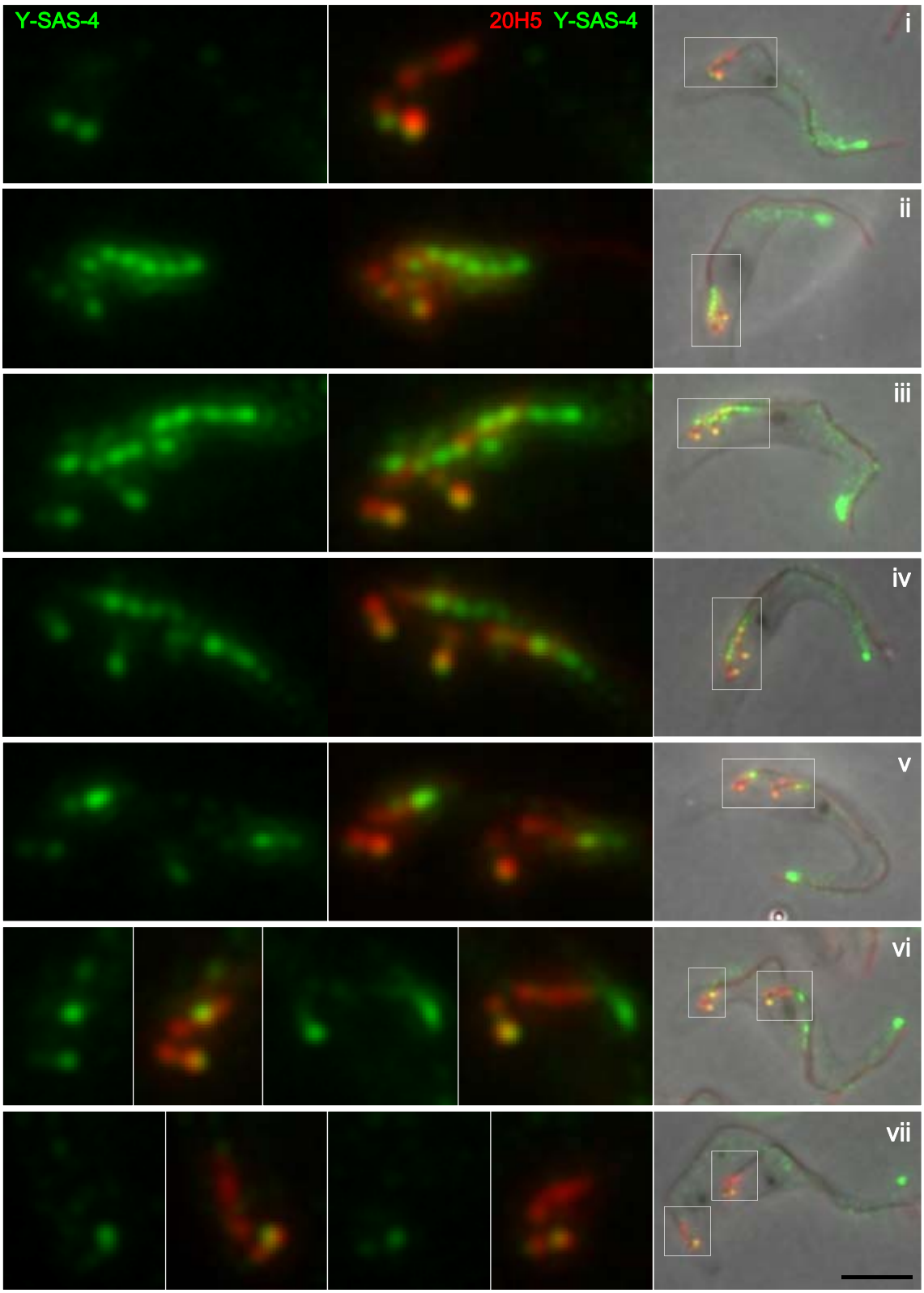

Figure 6.5 **The Y-SAS-4 signal near the exit of the flagellum from the pocket does not colocalise with 20H5.** Cytoskeleton preparation of cells expressing Y-SAS-4 (green) were immunolabelled with 20H5 (anti-centrin, red). This showed that Y-SAS-4 does not colocalise with centrin, a marker for the bilobe. DNA was labelled with DAPI (blue). Insets show the proximal end of the flagellum. Scale bar: 5μm.

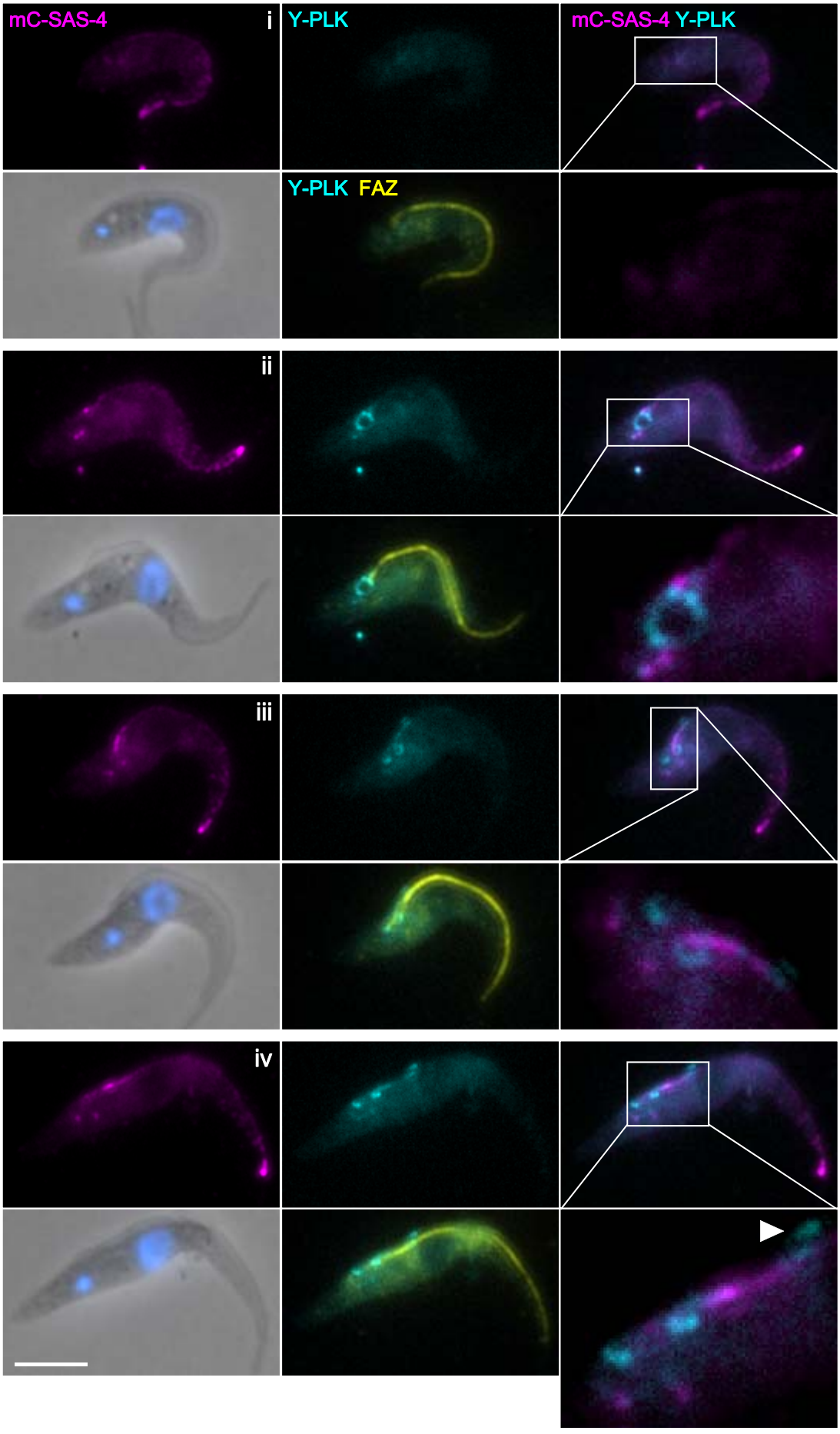

Figure 6.6 **SAS-4 does not colocalise with Polo-like Kinase.** (figure legend next page)

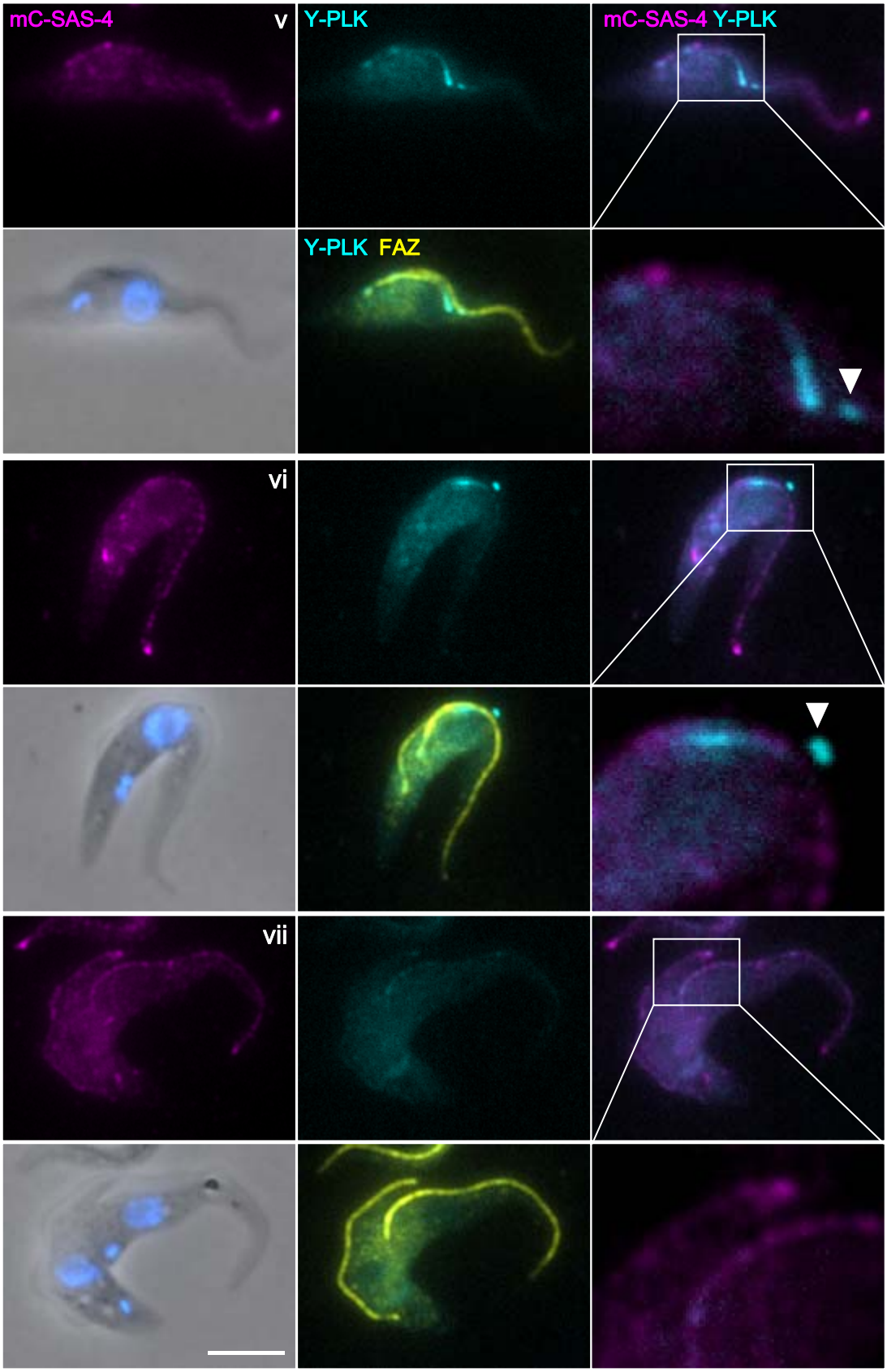

Continuation of Figure 6.6 **SAS-4 does not colocalise with Polo-like Kinase.** Cells expressing mC-SAS-4 and Y-PLK showing that the two proteins have different localisation patterns throughout the cell cycle. Both proteins localise to the distal tip of the new FAZ (L3B2, yellow). PLK was present early during the cell cycle (1K1N and 2K1N), while SAS-4 localised there later (2K1N and 2K2N). Arrow head indicates a site consistent with the flagellar connector. DNA was labelled with DAPI (blue). Scale bars: 5μm.

confirmed that the short hairpin construct against *SAS-4* (*shSAS-4*) was effective in reducing the amount of the protein to undetectable levels by 36h post RNAi induction (Fig. 6.7 A). Microscopic examination showed homogenous ablation of Y-SAS-4 across the population and the accumulation of aberrant multinucleated cells (Fig. 6.7 B). Induction of SAS-4 RNAi resulted in a strong growth defect within 24h, which revealed that SAS-4 was an essential protein for cell division (Fig. 6.7 C).

6.5 Flagellum assembly continues in SAS-4 depleted cells but cytokinesis does not

To characterise the phenotype associated with the depletion of SAS-4, cells were analysed by fluorescence microscopy. Counts of kinetoplasts and nuclei showed the accumulation of aberrant multinucleated cells across the population after SAS-4 ablation (Fig. 6.8 A). The ratio of the number of nuclei to the number of flagella remained relatively constant after SAS-4 RNAi induction, which is in stark contrast to the SAS-6 RNAi phenotype where this ratio increases 400% (Fig. 6.8 B, compare to Fig. 4.8 B). This suggested that flagellum assembly continued at normal speed compared to mitosis after SAS-4 depletion. 48h post SAS-4 RNAi induction 30% of the cells possessed more than two nuclei and more than two flagella (Fig. 6.8 C). These data indicated a cytokinesis defect, but surprisingly not a basal body duplication defect.

6.6 SAS-4 depleted cells assemble normal basal bodies

The presence of a multitude of flagella in SAS-4 depleted trypanosomes (F>2 in 50% of the cells 72h post RNAi induction) was unexpected since SAS-4 in all eukaryotes tested so far is required for proper centriole and/or basal body assembly (Basto et al., 2006; Gogendeau et al., 2011; Kirkham et al., 2003; Kleylein-Sohn et al., 2007; Leidel and Gonczy, 2003). To study the composition of basal bodies in SAS-4 depleted trypanosomes, Y-SAS-6 was expressed together

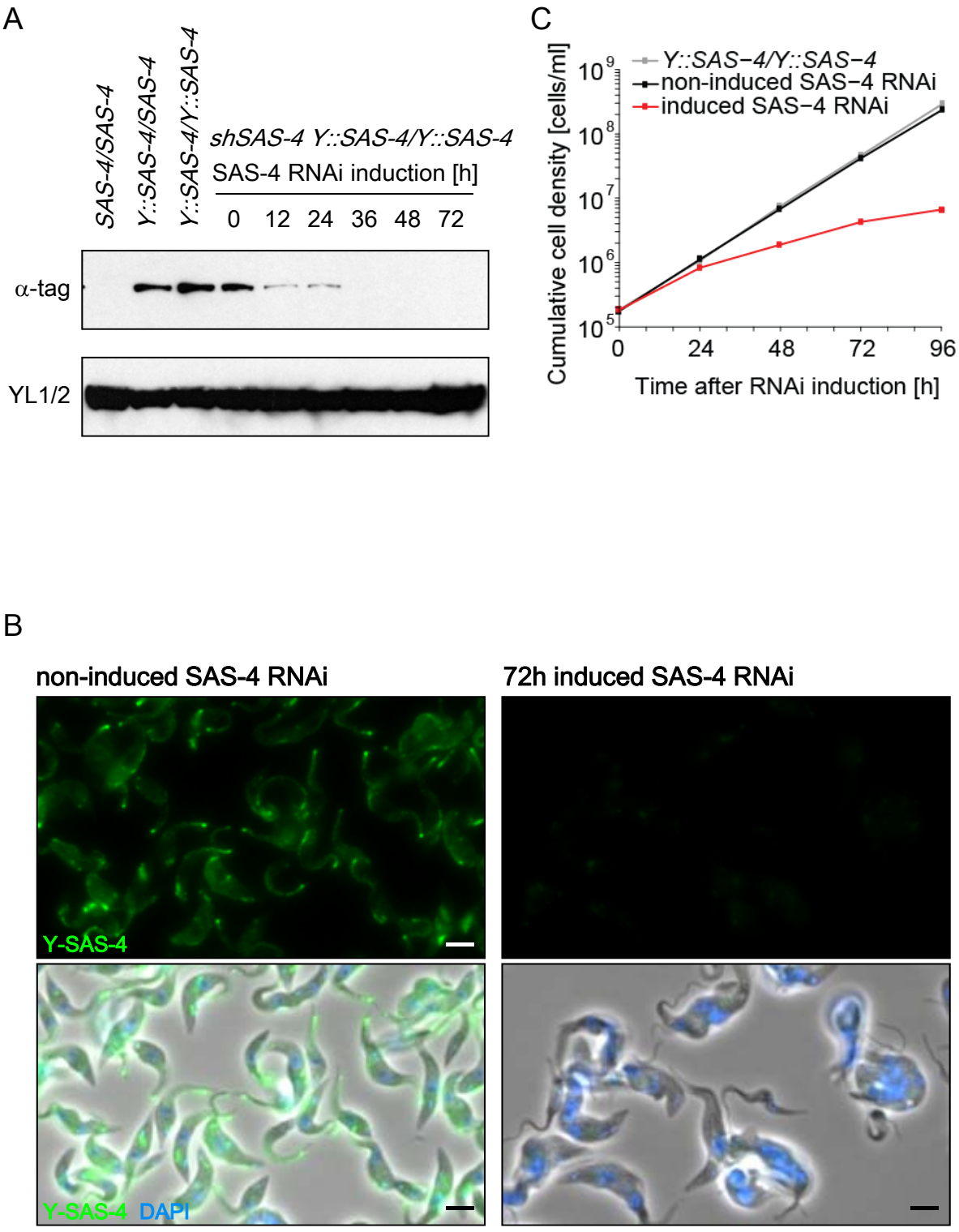

Figure 6.7 **Depletion of SAS-4 results in a lethal growth defect.** (A) Immunoblot analysis of cells given above image with anti-tag antibodies (anti-GFP, anti-Ty) showing the depletion of Y-SAS-4 after induction of RNAi against SAS-4. (B) Fluorescence microscopy analysis of non-induced and 72h induced SAS-4 RNAi cells confirmed the depletion of Y-SAS-4 and revealed the aberrant morphology of cells post SAS-4 RNAi induction. DNA was labelled with DAPI (blue). Scale bar: 5μm. (C) Population growth measured every 24h over 96h with cultures diluted every 48h showed that the ablation of SAS-4 resulted in a dramatic reduction in cell duplication.

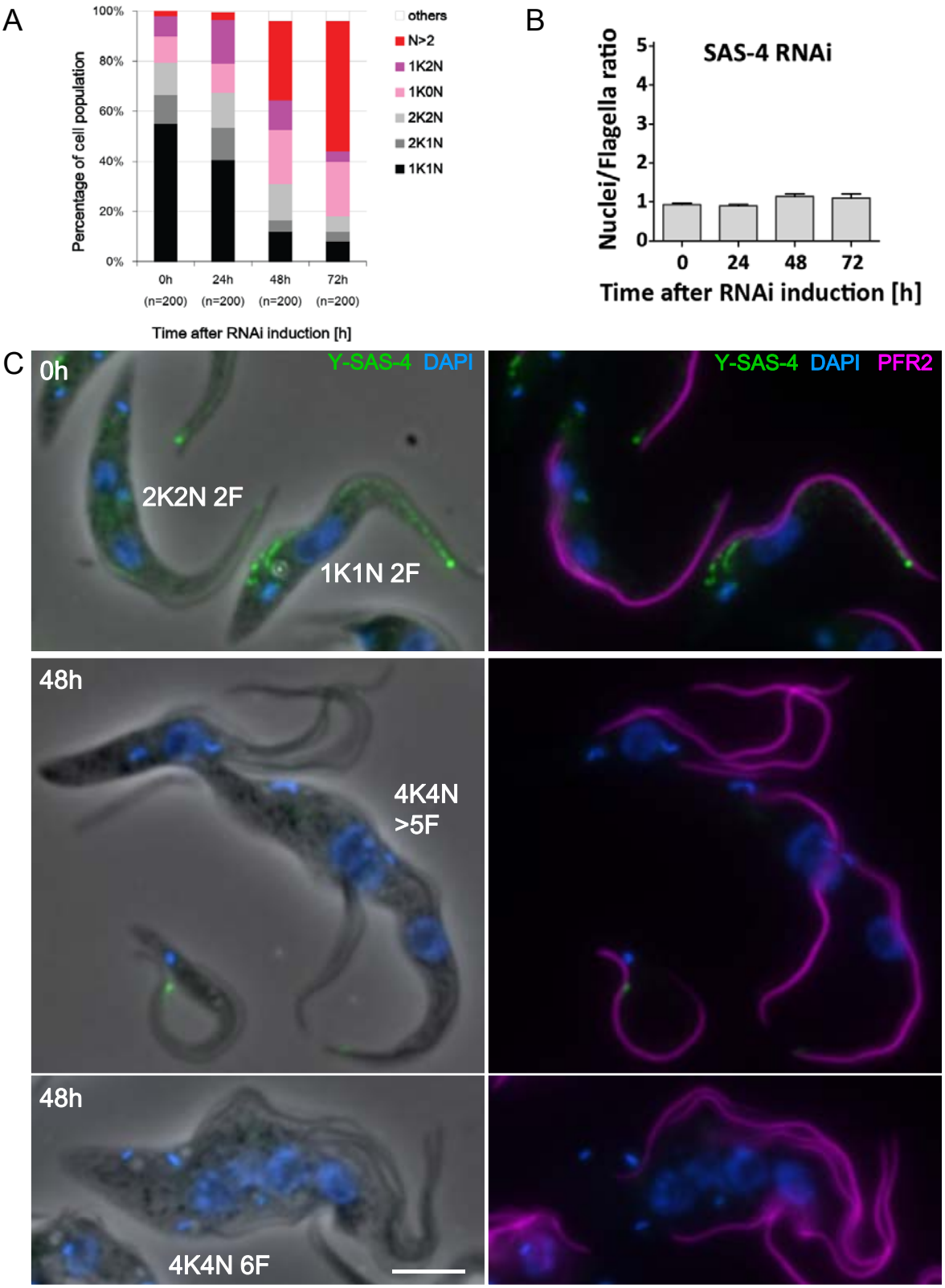

Figure 6.8 **Depletion of SAS-4 leads to failure of cytokinesis but flagellum assembly continues.** (A) Kinetoplast and nucleus counts at several time points after SAS-4 RNAi induction demonstrating an increase of abnormal cell cycle stages (redish colours). (B) Immunolabelling of whole cell preparations of non-induced and 48h induced SAS-4 RNAi cells with L8C4 (anti-PFR2, magenta), and fluorescence microscopy showed the accumulation of multinucleated cells with a high number of flagella post SAS-4 RNAi induction. DNA was labelled with DAPI (blue). Scale bar: 5μm. (C) Ratio of the number of nuclei to number of flagella remained unaffected of SAS-4 ablation suggesting that flagellum assembly continued at normal speed or changed at the same rate as mitosis. N=200/time point. Error bars: standard deviation.

with mC-SAS-4 in cells with inducible SAS-4 RNAi. Cells which had additional flagella had the same number of additional pairs of Y-SAS-6 dots (Fig. 6.9 A). This showed that SAS-4 depleted basal bodies and pro-basal bodies still contained SAS-6. YL1/2 and LAZ1 immunolabelling also supported that basal bodies assembly continued in SAS-4 depleted cells despite cytokinesis defect and SAS-4 ablation (Fig. 6.9 B,C). Thin section electron microscopy demonstrated that the ultrastructure of basal bodies and axonemes in SAS-4 depleted cell was indistinguishable from wild-type cells (Fig. 6.10 A,B). Collectively, these data showed that basal body assembly continued normally, and thus was unlikely to be the source of the observed cytokinesis defect.

6.7 Normal organisation of MTs at the anterior tip in SAS-4 depleted cells

SAS-4 depletion led to a cytokinesis defect. The protein localises to the anterior tip and the ingression of the cleavage furrow starts from the anterior site. To test whether SAS-4 depletion causes disorganisation of the anterior end, whole-mount cytoskeleton preparations were inspected. The old anterior end of the subpellicular cytoskeleton of cells 36h after SAS-4 RNAi induction was indistinguishable from that in non-induced cells (Fig. 6.11).

6.8 Ty-YFP-tagged SAS-4 complements the loss of wild-type SAS-4

To test whether tagged SAS-4 was functional, I generated a cell line in which both endogenous *SAS-4* alleles where modified to express Y-SAS-4. Integration of the targeting constructs and presence of the wild-type *SAS-4* allele was checked by PCR. This validated that *Y::SAS-4/Y::SAS-4* cells possessed only modified and no wild-type alleles of *SAS-4* (Fig. 6.12 A). Western blot analysis of whole cell extracts using anti-tag antibodies demonstrated that the cells with two *Y::SAS-4* alleles expressed a higher amount of the tagged protein compared to cells with

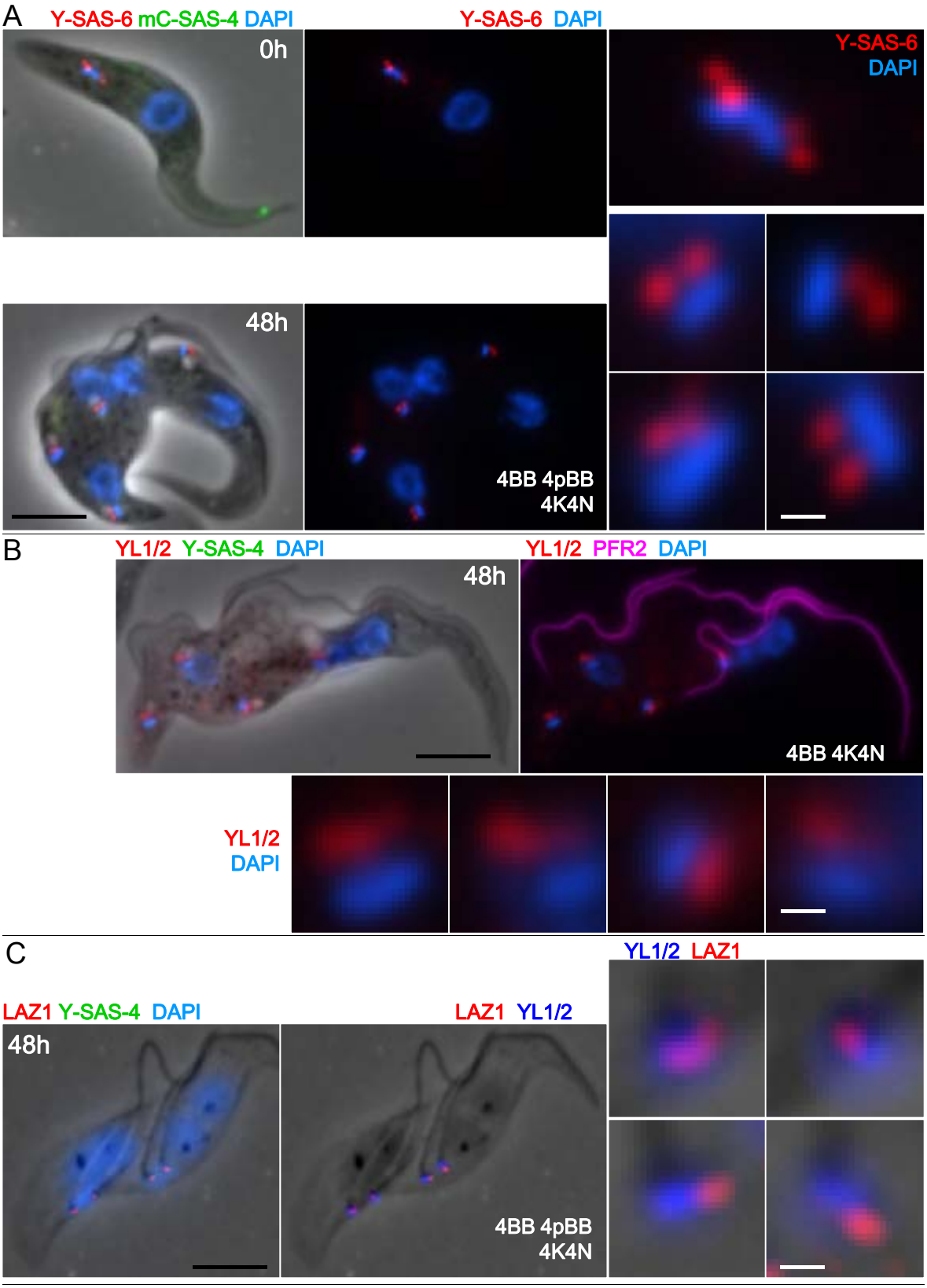

Figure 6.9 **Basal body assembly continues in SAS-4 depleted cells**. (A) Whole cell preparations of cells expressing mC-SAS-4 (green) and Y-SAS-6 (red) after SAS-4 RNAi induction showed that SAS-4 depleted cells possessed an increased number of Y-SAS-6 dots suggesting that BB assembly continued despite a reduced level of SAS-4. (B) Whole cell preparation of SAS-4 RNAi induced cells labelled with YL1/2 (red) showed increased numbers of YL1/2 dots supporting that BB assembly continued. (C) Cytoskeleton preparation of SAS-4 RNAi induced cells labelled with LAZ1 (red) and YL1/2 (dark blue) showed an increased number of LAZ1 dots indicating that pBB assembly continued. Insets show basal body area. White scale bars: 500nm. Black scale bars: 5μm.

A

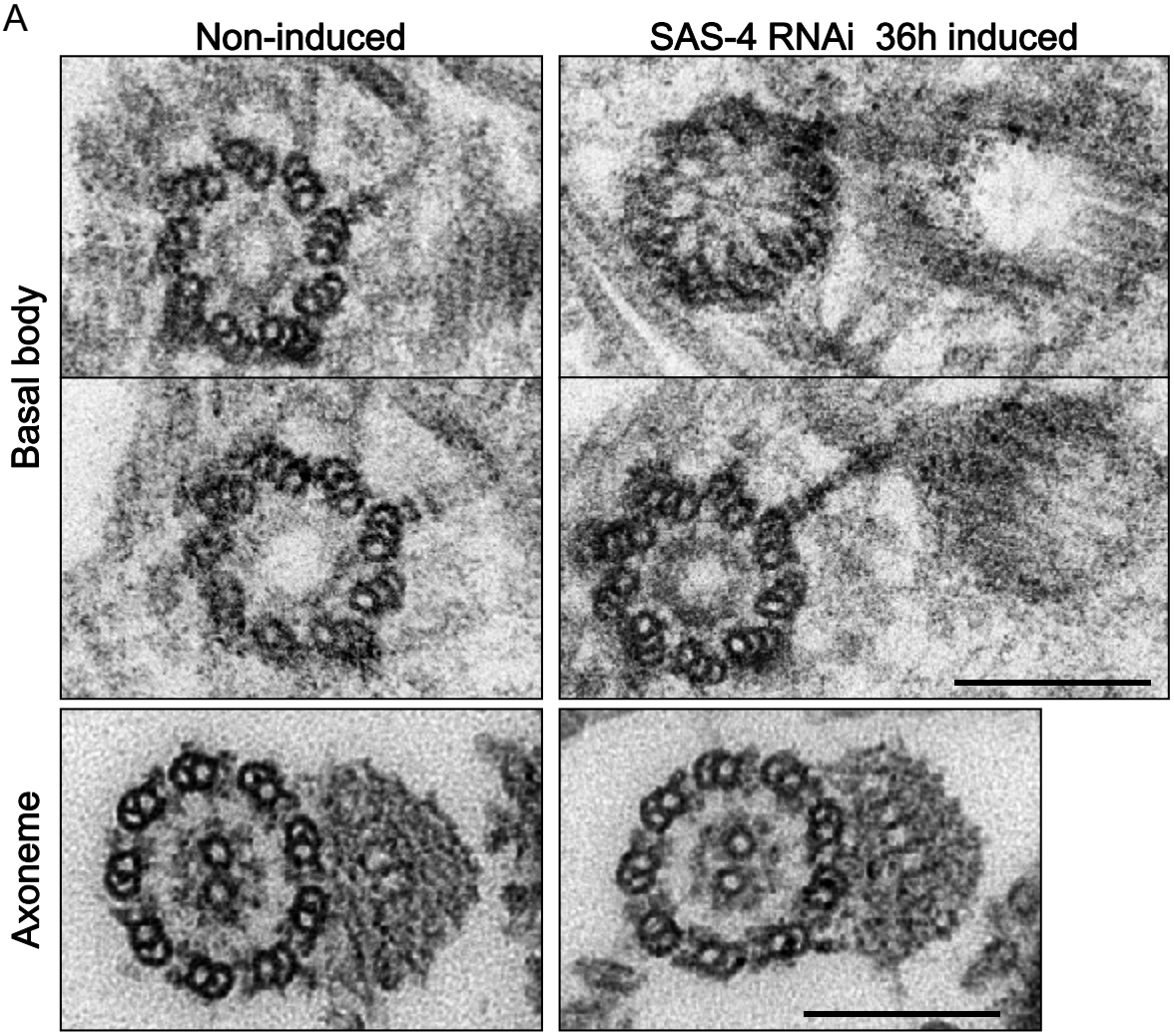

B

	Basal bodies & pro-basal bodies		Transition zones		Axonemes	
	non-induced n = 50	SAS-6 RNAi 36h induced n = 50	non-induced n = 50	SAS-6 RNAi 36h induced n = 50	non-induced n = 50	SAS-6 RNAi 36h induced n = 50
normal	49	49	50	50	47	48
abnormal	1	1	0	0	3	2
χ^2	p=1		-		p=0.55	

Figure 6.10 **The ultrastructure of SAS-4 depleted basal bodies appears normal**. (A) TEM thin sections of basal bodies and axonemes of cytoskeleton preparations of non-induced and 36h induced SAS-4 RNAi cells showed that the ultrastructure of basal bodies from SAS-4 RNAi induced cells looks indistinguishable from those from non-induced cells. Scale bars: 200nm. (B) Counts of normal and abnormal basal bodies, transition zones and axonemes of non-induced and 36h induced SAS-4 RNAi cells. Counts were done on TEM thin sections.

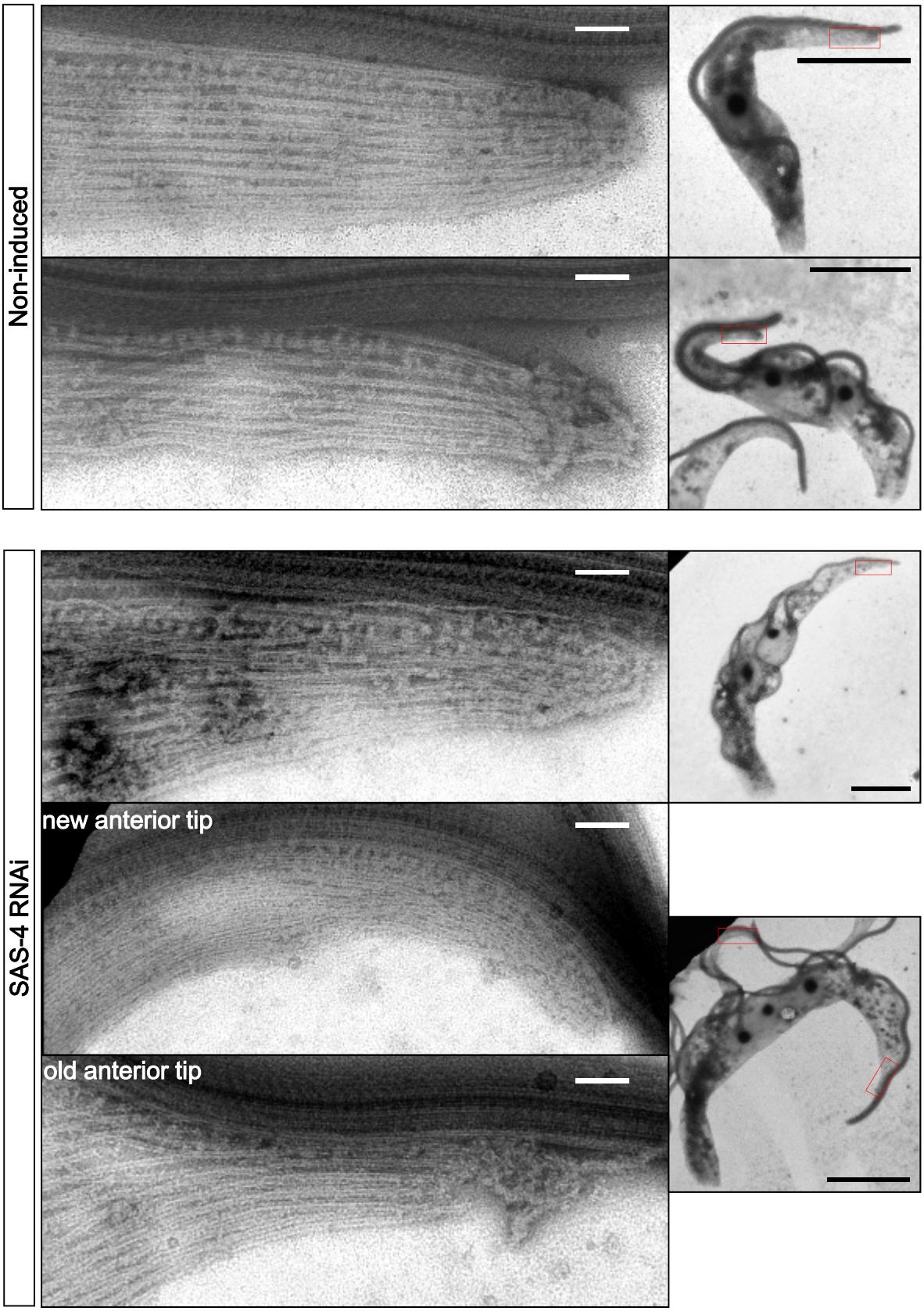

Figure 6.11 **The anterior end of the subpellicular cytoskeleton is still organised in SAS-4 depleted cells.** TEM images of anterior ends of the subpellicular MT array of negatively stained whole-mount cytoskeletons of non-induced and 36h induced SAS-6 RNAi cells. The cell cytoskeleton of the respective anterior tip is shown on the right. White scale bars: 200nm. Black scale bars: 5μm

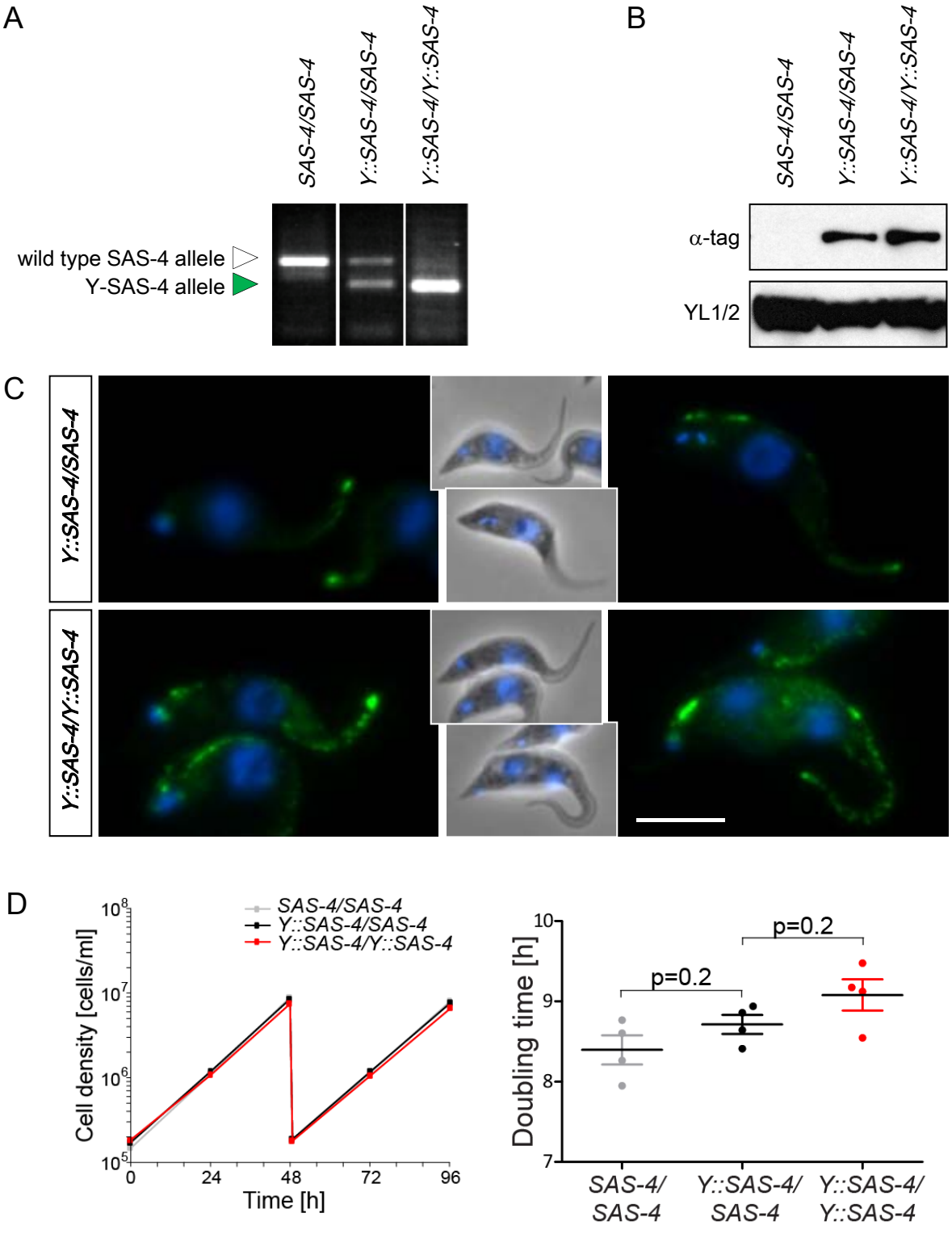

Figure 6.12 **Y-SAS-4 is functional.** In *Y::SAS-4/SAS-4* cells one endogenous *SAS-4* allele and in *Y::SAS-4/Y::SAS-4* cells both endogenous *SAS-4* alleles were modified to express Y-SAS-4. This abolished expression of wild-type SAS-4 in the latter cell line. (A) Examination of genomic DNA of cells given above image for wild-type and modified SAS-4 alleles. The PCR confirmed that *Y::SAS-4/Y::SAS-4* has no wild-type allele left. (B) Immunoblot analysis of cells given above image with anti-tag antibodies (anti-GFP, anti-Ty) showing that *Y::SAS-4/Y::SAS-4* has a higher amount of Y-SAS-4. (C) Microscopy showed that *Y::SAS-4/Y::SAS-4* cells looked morphologically normal and that YFP signal appeared brighter. DNA was labelled with DAPI (blue). Scale bar: 5μm. (D) Population growth was measured every 24h over 96h and cultures were diluted every 48h. This showed that doubling time of *Y::SAS-4/Y::SAS-4* was comparable to wild-type cells.

a single *Y::SAS-4* allele (Fig. 6.12 B). In agreement with this, the YFP fluorescence signal in *Y::SAS-4/Y::SAS-4* cells was more intense than in cells with a single *Y::SAS-4* allele (Fig. 6.12 C). Cells expressing only Y-SAS-4 were morphologically indistinguishable from cells expressing wild-type SAS-4. The doubling time of *Y::SAS-4/Y::SAS-4* cells was comparable to wild-type cells (Fig. 6.12 D). This analysis showed that Y-SAS-4 can complement the essential roles of wild-type SAS-4. The fact that tagged SAS-4 is functional makes it also less likely that the localisation observed for this protein is an artefact.

6.9 Overexpression of SAS-4 has no effect on growth or cell morphology

Overexpression of CPAP, the human SAS-4 homologue, results in the elongation of centriolar MTs (Kohlmaier et al., 2009; Schmidt et al., 2009; Tang et al., 2009). To investigate whether an increased amount of SAS-4 leads to any cellular phenotypes, I generated a cell line with inducible Y-SAS-4 expression from an ectopic locus additionally to the endogenous Y*::SAS-4/Y::SAS-4* background. This allowed the visualisation of all SAS-4 in a cell. Western blot analysis with an anti-GFP and an anti-tag antibody confirmed that doxycycline-mediated induction led to an increase of Y-SAS-4 above wild-type levels in these cells (Fig. 6.13 A). However, over-expression of Y-SAS-4 monitored over five days had no effect on the population growth rate (Fig. 6.13 B). Fluorescence microscopy showed that the additional Y-SAS-4 was resident at normal SAS-4 localisation sites such as the anterior tip and along the FAZ (Fig. 6.13 C). Nevertheless, the high amount of Y-SAS-4 was not associated with a phenotype.

6.10 Summary

Here I show that SAS-4 localises to multiple sites in trypanosomes, namely the pro-basal body, the anterior tip of the cell body and a site close to the exit of the flagellum from the pocket. SAS-4 is an

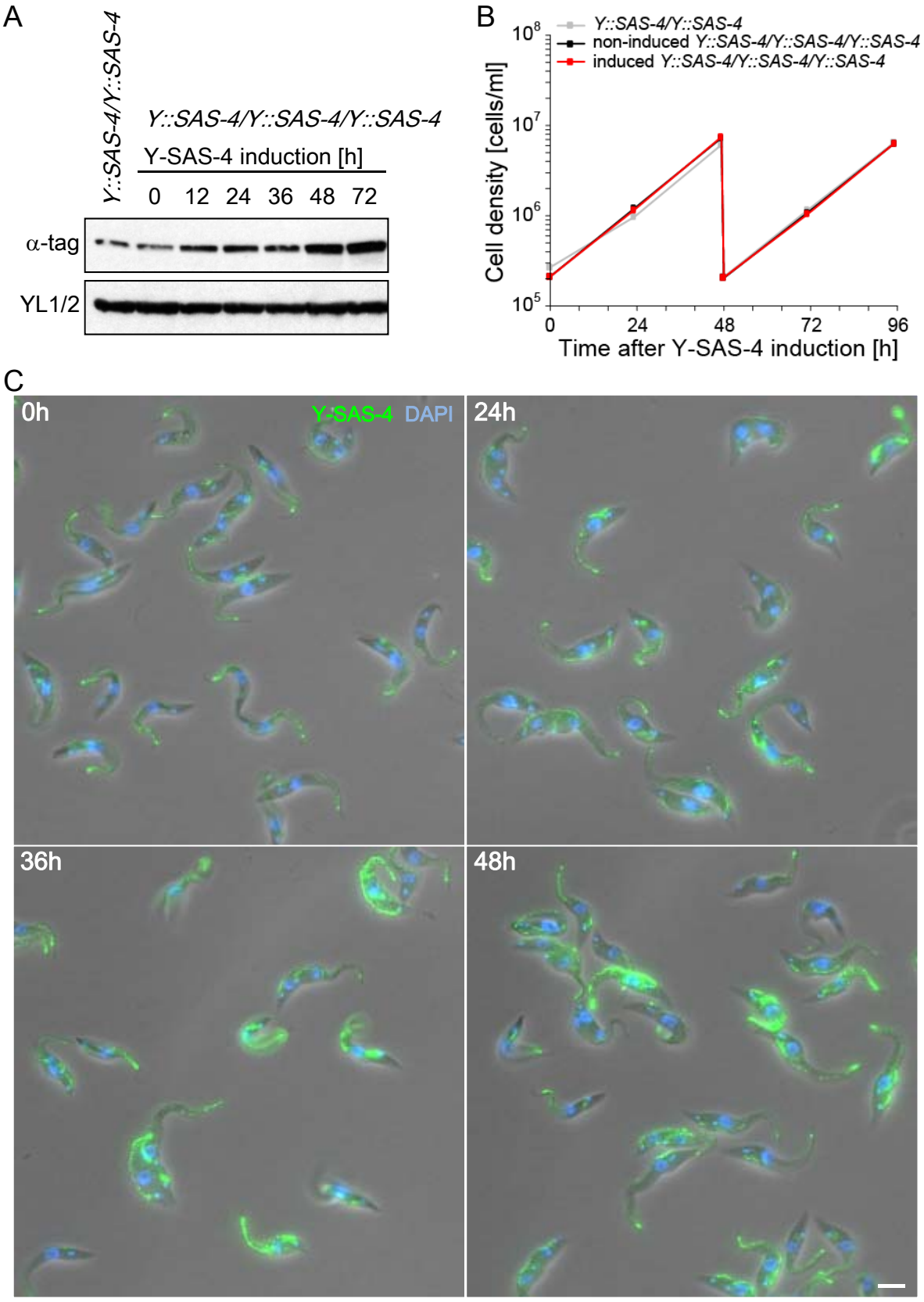

Figure 6.13 **Overexpression of Y-SAS-4 has no effect on the population growth rate or cell morphology.** (A) Immunoblot analysis of cells given above image with anti-tag antibodies (anti-GFP, anti-Ty) showing that *Y::SAS-4/Y::SAS-4/Y::SAS-4* cells express more SAS-4 after induction. Loading control: YL1/2. (B) Population growth measured every 24h over 96h with dilution every 48h showed that SAS-4 overexpression did not cause a change in the population growth rate. (C) Overview images of non-induced and Y-SAS-4 over-expressing *Y::SAS-4/Y::SAS-4/Y::SAS-4* cells. Scale bar: 5μm.

essential protein in *T. brucei* whose ablation results in a cytokinesis defect. Interestingly, I found that basal bodies assemble normally in the absence of SAS-4 and that their composition (apart from lacking SAS-4) and ultrastructure are unaffected. Ectopic overexpression of SAS-4 does not affect cell growth or cell morphology in *T. brucei*.

CHARACTERISATION OF TRYPANOSOMAL WDR16

7.1 Preface

In Chapter 3, WDR16 was identified as part of a core set of proteins that is conserved in cilia-producing species but not in species without cilia. This suggested that WDR16 is important in the eukaryotic centriole assembly pathway.

In the mammalian systems investigated, WDR16 is expressed at low levels in normal tissue but higher levels in testis and cilia-bearing ependymal cells of the brain hinting towards WDR16 involvement with cilia (Hirschner et al., 2007; Silva et al., 2005). Ablation of WDR16 in *Danio rerio* causes severe hydrocephalus. The reason for this, however, is unclear as no change in the beat of cilia of ependymal cells was observed (Hirschner et al., 2007).

WDR16, encoded by Tb11.02.5550, was also identified in the flagella proteome of *Trypanosoma brucei* (Broadhead et al., 2006). Further analysis suggested that Ty-GFP-WDR16 localises to the axoneme, the basal body and the pro-basal body in trypanosomes (Farr, 2007). RNA interference against the *WDR16* in procyclic form cells did not show a phenotype (Farr, 2007). This, however, was not conclusive as the protein level of WDR16 was not analysed after RNAi induction.

My aim in this chapter was to continue the study of the role of WDR16 in the model organism *T. brucei*.

7.2 WDR16 is remarkably conserved across ciliated eukaryotes

To analyse the conservation of *T. brucei* WDR16 with homologues of other eukaryotes, WDR16 protein sequences of a wide range of diverse eukaryotes were aligned with that of trypanosomes. This showed a high degree of similarity of WDR16 proteins across all ciliated eukaryotes (Fig. 7.1).

As the name implies, WDR16 proteins contain WD40 domains. Searching of WDR16 for WD40 identified ten to twelve of the domains per protein (Fig. 7.2 A). WD40 domains are amongst the most abundant protein domain in eukaryotes (for a review see Xu and Min, 2011). The domain is 39 amino acids in length and was named for a signature WD dipeptide found at the C-terminus (Fig. 7.2 B). WD40 domains are commonly found as repeats of four to eight which together form a β-propeller with each domain forming a blade. The conserved residues of the domain form a network of strong hydrogen bonds that stabilises the protein structure. WD40-containing proteins are involved in a range of cellular processes such as signal transduction, cytoskeletal assembly, vesicle trafficking, cell cycle control, chromatin dynamics, apoptosis, and transcription regulation. Their common function is to provide a rigid scaffold for protein-protein interactions.

7.3 WDR16 localises to the transition zone, axoneme, and pro-basal body

Previous studies by Dr Helen Farr (University of Oxford) had shown that *T. brucei* WDR16 with an N-terminal Ty-GFP tag (G-WDR16) expressed from the endogenous *WDR16* locus localises to the axoneme and the basal body region in procyclic form cells (Farr, 2007). In contrast to the cell line used by Helen Farr, the procyclic cell line used for the majority of the experiments presented in this thesis was a single marker cell line (SiMPs), generated by only one targeting cassette including the

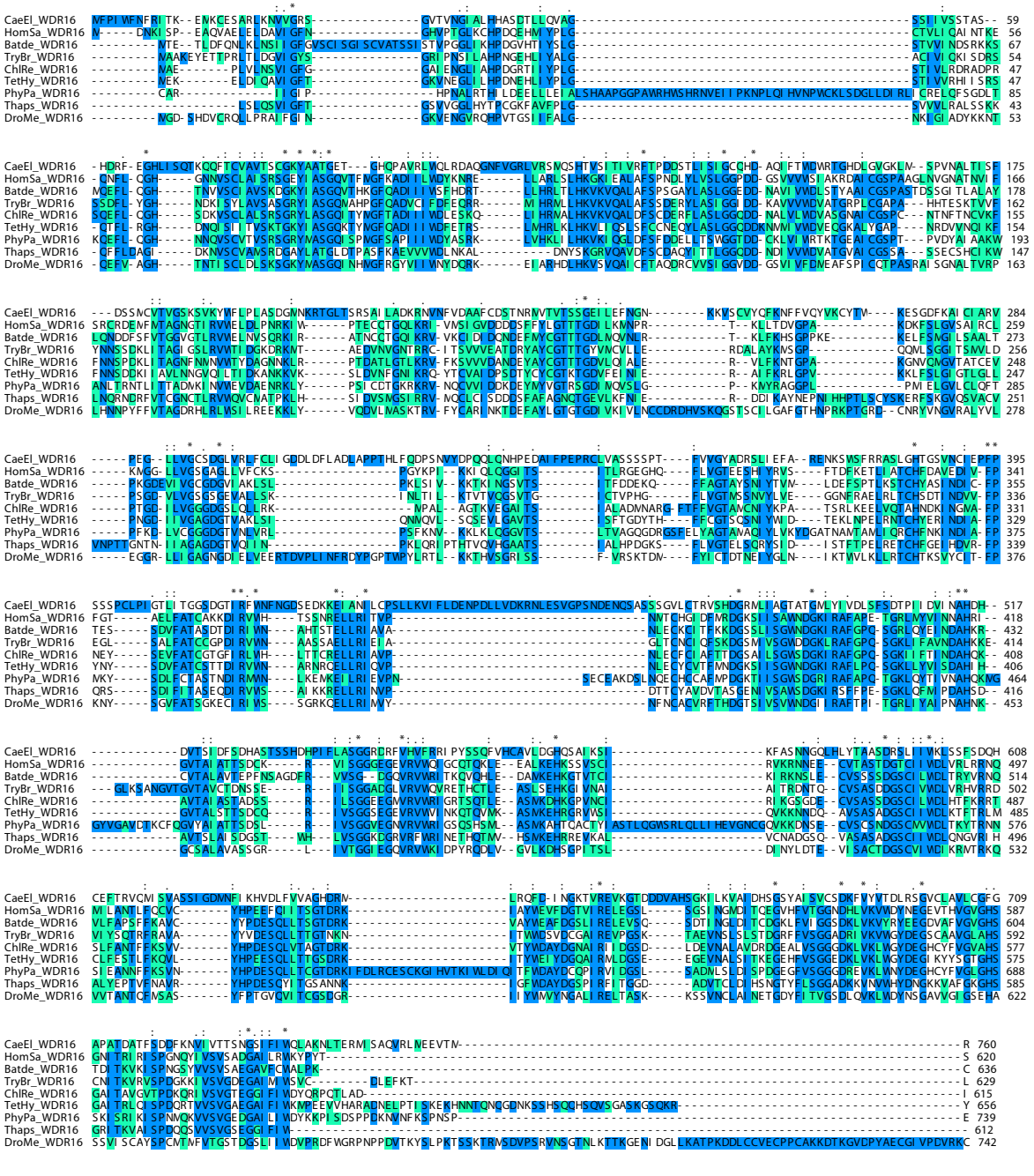

Figure 7.1 **WDR16 is highly conserved across ciliated eukaryotes.** Amino acid alignment of WDR16 protein sequences was generated with MAFFT version 6 E-INS-I (http://mafft.cbrc.jp/alignment/server/). Amino acids are shown with blue backgorund when they are identical to the majority consensus, and in cyan when they are similar. CaeEl = *Caenorhabditis elegans*, HomSa = *Homo sapiens*, Batde = *Batrachochytrium dendrobatidis*, TryBr = *Trypanosoma brucei*, ChlRe = *Chlamydomonas reinhardtii*, TetHy = *Tetrahymena thermophilia*, PhyPa = *Physcomitrella patens*, Thaps = *Thalassiosira pseudonana*, DroMe = *Drosophila melanogaster*.

A

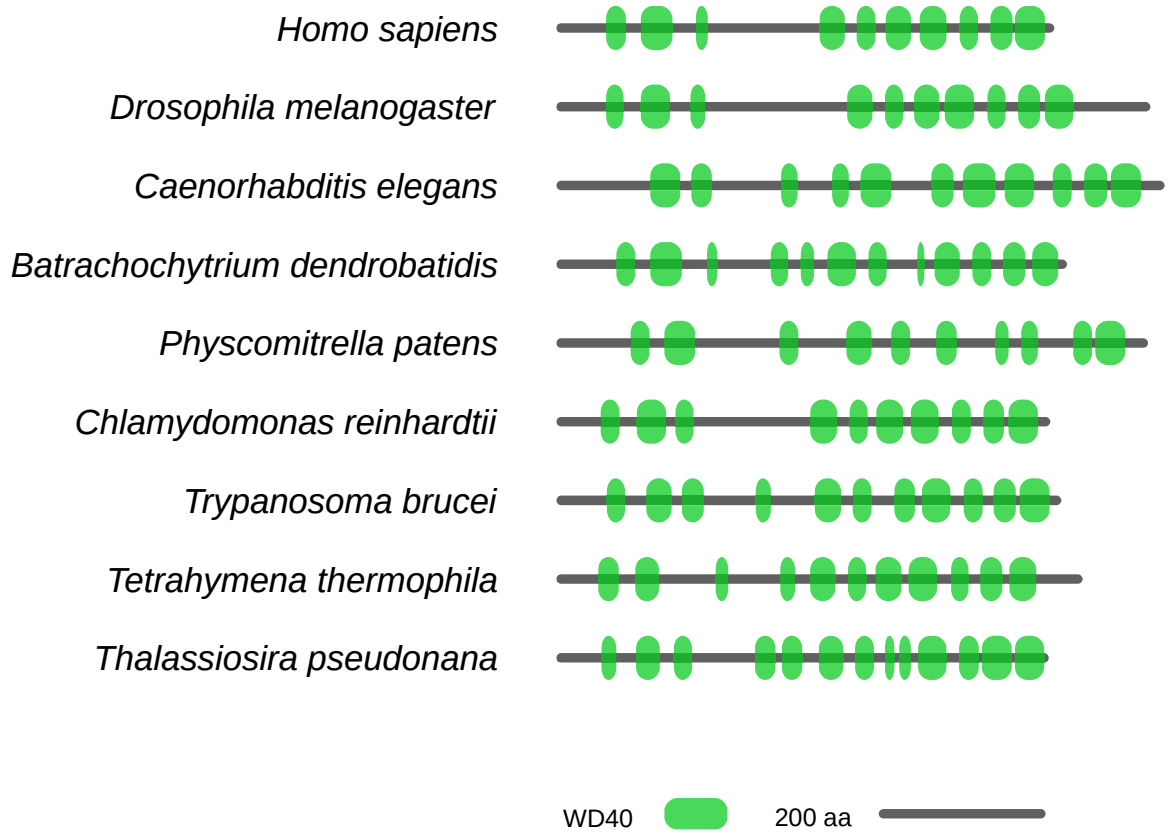

B

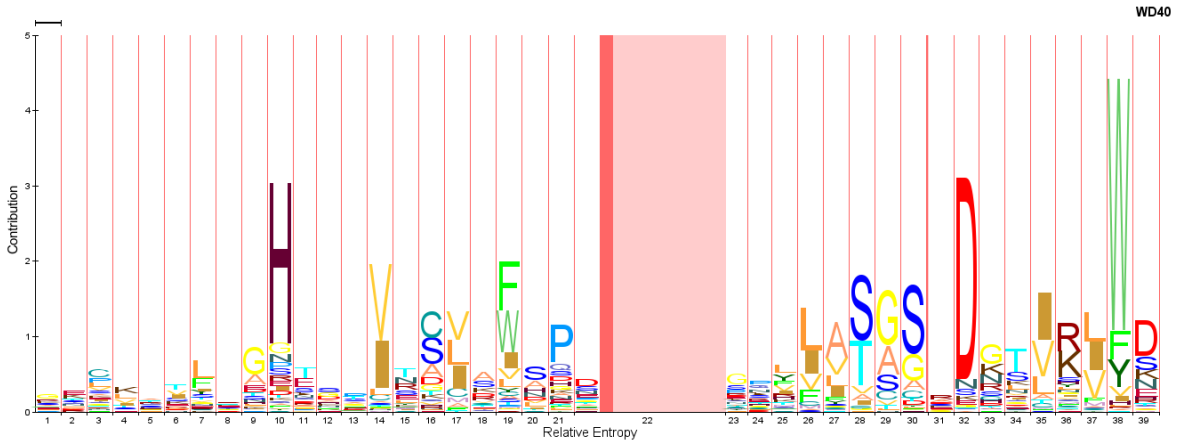

Figure 7.2 **WDR16 proteins across eukaryotes contain several WD40 domains.** (A) Domain architecture of eukaryotic WDR16 proteins. Protein sequences were initially scanned for domains using Pfam (http://pfam.sanger.ac.uk/), which identified several WD40 domains. The sequences were then specifically searched for WD40 domains with a cut off e-value of e-1. (B) Pfam Hmm logo of the WD40 domain.

gene for the T7 RNA Polymerase, the tetracycline repressor, and a single resistance marker. The possession of only one, instead of two, resistance marker allows more future genetic modifications.

Localisation of G-WDR16 in this single marker cell line was identical to the localisation shown by Helen Farr (Fig 7.3). To test whether WDR16 has the same localisation in bloodstream trypanosomes, I generated a bloodstream cell line which expressed G-WDR16 from the endogenous *WDR16* locus. This also demonstrated localisation of G-WDR16 to the axoneme and the basal body region (Fig 7.4).

To investigate the G-WDR16 signal in the basal body region, procyclic form cells were immunolabelled with a marker for mature basal bodies, YL1/2. The YL1/2 antibody recognises tyrosinated α-tubulin which is found at the posterior end of the subpellicular MT cytoskeleton and around the distal appendages of the basal body (Kilmartin et al., 1982; Stephan et al., 2007). The GFP signal is found only distal of the YL1/2 labelling, suggesting that WDR16 localises to the transition zone and the axoneme but not to the basal body (Fig. 7.5). Comparing the localisation of Y-SAS-6 to G-WDR16 using a combination of the basal body markers YL1/2 and BBA4 as reference showed that WDR16 is present only distal to SAS-6 (Fig. 7.6 A). This result was further confirmed by co-expression of Y-SAS-6 and Ty-mCherry-WDR16 (mC-WDR16, Fig. 7.6 B). The localisation of WDR16 is consistent with the results in Chapter 5, where measurements of the position of different markers in the basal body and along the axoneme showed that the most proximal localisation of mC-WDR16 was at a position consistent with the transition zone (Fig. 5.6 C).

Although WDR16 was absent from the basal body, the protein localised to a position consistent with the pro-basal body as demonstrated by co-localisation with Y-SAS-6 at this site (Fig. 7.6 B).

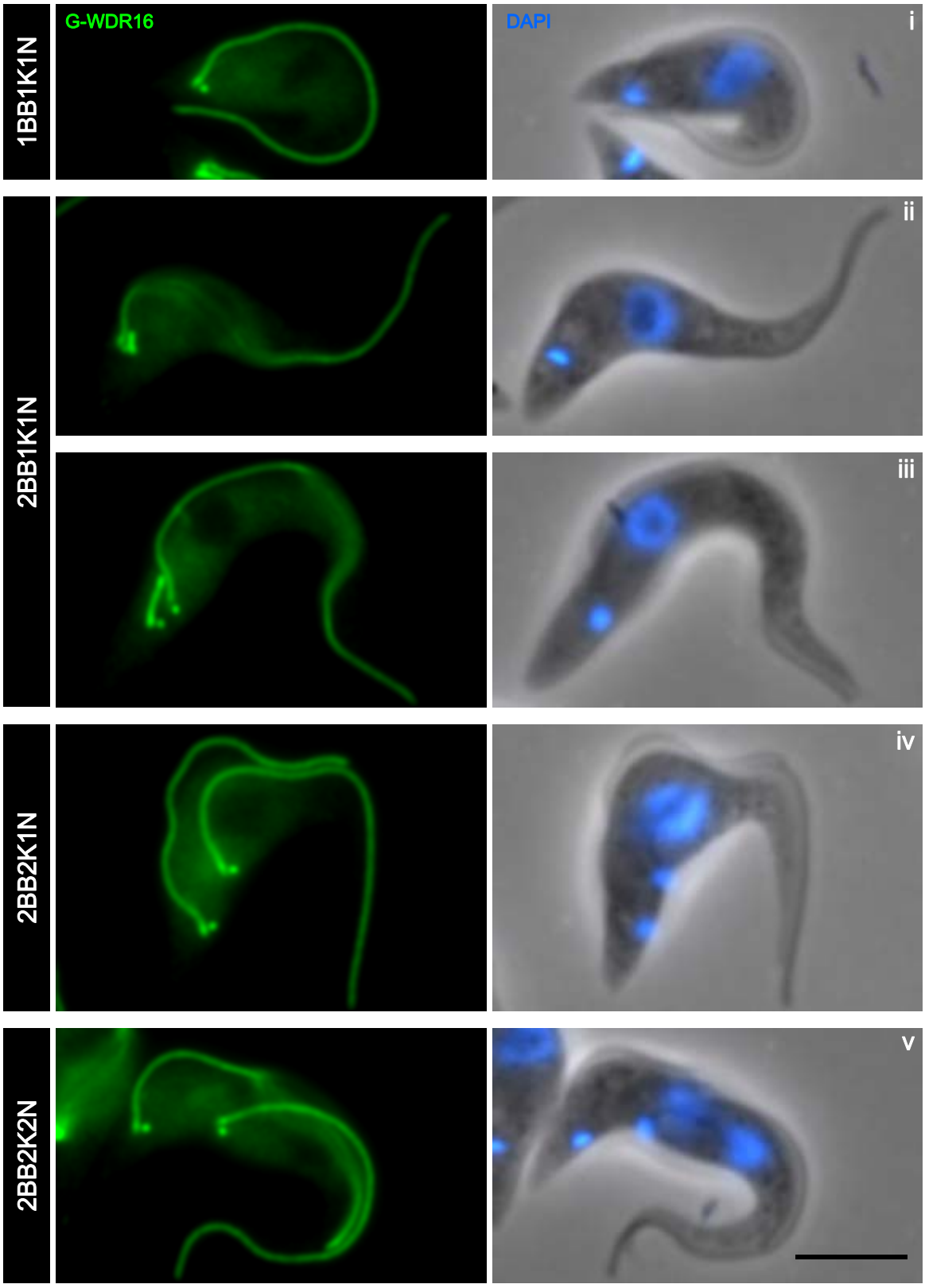

Figure 7.3 **G-WDR16 localises to the basal body area and the axoneme in procyclic form cells.** *T. brucei* WDR16 N-terminally tagged with Ty-GFP (G-WDR16, green) was expressed from the endogenous *WDR16* locus in procyclic forms. Cells were fixed with formaldehyde. DNA was labelled with DAPI (blue). Scale bar: 5μm.

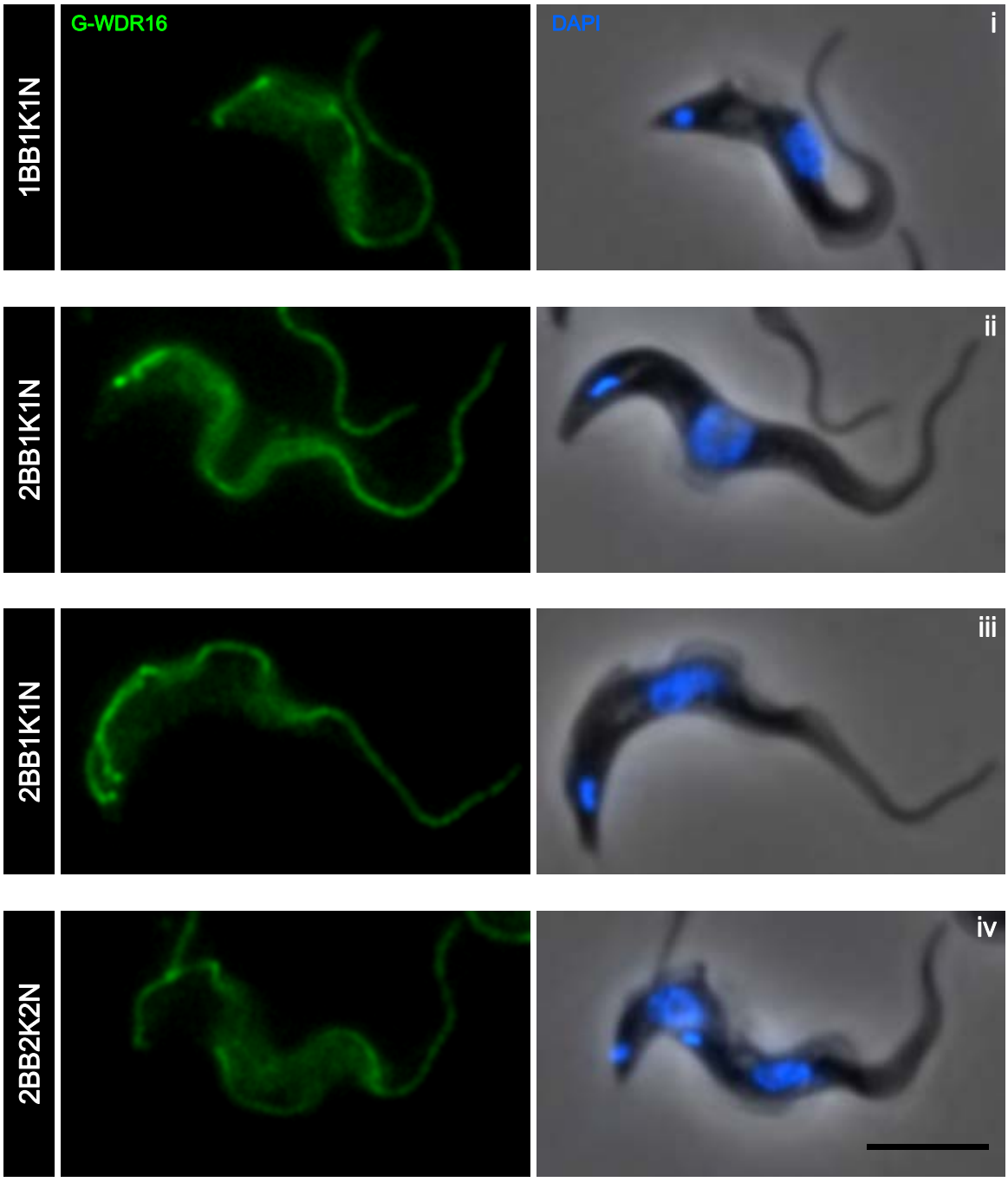

Figure 7.4 **G-WDR16 localises to the basal body area and the axoneme in bloodstream form cells.** *T. brucei* WDR16 N-terminally tagged with Ty-GFP (G-WDR16, green) was expressed from the endogenous *WDR16* locus in bloodstream forms. Cells were fixed with formaldehyde. DNA was labelled with DAPI (blue). Scale bar: 5μm.

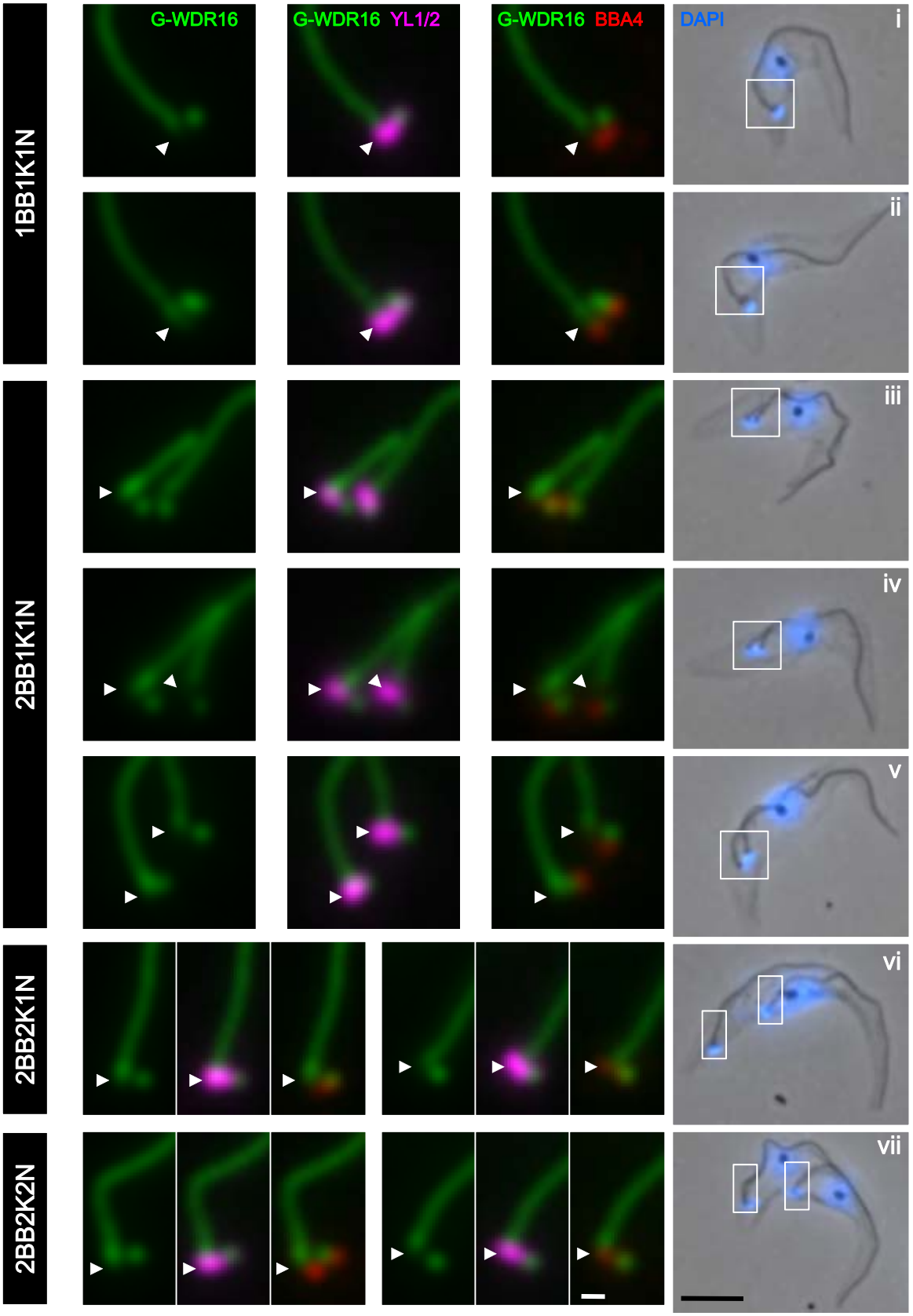

Figure 7.5 **G-WDR16 localises distal to YL1/2 suggesting G-WDR16 is not in the basal body but in the transition zone and axoneme.** Cells expressing G-WDR16 (green) were detergent-extracted, fixed in methanol and immunolabelled with YL1/2 (magenta) and BBA4 (red). DNA was labelled with DAPI (blue). Insets show basal body area. White arrow heads point towards basal body. White scale bar: 500nm. Black scale bar: 5μm.

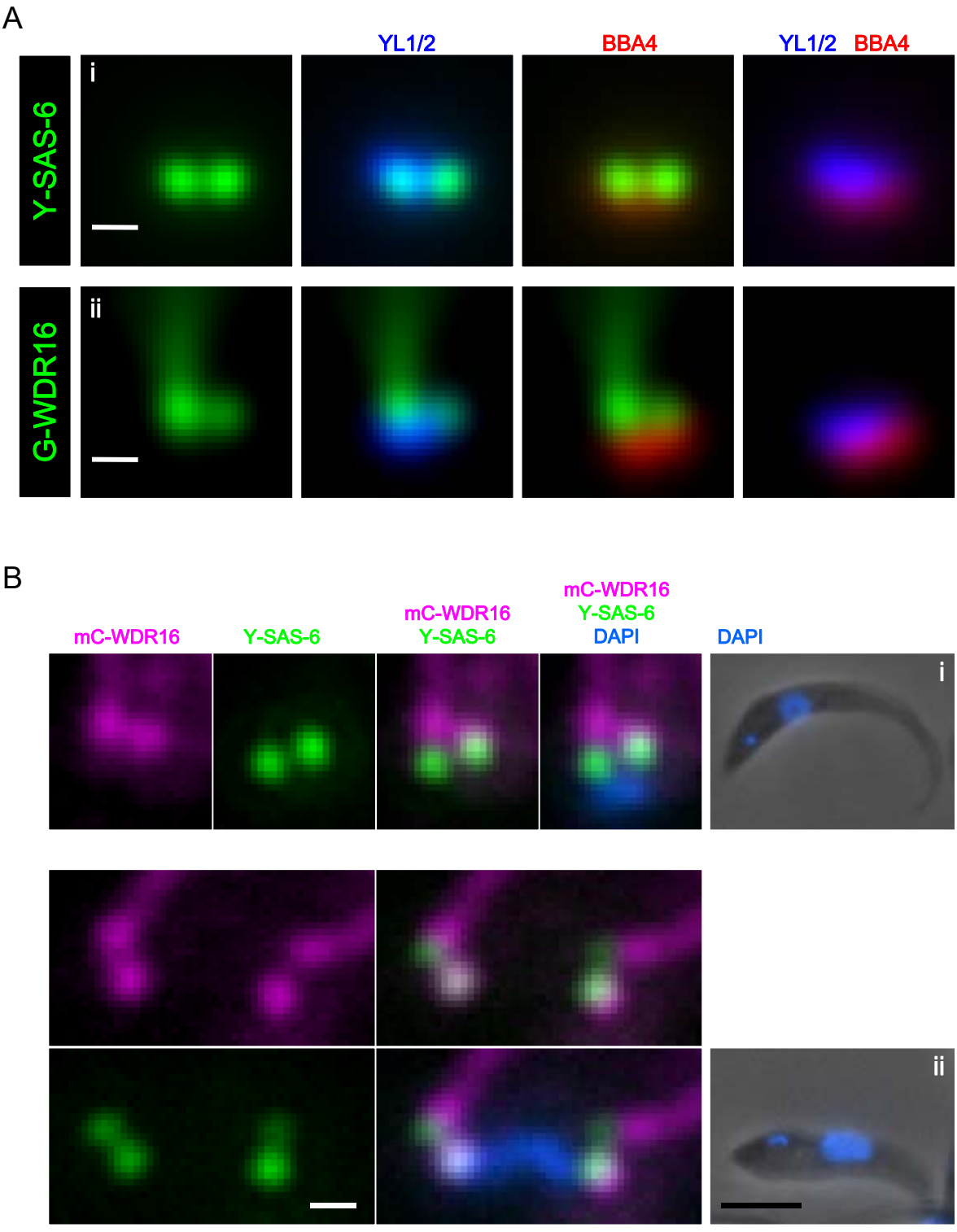

Figure 7.6 **WDR16 is distal to SAS-6 in the BB.** (A) Cells expressing Y-SAS-6 or G-WDR16 were detergent-extracted, fixed in methanol and immunolabelled with YL1/2 (magenta) and BBA4 (red). Images of the basal bodies region of 1BB1K1N cells (n=58 for Y-SAS-6, n=24 for G-WDR16) were aligned with BB in the centre for Y-SAS-6 and the transition zone in the centre for G-WDR16, and the pBB to the right, summed up and normalised according to number of input images. Basal bodies were distinguished of pro-basal bodies by the presence of YL1/2 (blue). Scale bar 500nm. (B) Cells expressing Y-SAS-6 and mCherry-WDR16 fixed with formaldehyde. DNA was labelled with DAPI (blue). Insets show basal body area. White scale bar: 500nm. Black scale bar: 5μm.

7.4 Knockdown of WDR16 does not cause a defect

For the purpose of detection of all WDR16 during RNA interference, I first generated a cell line in which both endogenous *WDR16* alleles where modified to express G-WDR16. Correct integration of the targeting constructs and absence of the wild-type *WDR16* allele was confirmed by PCR (Fig. 7.7 A). As G-WDR16 showed aberrant running behaviour in SDS gels electrophoresis, G-WDR16 levels were analysed by dot blot of whole cell extracts using anti-tag antibodies. This demonstrated that the cells with two *G::WDR16* alleles expressed a higher amount of the tagged protein compared to cells with a single *G::WDR16* allele (Fig. 7.7 B). Consistent with this, the YFP fluorescence signal in *G::WDR16/G::WDR16* cells was more intense than in cells with a single *G::WDR16* allele (Fig. 7.7 C). Cells expressing only G-WDR16 were morphologically indistinguishable from cells expressing wild-type WDR16. However, the population growth of *G::WDR16/G::WDR16* cells was slower compared to wild-type cells (Fig. 7.7 D).

To investigate the function of WDR16, I generated a cell line with inducible RNA interference against *WDR16* in the *G::WDR16/G::WDR16* background. Dot Blot analysis of doxycycline-induced cells confirmed that the RNAi construct was effective in reducing the amount of WDR16 (Fig. 7.8 A). However, the protein remained detectable even 72h after RNAi induction. Induction of WDR16 RNAi did not affect the population growth rate or the cell volume (Fig. 7.8 B,C). Microscopic examination showed a reduction of GFP-WDR16 across the population (Fig. 7.9). Nevertheless, the cells looked morphologically normal after RNAi induction.

Since the protein was still detectable after RNAi induction, it can not be excluded that small amounts of residual WDR16 are sufficient to fulfil an essential function. However, as strong reduction of the protein does not cause any defect, it is unlikely that WDR16 is an essential protein.

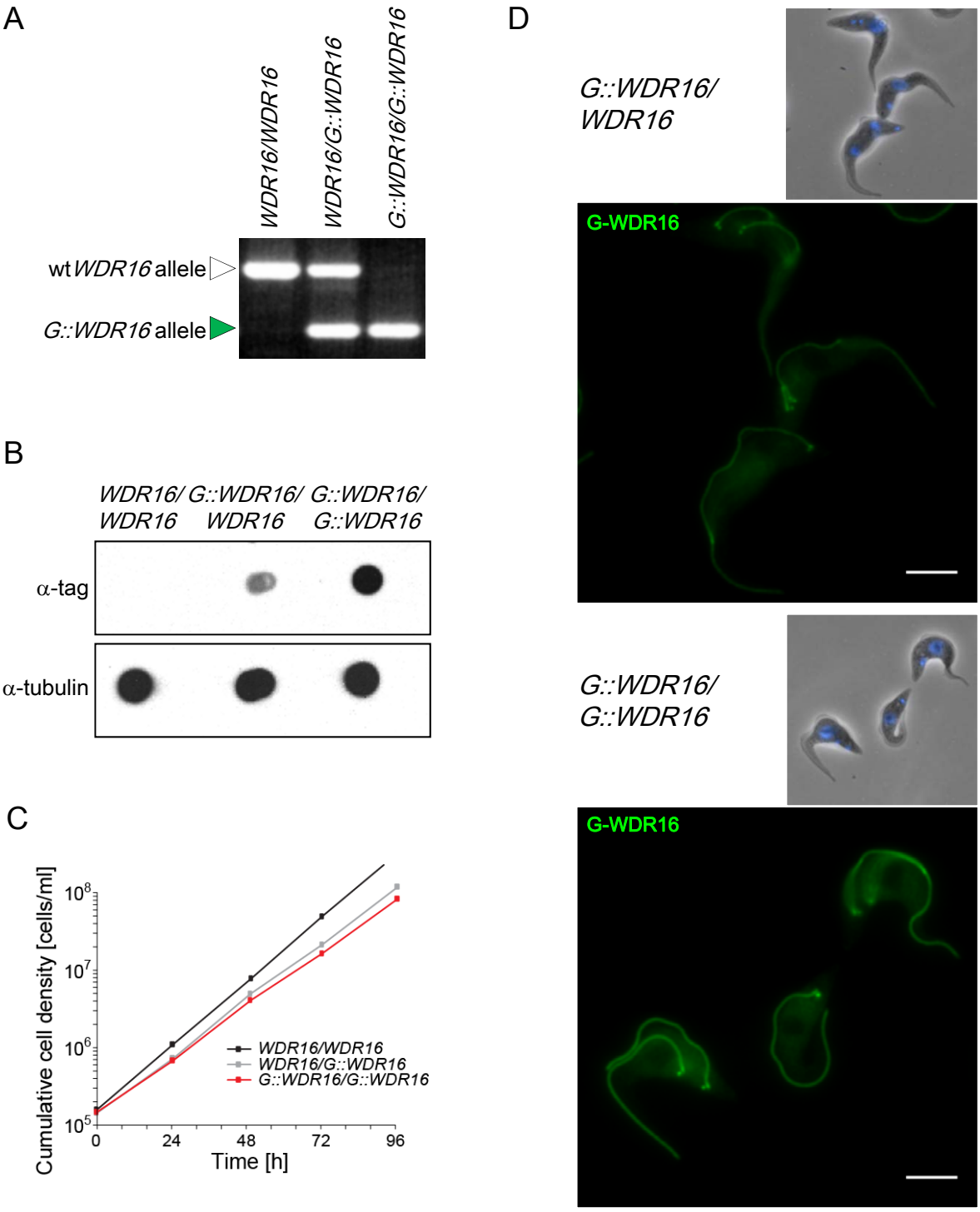

Figure 7.7 **Cells expressing only G-WDR16 without wild-type WDR16 look normal.** In *G::WDR16/WDR16* cells one endogenous *WDR16* allele and in *G::WDR16/G::WDR16* cells both endogenous *WDR16* alleles were modified to express G-WDR16. This abolished expression of wild-type WDR16 in the latter cell line. (A) Examination of genomic DNA of cells given above image for wild-type and modified WDR16 alleles. The PCR confirmed that *G::WDR16/G::WDR16* has no wild-type allele left. (B) Dot blot analysis of cells given above image with anti-tag (anti-GFP, anti-Ty) antibody showing that *G::WDR16/G::WDR16* has a higher amount of G-WDR16. (C) Population growth was measured every 24h over 96h and cultures were diluted every 48h. This showed that although *G::WDR16/G::WDR16* grow slower than wild-type cells, they are viable. (D) Microscopy showed that *G::WDR16/G::WDR16* cells looked morphologically normal and that their GFP signal appeared brighter compared to *G::WDR16/WDR16*. DNA was labelled with DAPI (blue). Scale bar: 5μm.

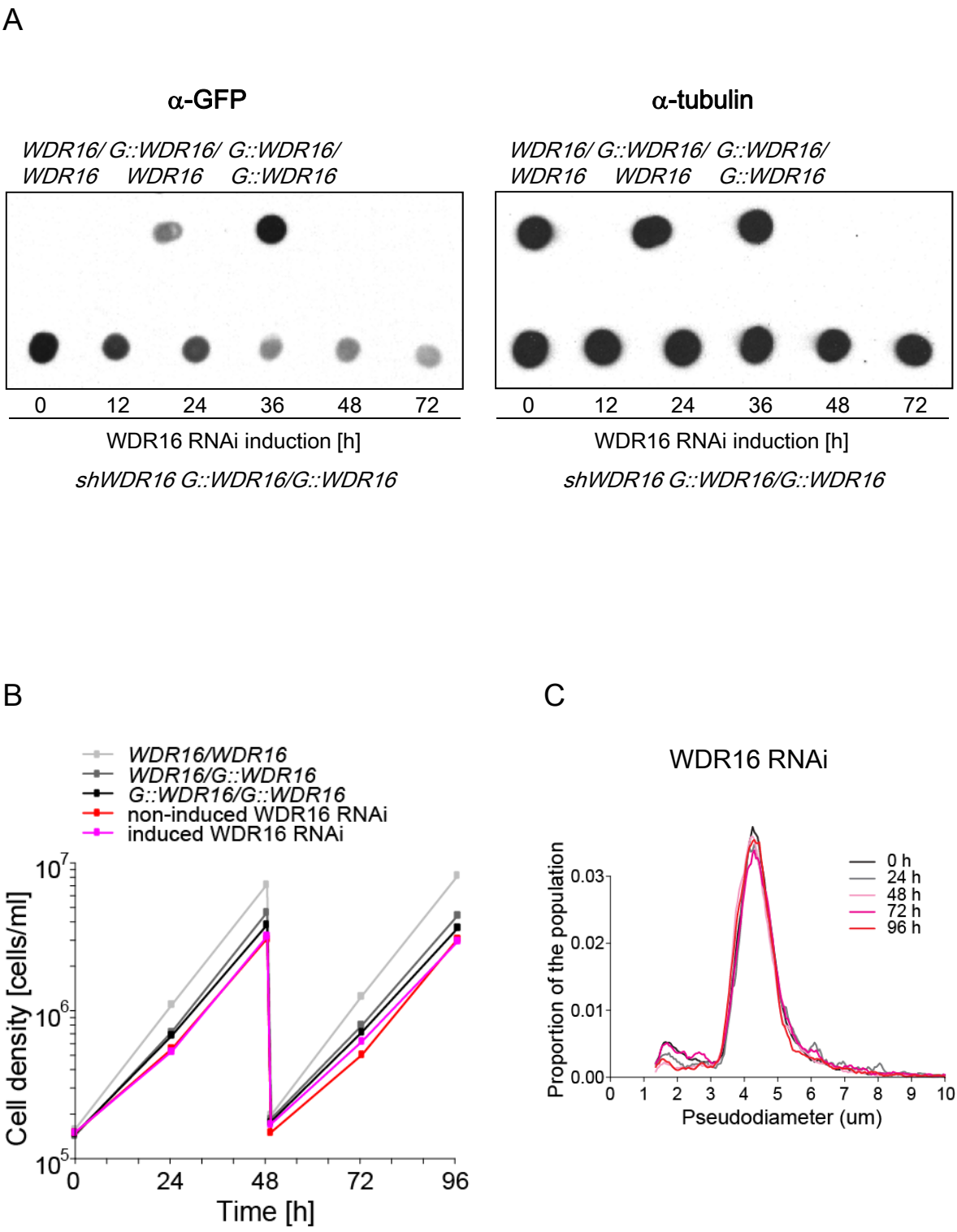

Figure 7.8 **Ablation of WDR16 has no effect on population growth.** (A) Dot blot analysis of cells given above and below image with anti-tag (anti-GFP, anti-Ty) showing the reduction of WDR16 after induction of RNAi against *WDR16*. WDR16 remained detectable 72h after RNAi induction. (B) Population growth measured every 24h over 96h with cultures diluted every 48h showed that the depletion of WDR16 did not resulted in a dramatic reduction in cell duplication. (C) Histogram of the cell volume after WDR16 RNAi induction showing that cells did not change in size.

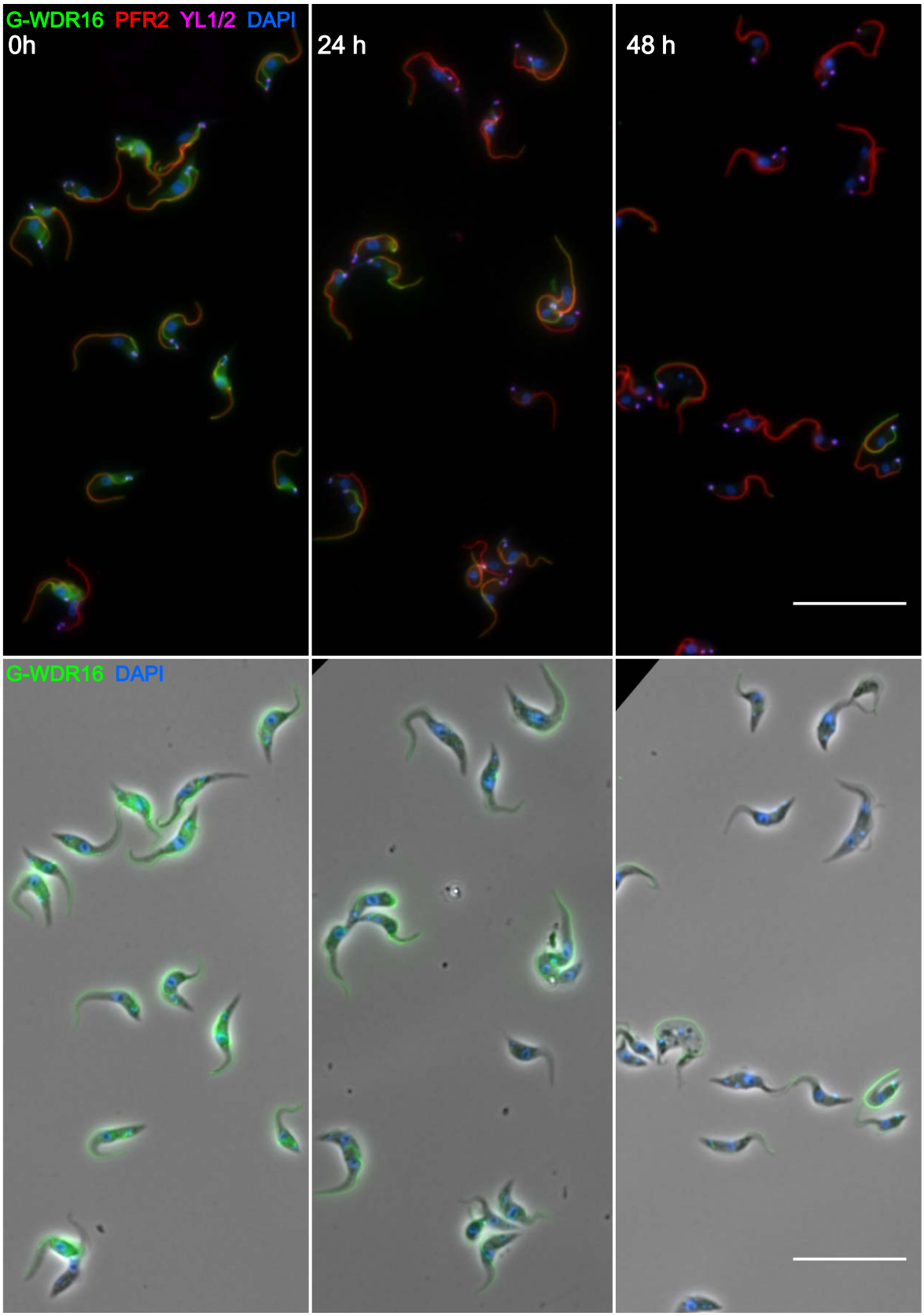

Figure 7.9 **WDR16-depleted cells look morphologically normal.** *G::WDR16/G::WDR16* cells with WDR16 RNAi induced and non-induced were fixed with formaldehyde, permeabilised in methanol and immunolabelled with L8C4 (anti-PFR2, red) and YL1/2 (anti-tyrosinated alpha-tubulin). Fluorescence microscopy confirmed the depletion of G-WDR16 (green). DNA was labelled with DAPI (blue). Scale bar: 25μm.

7.5 WDR16 is a stable component of the axoneme

Interestingly, after reduction of G-WDR16 by RNAi the fluorescence intensity indicated the protein was still present in the old flagellum while its level was strongly reduced in the new flagellum on the posterior side of the cell (Fig. 7.10). Some old flagella in these cells exhibit a fluorescent signal only at the proximal end but not towards the distal end. These findings suggest that WDR16 is not in exchange with the cytoplasmic pool and that it is not very if at all mobile but that WDR16 is a stable component of the axoneme.

7.6 Depletion of WDR16 does not cause detectable changes in the ultrastructure of the axoneme

To investigate whether WDR16 knockdown causes any ultrastructural changes in the axoneme of trypanosomes, cytoskeletons of cells 0h and 84h post WDR16 RNAi induction were prepared for electron microscopy. Thin section electron microscopy demonstrated that the ultrastructure of axonemes from cells with reduced levels of WDR16 were indistinguishable from axonemes from wild-type cells (Fig. 7.11).

7.7 Summary

WDR16 in *T. brucei* was previously identified in the flagellar proteome and localised to the basal body, pro-basal body and axoneme. It shows high sequence conservation and its presence in almost all ciliated species analysed in Chapter 3 strongly suggests that the protein is involved and important in cilia function. I showed that WDR16 is a stable component of the axoneme but that its knockdown does not cause a change in cell growth, cell morphology or axonemal ultrastructure in *T. brucei*.

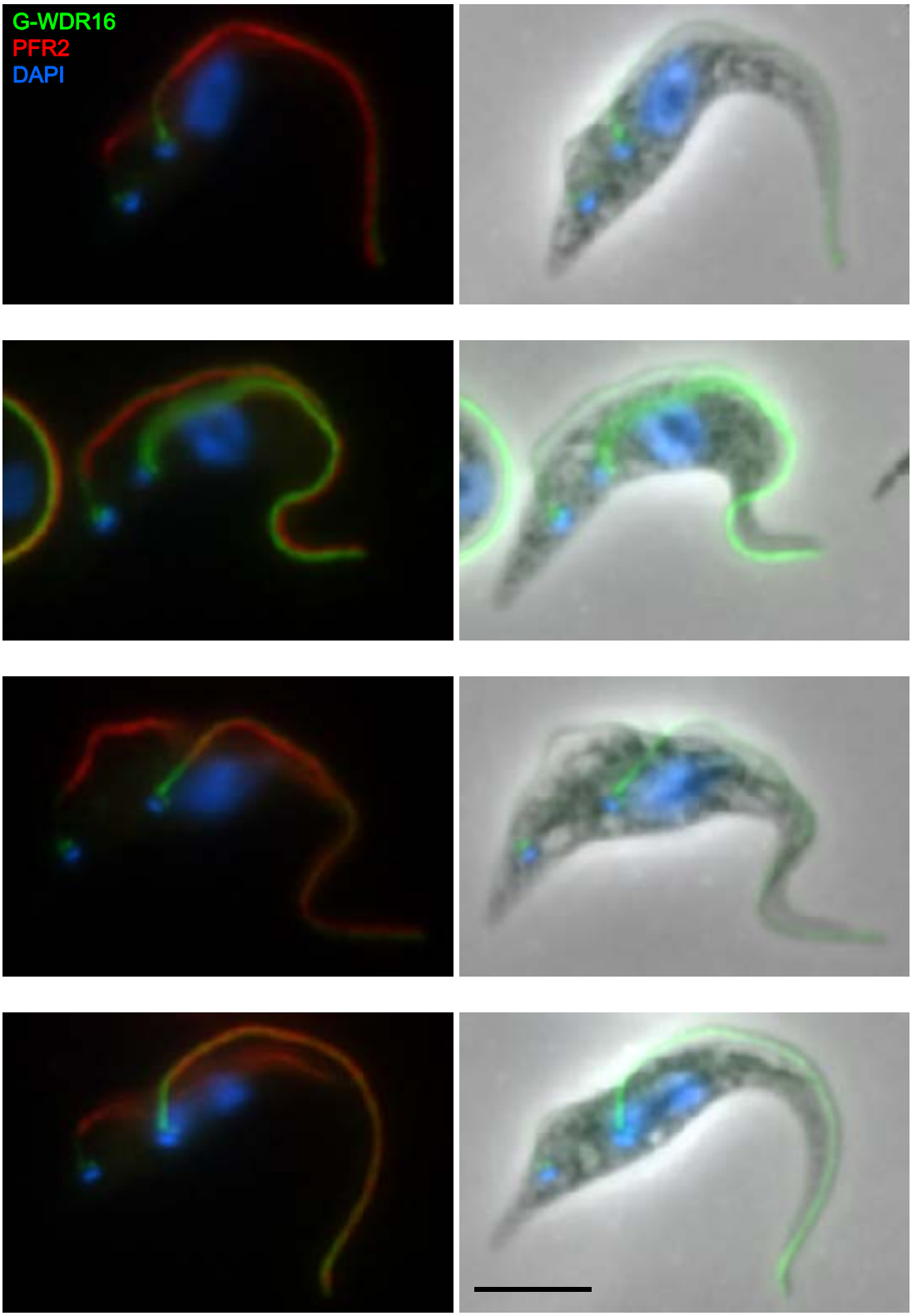

Figure 7.10 **WDR16 is stably integrated into the axoneme.** *G::WDR16/G::WDR16* cells 24h post WDR16 RNAi induction were fixed with formaldehyde, permeabilised in methanol and immunolabelled with L8C4 (anti-PFR2, red) and YL1/2 (anti-tyrosinated alpha-tubulin). 2BB2K1N cells show that G-WDR16 remained in the old axoneme after G-WDR16 level was reduced and less/no G-WDR16 was incorporate into the new axoneme. DNA was labelled with DAPI (blue). Scale bar: 5μm.

A non-induced WDR16 RNAi

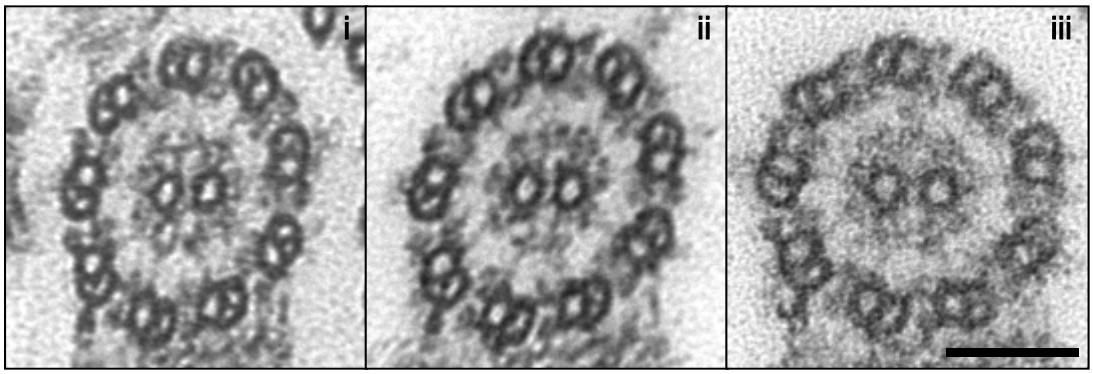

B 84h induced WDR16 RNAi

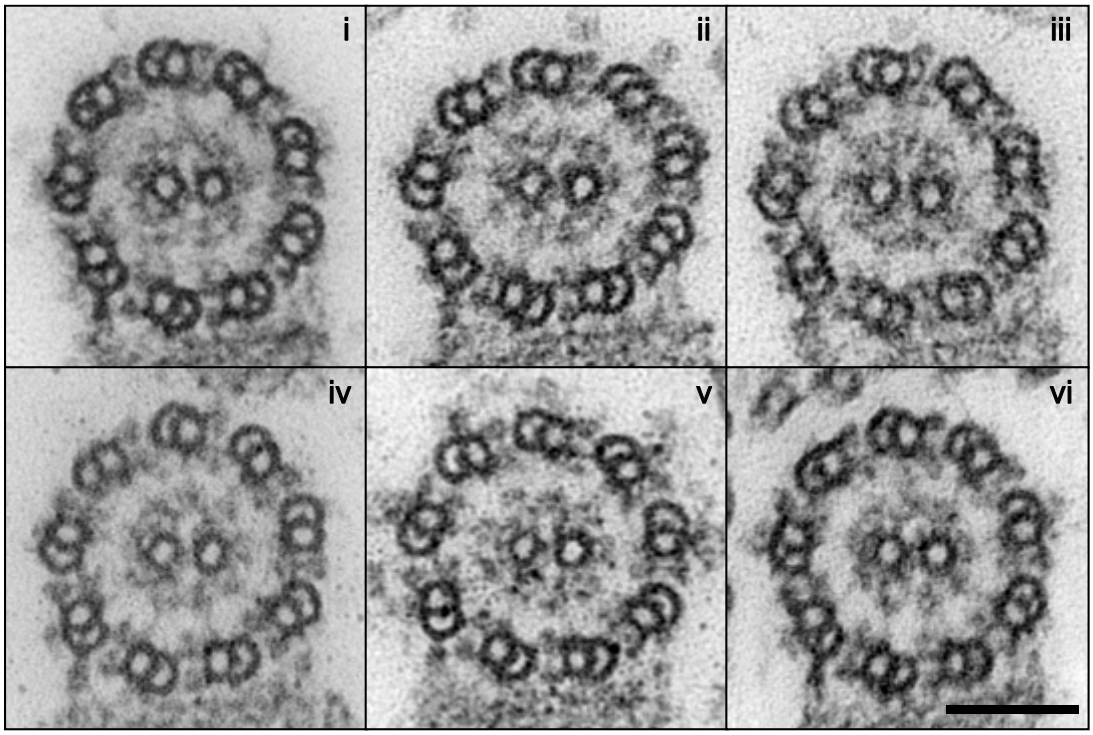

Figure 7.11 **The ultrastructure of axonemes of cells with reduced WDR16 looks normal.** TEM thin sections of axonemes of cytoskeleton preparations of non-induced (A) and 84h induced (B) WDR16 RNAi cells showed that the ultrastructure of axonemes of WDR16 RNAi induced cells looks indistinguishable from those from non-induced cells. Scale bars: 100nm.

DISCUSSION

8.1 Evolution of the centriole and basal body

Centrioles are highly conserved structures fulfilling important cellular functions such as nucleation of cilia (basal body function) and organisation of pericentriolar material to form the centrosome. The importance of cilia during development in cell signalling is increasingly acknowledged due to the discovery that multiple pathologies are caused by cilia dysfunction. In Chapter 3, I describe work undertaken by myself and another graduate student, Matthew Hodges, concerning the evolution of 53 proteins known either for centriolar association or for involvement in cilia-associated pathologies. The distribution of these proteins in 45 diverse eukaryotes was linked with the presence and absence of cilia.

8.1.1 The ancestor of all eukaryotes

This bioinformatic analysis provided molecular evidence that the basal body function is ancestral to eukaryotes, whereas centrosome components are specific to the Holozoa. Hence, it suggests that the cenancestor of eukaryotes possessed a basal body with no association to the centrosome. Furthermore, the phylogenetic distribution of the BBSome, which is involved in the transport of signalling molecules (Jin et al., 2010; Lechtreck et al., 2009; Nachury et al., 2007), suggests that this complex is also ancestral. The observation that the BBSome is absent from organisms that produce cilia only for motility further supports a role for the BBS complex in the sensory function of

cilia. Most importantly, it suggests that the cenancestor had a cilium or cilia capable of signalling and sensing.

This cenancestor possessed 14 centriolar proteins still present in extant ciliated eukaryotes. Interestingly, the morphology of the extant centrioles/basal bodies seems surprisingly insensitive to multiple losses from the centriolar set. Thus, the cenancestral basal body likely had a similar ultrastructure to canonical extant centrioles/basal bodies with a nine-fold symmetrical MT triplet arrangement.

The distribution of PLK homologues suggest that the enzyme was present in the cenancestor, wherein it may or may not have had a role that included initiation of centriole/basal body duplication. However, the non-identification of the PLK family from nine out of 29 ciliated species makes it unlikely that the kinase has a conserved role in the initiation of centriole/basal body duplication outside animals and suggests that another mechanism for the initiation of organelle duplication must exist.

8.1.2 Centrosome - a holozoan innovation

Our bioinformatic analysis provides evidence that centrosome components are specific to the Holozoa (animal and the choanoflagellate *Monosiga brevicollis* in our analysis) and hence suggests that the centrosome may be a holozoan innovation. One hypothesis is that association of basal bodies with spindle poles allowed fidelity in inheritance of the organelle during cell division (Pickett-Heaps, 1971; see also Beisson and Wright, 2003; Bornens and Azimzadeh, 2007). In the course of holozoan evolution basal bodies and spindle pole/pericentriolar material became interlinked to form the centrosome. Judging from the range of functions centrosomes perform in extant animal, it seems plausible to assume that the emergence of the centrosome contributed to the complex development of Holozoa. Centrosomes in most animal cells are critical for precise cell division, which is critical during the complex development of animals with up to 10^{14} cells. Furthermore, a centrosome pair can facilitate the asymmetric accumulation of factors and form an asymmetric

spindle leading to the formation of different daughter cells, which is a crucial prerequisite for the complex development of Holozoa (Wang et al., 2009).

Our analysis also showed that the PLK4 family is specific to Holozoa. This suggests that centriole duplication initiated by PLK4 activity is also a holozoan development, probably associated with the emergence of the centrosome.

8.1.3 Divergence of the model organism *Caenorhabditis elegans*

Caenorhabditis elegans has MT singlet centrioles lacking a defined cartwheel structure at the proximal end and non-motile cilia without apparent basal bodies (Perkins et al., 1986). This ultrastructural abnormality is also reflected in the higher degree of divergence and lack of molecular components compared to other species. The centriolar proteins SAS-4 and SAS-6, as well as and the centrosomal components SPD-2 and SZY-20, originally identified in the nematode (Dammermann et al., 2004; Kemp et al., 2004; Kirkham et al., 2003; Leidel et al., 2005; Leidel and Gonczy, 2003; Pelletier et al., 2006; Song et al., 2008), were not found by our method. WDR16 in *C. elegans* was identified by BLASTp search in Chapter 7, but too divergent to be found by our bioinformatic approach. We showed further that ZYG-1, functionally analogous to PLK4 and SAK (Bettencourt-Dias et al., 2005; Habedanck et al., 2005; O'Connell et al., 2001), can neither be grouped within the PLK4 family nor with any other kinase families either. The orphan nature of ZYG-1 is another molecular demonstration of the atypical nature of *C. elegans* centrioles. The extreme divergence of the nematode must be considered when functions of centriolar proteins are investigated and inferred to other model systems. While SAS-6 in *C. elegans* is involved in the assembly of the central tube (Pelletier et al., 2006), SAS-6 homologues in other eukaryotes constitutes the cartwheel (Nakazawa et al., 2007). SAS-4 in *C. elegans* has been suggest being involved in the attachment of centriolar MTs (Pelletier et al., 2006), while homologues in other species have been suggest to have a role in elongation of the MTs (Tang et al., 2009).

8.1.4 Comparison to another bioinformatic analysis

Parallel to our analysis another bioinformatic study of a small set of centriole proteins, which included SAS-4, SAS-6, Cep135, PLK4/SASK, PLK, CP110 and SPD2, was published (Carvalho-Santos et al., 2010). The distribution patterns of the centriole proteins found by the Bettencourt-Dias lab were very similar to the ones described by us. However, a major difference is their conclusion that PLK is involved in the initiation of centriole/basal body duplication across ciliated eukaryotes. Two circumstances lead to this difference: 1) the use of a different methodology to search for homologues led to the identification of PLK in *Batrachochytrium dendrobatidis*, *Chlamydomonas reinhardtii*, *Giardia lamblia* and *Trichomonas vaginalis*; 2) due to a lower number of representatives of Chromalveolata, species where we did not identify PLK homologues like *Toxoplasma gondii*, *Aureococcus anophagefferens* and Phytophthora sojae are not investigated at all. We could not find PLK homologues in nine out of the 29 analysed ciliated species, which made us conclude that PLK is ancestral but not the initiator of centriole/basal body duplication across eukaryotes. Some minor differences between the two bioinformatic analyses, probably also due to the different methodology used, include identification in the Bettencourt-Dias lab of a SPD2 homologue in *Dictyostelium discoideum*, of a PLK4 homologue in *Batrachochytrium dendrobatidis*, and of a Cep135/Bld10 homologue in trypanosomes.

8.2 SAS-6 in *T. brucei* - a basal body protein

SAS-6 is a central component of the cartwheel in several eukaryotes (or central tube in *C. elegans*) and as such required in the assembly of centrioles and basal bodies in all species studied (Culver et al., 2009; Dammermann et al., 2004; Jerka-Dziadosz et al., 2010; Kitagawa et al., 2011c; Kleylein-Sohn et al., 2007; Leidel et al., 2005; Nakazawa et al., 2007; Peel et al., 2007; Rodrigues-Martins et al., 2007a; van Breugel et al., 2011; Vladar and Stearns, 2007). In this thesis, I characterised the SAS-6 orthologue in *Trypanosoma brucei*, which is distantly-related to all species

where SAS-6 has been studied to-date. I showed that tagged SAS-6 localises to the basal body and the pro-basal body, and that this tag does not impede with the functionality of the protein. The amount of SAS-6 at the basal body and pro-basal body is cell-cycle dependent, with the highest amount residing at assembling pro-basal bodies. Furthermore, I demonstrated that SAS-6 is not stably integrated into the basal body but that it is in dynamic exchange probably with a cytoplasmic pool. SAS-6 in *T. brucei* is an essential protein whose RNAi-mediated depletion results in defective basal body assembly. Thin section electron microscopy revealed both ultrastructural defects of basal bodies and a complete lack of pro-basal bodies in the absence of SAS-6. Moreover, ectopic overexpression of SAS-6 does not induce a general basal body overduplication.

8.2.1 SAS-6 localisation to the basal body in *T. brucei*

Ty-YFP-tagged SAS-6 localises to the basal body and pro-basal body throughout the cell cycle in *T. brucei*. The amount of protein changes during the cell cycle with the highest levels of SAS-6 observed at pro-basal bodies in the 4BB1K1N cells. These cells are in S and G2 phase of the cycle (Woodward and Gull, 1990). By the time nuclear mitosis starts, the SAS-6 level at the pro-basal body is decreased but remains detectable.

The localisation of SAS-6 in *T. brucei* is consistent with the localisation of SAS-6 homologues to the centriole or basal body in *Caenorhabditis elegans*, *Drosophila melanogaster*, *Homo sapiens*, *Chlamydomonas reinhardtii*, *Tetrahymena thermophila* and *Paramecium tetraurelia* (Culver et al., 2009; Dammermann et al., 2004; Jerka-Dziadosz et al., 2010; Kleylein-Sohn et al., 2007; Leidel et al., 2005; Nakazawa et al., 2007; Peel et al., 2007; Rodrigues-Martins et al., 2007a). However, the dynamics of the protein to these structures vary across species. Cellular/centriolar levels of human SAS-6 oscillate during the cell cycle, with increasing levels in S phase and decreasing ones during the metaphase/anaphase transition in mitosis (Strnad et al., 2007). In contrast to the finding in *T. brucei*, SAS-6 is completely lost from pro-centrioles during disengagement in human cells (Kleylein-Sohn et al., 2007; Strnad et al., 2007). This loss is associated with the cell-cycle

dependent degradation of the human protein by APC/Cdh1 (Strnad et al., 2007). The centriolar SAS-6 levels in *C. elegans* embryos decrease only by 50% in the second half of mitosis (Dammermann et al., 2008). Whether this is representative for SAS-6 dynamics in all cells of the nematode, or whether the SAS-6 maintenance is an embryo-specific phenomenon due to short cell cycles with essentially no G1 phase to prepare for the next cycle, is not clear (Dammermann et al., 2008). One commonality between the SAS-6 dynamics in these three species is the increased amount of protein at the centriole/basal body during S phase while new structures assemble. However, the time points in the cell-cycle at which SAS-6 level change earlier in *T. brucei* than in animal cells. This finding demonstrates that SAS-6 levels and basal body duplication are also coupled to the cell cycle in *T. brucei*. However, the different timing and degree of SAS-6 removal indicate the molecular mechanisms linking cell cycle and SAS-6 regulation might by different between the three species.

Two models have been suggested for the SAS-6 dynamics observed in *C. elegans* (Dammermann et al., 2008), both of which could also apply to *T. brucei* and explain the partial decrease: (1) SAS-6 is recruited and directly integrated into the assembling pro-basal body without excess protein accumulating around the structure. In this case the following SAS-6 decrease would correspond to the loss of a structural component (such as the cartwheel). (2) SAS-6 accumulates initially around the basal body and a proportion of the protein is integrated into the assembling pro-basal body. In this scenario the decrease of SAS-6 would reflect the clearance of excess protein after pro-basal body assembly is finished. Whereas the authors of the *C. elegans* study favour the second model for centriole assembly in *C. elegans*, both models could be envisioned plausible for basal body assembly in *T. brucei*. The association of the high SAS-6 level with the pro-basal bodies and not with the basal bodies in 4BB1K1N cells supports the first model but does not exclude the second model. Despite efforts to identify a cartwheel in mature basal bodies in *T. brucei*, the presence of this structure could not be demonstrated so far; the absence of the cartwheel would also support the first model (discussed below).

8.2.2 SAS-6 function in basal body assembly in *T. brucei*

A range of experiments have provided substantial evidence that SAS-6 forms the central hub of the cartwheel and probably parts of the spokes (Kitagawa et al., 2011c; Nakazawa et al., 2007; van Breugel et al., 2011). The SAS-6 RNAi phenotype in *T. brucei* is consistent with this role. RNAi-mediated depletion of SAS-6 in *T. brucei* leads to defects in basal body duplication, which establishes either as the complete absence of a pro-basal body or as basal bodies with a reduced number of MT triplets. The complete failure of pro-basal body assembly is comparable to the phenotypes observed in other eukaryotes where absence of functional SAS-6 leads to complete failure of centriole assembly (Dammermann et al., 2004; Kleylein-Sohn et al., 2007; Leidel et al., 2005; Nakazawa et al., 2007; Peel et al., 2007; Rodrigues-Martins et al., 2007a; Vladar and Stearns, 2007). *Chlamydomonas bld12*, a null mutant of the *SAS-6* homologue, also does not form basal bodies under normal circumstances. However, after treatment of the cells with autolysin which removes cell wall, 20% of the cells in the *bld12* strain assemble basal bodies, although often with an aberrant number of MT triplets (Nakazawa et al., 2007). This is similarly to the basal bodies with a reduced number of MT triplets in *T. brucei*.

The assembly of these defective basal bodies in *T. brucei* could have occurred under two different conditions: (1) in complete absence of SAS-6, or (2) in the presence of small residual amounts of SAS-6. In support for the latter condition is that non-induced cells, which have reduced levels of SAS-6 (Fig. 4.6), have occasionally defective basal bodies (Fig 4.9). Furthermore, all defective basal bodies observed lacked a pro-basal body. This could mean that assembly of the defective basal bodies occurred when small amounts of residual SAS-6 were still present, whereas at the time when pro-basal body would have occurred no SAS-6 was present anymore. As SAS-6 is likely to form the cartwheel, it seems plausible that reduced amounts of SAS-6 facilitated the formation of a smaller cartwheel with fewer spokes that accommodate less MT triplets.

Ectopic overexpression of SAS-6 in *T. brucei* was not sufficient to induce general overduplication of

basal bodies. Overduplication of centrioles has been observed after overexpression of SAS-6 in unfertilised *D. melanogaster* eggs and after the expression of degradation-resistant SAS-6 in human cells (Peel et al., 2007; Strnad et al., 2007) In other instances overexpression of SAS-6 is not sufficient to induced overduplication of bona fide centrioles (Rodrigues-Martins et al., 2007a; Stevens et al., 2010b). My finding indicates that even though SAS-6 is an early structural component, basal body duplication in *T. brucei* requires a mechanism other than just presence of SAS-6 to trigger assembly of pro-basal bodies.

8.2.3 SAS-6 dynamics and implications for the cartwheel

As detailed in the introduction, our current understanding is that SAS-6 constitutes the central hub and probably parts of the spokes of the cartwheel (Kitagawa et al., 2011c; Nakazawa et al., 2007; van Breugel et al., 2011). SAS-6 consists of a globular head domain at the N-terminus, a central coiled coil region and a less defined C-terminus. Models predict that SAS-6 forms homodimers via the central coiled coil domain, and that nine of these dimers form into a ring via hydrophobic interactions between the N-terminal head domains to constitute the central part of the cartwheel (Kitagawa et al., 2011c; van Breugel et al., 2011).

In *T. brucei* a canonical cartwheel is present in pro-basal bodies, but seems to be absent from basal bodies (tomograms and serial sections from the Gull lab, (Lacomble et al., 2010)). Although the level of SAS-6 is higher at assembling pro-basal bodies, SAS-6 remains present throughout the cell cycle. If SAS-6 constitutes the cartwheel and nothing else in the basal body and pro-basal body, the presence of SAS-6 should be an indication for the presence of a cartwheel. This correlation fits well in *H. sapiens*, where cartwheel loss from the mature centriole is accompanied by the complete loss of SAS-6 (Alvey, 1986; Kleylein-Sohn et al., 2007). If the correlation was true in *T. brucei*, the presence of SAS-6 throughout the cell cycle would suggest that the cartwheel is not lost from the basal body in *T. brucei*. Conversely, electron tomography studies which do not show the presence of a cartwheel in the basal body would predict that SAS-6 is lost from the basal body after

assembly. However, both predictions are wrong. One explanation for this could be that the initial assumption of SAS-6 forming only the cartwheel is wrong. Another possibility is that tagged SAS-6 has different dynamics to wild-type SAS-6 and resides in basal bodies whereas wild-type protein leaves the structure. This would lead to a discrepancy between EM data on wild-type cells and dynamics of tagged SAS-6. However, as tagged SAS-6 has been shown to complement the essential functions of wild-type SAS-6, it seems unlikely that it behaves very differently to wild-type protein. Therefore, these data raise the question whether SAS-6 localises in a different shape than the cartwheel to the basal body in *T. brucei*.

The finding that SAS-6 is not a stably integrated component of the basal body was surprising. Individual molecules were readily exchanged as the displacement of YFP-tagged SAS-6 with mCherry-tagged SAS-6. This observation suggested either that the nature of the cartwheel allows exchange of molecules, or that the exchanged SAS-6 is not part of the cartwheel but another more dynamic pool in the basal body.

Together, these data indicate that SAS-6 localises to the basal body not only as part of the cartwheel.

8.2.4 Incomplete basal bodies support the assembly of associated structures

SAS-6 depletion led to the assembly of basal bodies with a reduced number of MT triplets. While structures with six to eight MT triplets still formed a closed circular arrangement of MT triplets, structures with less MT triplets organised in an open, half-circular arrangement were also observed. Nevertheless, the incomplete assemblies were still competent to support the formation of a transition zone with radial. A similar phenotype was observed in a SAS-6 loss-of-function mutant in *D. melanogaster*, where centrioles with a reduced number of MT triplets are assembled (Rodrigues-Martins et al., 2007a). Even structures that formed only a half circles arrangement of MT triplets appeared to support the formation of axonemes as some spermatocytes possessed axonemes with a half circle of outer MT doublets (Rodrigues-Martins et al., 2007a). My work and

the fly studies, both suggest that many assembly steps do not require a complete basal body/centriole but that MT triplets are sufficient to trigger subsequent steps.

8.3 SAS6L in *T. brucei* - a filament forming protein

In this thesis a novel family of proteins with similarity to the N-terminal proportion of SAS-6 is described. This SAS-6-like (SAS6L) protein family was shown to be most likely ancestral to all eukaryotes but lost near the root of Holozoa. I showed localisation of YFP-tagged SAS6L to a position consistent with the basal plate and around the exit of the flagellum from the pocket in *T. brucei*. Ectopic overexpression of the protein led to the formation of long cytoplasmic filaments that most likely originated from the latter localisation site.

8.3.1 SAS6L overexpression leads to filament formation

Eukaryotic SAS6L proteins are shorter than SAS-6 proteins and consist mainly of the N-terminal Pfam-B domain that is also contained in the N-terminus of SAS-6 proteins. Models based on crystallisation of the globular N-terminal head domain of SAS-6 from *C. elegans*, *D. rerio* and *C. reinhardtii* and polymerisation experiments have shown that this proportion of SAS-6 forms dimers via hydrophobic interactions (Kitagawa et al., 2011c; van Breugel et al., 2011). However, higher order oligomers require the coiled coil region of SAS-6 protein.

Interestingly, I showed that the overexpression of MH-YFP-TAP-tagged SAS6L in *T. brucei* leads to the formation of cytoplasmic filaments containing SAS6L but no tubulin. The filaments appeared to originate from the SAS6L localisation site around the exit of the flagellum from the flagellar pocket. It cannot be excluded that filament formation is an artefact that is supported by interaction/polymerisation of the tag. However, a comparable phenotype was also observed by our collaborators after the ectopic overexpression of YFP-tagged TgSAS6L in *Toxoplasma gondii* tachizoites. Furthermore, the similarity between SAS6L and SAS-6, and data showing dimerisation

of the N-terminal fragment of SAS-6 (Kitagawa et al., 2011c; van Breugel et al., 2011), indicates that SAS6L might have the potential to dimerise as well. However, since SAS6L lacks a coiled coil region it is not clear how the step from dimerisation to oligomerisation into rings and stacking into filaments is facilitated. Although the absence of α-tubulin, SAS-4 and centrin from the filaments was demonstrate, it remains to be shown whether the filaments are made only of SAS6L or if other proteins contribute to the formation.

The suggested nucleation site of the ectopic filaments is around the exit of the flagellum from the pocket. Recently, a fibre was described in this area (Esson et al., 2012). If SAS6L localise to this fibre and/or even forms it, the frequently observed forking of the ectopic filaments could be explained by two-sided extension of the fibre bending around the neck which could lead to the V-shaped filament.

8.3.2 Possible role for SAS6L in *T. brucei* and other eukaryotes

A genome-wide RNAi screen suggested that SAS6L is not essential for cell growth in *T. brucei* (Alsford et al., 2011). SAS6L presence in cilia-forming species (except Holozoa) and general absence form non-ciliated species suggests that it has a function in cilia formation. The major localisation sites of SAS6L are the basal plate, and around the exit of the flagellum from the pocket. Whether either, both or none of these sites are associated with the ancestral function is unclear. Basal plates exist in cilia of most cilia-forming species, which is suggestive of SAS6L at the basal plate being involved in the ancestral function. However, the function of SAS6L remains to be shown and could be addressed by ultrastructural investigations in a cell line with RNA interference against *SAS6L* or with *SAS6L* knockout.

The loss of SAS6L from Holozoa raises the question whether this loss is linked to the adaptation of the centriole and cilia to the emergence of the centrosome. In *T. brucei* SAS-6 localises to the basal body and SAS6L localises to a position consistent with the basal plate. In contrast, in multi-ciliated rat epithelia cells, which as holozoan cells lack a SAS6L homologue, SAS6 localises to the

basal body of cilia but also to a more distal site which is consistent with the position of the basal plate (Vladar and Stearns, 2007). In *D. melanogaster* spermatocytes SAS-6 localises to the proximal and distal side of centrioles, which is consistent with the position of the cartwheel and the basal plate (Peel et al., 2007; Rodrigues-Martins et al., 2007a). These localisation data suggests that SAS-6 in Holozoa might have evolved to fulfil the function that SAS6L accomplishes at the basal plate in species outside the Holozoa.

8.4 SAS-4 in *T. brucei* - a protein with diverged function

SAS-4 is well known for its essential role in assembly of centriolar MTs during centriole formation in metazoa (Dammermann et al., 2004; Kohlmaier et al., 2009; Leidel and Gonczy, 2003; Pelletier et al., 2006; Schmidt et al., 2009; Tang et al., 2009). In my thesis I show that SAS-4 localises to multiple sites in trypanosomes, namely the pro-basal body, the anterior tip of the cell body and a site close to the exit of the flagellum from the pocket. SAS-4 is an essential protein in *T. brucei* whose ablation results in a cytokinesis defect. Interestingly, I found that basal bodies assemble normally in the absence of SAS-4 and that their composition (apart from lacking SAS-4) and ultrastructure are unaffected. Ectopic overexpression of SAS-4 does not affect cell growth or cell morphology in *T. brucei*.

8.4.1 SAS-4 domain architecture

Comparing the domain architecture of SAS-4 protein across eukaryotes reinforced that Tb11.02.0810 encodes a SAS-4 protein. The similarity is mainly found in the region of the Tcp10 domain. This domain was initially identified in a protein in *H. sapiens* that is expressed only in spermatocytes (Islam et al., 1993). While overexpression of CPAP (human SAS-4 homologue) leads to elongation of centriolar MTs; overexpression of a mutant lacking the Tcp10 domain still leads to the localisation of the protein to the centriole but it is unable to induced the formation of long centriolar MTs (Kitagawa et al., 2011b). This suggests that the Tcp10 domain is involved in

the process of MT elongation, even though it is not the region of tubulin interaction (that is the PN2-3 motif described in *H. sapiens* and *D. melanogaster* (Cormier et al., 2009; Hsu et al., 2008; Hung et al., 2004)).

Interestingly, SAS-4 in *T. brucei* lacks the Pfam-B_19564 domain that is found in most SAS-4 homologues (including *H. sapiens*, *D. melanogaster*, *C. reinhardtii*, *T. thermophila*, but excluding *C. elegans*). The Pfam-B_19564 domain was also not identified in SAS-4 homologues of other excavates such as *Leishmania major*, *Giardia lamblia* and *Naegleria gruberi*. This suggests loss of this domain or a higher degree of sequence divergence in this part of SAS-4 proteins in excavates compared to homologues in other eukaryotes.

8.4.2 Divergent localisation of SAS-4 in *T. brucei*

SAS-4 localises to multiple sites in trypanosomes: the pro-basal body, the anterior tip of the cell body and a site close to the exit of the flagellum from the pocket. Localisation to sites other than the basal body was surprising, as SAS-4 homologues in three metazoan species and *P. tetraurelia* localise almost exclusively to the centrosome/centriole or the basal body (Basto et al., 2006; Gogendeau et al., 2011; Hung et al., 2000; Kirkham et al., 2003; Leidel and Gonczy, 2003). There has been one report showing CPAP localisation to the midbody ring during cytokinesis in HeLa cells using immunofluorescence (Paramasivam et al., 2007). Nevertheless, the SAS-4 localisation observed in *T. brucei* is unlikely to be an artefact, since tagged SAS-4 was expressed at levels comparable to wild-type levels and could complement the complete loss of the essential wild-type protein.

The dynamics of SAS-4 at the basal body in *T. brucei* are different to all eukaryotes studied to date. Whereas SAS-4 remains present at the centriole and basal body after maturation in metazoa and *P. tetraurelia*, SAS-4 in *T. brucei* is essentially gone from the structure after pro-basal body assembly is completed (Basto et al., 2006; Dammermann et al., 2008; Gogendeau et al., 2011; Hung et al., 2000; Kirkham et al., 2003; Leidel and Gonczy, 2003). This suggests that SAS-4 in

T. brucei is not involved in the maintenance of the basal body structure and hence not likely to fulfil a structural role in MT attachment. SAS-4 localisation to the pro-basal body, however, suggests that it may be involved in the assembly process. This seems plausible as abnormal elongation of centriolar MTs was previously observed after overexpression of CPAP in human cells (Kohlmaier et al., 2009; Schmidt et al., 2009; Tang et al., 2009). However, the contribution of SAS-4 in *T. brucei* to basal body assembly might be a different one.

The anterior end of the cell body accommodates many MT minus ends from the subpellicular MT cytoskeleton with the minus end orientation of MTs to the anterior end (except of four specialised MTs which have the opposite orientation). If SAS-4 in *T. brucei*, as its human homologue CPAP (Hung et al., 2004) possesses the capability to interact with tubulin and/or MTs, the localisation to this site might be linked to the high occurrence of MT ends. Another protein that localises to the anterior end of trypanosomes is γ-tubulin. An interaction between CPAP and γ-tubulin was previously suggested in human cells (Hung et al., 2000). Therefore, it seems also possible that SAS-4 localises via a γ-tubulin mediated interaction (or inverse/mutual dependency) to this anterior end in *T. brucei*.

It is still unclear what the localisation of SAS-4 close to the exit of the flagellum from the pocket represents on a structural level. If SAS-4 has a preference for MT minus ends, one might predict that it localises to the minus ends of the four specialised MTs that originate from between the basal body and the pro-basal body and run along the FAZ. However, the signal of SAS-4 is too far to the anterior of the cell to correspond to the minus end of the four specialised MTs (Lacomble et al., 2009). The shape of the SAS-4 signal in this region is different from centrin and SAS6L, and therefore seems unlikely to label any of the fibres/filament in this region (Esson et al., 2012). The SAS-4 signal close to the exit of the flagellum from the pocket is only present during flagellum biogenesis. Considering the timing, SAS-4 could be involved in a process linked to the duplication of the flagellum, an associated structure or the whole cell. Depletion of SAS-4 results in a similar cytokinesis defect observed after PLK depletion (Kumar and Wang, 2006). However the two

proteins do not colocalise.

8.4.3 Divergent SAS-4 function in *T. brucei*

Using RNA interference against *SAS-4*, I showed that SAS-4 is required for cytokinesis in *T. brucei*. However, SAS-4 was dispensable for basal body assembly. This is in stark contrast to the requirement of SAS-4 for centriole and basal body assembly in all species investigated so far (Basto et al., 2006; Gogendeau et al., 2011; Hung et al., 2000; Kirkham et al., 2003; Leidel and Gonczy, 2003). However, it cannot be completely excluded that small residual amounts of SAS-4, undetectable by Western blot, remained present in trypanosomes after SAS-4 ablation, and that these amounts were sufficient to support an essential function in pro-basal body assembly but not in cytokinesis. In any case, the RNAi phenotype together with the localisation suggests that the function of SAS-4 in *T. brucei* is different from that in other eukaryotes.

The way in which SAS-4 depletion leads to a defect in cytokinesis is unknown. The obvious connection is that the protein localises to the anterior tip and the ingression of the cleavage furrow starts from the anterior site. However, the role of SAS-4 at this site and how its absence leads to the defect were not elucidated in this work. Several scenarios are possible:

1) SAS-4 is involved in MT nucleation, stabilisation or capping. In this case, depletion of SAS-4 would lead to an insufficient number of MTs to form a new anterior end. In line with this idea is that new anterior ends are observed only rarely. Furthermore, CPAP has been shown to interact with γ-tubulin in *H. sapiens*, which would support this idea (Dammermann et al., 2008; Hung et al., 2000).

2) SAS-4 is required for MT elongation. In this case depletion of SAS-4 would also result in an insufficient number of MTs to form a new anterior end. Overexpression of CPAP in human cells causes overly long centriolar MTs which suggest a role in MT elongation which would support this idea (Kohlmaier et al., 2009; Schmidt et al., 2009; Tang et al., 2009). However, if SAS-4 would be

required for MT growth all the way, it would not localise only to the minus end of MT but it would probably also localise along the MTs or at least at the growing plus end of the MTs.

(Both hypotheses imply that nucleation or elongation of basal body MTs would have different molecular requirements than nucleation or elongation of subpellicular MTs. A possible inconsistency with the explanations is that despite the cytokinesis defect, SAS-4 depleted cells increase in size due to multiplication of nuclei and other organelles, which probably involves the nucleation and elongation of new intercalating MTs into the existing subpellicular MT array.)

3) SAS-4 is involved in MT bundling or connecting MTs at the anterior end. In this case depletion of SAS-4 would make it difficult to get the formation of a new anterior end started. Support for this idea comes from SAS-4 depleted *C. elegans* embryos, which assemble a central tube that lacks distinct hook formations observed during normal centriole assembly. This observation has led to the suggestion that SAS-4 is involved in the formation of these hook structures that facilitate MT attachment (Pelletier et al., 2006). Furthermore, CPAP has been suggested to form a homodimer via a coiled coil domain towards the C-terminus, which supports cohesion of the centrosome (Zhao et al., 2010).

4) SAS-4 is involved in a non-MT function, such as marking the new end or forming a scaffold at the anterior end.

At least one SAS-4 homologue has been identified in all cilia forming species analysed in Chapter 3 (except in *Physcomitrella patens*). This suggested that the essential function of SAS-4 shown in centriole and basal body assembly in Metazoa and *Paramecium* is conserved across eukaryotes. The finding that SAS-4 is not required for basal body assembly in *T. brucei* was unexpected. Nevertheless, this is in line with the difference in the molecular composition of extant centrioles described in our bioinformatic analysis in Chapter 3. The work on SAS-4 presented here, is the first analysis showing that the SAS-4 is not universally required for in centriole/basal body assembly

across all eukaryotes. It shows that the protein is divergent in *T. brucei* demonstrated by the divergent localisation pattern and RNAi phenotype. Whether SAS-4 is not involved in the assembly of the basal body MTs or whether its loss can be compensate by another protein in *T. brucei* remains to be shown.

8.5 WDR16 in *T. brucei*

WDR16 in *T. brucei* was previously identified in the flagellar proteome and localised to the basal body, pro-basal body and axoneme (Broadhead et al., 2006; Farr, 2007). However, the function of the protein is unknown. Its high sequence conservation and its presence in almost all ciliated species analysed in Chapter 3, led me to continue the previous studies on the protein. I showed that WDR16 is a stable component of the axoneme but that its knockdown does not cause a change in cell growth, cell morphology or axonemal ultrastructure in *T. brucei*.

8.5.1 High sequence conservation of WDR16

WDR16 proteins across ciliated eukaryotes show high sequence conservation and possess a high number of WD40 domains.

WDR16 proteins contains up to 13 WD40 domains. WD40 domains form a β-propeller comprising usually seven to eight blades. Multiple β-propellers in one protein have been observed for example in the actin-interacting protein 1, Aip1 (Voegtli et al., 2003). WDR16 contains too many WD40 domains for only one β-propeller. Although the number of identified WD40 domains is not high enough for the formation of two seven-blade β-propellers, it seems plausible to suggest that WDR16 might form two β-propeller. It could be either that some WD40 domains are more divergent and were not identified at the applied threshold, or that the β-propeller contains less than seven blades (Xu and Min, 2011). WD40 containing proteins are involved in mediating protein-protein interaction in many cellular processes, which makes it impossible to make a meaningful

assumption about the function that WDR16 might be involved in.

8.5.2 WDR16 localisation to the axoneme and transition zone but not to the basal body

Measuring the distance between markers along the basal body and axoneme, I showed that GFP-tagged WDR16 localises only to the transition zone and the axoneme but not to the triplet basal body. This was surprising because of two observations: Firstly, the shape and intensity of the fluorescent signal is such that the proximal end is slightly wider and more intense then the signal along the axoneme. This led to the assumption that the very proximal part of the signal corresponds to triplet MTs region whereas the lower intensity along the axoneme reflects association to only doublet MTs. Secondly, WDR16 localises to a position consistent with the pro-basal body.

However, the two observations can be explained differently: First, the slightly wider and more intense proximal GFP-WDR16 signal might correspond to the transitional fibres. Second, material that accumulates at the pro-basal body is not necessarily integrated into the basal body. This phenomenon was observed also in Chapter 5 for SAS6L which accumulates at the pro-basal body in a late assembly stage and localises later to the basal plate of the axoneme but not the mature basal body.

8.5.3 WDR16 function

The remaining question is which function WDR16 fulfils in the axoneme. RNAi-mediated knock-down of WDR16 did not cause a change in cell growth or cell morphology. However, even 72h after RNAi induction WDR16 remained detectable by dot blot. Whether this amount of residual protein represents only WDR16 integrated into old axonemes or whether the knockdown is incomplete was not tested. It cannot be excluded that the residual amount of WDR16 is sufficient to fulfil an essential function. It seems however, that wild-type levels of WDR16 are not necessary for normal growth and cell morphology.

I showed that WDR16 is a stable component of the axonemes that remains present in old axoneme during RNAi-mediated depletion of *WDR16*. However, *C. elegans*, which forms only primary cilia, possesses a WDR16 homologue, which was identified by BLASTp search (it is divergent and hence was not identified by our bioinformatic approach in Chapter 3). As *C. elegans* does not possess a central MT pair and does not require inner and outer dynein arms for motility, it seems more likely that WDR16 is involved with the outer MT doublets or connections between them. As WDR16 contains a high number of WD40 domains, the protein is likely involved in a scaffolding function in the axoneme.

8.6 Summary

Cilia are crucial for cell signalling and motility. Understanding the biology and functioning of these organelles has gained huge scientific interest, especially because of the recognition that several developmental pathologies are caused by dysfunctional cilia. The study of proteins involved in basal body assembly provides information critical for understanding the biological processes underlying cilia assembly and functioning. Furthermore, the emerging mechanisms of eukaryotic centriole/basal body assembly, which are mostly based on studies in metazoan cells, need to be evaluated by comparison to distantly-related eukaryotes, such as *T. brucei*, in order to distinguish basic eukaryotic concepts from centriole-specific adaptations in the centrosomal context.

My thesis provides additional information on the evolution and function of centriolar proteins. The bioinformatic survey of centriolar and ciliopathy-associated proteins established that the cilia formation is the ancient function of centrioles/basal body and that the centrosome organisation is an adaptation specific to Holozoa. Furthermore, the survey gave insight into the molecular composition of the ancestral and extant centrioles/basal bodies which formed the foundation of my cell biological work. Analysis of the four conserved centriole/cilium proteins SAS-6, SAS6L, SAS-4 and WDR16 gave insight into their function and/or localisation in an evolutionary distant species to

metazoa. I demonstrated that in *T. brucei* the essential SAS-6 function in basal body assembly is conserved, whereas SAS-4 function is divergent from the role of metazoan and ciliate homologues. This work also identifies and introduces a novel protein family which possess similarity to SAS-6 and is suggested to have a non-essential but conserved function at the basal plate.

REFERENCES

Adams, G.M., R.L. Wright, and J.W. Jarvik. 1985. Defective temporal and spatial control of flagellar assembly in a mutant of *Chlamydomonas reinhardtii* with variable flagellar number. *J. Cell Biol.* 100:955-964.

Allen, R.D. 1969. The morphogenesis of basal bodies and accessory structures of the cortex of the ciliated protozoan *Tetrahymena pyriformis*. *J. Cell Biol.* 40:716-733.

Alsford, S., D.J. Turner, S.O. Obado, A. Sanchez-Flores, L. Glover, M. Berriman, C. Hertz-Fowler, and D. Horn. 2011. High-throughput phenotyping using parallel sequencing of RNA interference targets in the African trypanosome. *Genome Res.* 21:915-924.

Altschul, S.F., W. Gish, W. Miller, E.W. Myers, and D.J. Lipman. 1990. Basic local alignment search tool. *J. Mol. Biol.* 215:403-410.

Alvey, P.L. 1986. Do adult centrioles contain cartwheels and lie at right angles to each other? *Cell Biol. Int. Rep.* 10:589-598.

Andersen, J.S., C.J. Wilkinson, T. Mayor, P. Mortensen, E.A. Nigg, and M. Mann. 2003. Proteomic characterization of the human centrosome by protein correlation profiling. *Nature*. 426:570-574.

Archambault, V., and D.M. Glover. 2009. Polo-like kinases: conservation and divergence in their functions and regulation. *Nat. Rev. Mol. Cell Biol.* 10:265-275.

Armbrust, E.V. 1990. The Life Cycle of the Centric Diatom *Thalassiosira weissflogii*: Control of Gametogenesis and Cell Size. *Doctoral Dissertation at Woods Hole Oceanographic Institution Massachusetts Institute of Technology*.

Arquint, C., K.F. Sonnen, Y.D. Stierhof, and E.A. Nigg. 2012. Cell-cycle-regulated expression of STIL controls centriole number in human cells. *J. Cell Sci.*

Arts, H.H., D. Doherty, S.E. van Beersum, M.A. Parisi, S.J. Letteboer, N.T. Gorden, T.A. Peters, T. Marker, K. Voesenek, A. Kartono, H. Ozyurek, F.M. Farin, H.Y. Kroes, U. Wolfrum, H.G. Brunner, F.P. Cremers, I.A. Glass, N.V. Knoers, and R. Roepman. 2007. Mutations in the gene encoding the basal body protein RPGRIP1L, a nephrocystin-4 interactor, cause Joubert syndrome. *Nat. Genet.* 39:882-888.

Avidor-Reiss, T., A.M. Maer, E. Koundakjian, A. Polyanovsky, T. Keil, S. Subramaniam, and C.S. Zuker. 2004. Decoding cilia function: defining specialized genes required for compartmentalized cilia biogenesis. *Cell.* 117:527-539.

Azimzadeh, J., P. Hergert, A. Delouvee, U. Euteneuer, E. Formstecher, A. Khodjakov, and M. Bornens. 2009. hPOC5 is a centrin-binding protein required for assembly of full-length centrioles. *J. Cell Biol.* 185:101-114.

Azimzadeh, J., and W.F. Marshall. 2010. Building the centriole. *Curr. Biol.* 20:R816-825.

Azimzadeh, J., M.L. Wong, D.M. Downhour, A. Sanchez Alvarado, and W.F. Marshall. 2012. Centrosome loss in the evolution of planarians. *Science*. 335:461-463.

Badano, J.L., N. Mitsuma, P.L. Beales, and N. Katsanis. 2006. The ciliopathies: an emerging class of human genetic disorders. *Annu. Rev. Genomics Hum. Genet.* 7:125-148.

Bahtz, R., J. Seidler, M. Arnold, U. Haselmann-Weiss, C. Antony, W.D. Lehmann, and I. Hoffmann. 2012. GCP6 is a substrate of Plk4 and required for centriole duplication. *J. Cell Sci.* 125:486-496.

Barry, J.D., and R. McCulloch. 2001. Antigenic variation in trypanosomes: enhanced phenotypic variation in a eukaryotic parasite. *Adv. Parasitol.* 49:1-70.

Bastin, P., Z. Bagherzadeh, K.R. Matthews, and K. Gull. 1996. A novel epitope tag system to study protein targeting and organelle biogenesis in *Trypanosoma brucei*. *Mol. Biochem. Parasitol.* 77:235-239.

Basto, R., J. Lau, T. Vinogradova, A. Gardiol, C.G. Woods, A. Khodjakov, and J.W. Raff. 2006. Flies without centrioles. *Cell.* 125:1375-1386.

Bastos, R.N., and F.A. Barr. 2010. Plk1 negatively regulates Cep55 recruitment to the midbody to ensure orderly abscission. *J. Cell Biol.* 191:751-760.

Beisson, J., and M. Wright. 2003. Basal body/centriole assembly and continuity. *Curr. Opin. Cell Biol.* 15:96-104.

Berbari, N.F., A.K. O'Connor, C.J. Haycraft, and B.K. Yoder. 2009. The Primary Cilium as a Complex Signaling Center. *Curr. Biol.* 19:R526-R535.

Berger, L., A.D. Hyatt, R. Speare, and J.E. Longcore. 2005. Life cycle stages of the amphibian chytrid *Batrachochytrium dendrobatidis*. *Dis. Aquat. Organ.* 68:51-63.

Berriman, M., E. Ghedin, C. Hertz-Fowler, G. Blandin, H. Renauld, D.C. Bartholomeu, N.J. Lennard, E. Caler, N.E. Hamlin, B. Haas, U. Bohme, L. Hannick, M.A. Aslett, J. Shallom, L. Marcello, L. Hou, B. Wickstead, U.C. Alsmark, C. Arrowsmith, R.J. Atkin, A.J. Barron, F. Bringaud, K. Brooks, M. Carrington, I. Cherevach, T.J. Chillingworth, C. Churcher, L.N. Clark, C.H. Corton, A. Cronin, R.M. Davies, J. Doggett, A. Djikeng, T. Feldblyum, M.C. Field, A. Fraser, I. Goodhead, Z. Hance, D. Harper, B.R. Harris, H. Hauser, J. Hostetler, A. Ivens, K. Jagels, D. Johnson, J. Johnson, K. Jones, A.X. Kerhornou, H. Koo, N. Larke, S. Landfear, C. Larkin, V. Leech, A. Line, A. Lord, A. Macleod, P.J. Mooney, S. Moule, D.M. Martin, G.W. Morgan, K. Mungall, H. Norbertczak, D. Ormond, G. Pai, C.S. Peacock, J. Peterson, M.A. Quail, E. Rabbinowitsch, M.A. Rajandream, C. Reitter, S.L. Salzberg, M. Sanders, S. Schobel, S. Sharp, M. Simmonds, A.J. Simpson, L. Tallon, C.M. Turner, A. Tait, A.R. Tivey, S. Van Aken, D. Walker, D. Wanless, S. Wang, B. White, O. White, S. Whitehead, J. Woodward, J. Wortman, M.D. Adams, T.M. Embley, K. Gull, E. Ullu, J.D. Barry, A.H. Fairlamb, F. Opperdoes, B.G. Barrell, J.E. Donelson, N. Hall, C.M. Fraser, et al. 2005. The genome of the African trypanosome *Trypanosoma brucei*. *Science*. 309:416-422.

Bettencourt-Dias, M., A. Rodrigues-Martins, L. Carpenter, M. Riparbelli, L. Lehmann, M.K. Gatt, N. Carmo, F. Balloux, G. Callaini, and D.M. Glover. 2005. SAK/PLK4 is required for centriole duplication and flagella development. *Curr. Biol.* 15:2199-2207.

Blachon, S., J. Gopalakrishnan, Y. Omori, A. Polyanovsky, A. Church, D. Nicastro, J. Malicki, and T. Avidor-Reiss. 2008. *Drosophila* asterless and vertebrate Cep152 Are orthologs essential for centriole duplication. *Genetics*. 180:2081-2094.

Blacque, O.E., and M.R. Leroux. 2006. Bardet-Biedl syndrome: an emerging pathomechanism of intracellular transport. *Cell. Mol. Life Sci.* 63:2145-2161.

Blacque, O.E., M.J. Reardon, C. Li, J. McCarthy, M.R. Mahjoub, S.J. Ansley, J.L. Badano, A.K. Mah, P.L. Beales, W.S. Davidson, R.C. Johnsen, M. Audeh, R.H. Plasterk, D.L. Baillie, N. Katsanis, L.M. Quarmby, S.R. Wicks, and M.R. Leroux. 2004. Loss of *C. elegans* BBS-7 and BBS-8 protein function results in cilia defects and compromised intraflagellar transport. *Genes Dev.* 18:1630-1642.

Blaineau, C., M. Tessier, P. Dubessay, L. Tasse, L. Crobu, M. Pages, and P. Bastien. 2007. A novel microtubule-depolymerizing kinesin involved in length control of a eukaryotic flagellum. *Curr. Biol.* 17:778-782.

Bond, J., E. Roberts, K. Springell, S.B. Lizarraga, S. Scott, J. Higgins, D.J. Hampshire, E.E. Morrison, G.F. Leal, E.O. Silva, S.M. Costa, D. Baralle, M. Raponi, G. Karbani, Y. Rashid, H. Jafri, C. Bennett, P. Corry, C.A. Walsh, and C.G. Woods. 2005. A centrosomal mechanism involving CDK5RAP2 and CENPJ controls brain size. *Nat. Genet.* 37:353-355.

Bornens, M. 2012. The centrosome in cells and organisms. *Science*. 335:422-426.

Bornens, M., and J. Azimzadeh. 2007. Origin and evolution of the centrosome. *In* Eukaryotic membranes and cytoskeleton: Origins and evolution. G. Jékely, editor. Landes Bioscience. 119-129.

Briggs, L.J., J.A. Davidge, B. Wickstead, M.L. Ginger, and K. Gull. 2004a. More than one way to build a flagellum: comparative genomics of parasitic protozoa. *Curr. Biol.* 14:R611-612.

Briggs, L.J., P.G. McKean, A. Baines, F. Moreira-Leite, J. Davidge, S. Vaughan, and K. Gull. 2004b. The flagella connector of *Trypanosoma brucei*: an unusual mobile transmembrane junction. *J. Cell Sci.* 117:1641-1651.

Broadhead, R., H.R. Dawe, H. Farr, S. Griffiths, S.R. Hart, N. Portman, M.K. Shaw, M.L. Ginger, S.J. Gaskell, P.G. McKean, and K. Gull. 2006. Flagellar motility is required for the viability of the bloodstream trypanosome. *Nature*. 440:224-227.

Brouhard, G.J., J.H. Stear, T.L. Noetzel, J. Al-Bassam, K. Kinoshita, S.C. Harrison, J. Howard, and A.A. Hyman. 2008. XMAP215 is a processive microtubule polymerase. *Cell.* 132:79-88.

Brownlee, C.W., J.E. Klebba, D.W. Buster, and G.C. Rogers. 2011. The Protein Phosphatase 2A regulatory subunit Twins stabilizes Plk4 to induce centriole amplification. *J. Cell Biol.* 195:231-243.

Brun, R., and L. Jenni. 1977. A new semi-defined medium for *Trypanosoma brucei* sspp. *Acta Trop.* 34:21-33.

Callaini, G., W.G. Whitfield, and M.G. Riparbelli. 1997. Centriole and centrosome dynamics during the embryonic cell cycles that follow the formation of the cellular blastoderm in *Drosophila*. *Exp. Cell Res.* 234:183-190.

Carlton, J.G., M. Agromayor, and J. Martin-Serrano. 2008. Differential requirements for Alix and ESCRT-III in cytokinesis and HIV-1 release. *Proc. Natl. Acad. Sci. U. S. A.* 105:10541-10546.

Carvalho-Santos, Z., J. Azimzadeh, J.B. Pereira-Leal, and M. Bettencourt-Dias. 2011. Evolution: Tracing the origins of centrioles, cilia, and flagella. *J. Cell Biol.* 194:165-175.

Carvalho-Santos, Z., P. Machado, P. Branco, F. Tavares-Cadete, A. Rodrigues-Martins, J.B. Pereira-Leal, and M. Bettencourt-Dias. 2010. Stepwise evolution of the centriole-assembly pathway. *J. Cell Sci.* 123:1414-1426.

Cavalier-Smith, T. 1987. The origin of eukaryotic and archaebacterial cells. *Ann. N. Y. Acad. Sci.* 503:17-54.

Chan, K.Y., and K. Ersfeld. 2010. The role of the Kinesin-13 family protein TbKif13-2 in flagellar length control of *Trypanosoma brucei*. *Mol. Biochem. Parasitol.* 174:137-140.

Chang, J., O. Cizmecioglu, I. Hoffmann, and K. Rhee. 2010. PLK2 phosphorylation is critical for CPAP function in procentriole formation during the centrosome cycle. *EMBO J.* 29:2395-2406.

Chang, P., T.H. Giddings, Jr., M. Winey, and T. Stearns. 2003. Epsilon-tubulin is required for centriole duplication and microtubule organization. *Nat. Cell Biol.* 5:71-76.

Chang, P., and T. Stearns. 2000. Delta-tubulin and epsilon-tubulin: two new human centrosomal tubulins reveal new aspects of centrosome structure and function. *Nat. Cell Biol.* 2:30-35.

Chen, Z., V.B. Indjeian, M. McManus, L. Wang, and B.D. Dynlacht. 2002. CP110, a cell cycle-dependent CDK substrate, regulates centrosome duplication in human cells. *Dev. Cell.* 3:339-350.

Chiang, A.P., J.S. Beck, H.J. Yen, M.K. Tayeh, T.E. Scheetz, R.E. Swiderski, D.Y. Nishimura, T.A. Braun, K.Y. Kim, J. Huang, K. Elbedour, R. Carmi, D.C. Slusarski, T.L. Casavant, E.M. Stone, and V.C. Sheffield. 2006. Homozygosity mapping with SNP arrays identifies TRIM32, an E3 ubiquitin ligase, as a Bardet-Biedl syndrome gene (BBS11). *Proc. Natl. Acad. Sci. U. S. A.* 103:6287-6292.

Chih, B., P. Liu, Y. Chinn, C. Chalouni, L.G. Komuves, P.E. Hass, W. Sandoval, and A.S. Peterson. 2012. A ciliopathy complex at the transition zone protects the cilia as a privileged membrane domain. *Nat. Cell Biol.* 14:61-72.

Cizmecioglu, O., M. Arnold, R. Bahtz, F. Settele, L. Ehret, U. Haselmann-Weiss, C. Antony, and I. Hoffmann. 2010. Cep152 acts as a scaffold for recruitment of Plk4 and CPAP to the centrosome. *J. Cell Biol.* 191:731-739.

Collin, G.B., J. Won, W.L. Hicks, S.A. Cook, P.M. Nishina, and J.K. Naggert. 2012. Meckelin is necessary for photoreceptor intraciliary transport and outer segment morphogenesis. *Invest. Ophthalmol. Vis. Sci.* 53:967-974.

Corbit, K.C., A.E. Shyer, W.E. Dowdle, J. Gaulden, V. Singla, M.H. Chen, P.T. Chuang, and J.F. Reiter. 2008. Kif3a constrains beta-catenin-dependent Wnt signalling through dual ciliary and non-ciliary mechanisms. *Nat. Cell Biol.* 10:70-76.

Cormier, A., M.J. Clement, M. Knossow, S. Lachkar, P. Savarin, F. Toma, A. Sobel, B. Gigant, and P.A. Curmi. 2009. The PN2-3 domain of centrosomal P4.1-associated protein implements a novel mechanism for tubulin sequestration. *J. Biol. Chem.* 284:6909-6917.

Coss, R.A. 1974. Mitosis in *Chlamydomonas reinhardtii* basal bodies and mitotic apparatus. *J. Cell Biol.* 63:325-329.

Cottee, M.A., J.W. Raff, S.M. Lea, and H. Roque. 2011. SAS-6 oligomerization: the key to the centriole? *Nat. Chem. Biol.* 7:650-653.

Craige, B., C.C. Tsao, D.R. Diener, Y. Hou, K.F. Lechtreck, J.L. Rosenbaum, and G.B. Witman. 2010. CEP290 tethers flagellar transition zone microtubules to the membrane and regulates flagellar protein content. *J. Cell Biol.* 190:927-940.

Cross, G.A. 1977. Antigenic variation in trypanosomes. *Am. J. Trop. Med. Hyg.* 26:240-244.

Cui, C., B. Chatterjee, D. Francis, Q. Yu, J.T. SanAgustin, R. Francis, T. Tansey, C. Henry, B. Wang, B. Lemley, G.J. Pazour, and C.W. Lo. 2011. Disruption of Mks1 localization to the mother centriole causes cilia defects and developmental malformations in Meckel-Gruber syndrome. *Dis. Model. Mech.* 4:43-56.

Culver, B.P., J.B. Meehl, T.H. Giddings, Jr., and M. Winey. 2009. The two SAS-6 homologs in *Tetrahymena thermophila* have distinct functions in basal body assembly. *Mol. Biol. Cell.* 20:1865-1877.

Cunha-Ferreira, I., A. Rodrigues-Martins, I. Bento, M. Riparbelli, W. Zhang, E. Laue, G. Callaini, D.M. Glover, and M. Bettencourt-Dias. 2009. The SCF/Slimb ubiquitin ligase limits centrosome amplification through degradation of SAK/PLK4. *Curr. Biol.* 19:43-49.

D'Angiolella, V., V. Donato, S. Vijayakumar, A. Saraf, L. Florens, M.P. Washburn, B. Dynlacht, and M. Pagano. 2010. SCF(Cyclin F) controls centrosome homeostasis and mitotic fidelity through CP110 degradation. *Nature.* 466:138-142.

Dammermann, A., P.S. Maddox, A. Desai, and K. Oegema. 2008. SAS-4 is recruited to a dynamic structure in newly forming centrioles that is stabilized by the gamma-tubulin-mediated addition of centriolar microtubules. *J. Cell Biol.* 180:771-785.

Dammermann, A., and A. Merdes. 2002. Assembly of centrosomal proteins and microtubule organization depends on PCM-1. *J. Cell Biol.* 159:255-266.

Dammermann, A., T. Muller-Reichert, L. Pelletier, B. Habermann, A. Desai, and K. Oegema. 2004. Centriole assembly requires both centriolar and pericentriolar material proteins. *Dev. Cell.* 7:815-829.

Dammermann, A., H. Pemble, B.J. Mitchell, I. McLeod, J.R. Yates, 3rd, C. Kintner, A.B. Desai, and K. Oegema. 2009. The hydrolethalus syndrome protein HYLS-1 links core centriole structure to cilia formation. *Genes Dev.* 23:2046-2059.

Davidge, J.A., E. Chambers, H.A. Dickinson, K. Towers, M.L. Ginger, P.G. McKean, and K. Gull. 2006. Trypanosome IFT mutants provide insight into the motor location for mobility of the flagella connector and flagellar membrane formation. *J. Cell Sci.* 119:3935-3943.

Davis, R.E., R.E. Swiderski, K. Rahmouni, D.Y. Nishimura, R.F. Mullins, K. Agassandian, A.R. Philp, C.C. Searby, M.P. Andrews, S. Thompson, C.J. Berry, D.R. Thedens, B. Yang, R.M. Weiss, M.D. Cassell, E.M. Stone, and V.C. Sheffield. 2007. A knockin mouse model of the Bardet-Biedl syndrome 1 M390R mutation has cilia defects, ventriculomegaly, retinopathy, and obesity. *Proc. Natl. Acad. Sci. U. S. A.* 104:19422-19427.

Dawe, H.R., U.M. Smith, A.R. Cullinane, D. Gerrelli, P. Cox, J.L. Badano, S. Blair-Reid, N. Sriram, N. Katsanis, T. Attie-Bitach, S.C. Afford, A.J. Copp, D.A. Kelly, K. Gull, and C.A. Johnson. 2007. The Meckel-Gruber Syndrome proteins MKS1 and meckelin interact and are required for primary cilium formation. *Hum. Mol. Genet.* 16:173-186.

de Graffenried, C.L., H.H. Ho, and G. Warren. 2008. Polo-like kinase is required for Golgi and bilobe biogenesis in *Trypanosoma brucei*. *J. Cell Biol.* 181:431-438.

Deane, J.A., D.G. Cole, E.S. Seeley, D.R. Diener, and J.L. Rosenbaum. 2001. Localization of intraflagellar transport protein IFT52 identifies basal body transitional fibers as the docking site for IFT particles. *Curr. Biol.* 11:1586-1590.

Delattre, M., C. Canard, and P. Gonczy. 2006. Sequential protein recruitment in *C. elegans* centriole formation. *Curr. Biol.* 16:1844-1849.

Delattre, M., S. Leidel, K. Wani, K. Baumer, J. Bamat, H. Schnabel, R. Feichtinger, R. Schnabel, and P. Gonczy. 2004. Centriolar SAS-5 is required for centrosome duplication in *C. elegans*. *Nat. Cell Biol.* 6:656-664.

Delgehyr, N., H. Rangone, J. Fu, G. Mao, B. Tom, M.G. Riparbelli, G. Callaini, and D.M. Glover. 2012. Klp10A, a Microtubule-Depolymerizing Kinesin-13, Cooperates with CP110 to Control *Drosophila* Centriole Length. *Curr. Biol.* 22(6):502-9.

Delgehyr, N., J. Sillibourne, and M. Bornens. 2005. Microtubule nucleation and anchoring at the centrosome are independent processes linked by ninein function. *J. Cell Sci.* 118:1565-1575.

Delous, M., L. Baala, R. Salomon, C. Laclef, J. Vierkotten, K. Tory, C. Golzio, T. Lacoste, L. Besse, C. Ozilou, I. Moutkine, N.E. Hellman, I. Anselme, F. Silbermann, C. Vesque, C. Gerhardt, E. Rattenberry, M.T. Wolf, M.C. Gubler, J. Martinovic, F. Encha-Razavi, N. Boddaert, M. Gonzales, M.A. Macher, H. Nivet, G. Champion, J.P. Bertheleme, P. Niaudet, F. McDonald, F. Hildebrandt, C.A. Johnson, M. Vekemans, C. Antignac, U. Ruther, S. Schneider-Maunoury, T. Attie-Bitach, and S. Saunier. 2007. The ciliary gene RPGRIP1L is mutated in cerebello-oculo-renal syndrome (Joubert syndrome type B) and Meckel syndrome. *Nat. Genet.* 39:875-881.

Devaux, S., S. Kelly, L. Lecordier, B. Wickstead, D. Perez-Morga, E. Pays, L. Vanhamme, and K. Gull. 2007. Diversification of function by different isoforms of conventionally shared RNA polymerase subunits. *Mol. Biol. Cell.* 18:1293-1301.

Dietzl, G., D. Chen, F. Schnorrer, K.C. Su, Y. Barinova, M. Fellner, B. Gasser, K. Kinsey, S. Oppel, S. Scheiblauer, A. Couto, V. Marra, K. Keleman, and B.J. Dickson. 2007. A genome-wide transgenic RNAi library for conditional gene inactivation in *Drosophila*. *Nature*. 448:151-156.

Dingle, A.D., and C. Fulton. 1966. Development of the flagellar apparatus of *Naegleria*. *J. Cell Biol.* 31:43-54.

Dippell, R.V. 1968. The development of basal bodies in *paramecium*. *Proc. Natl. Acad. Sci. U. S. A.* 61:461-468.

Dix, C.I., and J.W. Raff. 2007. *Drosophila* Spd-2 recruits PCM to the sperm centriole, but is dispensable for centriole duplication. *Curr. Biol.* 17:1759-1764.

Dobbelaere, J., F. Josue, S. Suijkerbuijk, B. Baum, N. Tapon, and J. Raff. 2008. A genome-wide RNAi screen to dissect centriole duplication and centrosome maturation in *Drosophila*. *PLoS Biol.* 6:e224.

Dupuis-Williams, P., A. Fleury-Aubusson, N.G. de Loubresse, H. Geoffroy, L. Vayssie, A. Galvani, A. Espigat, and J. Rossier. 2002. Functional role of epsilon-tubulin in the assembly of the centriolar microtubule scaffold. *J. Cell Biol.* 158:1183-1193.

Dutcher, S.K. 2003. Elucidation of basal body and centriole functions in *Chlamydomonas reinhardtii*. *Traffic.* 4:443-451.

Dutcher, S.K., N.S. Morrissette, A.M. Preble, C. Rackley, and J. Stanga. 2002. Epsilon-tubulin is an essential component of the centriole. *Mol. Biol. Cell.* 13:3859-3869.

Dutcher, S.K., and E.C. Trabuco. 1998. The *UNI3* gene is required for assembly of basal bodies of *Chlamydomonas* and encodes delta-tubulin, a new member of the tubulin superfamily. *Mol. Biol. Cell.* 9:1293-1308.

Dzhindzhev, N.S., Q.D. Yu, K. Weiskopf, G. Tzolovsky, I. Cunha-Ferreira, M. Riparbelli, A. Rodrigues-Martins, M. Bettencourt-Dias, G. Callaini, and D.M. Glover. 2010. Asterless is a scaffold for the onset of centriole assembly. *Nature*. 467:714-718.

Esson, H.J., B. Morriswood, S. Yavuz, K. Vidilaseris, G. Dong, and G. Warren. 2012. Morphology of the trypanosome bilobe, a novel cytoskeletal structure. *Eukaryot. Cell.* 11(6):761-72

Fan, Y., M.A. Esmail, S.J. Ansley, O.E. Blacque, K. Boroevich, A.J. Ross, S.J. Moore, J.L. Badano, H. May-Simera, D.S. Compton, J.S. Green, R.A. Lewis, M.M. van Haelst, P.S. Parfrey, D.L. Baillie, P.L. Beales, N. Katsanis, W.S. Davidson, and M.R. Leroux. 2004. Mutations in a member of the Ras superfamily of small GTP-binding proteins causes Bardet-Biedl syndrome. *Nat. Genet.* 36:989-993.

Farr, H. 2007. The eukaryotic flagellum in health and disease. *In* Sir William Dunn School of Pathology. Vol. D. Phil. Universtity of Oxford.

Ferrante, A. and A. C. Allison (1983). "Alternative pathway activation of complement by African trypanosomes lacking a glycoprotein coat." Parasite Immunol 5(5): 491-498

Fliegauf, M., J. Horvath, C. von Schnakenburg, H. Olbrich, D. Muller, J. Thumfart, B. Schermer, G.J. Pazour, H.P. Neumann, H. Zentgraf, T. Benzing, and H. Omran. 2006. Nephrocystin specifically localizes to the transition zone of renal and respiratory cilia and photoreceptor connecting cilia. *J. Am. Soc. Nephrol.* 17:2424-2433.

Gadelha, C., S. Rothery, M. Morphew, J.R. McIntosh, N.J. Severs, and K. Gull. 2009. Membrane domains and flagellar pocket boundaries are influenced by the cytoskeleton in African trypanosomes. *Proc. Natl. Acad. Sci. U. S. A.* 106:17425-17430.

Gadelha, C., B. Wickstead, P.G. McKean, and K. Gull. 2006. Basal body and flagellum mutants reveal a rotational constraint of the central pair microtubules in the axonemes of trypanosomes. *J. Cell Sci.* 119:2405-2413.

Garcia-Gonzalo, F.R., K.C. Corbit, M.S. Sirerol-Piquer, G. Ramaswami, E.A. Otto, T.R. Noriega, A.D. Seol, J.F. Robinson, C.L. Bennett, D.J. Josifova, J.M. Garcia-Verdugo, N. Katsanis, F. Hildebrandt, and J.F. Reiter. 2011. A transition zone complex regulates mammalian ciliogenesis and ciliary membrane composition. *Nat. Genet.* 43:776-784.

Garreau de Loubresse, N., F. Ruiz, J. Beisson, and C. Klotz. 2001. Role of delta-tubulin and the C-tubule in assembly of *Paramecium* basal bodies. *BMC Cell Biol.* 2:4.

Gascue, C., P.L. Tan, M. Cardenas-Rodriguez, G. Libisch, T. Fernandez-Calero, Y.P. Liu, S. Astrada, C. Robello, H. Naya, N. Katsanis, and J.L. Badano. 2012. Direct role of Bardet-Biedl syndrome proteins in transcriptional regulation. *J. Cell Sci.* 125:362-375.

Geimer, S., and M. Melkonian. 2005. Centrin scaffold in *Chlamydomonas* reinhardtii revealed by immunoelectron microscopy. *Eukaryot. Cell.* 4:1253-1263.

Gibbons, I.R. 1961. The relationship between the fine structure and direction of beat in gill cilia of a lamellibranch mollusc. *The Journal of biophysical and biochemical cytology.* 11:179-205.

Gibbons, I.R., and A.V. Grimstone. 1960. On flagellar structure in certain flagellates. *The Journal of biophysical and biochemical cytology.* 7:697-716.

Gluenz, E., J.L. Hoog, A.E. Smith, H.R. Dawe, M.K. Shaw, and K. Gull. 2010. Beyond 9+0: noncanonical axoneme structures characterize sensory cilia from protists to humans. *FASEB J.* 24:3117-3121.

Gogendeau, D., I. Hurbain, G. Raposo, J. Cohen, F. Koll, and R. Basto. 2011. Sas-4 proteins are required during basal body duplication in Paramecium. *Mol. Biol. Cell.* 22:1035-1044.

Gomez-Ferreria, M.A., U. Rath, D.W. Buster, S.K. Chanda, J.S. Caldwell, D.R. Rines, and D.J. Sharp. 2007. Human Cep192 is required for mitotic centrosome and spindle assembly. *Curr. Biol.* 17:1960-1966.

Goodenough, U.W., and H.S. StClair. 1975. BALD-2: a mutation affecting the formation of doublet and triplet sets of microtubules in *Chlamydomonas reinhardtii*. *J. Cell Biol.* 66:480-491.

Gopalakrishnan, J., V. Mennella, S. Blachon, B. Zhai, A.H. Smith, T.L. Megraw, D. Nicastro, S.P. Gygi, D.A. Agard, and T. Avidor-Reiss. 2011. Sas-4 provides a scaffold for cytoplasmic complexes and tethers them in a centrosome. *Nature communications.* 2:359.

Gorden, N.T., H.H. Arts, M.A. Parisi, K.L. Coene, S.J. Letteboer, S.E. van Beersum, D.A. Mans, A. Hikida, M. Eckert, D. Knutzen, A.F. Alswaid, H. Ozyurek, S. Dibooglu, E.A. Otto, Y. Liu, E.E. Davis, C.M. Hutter, T.K. Bammler, F.M. Farin, M. Dorschner, M. Topcu, E.H. Zackai, P. Rosenthal, K.N. Owens, N. Katsanis, J.B. Vincent, F. Hildebrandt, E.W. Rubel, D.W. Raible, N.V. Knoers, P.F. Chance, R. Roepman, C.B. Moens, I.A. Glass, and D. Doherty. 2008. CC2D2A is mutated in Joubert syndrome and interacts with the ciliopathy-associated basal body protein CEP290. *Am. J. Hum. Genet.* 83:559-571.

Graham, T.M., A. Tait, and G. Hide. 1998. Characterisation of a polo-like protein kinase gene homologue from an evolutionary divergent eukaryote, *Trypanosoma brucei*. *Gene*. 207:71-77.

Graser, S., Y.D. Stierhof, S.B. Lavoie, O.S. Gassner, S. Lamla, M. Le Clech, and E.A. Nigg. 2007a. Cep164, a novel centriole appendage protein required for primary cilium formation. *J. Cell Biol.* 179:321-330.

Graser, S., Y.D. Stierhof, and E.A. Nigg. 2007b. Cep68 and Cep215 (Cdk5rap2) are required for centrosome cohesion. *J. Cell Sci.* 120:4321-4331.

Gray, R.S., P.B. Abitua, B.J. Wlodarczyk, H.L. Szabo-Rogers, O. Blanchard, I. Lee, G.S. Weiss, K.J. Liu, E.M. Marcotte, J.B. Wallingford, and R.H. Finnell. 2009. The planar cell polarity effector Fuz is essential for targeted membrane trafficking, ciliogenesis and mouse embryonic development. *Nat. Cell Biol.* 11:1225-1232.

Gromley, A., A. Jurczyk, J. Sillibourne, E. Halilovic, M. Mogensen, I. Groisman, M. Blomberg, and S. Doxsey. 2003. A novel human protein of the maternal centriole is required for the final stages of cytokinesis and entry into S phase. *J. Cell Biol.* 161:535-545.

Gromley, A., C. Yeaman, J. Rosa, S. Redick, C.T. Chen, S. Mirabelle, M. Guha, J. Sillibourne, and S.J. Doxsey. 2005. Centriolin anchoring of exocyst and SNARE complexes at the midbody is required for secretory-vesicle-mediated abscission. *Cell.* 123:75-87.

Guderian, G., J. Westendorf, A. Uldschmid, and E.A. Nigg. 2010. Plk4 trans-autophosphorylation regulates centriole number by controlling betaTrCP-mediated degradation. *J. Cell Sci.* 123:2163-2169.

Guichard, P., D. Chretien, S. Marco, and A.M. Tassin. 2010. Procentriole assembly revealed by cryo-electron tomography. *EMBO J.* 29:1565-1572.

Gull, K. (1999). "The cytoskeleton of trypanosomatid parasites." Annu Rev Microbiol 53: 629-655.

Habbig, S., M.P. Bartram, R.U. Muller, R. Schwarz, N. Andriopoulos, S. Chen, J.G. Sagmuller, M. Hoehne, V. Burst, M.C. Liebau, H.C. Reinhardt, T. Benzing, and B. Schermer. 2011. NPHP4, a cilia-associated protein, negatively regulates the Hippo pathway. *J. Cell Biol.* 193:633-642.

Habedanck, R., Y.D. Stierhof, C.J. Wilkinson, and E.A. Nigg. 2005. The Polo kinase Plk4 functions in centriole duplication. *Nat. Cell Biol.* 7:1140-1146.

Hammarton, T.C. 2007. Cell cycle regulation in *Trypanosoma brucei*. *Mol. Biochem. Parasitol.* 153:1-8.

Haren, L., M.H. Remy, I. Bazin, I. Callebaut, M. Wright, and A. Merdes. 2006. NEDD1-dependent recruitment of the gamma-tubulin ring complex to the centrosome is necessary for centriole duplication and spindle assembly. *J. Cell Biol.* 172:505-515.

He, C.Y., M. Pypaert, and G. Warren. 2005. Golgi duplication in *Trypanosoma brucei* requires Centrin2. *Science*. 310:1196-1198.

Hearn, T., C. Spalluto, V.J. Phillips, G.L. Renforth, N. Copin, N.A. Hanley, and D.I. Wilson. 2005. Subcellular localization of ALMS1 supports involvement of centrosome and basal body dysfunction in the pathogenesis of obesity, insulin resistance, and type 2 diabetes. *Diabetes*. 54:1581-1587.

Henderson, G.P., L. Gan, and G.J. Jensen. 2007. 3-D ultrastructure of *O. tauri*: electron cryotomography of an entire eukaryotic cell. *PLoS ONE*. 2:e749.

Hiraki, M., Y. Nakazawa, R. Kamiya, and M. Hirono. 2007. Bld10p constitutes the cartwheel-spoke tip and stabilizes the 9-fold symmetry of the centriole. *Curr. Biol.* 17:1778-1783.

Hirschner, W., H.M. Pogoda, C. Kramer, U. Thiess, B. Hamprecht, K.H. Wiesmuller, M. Lautner, and S. Verleysdonk. 2007. Biosynthesis of Wdr16, a marker protein for kinocilia-bearing cells, starts at the time of kinocilia formation in rat, and wdr16 gene knockdown causes hydrocephalus in zebrafish. *J. Neurochem.* 101:274-288.

Hirumi, H., and K. Hirumi. 1989. Continuous cultivation of *Trypanosoma brucei* blood stream forms in a medium containing a low concentration of serum protein without feeder cell layers. *J. Parasitol.* 75:985-989.

Hodges, M.E., N. Scheumann, B. Wickstead, J.A. Langdale, and K. Gull. 2010. Reconstructing the evolutionary history of the centriole from protein components. *J. Cell Sci.* 123:1407-1413.

Hoyer-Fender, S. 2010. Centriole maturation and transformation to basal body. *Semin. Cell Dev. Biol.* 21:142-147.

Hsu, W.B., L.Y. Hung, C.J. Tang, C.L. Su, Y. Chang, and T.K. Tang. 2008. Functional characterization of the microtubule-binding and -destabilizing domains of CPAP and d-SAS-4. *Exp. Cell Res.* 314:2591-2602.

Hu, Q., L. Milenkovic, H. Jin, M.P. Scott, M.V. Nachury, E.T. Spiliotis, and W.J. Nelson. 2010. A septin diffusion barrier at the base of the primary cilium maintains ciliary membrane protein distribution. *Science.* 329:436-439.

Huangfu, D., A. Liu, A.S. Rakeman, N.S. Murcia, L. Niswander, and K.V. Anderson. 2003. Hedgehog signalling in the mouse requires intraflagellar transport proteins. *Nature.* 426:83-87.

Hung, L.Y., H.L. Chen, C.W. Chang, B.R. Li, and T.K. Tang. 2004. Identification of a novel microtubule-destabilizing motif in CPAP that binds to tubulin heterodimers and inhibits microtubule assembly. *Mol. Biol. Cell.* 15:2697-2706.

Hung, L.Y., C.J. Tang, and T.K. Tang. 2000. Protein 4.1 R-135 interacts with a novel centrosomal protein (CPAP) which is associated with the gamma-tubulin complex. *Mol. Cell. Biol.* 20:7813-7825.

Ibi, M., P. Zou, A. Inoko, T. Shiromizu, M. Matsuyama, Y. Hayashi, M. Enomoto, D. Mori, S. Hirotsune, T. Kiyono, S. Tsukita, H. Goto, and M. Inagaki. 2011. Trichoplein controls microtubule anchoring at the centrosome by binding to Odf2 and ninein. *J. Cell Sci.* 124:857-864.

Ishikawa, H., A. Kubo, S. Tsukita, and S. Tsukita. 2005. Odf2-deficient mother centrioles lack distal/subdistal appendages and the ability to generate primary cilia. *Nat. Cell Biol.* 7:517-524.

Ishikawa, H., and W.F. Marshall. 2011. Ciliogenesis: building the cell's antenna. *Nat. Rev. Mol. Cell Biol.* 12:222-234.

Islam, S.D., S.H. Pilder, C.L. Decker, J.A. Cebra-Thomas, and L.M. Silver. 1993. The human homolog of a candidate mouse t complex responder gene: conserved motifs and evolution with punctuated equilibria. *Hum. Mol. Genet.* 2:2075-2079.

Jensen, K.G., O. Moestrup, and A.M.M. Schmid. 2003. Ultrastructure of the male gametes from two centric diatoms, *Chaetoceros laciniosus* and *Coscinodiscus wailesii* (*Bacillariophyceae*). *Phycologia.* 42:98-105.

Jerka-Dziadosz, M., D. Gogendeau, C. Klotz, J. Cohen, J. Beisson, and F. Koll. 2010. Basal body duplication in *Paramecium*: the key role of Bld10 in assembly and stability of the cartwheel. *Cytoskeleton.* 67:161-171.

Jin, H., and M.V. Nachury. 2009. The BBSome. *Curr. Biol.* 19:R472-473.

Jin, H., S.R. White, T. Shida, S. Schulz, M. Aguiar, S.P. Gygi, J.F. Bazan, and M.V. Nachury. 2010. The conserved Bardet-Biedl syndrome proteins assemble a coat that traffics membrane proteins to cilia. *Cell.* 141:1208-1219.

Joukov, V., A. De Nicolo, A. Rodriguez, J.C. Walter, and D.M. Livingston. 2010. Centrosomal protein of 192 kDa (Cep192) promotes centrosome-driven spindle assembly by engaging in organelle-specific Aurora A activation. *Proc. Natl. Acad. Sci. U. S. A.* 107:21022-21027.

Kato, A., Y. Nagata, and K. Todokoro. 2004. Delta-tubulin is a component of intercellular bridges and both the early and mature perinuclear rings during spermatogenesis. *Dev. Biol.* 269:196-205.

Katoh, K., K. Kuma, H. Toh, and T. Miyata. 2005. MAFFT version 5: improvement in accuracy of multiple sequence alignment. *Nucleic Acids Res.* 33:511-518.

Katoh, K., K. Misawa, K. Kuma, and T. Miyata. 2002. MAFFT: a novel method for rapid multiple sequence alignment based on fast Fourier transform. *Nucleic Acids Res.* 30:3059-3066.

Keller, L.C., S. Geimer, E. Romijn, J. Yates, 3rd, I. Zamora, and W.F. Marshall. 2009. Molecular architecture of the centriole proteome: the conserved WD40 domain protein POC1 is required for centriole duplication and length control. *Mol. Biol. Cell.* 20:1150-1166.

Keller, L.C., E.P. Romijn, I. Zamora, J.R. Yates, 3rd, and W.F. Marshall. 2005. Proteomic analysis of isolated *Chlamydomonas* centrioles reveals orthologs of ciliary-disease genes. *Curr. Biol.* 15:1090-1098.

Kelly, S., J. Reed, S. Kramer, L. Ellis, H. Webb, J. Sunter, J. Salje, N. Marinsek, K. Gull, B. Wickstead, and M. Carrington. 2007. Functional genomics in *Trypanosoma brucei*: a collection of vectors for the expression of tagged proteins from endogenous and ectopic gene loci. *Mol. Biochem. Parasitol.* 154:103-109.

Kemp, C.A., K.R. Kopish, P. Zipperlen, J. Ahringer, and K.F. O'Connell. 2004. Centrosome maturation and duplication in *C. elegans* require the coiled-coil protein SPD-2. *Dev. Cell.* 6:511-523.

Keryer, G., J.R. Pineda, G. Liot, J. Kim, P. Dietrich, C. Benstaali, K. Smith, F.P. Cordelieres, N. Spassky, R.J. Ferrante, I. Dragatsis, and F. Saudou. 2011. Ciliogenesis is regulated by a huntingtin-HAP1-PCM1 pathway and is altered in Huntington disease. *J. Clin. Invest.* 121:4372-4382.

Kilburn, C.L., C.G. Pearson, E.P. Romijn, J.B. Meehl, T.H. Giddings, Jr., B.P. Culver, J.R. Yates, 3rd, and M. Winey. 2007. New *Tetrahymena* basal body protein components identify basal body domain structure. *J. Cell Biol.* 178:905-912.

Kilmartin, J.V., B. Wright, and C. Milstein. 1982. Rat monoclonal antitubulin antibodies derived by using a new nonsecreting rat cell line. *J. Cell Biol.* 93:576-582.

Kim, J.C., Y.Y. Ou, J.L. Badano, M.A. Esmail, C.C. Leitch, E. Fiedrich, P.L. Beales, J.M. Archibald, N. Katsanis, J.B. Rattner, and M.R. Leroux. 2005. MKKS/BBS6, a divergent chaperonin-like protein linked to the obesity disorder Bardet-Biedl syndrome, is a novel centrosomal component required for cytokinesis. *J. Cell Sci.* 118:1007-1020.

Kim, K., S. Lee, J. Chang, and K. Rhee. 2008. A novel function of CEP135 as a platform protein of C-NAP1 for its centriolar localization. *Exp. Cell Res.* 314:3692-3700.

Kim, S.K., A. Shindo, T.J. Park, E.C. Oh, S. Ghosh, R.S. Gray, R.A. Lewis, C.A. Johnson, T. Attie-Bittach, N. Katsanis, and J.B. Wallingford. 2010. Planar cell polarity acts through septins to control collective cell movement and ciliogenesis. *Science.* 329:1337-1340.

Kirkham, M., T. Muller-Reichert, K. Oegema, S. Grill, and A.A. Hyman. 2003. SAS-4 is a *C. elegans* centriolar protein that controls centrosome size. *Cell.* 112:575-587.

Kitagawa, D., C. Busso, I. Fluckiger, and P. Gonczy. 2009. Phosphorylation of SAS-6 by ZYG-1 is critical for centriole formation in *C. elegans* embryos. *Dev. Cell.* 17:900-907.

Kitagawa, D., I. Fluckiger, J. Polanowska, D. Keller, J. Reboul, and P. Gonczy. 2011a. PP2A phosphatase acts upon SAS-5 to ensure centriole formation in *C. elegans* embryos. *Dev. Cell.* 20:550-562.

Kitagawa, D., G. Kohlmaier, D. Keller, P. Strnad, F.R. Balestra, I. Fluckiger, and P. Gonczy. 2011b. Spindle positioning in human cells relies on proper centriole formation and on the microcephaly proteins CPAP and STIL. *J. Cell Sci.* 124:3884-3893.

Kitagawa, D., I. Vakonakis, N. Olieric, M. Hilbert, D. Keller, V. Olieric, M. Bortfeld, M.C. Erat, I. Fluckiger, P. Gonczy, and M.O. Steinmetz. 2011c. Structural basis of the 9-fold symmetry of centrioles. *Cell.* 144:364-375.

Kleylein-Sohn, J., J. Westendorf, M. Le Clech, R. Habedanck, Y.D. Stierhof, and E.A. Nigg. 2007. Plk4-induced centriole biogenesis in human cells. *Dev. Cell.* 13:190-202.

Knorz, V.J., C. Spalluto, M. Lessard, T.L. Purvis, F.F. Adigun, G.B. Collin, N.A. Hanley, D.I. Wilson, and T. Hearn. 2010. Centriolar association of ALMS1 and likely centrosomal functions of the ALMS motif-containing proteins C10orf90 and KIAA1731. *Mol. Biol. Cell.* 21:3617-3629.

Kobayashi, T., W.Y. Tsang, J. Li, W. Lane, and B.D. Dynlacht. 2011. Centriolar kinesin Kif24 interacts with CP110 to remodel microtubules and regulate ciliogenesis. *Cell.* 145:914-925.

Koblenz, B., J. Schoppmeier, A. Grunow, and K.F. Lechtreck. 2003. Centrin deficiency in *Chlamydomonas* causes defects in basal body replication, segregation and maturation. *J. Cell Sci.* 116:2635-2646.

Kohl, L., T. Sherwin, and K. Gull. 1999. Assembly of the paraflagellar rod and the flagellum attachment zone complex during the *Trypanosoma brucei* cell cycle. *J. Eukaryot. Microbiol.* 46:105-109.

Kohlmaier, G., J. Loncarek, X. Meng, B.F. McEwen, M.M. Mogensen, A. Spektor, B.D. Dynlacht, A. Khodjakov, and P. Gonczy. 2009. Overly long centrioles and defective cell division upon excess of the SAS-4-related protein CPAP. *Curr. Biol.* 19:1012-1018.

Kozminski, K.G., K.A. Johnson, P. Forscher, and J.L. Rosenbaum. 1993. A motility in the eukaryotic flagellum unrelated to flagellar beating. *Proc. Natl. Acad. Sci. U. S. A.* 90:5519-5523.

Kramer-Zucker, A.G., F. Olale, C.J. Haycraft, B.K. Yoder, A.F. Schier, and I.A. Drummond. 2005. Cilia-driven fluid flow in the zebrafish pronephros, brain and Kupffer's vesicle is required for normal organogenesis. *Development.* 132:1907-1921.

Kubo, A., H. Sasaki, A. Yuba-Kubo, S. Tsukita, and N. Shiina. 1999. Centriolar satellites: molecular characterization, ATP-dependent movement toward centrioles and possible involvement in ciliogenesis. *J. Cell Biol.* 147:969-980.

Kumar, P., and C.C. Wang. 2006. Dissociation of cytokinesis initiation from mitotic control in a eukaryote. *Eukaryot. Cell.* 5:92-102.

Kunimoto, K., Y. Yamazaki, T. Nishida, K. Shinohara, H. Ishikawa, T. Hasegawa, T. Okanoue, H. Hamada, T. Noda, A. Tamura, S. Tsukita, and S. Tsukita. 2012. Coordinated ciliary beating requires Odf2-mediated polarization of basal bodies via basal feet. *Cell.* 148:189-200.

Lacomble, S., S. Vaughan, C. Gadelha, M.K. Morphew, M.K. Shaw, J.R. McIntosh, and K. Gull. 2009. Three-dimensional cellular architecture of the flagellar pocket and associated cytoskeleton in trypanosomes revealed by electron microscope tomography. *J. Cell Sci.* 122:1081-1090.

Lacomble, S., S. Vaughan, C. Gadelha, M.K. Morphew, M.K. Shaw, J.R. McIntosh, and K. Gull. 2010. Basal body movements orchestrate membrane organelle division and cell morphogenesis in *Trypanosoma brucei*. *J. Cell Sci.* 123:2884-2891.

Lange, B.M., and K. Gull. 1995. A molecular marker for centriole maturation in the mammalian cell cycle. *J. Cell Biol.* 130:919-927.

Le Clech, M. 2008. Role of CAP350 in centriolar tubule stability and centriole assembly. *PLoS ONE*. 3:e3855.

Lechtreck, K.F., E.C. Johnson, T. Sakai, D. Cochran, B.A. Ballif, J. Rush, G.J. Pazour, M. Ikebe, and G.B. Witman. 2009. The *Chlamydomonas* reinhardtii BBSome is an IFT cargo required for export of specific signaling proteins from flagella. *J. Cell Biol.* 187:1117-1132.

Leidel, S., M. Delattre, L. Cerutti, K. Baumer, and P. Gonczy. 2005. SAS-6 defines a protein family required for centrosome duplication in *C. elegans* and in human cells. *Nat. Cell Biol.* 7:115-125.

Leidel, S., and P. Gonczy. 2003. SAS-4 is essential for centrosome duplication in *C. elegans* and is recruited to daughter centrioles once per cell cycle. *Dev. Cell.* 4:431-439.

Li, S., and X.J. Li. 2012. A huntingtin-HAP1-PCM1 pathway in ciliogenesis. *Expert Rev. Proteomics*. 9:17-19.

Liu, L., M. Zhang, Z. Xia, P. Xu, L. Chen, and T. Xu. 2011. Caenorhabditis elegans ciliary protein NPHP-8, the homologue of human RPGRIP1L, is required for ciliogenesis and chemosensation. *Biochem. Biophys. Res. Commun.* 410:626-631.

Locke, M., C.L. Tinsley, M.A. Benson, and D.J. Blake. 2009. TRIM32 is an E3 ubiquitin ligase for dysbindin. *Hum. Mol. Genet.* 18:2344-2358.

Loncarek, J., P. Hergert, V. Magidson, and A. Khodjakov. 2008. Control of daughter centriole formation by the pericentriolar material. *Nat. Cell Biol.* 10:322-328.

Mardin, B.R., F.G. Agircan, C. Lange, and E. Schiebel. 2011. Plk1 controls the Nek2A-PP1gamma antagonism in centrosome disjunction. *Curr. Biol.* 21:1145-1151.

Mardin, B.R., C. Lange, J.E. Baxter, T. Hardy, S.R. Scholz, A.M. Fry, and E. Schiebel. 2010. Components of the Hippo pathway cooperate with Nek2 kinase to regulate centrosome disjunction. *Nat. Cell Biol.* 12:1166-1176.

Marion, V., C. Stoetzel, D. Schlicht, N. Messaddeq, M. Koch, E. Flori, J.M. Danse, J.L. Mandel, and H. Dollfus. 2009. Transient ciliogenesis involving Bardet-Biedl syndrome proteins is a fundamental characteristic of adipogenic differentiation. *Proc. Natl. Acad. Sci. U. S. A.* 106:1820-1825.

Matsuura, K., P.A. Lefebvre, R. Kamiya, and M. Hirono. 2004. Bld10p, a novel protein essential for basal body assembly in *Chlamydomonas*: localization to the cartwheel, the first ninefold symmetrical structure appearing during assembly. *J. Cell Biol.* 165:663-671.

Matthews, K.R. 2005. The developmental cell biology of *Trypanosoma brucei*. *J. Cell Sci.* 118:283-290.

Mayor, T., U. Hacker, Y.D. Stierhof, and E.A. Nigg. 2002. The mechanism regulating the dissociation of the centrosomal protein C-Nap1 from mitotic spindle poles. *J. Cell Sci.* 115:3275-3284.

McKean, P.G. 2003. Coordination of cell cycle and cytokinesis in *Trypanosoma brucei*. *Curr. Opin. Microbiol.* 6:600-607.

McCulloch, R. (2004). "Antigenic variation in African trypanosomes: monitoring progress." Trends Parasitol 20(3): 117-121.

Megraw, T.L., J.T. Sharkey, and R.S. Nowakowski. 2011. Cdk5rap2 exposes the centrosomal root of microcephaly syndromes. *Trends Cell Biol.* 21:470-480.

Merchant, S.S., S.E. Prochnik, O. Vallon, E.H. Harris, S.J. Karpowicz, G.B. Witman, A. Terry, A. Salamov, L.K. Fritz-Laylin, L. Marechal-Drouard, W.F. Marshall, L.H. Qu, D.R. Nelson, A.A. Sanderfoot, M.H. Spalding, V.V. Kapitonov, Q. Ren, P. Ferris, E. Lindquist, H. Shapiro, S.M. Lucas, J. Grimwood, J. Schmutz, P. Cardol, H. Cerutti, G. Chanfreau, C.L. Chen, V. Cognat, M.T. Croft, R. Dent, S. Dutcher, E. Fernandez, H. Fukuzawa, D. Gonzalez-Ballester, D. Gonzalez-Halphen, A. Hallmann, M. Hanikenne, M. Hippler, W. Inwood, K. Jabbari, M. Kalanon, R. Kuras, P.A. Lefebvre, S.D. Lemaire, A.V. Lobanov, M. Lohr, A. Manuell, I. Meier, L. Mets, M. Mittag, T. Mittelmeier, J.V. Moroney, J. Moseley, C. Napoli, A.M. Nedelcu, K. Niyogi, S.V. Novoselov, I.T. Paulsen, G. Pazour, S. Purton, J.P. Ral, D.M. Riano-Pachon, W. Riekhof, L. Rymarquis, M. Schroda, D. Stern, J. Umen, R. Willows, N. Wilson, S.L. Zimmer, J. Allmer, J. Balk, K. Bisova, C.J. Chen, M. Elias, K. Gendler, C. Hauser, M.R. Lamb, H. Ledford, J.C. Long, J. Minagawa, M.D. Page, J. Pan, W. Pootakham, S. Roje, A. Rose, E. Stahlberg, A.M. Terauchi, P. Yang, S. Ball, C. Bowler, C.L. Dieckmann, V.N. Gladyshev, P. Green, R. Jorgensen, S. Mayfield, B. Mueller-Roeber, S. Rajamani, R.T. Sayre, P. Brokstein, et al. 2007. The *Chlamydomonas* genome reveals the evolution of key animal and plant functions. *Science*. 318:245-250.

Mogensen, M.M., A. Malik, M. Piel, V. Bouckson-Castaing, and M. Bornens. 2000. Microtubule minus-end anchorage at centrosomal and non-centrosomal sites: the role of ninein. *J. Cell Sci.* 113 (Pt 17):3013-3023.

Moreira-Leite, F.F., T. Sherwin, L. Kohl, and K. Gull. 2001. A trypanosome structure involved in transmitting cytoplasmic information during cell division. *Science*. 294:610-612.

Morita, E., V. Sandrin, H.Y. Chung, S.G. Morham, S.P. Gygi, C.K. Rodesch, and W.I. Sundquist. 2007. Human ESCRT and ALIX proteins interact with proteins of the midbody and function in cytokinesis. *EMBO J.* 26:4215-4227.

Morriswood, B., C. Y. He, et al. (2009). "The bilobe structure of *Trypanosoma brucei* contains a MORN-repeat protein." Mol Biochem Parasitol 167(2): 95-103.

Mottier-Pavie, V., and T.L. Megraw. 2009. *Drosophila* bld10 is a centriolar protein that regulates centriole, basal body, and motile cilium assembly. *Mol. Biol. Cell.* 20:2605-2614.

Mykytyn, K., R.F. Mullins, M. Andrews, A.P. Chiang, R.E. Swiderski, B. Yang, T. Braun, T. Casavant, E.M. Stone, and V.C. Sheffield. 2004. Bardet-Biedl syndrome type 4 (BBS4)-null mice implicate Bbs4 in flagella formation but not global cilia assembly. *Proc. Natl. Acad. Sci. U. S. A.* 101:8664-8669.

Nachury, M.V., A.V. Loktev, Q. Zhang, C.J. Westlake, J. Peranen, A. Merdes, D.C. Slusarski, R.H. Scheller, J.F. Bazan, V.C. Sheffield, and P.K. Jackson. 2007. A core complex of BBS proteins cooperates with the GTPase Rab8 to promote ciliary membrane biogenesis. *Cell.* 129:1201-1213.

Nachury, M.V., E.S. Seeley, and H. Jin. 2010. Trafficking to the ciliary membrane: how to get across the periciliary diffusion barrier? *Annu. Rev. Cell Dev. Biol.* 26:59-87.

Nakata, K., D. Shiba, D. Kobayashi, and T. Yokoyama. 2012. Targeting of Nphp3 to the primary cilia is controlled by an N-terminal myristoylation site and coiled-coil domains. *Cytoskeleton.* 69(4):221-34.

Nakazawa, Y., M. Hiraki, R. Kamiya, and M. Hirono. 2007. SAS-6 is a cartwheel protein that establishes the 9-fold symmetry of the centriole. *Curr. Biol.* 17:2169-2174.

Nasmyth, K., J.M. Peters, and F. Uhlmann. 2000. Splitting the chromosome: cutting the ties that bind sister chromatids. *Science.* 288:1379-1385.

Nauli, S.M., F.J. Alenghat, Y. Luo, E. Williams, P. Vassilev, X. Li, A.E. Elia, W. Lu, E.M. Brown, S.J. Quinn, D.E. Ingber, and J. Zhou. 2003. Polycystins 1 and 2 mediate mechanosensation in the primary cilium of kidney cells. *Nat. Genet.* 33:129-137.

Nigg, E.A., and T. Stearns. 2011. The centrosome cycle: Centriole biogenesis, duplication and inherent asymmetries. *Nat. Cell Biol.* 13:1154-1160.

Nonaka, S., Y. Tanaka, Y. Okada, S. Takeda, A. Harada, Y. Kanai, M. Kido, and N. Hirokawa. 1998. Randomization of left-right asymmetry due to loss of nodal cilia generating leftward flow of extraembryonic fluid in mice lacking KIF3B motor protein. *Cell.* 95:829-837.

O'Connell, K.F., C. Caron, K.R. Kopish, D.D. Hurd, K.J. Kemphues, Y. Li, and J.G. White. 2001. The *C. elegans* zyg-1 gene encodes a regulator of centrosome duplication with distinct maternal and paternal roles in the embryo. *Cell.* 105:547-558.

O'Toole, E.T., T.H. Giddings, J.R. McIntosh, and S.K. Dutcher. 2003. Three-dimensional organization of basal bodies from wild-type and delta-tubulin deletion strains of *Chlamydomonas reinhardtii*. *Mol. Biol. Cell.* 14:2999-3012.

Oakley, C.E., and B.R. Oakley. 1989. Identification of gamma-tubulin, a new member of the tubulin superfamily encoded by mipA gene of *Aspergillus nidulans*. *Nature.* 338:662-664.

Oh, E.C., and N. Katsanis. 2012. Cilia in vertebrate development and disease. *Development.* 139:443-448.

Olbrich, H., M. Fliegauf, J. Hoefele, A. Kispert, E. Otto, A. Volz, M.T. Wolf, G. Sasmaz, U. Trauer, R. Reinhardt, R. Sudbrak, C. Antignac, N. Gretz, G. Walz, B. Schermer, T. Benzing, F. Hildebrandt, and H. Omran. 2003. Mutations in a novel gene, NPHP3, cause adolescent nephronophthisis, tapeto-retinal degeneration and hepatic fibrosis. *Nat. Genet.* 34:455-459.

Omran, H. 2010. NPHP proteins: gatekeepers of the ciliary compartment. *J. Cell Biol.* 190:715-717.

Otto, E., J. Hoefele, R. Ruf, A.M. Mueller, K.S. Hiller, M.T. Wolf, M.J. Schuermann, A. Becker, R. Birkenhager, R. Sudbrak, H.C. Hennies, P. Nurnberg, and F. Hildebrandt. 2002. A gene mutated in nephronophthisis and retinitis pigmentosa encodes a novel protein, nephroretinin, conserved in evolution. *Am. J. Hum. Genet.* 71:1161-1167.

Otto, E.A., B. Loeys, H. Khanna, J. Hellemans, R. Sudbrak, S. Fan, U. Muerb, J.F. O'Toole, J. Helou, M. Attanasio, B. Utsch, J.A. Sayer, C. Lillo, D. Jimeno, P. Coucke, A. De Paepe, R. Reinhardt, S. Klages, M. Tsuda, I. Kawakami, T. Kusakabe, H. Omran, A. Imm, M. Tippens, P.A. Raymond, J. Hill, P. Beales, S. He, A. Kispert, B. Margolis, D.S. Williams, A. Swaroop, and F. Hildebrandt. 2005. Nephrocystin-5, a ciliary IQ domain protein, is mutated in Senior-Loken syndrome and interacts with RPGR and calmodulin. *Nat. Genet.* 37:282-288.

Ou, G., O.E. Blacque, J.J. Snow, M.R. Leroux, and J.M. Scholey. 2005. Functional coordination of intraflagellar transport motors. *Nature*. 436:583-587.

Ou, Y.Y., G.J. Mack, M. Zhang, and J.B. Rattner. 2002. CEP110 and ninein are located in a specific domain of the centrosome associated with centrosome maturation. *J. Cell Sci.* 115:1825-1835.

Paoletti, A., M. Moudjou, M. Paintrand, J.L. Salisbury, and M. Bornens. 1996. Most of centrin in animal cells is not centrosome-associated and centrosomal centrin is confined to the distal lumen of centrioles. *J. Cell Sci.* 109 (Pt 13):3089-3102.

Paramasivam, M., Y.J. Chang, and J.J. LoTurco. 2007. ASPM and citron kinase co-localize to the midbody ring during cytokinesis. *Cell Cycle*. 6:1605-1612.

Park, T.J., B.J. Mitchell, P.B. Abitua, C. Kintner, and J.B. Wallingford. 2008. Dishevelled controls apical docking and planar polarization of basal bodies in ciliated epithelial cells. *Nat. Genet.* 40:871-879.

Pazour, G.J., B.L. Dickert, Y. Vucica, E.S. Seeley, J.L. Rosenbaum, G.B. Witman, and D.G. Cole. 2000. *Chlamydomonas* IFT88 and its mouse homologue, polycystic kidney disease gene tg737, are required for assembly of cilia and flagella. *J. Cell Biol.* 151:709-718.

Pazour, G.J., J.T. San Agustin, J.A. Follit, J.L. Rosenbaum, and G.B. Witman. 2002. Polycystin-2 localizes to kidney cilia and the ciliary level is elevated in orpk mice with polycystic kidney disease. *Curr. Biol.* 12:R378-380.

Pearson, C.G., D.P. Osborn, T.H. Giddings, Jr., P.L. Beales, and M. Winey. 2009. Basal body stability and ciliogenesis requires the conserved component Poc1. *J. Cell Biol.* 187:905-920.

Pearson, C.G., and M. Winey. 2009. Basal body assembly in ciliates: the power of numbers. *Traffic*. 10:461-471.

Peel, N., N.R. Stevens, R. Basto, and J.W. Raff. 2007. Overexpressing centriole-replication proteins in vivo induces centriole overduplication and de novo formation. *Curr. Biol.* 17:834-843.

Pelletier, L., E. O'Toole, A. Schwager, A.A. Hyman, and T. Muller-Reichert. 2006. Centriole assembly in *Caenorhabditis elegans*. *Nature*. 444:619-623.

Perkins, L.A., E.M. Hedgecock, J.N. Thomson, and J.G. Culotti. 1986. Mutant sensory cilia in the nematode *Caenorhabditis elegans*. *Dev. Biol.* 117:456-487.

Pfannenschmid, F., V.C. Wimmer, R.M. Rios, S. Geimer, U. Krockel, A. Leiherer, K. Haller, Y. Nemcova, and W. Mages. 2003. *Chlamydomonas* DIP13 and human NA14: a new class of proteins associated with microtubule structures is involved in cell division. *J. Cell Sci.* 116:1449-1462.

Piao, T., M. Luo, L. Wang, Y. Guo, D. Li, P. Li, W.J. Snell, and J. Pan. 2009. A microtubule depolymerizing kinesin functions during both flagellar disassembly and flagellar assembly in Chlamydomonas. *Proc. Natl. Acad. Sci. U. S. A.* 106:4713-4718.

Pickett-Heaps, J. 1971. Autonomy of the centriole - fact or fallacy? *Cytobios*. 3:205.

Piel, M., P. Meyer, A. Khodjakov, C.L. Rieder, and M. Bornens. 2000. The respective contributions of the mother and daughter centrioles to centrosome activity and behavior in vertebrate cells. *J. Cell Biol.* 149:317-330.

Piperno, G., E. Siuda, S. Henderson, M. Segil, H. Vaananen, and M. Sassaroli. 1998. Distinct mutants of retrograde intraflagellar transport (IFT) share similar morphological and molecular defects. *J. Cell Biol.* 143:1591-1601.

Ploubidou, A., D.R. Robinson, R.C. Docherty, E.O. Ogbadoyi, and K. Gull. 1999. Evidence for novel cell cycle checkpoints in trypanosomes: kinetoplast segregation and cytokinesis in the absence of mitosis. *J. Cell Sci.* 112 (Pt 24):4641-4650.

Poon, S.K., L. Peacock, W. Gibson, K. Gull, and S. Kelly. 2012. A modular and optimized single marker system for generating *Trypanosoma brucei* cell lines expressing T7 RNA polymerase and the tetracyclin repressor. *In* Open Biology. Vol. 2(2):110037.

Popov, A.V., A. Pozniakovsky, I. Arnal, C. Antony, A.J. Ashford, K. Kinoshita, R. Tournebize, A.A. Hyman, and E. Karsenti. 2001. XMAP215 regulates microtubule dynamics through two distinct domains. *EMBO J.* 20:397-410.

Price, H.P., M.R. Hodgkinson, R.S. Curwen, L.M. Maclean, J.A. Brannigan, M. Carrington, B.A. Smith, D.A. Ashford, M. Stark, and D.F. Smith. 2012. The Orthologue of Sjogren's Syndrome Nuclear Autoantigen 1 (SSNA1) in *Trypanosoma brucei* Is an Immunogenic Self-Assembling Molecule. *PLoS ONE*. 7:e31842.

Puklowski, A., Y. Homsi, D. Keller, M. May, S. Chauhan, U. Kossatz, V. Grunwald, S. Kubicka, A. Pich, M.P. Manns, I. Hoffmann, P. Gonczy, and N.P. Malek. 2011. The SCF-FBXW5 E3-ubiquitin ligase is regulated by PLK4 and targets HsSAS-6 to control centrosome duplication. *Nat. Cell Biol.* 13:1004-1009.

Purvis, T.L., T. Hearn, C. Spalluto, V.J. Knorz, K.P. Hanley, T. Sanchez-Elsner, N.A. Hanley, and D.I. Wilson. 2010. Transcriptional regulation of the Alstrom syndrome gene ALMS1 by members of the RFX family and Sp1. *Gene*. 460:20-29.

Quarmby, L.M., and J.D. Parker. 2005. Cilia and the cell cycle? *J. Cell Biol.* 169:707-710.

Raynaud-Messina, B., and A. Merdes. 2007. Gamma-tubulin complexes and microtubule organization. *Curr. Opin. Cell Biol.* 19:24-30.

Rebollo, E., P. Sampaio, J. Januschke, S. Llamazares, H. Varmark, and C. Gonzalez. 2007. Functionally unequal centrosomes drive spindle orientation in asymmetrically dividing Drosophila neural stem cells. *Dev. Cell.* 12:467-474.

Ringo, D.L. 1967. Flagellar motion and fine structure of the flagellar apparatus in *Chlamydomonas*. *J. Cell Biol.* 33:543-571.

Robinson, D. R., T. Sherwin, et al. (1995). "Microtubule polarity and dynamics in the control of organelle positioning, segregation, and cytokinesis in the trypanosome cell cycle." J Cell Biol 128(6): 1163-1172.

Rodrigues-Martins, A., M. Bettencourt-Dias, M. Riparbelli, C. Ferreira, I. Ferreira, G. Callaini, and D.M. Glover. 2007a. DSAS-6 organizes a tube-like centriole precursor, and its absence suggests modularity in centriole assembly. *Curr. Biol.* 17:1465-1472.

Rodrigues-Martins, A., M. Riparbelli, G. Callaini, D.M. Glover, and M. Bettencourt-Dias. 2007b. Revisiting the role of the mother centriole in centriole biogenesis. *Science*. 316:1046-1050.

Rogers, G.C., N.M. Rusan, D.M. Roberts, M. Peifer, and S.L. Rogers. 2009. The SCF Slimb ubiquitin ligase regulates Plk4/Sak levels to block centriole reduplication. *J. Cell Biol.* 184:225-239.

Rohatgi, R., and W.J. Snell. 2010. The ciliary membrane. *Curr. Opin. Cell Biol.* 22:541-546.

Ronquist, F., and J.P. Huelsenbeck. 2003. MrBayes 3: Bayesian phylogenetic inference under mixed models. *Bioinformatics*. 19:1572-1574.

Ruiz, F., J. Beisson, J. Rossier, and P. Dupuis-Williams. 1999. Basal body duplication in *Paramecium* requires gamma-tubulin. *Curr. Biol.* 9:43-46.

Ruiz, F., N. Garreau de Loubresse, C. Klotz, J. Beisson, and F. Koll. 2005. Centrin deficiency in *Paramecium* affects the geometry of basal-body duplication. *Curr. Biol.* 15:2097-2106.

Salisbury, J.L., K.M. Suino, R. Busby, and M. Springett. 2002. Centrin-2 is required for centriole duplication in mammalian cells. *Curr. Biol.* 12:1287-1292.

Sandblad, L., K.E. Busch, P. Tittmann, H. Gross, D. Brunner, and A. Hoenger. 2006. The *Schizosaccharomyces pombe* EB1 homolog Mal3p binds and stabilizes the microtubule lattice seam. *Cell.* 127:1415-1424.

Sang, L., J.J. Miller, K.C. Corbit, R.H. Giles, M.J. Brauer, E.A. Otto, L.M. Baye, X. Wen, S.J. Scales, M. Kwong, E.G. Huntzicker, M.K. Sfakianos, W. Sandoval, J.F. Bazan, P. Kulkarni, F.R. Garcia-Gonzalo, A.D. Seol, J.F. O'Toole, S. Held, H.M. Reutter, W.S. Lane, M.A. Rafiq, A. Noor, M. Ansar, A.R. Devi, V.C. Sheffield, D.C. Slusarski, J.B. Vincent, D.A. Doherty, F. Hildebrandt, J.F. Reiter, and P.K. Jackson. 2011. Mapping the NPHP-JBTS-MKS protein network reveals ciliopathy disease genes and pathways. *Cell.* 145:513-528.

Schmidt, T.I., J. Kleylein-Sohn, J. Westendorf, M. Le Clech, S.B. Lavoie, Y.D. Stierhof, and E.A. Nigg. 2009. Control of centriole length by CPAP and CP110. *Curr. Biol.* 19:1005-1011.

Schockel, L., M. Mockel, B. Mayer, D. Boos, and O. Stemmann. 2011. Cleavage of cohesin rings coordinates the separation of centrioles and chromatids. *Nat. Cell Biol.* 13:966-972.

Schrevel, J., and C. Besse. 1975. [A functional flagella with a 6 + 0 pattern]. *J. Cell Biol.* 66:492-507.

Seo, S., L.M. Baye, N.P. Schulz, J.S. Beck, Q. Zhang, D.C. Slusarski, and V.C. Sheffield. 2010. BBS6, BBS10, and BBS12 form a complex with CCT/TRiC family chaperonins and mediate BBSome assembly. *Proc. Natl. Acad. Sci. U. S. A.* 107:1488-1493.

Shah, A.S., S.L. Farmen, T.O. Moninger, T.R. Businga, M.P. Andrews, K. Bugge, C.C. Searby, D. Nishimura, K.A. Brogden, J.N. Kline, V.C. Sheffield, and M.J. Welsh. 2008. Loss of Bardet-Biedl syndrome proteins alters the morphology and function of motile cilia in airway epithelia. *Proc. Natl. Acad. Sci. U. S. A.* 105:3380-3385.

Shang, Y., B. Li, and M.A. Gorovsky. 2002. *Tetrahymena* thermophila contains a conventional gamma-tubulin that is differentially required for the maintenance of different microtubule-organizing centers. *J. Cell Biol.* 158:1195-1206.

Sharma, R., E. Gluenz, L. Peacock, W. Gibson, K. Gull, and M. Carrington. 2009. The heart of darkness: growth and form of Trypanosoma brucei in the tsetse fly. *Trends Parasitol.* 25:517-524.

Sherwin, T., and K. Gull. 1989. The cell division cycle of *Trypanosoma brucei brucei*: timing of event markers and cytoskeletal modulations. *Philos. Trans. R. Soc. Lond. B. Biol. Sci.* 323:573-588.

Shi, J., J. B. Franklin, et al. (2008). "Centrin4 coordinates cell and nuclear division in *T. brucei*." J Cell Sci 121(Pt 18): 3062-3070.

Silflow, C.D., M. LaVoie, L.W. Tam, S. Tousey, M. Sanders, W. Wu, M. Borodovsky, and P.A. Lefebvre. 2001. The Vfl1 Protein in *Chlamydomonas* localizes in a rotationally asymmetric pattern at the distal ends of the basal bodies. *J. Cell Biol.* 153:63-74.

Silva, F.P., R. Hamamoto, Y. Nakamura, and Y. Furukawa. 2005. WDRPUH, a novel WD-repeat-containing protein, is highly expressed in human hepatocellular carcinoma and involved in cell proliferation. *Neoplasia*. 7:348-355.

Sinden, R.E., E.U. Canning, R.S. Bray, and M.E. Smalley. 1978. Gametocyte and gamete development in *Plasmodium falciparum*. *Proc. R. Soc. Lond. B Biol. Sci.* 201:375-399.

Sinden, R.E., E.U. Canning, and B. Spain. 1976. Gametogenesis and fertilization in *Plasmodium yoelii nigeriensis*: a transmission electron microscope study. *Proc. R. Soc. Lond. B Biol. Sci.* 193:55-76.

Singla, V., M. Romaguera-Ros, J.M. Garcia-Verdugo, and J.F. Reiter. 2010. Ofd1, a human disease gene, regulates the length and distal structure of centrioles. *Dev. Cell.* 18:410-424.

Sir, J.H., A.R. Barr, A.K. Nicholas, O.P. Carvalho, M. Khurshid, A. Sossick, S. Reichelt, C. D'Santos, C.G. Woods, and F. Gergely. 2011. A primary microcephaly protein complex forms a ring around parental centrioles. *Nat. Genet.* 43:1147-1153.

Smith, E., N. Hegarat, C. Vesely, I. Roseboom, C. Larch, H. Streicher, K. Straatman, H. Flynn, M. Skehel, T. Hirota, R. Kuriyama, and H. Hochegger. 2011. Differential control of Eg5-dependent centrosome separation by Plk1 and Cdk1. *EMBO J.* 30:2233-2245.

Smrzka, O.W., N. Delgehyr, and M. Bornens. 2000. Tissue-specific expression and subcellular localisation of mammalian delta-tubulin. *Curr. Biol.* 10:413-416.

Song, M.H., L. Aravind, T. Muller-Reichert, and K.F. O'Connell. 2008. The conserved protein SZY-20 opposes the Plk4-related kinase ZYG-1 to limit centrosome size. *Dev. Cell.* 15:901-912.

Song, M.H., Y. Liu, D.E. Anderson, W.J. Jahng, and K.F. O'Connell. 2011. Protein phosphatase 2A-SUR-6/B55 regulates centriole duplication in *C. elegans* by controlling the levels of centriole assembly factors. *Dev. Cell.* 20:563-571.

Sorokin, S. 1962. Centrioles and the formation of rudimentary cilia by fibroblasts and smooth muscle cells. *J. Cell Biol.* 15:363-377.

Spektor, A., W.Y. Tsang, D. Khoo, and B.D. Dynlacht. 2007. Cep97 and CP110 suppress a cilia assembly program. *Cell.* 130:678-690.

Stemm-Wolf, A.J., G. Morgan, T.H. Giddings, Jr., E.A. White, R. Marchione, H.B. McDonald, and M. Winey. 2005. Basal body duplication and maintenance require one member of the *Tetrahymena thermophila* centrin gene family. *Mol. Biol. Cell.* 16:3606-3619.

Stephan, A., S. Vaughan, M.K. Shaw, K. Gull, and P.G. McKean. 2007. An essential quality control mechanism at the eukaryotic basal body prior to intraflagellar transport. *Traffic.* 8:1323-1330.

Stevens, N.R., J. Dobbelaere, K. Brunk, A. Franz, and J.W. Raff. 2010a. *Drosophila* Ana2 is a conserved centriole duplication factor. *J. Cell Biol.* 188:313-323.

Stevens, N.R., H. Roque, and J.W. Raff. 2010b. DSas-6 and Ana2 coassemble into tubules to promote centriole duplication and engagement. *Dev. Cell.* 19:913-919.

Stoetzel, C., J. Muller, V. Laurier, E.E. Davis, N.A. Zaghloul, S. Vicaire, C. Jacquelin, F. Plewniak, C.C. Leitch, P. Sarda, C. Hamel, T.J. de Ravel, R.A. Lewis, E. Friederich, C. Thibault, J.M. Danse, A. Verloes, D. Bonneau, N. Katsanis, O. Poch, J.L. Mandel, and H. Dollfus. 2007. Identification of a novel BBS gene (BBS12) highlights the major role of a vertebrate-specific branch of chaperonin-related proteins in Bardet-Biedl syndrome. *Am. J. Hum. Genet.* 80:1-11.

Strnad, P., S. Leidel, T. Vinogradova, U. Euteneuer, A. Khodjakov, and P. Gonczy. 2007. Regulated HsSAS-6 levels ensure formation of a single procentriole per centriole during the centrosome duplication cycle. *Dev. Cell.* 13:203-213.

Tadenev, A.L., H.M. Kulaga, H.L. May-Simera, M.W. Kelley, N. Katsanis, and R.R. Reed. 2011. Loss of Bardet-Biedl syndrome protein-8 (BBS8) perturbs olfactory function, protein localization, and axon targeting. *Proc. Natl. Acad. Sci. U. S. A.* 108:10320-10325.

Tang, C.J., R.H. Fu, K.S. Wu, W.B. Hsu, and T.K. Tang. 2009. CPAP is a cell-cycle regulated protein that controls centriole length. *Nat. Cell Biol.* 11:825-831.

Tang, C.J., S.Y. Lin, W.B. Hsu, Y.N. Lin, C.T. Wu, Y.C. Lin, C.W. Chang, K.S. Wu, and T.K. Tang. 2011. The human microcephaly protein STIL interacts with CPAP and is required for procentriole formation. *EMBO J.* 30:4790-4804.

Tsang, W.Y., C. Bossard, H. Khanna, J. Peranen, A. Swaroop, V. Malhotra, and B.D. Dynlacht. 2008. CP110 suppresses primary cilia formation through its interaction with CEP290, a protein deficient in human ciliary disease. *Dev. Cell.* 15:187-197.

Tsang, W.Y., A. Spektor, S. Vijayakumar, B.R. Bista, J. Li, I. Sanchez, S. Duensing, and B.D. Dynlacht. 2009. Cep76, a centrosomal protein that specifically restrains centriole reduplication. *Dev. Cell.* 16:649-660.

Tsao, C.C., and M.A. Gorovsky. 2008. Tetrahymena IFT122A is not essential for cilia assembly but plays a role in returning IFT proteins from the ciliary tip to the cell body. *J. Cell Sci.* 121:428-436.

Tsou, M.F., and T. Stearns. 2006. Mechanism limiting centrosome duplication to once per cell cycle. *Nature.* 442:947-951.

Tsou, M.F., W.J. Wang, K.A. George, K. Uryu, T. Stearns, and P.V. Jallepalli. 2009. Polo kinase and separase regulate the mitotic licensing of centriole duplication in human cells. *Dev. Cell.* 17:344-354.

van Breugel, M., M. Hirono, A. Andreeva, H.A. Yanagisawa, S. Yamaguchi, Y. Nakazawa, N. Morgner, M. Petrovich, I.O. Ebong, C.V. Robinson, C.M. Johnson, D. Veprintsev, and B. Zuber. 2011. Structures of SAS-6 suggest its organization in centrioles. *Science.* 331:1196-1199.

Varmark, H., S. Llamazares, E. Rebollo, B. Lange, J. Reina, H. Schwarz, and C. Gonzalez. 2007. Asterless is a centriolar protein required for centrosome function and embryo development in *Drosophila*. *Curr. Biol.* 17:1735-1745.

Vickerman, K. (1969). "On the surface coat and flagellar adhesion in trypanosomes." J Cell Sci 5(1): 163-193.

Vickerman, K. 1985. Developmental cycles and biology of pathogenic trypanosomes. *Br. Med. Bull.* 41:105-114.

Vieira, O.V., K. Gaus, P. Verkade, J. Fullekrug, W.L. Vaz, and K. Simons. 2006. FAPP2, cilium formation, and compartmentalization of the apical membrane in polarized Madin-Darby canine kidney (MDCK) cells. *Proc. Natl. Acad. Sci. U. S. A.* 103:18556-18561.

Vitre, B., F.M. Coquelle, C. Heichette, C. Garnier, D. Chretien, and I. Arnal. 2008. EB1 regulates microtubule dynamics and tubulin sheet closure in vitro. *Nat. Cell Biol.* 10:415-421.

Vladar, E.K., and T. Stearns. 2007. Molecular characterization of centriole assembly in ciliated epithelial cells. *J. Cell Biol.* 178:31-42.

Voegtli, W.C., A.Y. Madrona, and D.K. Wilson. 2003. The structure of Aip1p, a WD repeat protein that regulates Cofilin-mediated actin depolymerization. *J. Biol. Chem.* 278:34373-34379.

Vorobjev, I.A., and S. Chentsov Yu. 1982. Centrioles in the cell cycle. I. Epithelial cells. *J. Cell Biol.* 93:938-949.

Wallingford, J.B., and B. Mitchell. 2011. Strange as it may seem: the many links between Wnt signaling, planar cell polarity, and cilia. *Genes Dev.* 25:201-213.

Wang, X., J.W. Tsai, J.H. Imai, W.N. Lian, R.B. Vallee, and S.H. Shi. 2009. Asymmetric centrosome inheritance maintains neural progenitors in the neocortex. *Nature*. 461:947-955.

Wang, X., Y. Yang, Q. Duan, N. Jiang, Y. Huang, Z. Darzynkiewicz, and W. Dai. 2008. sSgo1, a major splice variant of Sgo1, functions in centriole cohesion where it is regulated by Plk1. *Dev. Cell.* 14:331-341.

Welburn, S.C., and M. Odiit. 2002. Recent developments in human African trypanosomiasis. *Curr. Opin. Infect. Dis.* 15:477-484.

Whelan, S., and N. Goldman. 2001. A general empirical model of protein evolution derived from multiple protein families using a maximum-likelihood approach. *Mol. Biol. Evol.* 18:691-699.

Wickstead, B., J.T. Carrington, E. Gluenz, and K. Gull. 2010. The expanded Kinesin-13 repertoire of trypanosomes contains only one mitotic Kinesin indicating multiple extra-nuclear roles. *PLoS ONE*. 5:e15020.

Wickstead, B., and K. Gull. 2007. Dyneins across eukaryotes: a comparative genomic analysis. *Traffic*. 8:1708-1721.

Williams, C.L., C. Li, K. Kida, P.N. Inglis, S. Mohan, L. Semenec, N.J. Bialas, R.M. Stupay, N. Chen, O.E. Blacque, B.K. Yoder, and M.R. Leroux. 2011. MKS and NPHP modules cooperate to establish basal body/transition zone membrane associations and ciliary gate function during ciliogenesis. *J. Cell Biol.* 192:1023-1041.

Won, J., C. Marin de Evsikova, R.S. Smith, W.L. Hicks, M.M. Edwards, C. Longo-Guess, T. Li, J.K. Naggert, and P.M. Nishina. 2011. NPHP4 is necessary for normal photoreceptor ribbon synapse maintenance and outer segment formation, and for sperm development. *Hum. Mol. Genet.* 20:482-496.

Woods, A., T. Sherwin, R. Sasse, T.H. MacRae, A.J. Baines, and K. Gull. 1989. Definition of individual components within the cytoskeleton of *Trypanosoma brucei* by a library of monoclonal antibodies. *J. Cell Sci.* 93 (Pt 3):491-500.

Woodward, R., M.J. Carden, and K. Gull. 1995. Immunological characterization of cytoskeletal proteins associated with the basal body, axoneme and flagellum attachment zone of *Trypanosoma brucei*. *Parasitology.* 111 (Pt 1):77-85.

Woodward, R., and K. Gull. 1990. Timing of nuclear and kinetoplast DNA replication and early morphological events in the cell cycle of *Trypanosoma brucei*. *J. Cell Sci.* 95 (Pt 1):49-57.

Wright, K.J., L.M. Baye, A. Olivier-Mason, S. Mukhopadhyay, L. Sang, M. Kwong, W. Wang, P.R. Pretorius, V.C. Sheffield, P. Sengupta, D.C. Slusarski, and P.K. Jackson. 2011. An ARL3-UNC119-RP2 GTPase cycle targets myristoylated NPHP3 to the primary cilium. *Genes Dev.* 25:2347-2360.

Xu, C., and J. Min. 2011. Structure and function of WD40 domain proteins. *Protein & cell.* 2:202-214.

Yabe, T., X. Ge, and F. Pelegri. 2007. The zebrafish maternal-effect gene cellular atoll encodes the centriolar component sas-6 and defects in its paternal function promote whole genome duplication. *Dev. Biol.* 312:44-60.

Yamashita, Y.M., A.P. Mahowald, J.R. Perlin, and M.T. Fuller. 2007. Asymmetric inheritance of mother versus daughter centrosome in stem cell division. *Science*. 315:518-521.

Yan, X., R. Habedanck, and E.A. Nigg. 2006. A complex of two centrosomal proteins, CAP350 and FOP, cooperates with EB1 in microtubule anchoring. *Mol. Biol. Cell.* 17:634-644.

Yang, J., M. Adamian, and T. Li. 2006. Rootletin interacts with C-Nap1 and may function as a physical linker between the pair of centrioles/basal bodies in cells. *Mol. Biol. Cell.* 17:1033-1040.

Yu, Z., Y. Liu, and Z. Li. 2012. Structure-function relationship of the Polo-like kinase in *Trypanosoma brucei*. *J. Cell Sci.* 125(Pt 6):1519-30.

Zhang, Q., D. Nishimura, S. Seo, T. Vogel, D.A. Morgan, C. Searby, K. Bugge, E.M. Stone, K. Rahmouni, and V.C. Sheffield. 2011. Bardet-Biedl syndrome 3 (Bbs3) knockout mouse model reveals common BBS-associated phenotypes and Bbs3 unique phenotypes. *Proc. Natl. Acad. Sci. U. S. A.* 108:20678-20683.

Zhao, C., and J. Malicki. 2011. Nephrocystins and MKS proteins interact with IFT particle and facilitate transport of selected ciliary cargos. *EMBO J.* 30:2532-2544.

Zhao, L., C. Jin, Y. Chu, C. Varghese, S. Hua, F. Yan, Y. Miao, J. Liu, D. Mann, X. Ding, J. Zhang, Z. Wang, Z. Dou, and X. Yao. 2010. Dimerization of CPAP orchestrates centrosome cohesion plasticity. *J. Biol. Chem.* 285:2488-2497.

Zhou, Q., L. Gheiratmand, et al. (2010). "A comparative proteomic analysis reveals a new bilobe protein required for bi-lobe duplication and cell division in *Trypanosoma brucei*." PLoS One 5(3): e9660

Zhu, F., S. Lawo, A. Bird, D. Pinchev, A. Ralph, C. Richter, T. Muller-Reichert, R. Kittler, A.A. Hyman, and L. Pelletier. 2008. The mammalian SPD-2 ortholog Cep192 regulates centrosome biogenesis. *Curr. Biol.* 18:136-141.

APPENDIX

Reconstructing the evolutionary history of the centriole from protein components

Matthew E. Hodges[1,2,*], Nicole Scheumann[1,*], Bill Wickstead[1,*], Jane A. Langdale[2] and Keith Gull[1,‡]

[1]Sir William Dunn School of Pathology, University of Oxford, South Parks Road, Oxford OX1 3RE, UK
[2]Department of Plant Sciences, University of Oxford, South Parks Road, Oxford OX1 3RB, UK
*These authors contributed equally to this work
‡Author for correspondence (keith.gull@path.ox.ac.uk)

Accepted 9 February 2010
Journal of Cell Science 123, 1407-1413

doi:10.1242/jcs.064873

Summary

Centrioles are highly conserved structures that fulfil important cellular functions, such as nucleation of cilia and flagella (basal-body function) and organisation of pericentriolar material to form the centrosome. The evolution of these functions can be inferred from the distribution of the molecular components of extant centrioles and centrosomes. Here, we undertake an evolutionary analysis of 53 proteins known either for centriolar association or for involvement in cilia-associated pathologies. By linking protein distribution in 45 diverse eukaryotes with organism biology, we provide molecular evidence to show that basal-body function is ancestral, whereas the presence of the centrosome is specific to the Holozoa. We define an ancestral centriolar inventory of 14 core proteins, Polo-like-kinase, and proteins associated with Bardet-Biedl syndrome (BBS) and Meckel-Gruber syndrome. We show that the BBSome is absent from organisms that produce cilia only for motility, predicting a dominant and ancient role for this complex in sensory function. We also show that the unusual centriole of *Caenorhabditis elegans* is highly divergent in both protein composition and sequence. Finally, we demonstrate a correlation between the presence of specific centriolar proteins and eye evolution. This correlation is used to predict proteins with functions in the development of ciliary, but not rhabdomeric, eyes.

Key words: BBS, Basal body, Cenancestor, Cilia/flagellum, Ciliopathy, MKS

Introduction

Centrioles are highly conserved eukaryotic organelles consisting of nine microtubule triplets (or, more rarely, doublets or singlets) arranged in a radially symmetrical array. These structures are involved in a number of cellular functions, which include nucleating cilia and flagella – a context in which they are termed basal bodies (for a review, see Dawe et al., 2007) – and organising pericentriolar material to form the centrosome. The centrosome is a microtubule-organising centre in interphase cells and, in some eukaryotes, forms part of the spindle poles during cell division (see Delattre and Gonczy, 2004).

In recent years, experimental work on centrioles, centrosomes and basal bodies has elucidated a list of proteins that contribute to the formation of these structures (at least in the case of the individual model system studied). In addition to these proteins, several genes have been implicated in basal-body or ciliary function by their association with human pathologies caused by defects in cilia, collectively named ciliopathies (for a review, see Badano et al., 2006). Despite these insights, it remains difficult to determine whether an individual protein has a role in centriolar, centrosomal or basal-body function; furthermore, it cannot be assumed that a particular role in one model system extends to other model systems.

Here, we use a bioinformatics approach to determine the evolutionary history of the centriole from the perspective of its constituent proteins. We look at the conservation of multiple proteins that have either been physically localised to centrioles, centrosomes or basal bodies, or are genetically linked with basal-body or ciliary function by association with ciliopathies. By ascertaining the distribution of these proteins in a wide cross-section of eukaryotes, we are able to define a set of components that were present in the ancestral centriole. Linking this distribution to known organismal biology, we are also able to relate the loss of components to unusual centriolar morphologies and to predict a role for particular proteins in eye development.

Results and Discussion

Identification of centriolar proteins in diverse eukaryotes

To gain a deeper understanding of the biological role of known centriole- and ciliopathy-associated proteins, we analysed the phylogenetic presence and absence of these proteins among eukaryotes and linked the distribution pattern obtained to information about the protein and organism. We selected 45 organisms, each with a complete or near-complete genome sequence, which represent a wide evolutionary spread across six major groups of eukaryotes (namely: Plantae, Excavata, Chromalveolata, Holozoa, Fungi and Amoebozoa). The selected organisms exhibit a rich diversity of microtubule biology and represent species that either produce cilia or flagella during their lifecycle or do not (29 ciliated species and 16 non-ciliated species; supplementary material Table S1). We hypothesised that proteins that just have a centriolar and/or ciliary function would be present in cilia-forming species and absent in non-ciliated species.

We selected a set of 53 proteins that are known either for their centriolar, centrosomal or basal-body localisation, or for their involvement in cilia-associated pathologies that present with retinitis pigmentosa (supplementary material Table S2). We used these protein sequences to interrogate the 45 predicted proteomes for orthologous sequences. We found that reciprocal best BLAST approaches – in which only proteins that are the best match in their respective genomes are considered orthologues – were generally too conservative in identifying orthologues, in part because of

Journal of Cell Science

extensive gene duplications in particular lineages. By contrast, simple BLAST searches (identifying all similar sequences) were too noisy and unable to discriminate among paralogues. To overcome these problems, we used an approach based on the clustering of proteins by BLASTp score (Wickstead and Gull, 2007), with support from phylogenetic inference where necessary, as outlined in Materials and Methods.

To validate our approach, we searched for three proteins (γ-tubulin, EB1/Bim1p and XMAP215/ch-TOG) involved in microtubule dynamics that are expected to be widely present among the eukaryotes. As expected, γ-tubulin was found in all organisms analysed. Importantly, we were not only able to identify tubulin homologues, but could also unambiguously distinguish γ-tubulin from paralogous sequences (supplementary material Fig. S1). The approach also performed well in identifying EB1 and XMAP215 orthologues; the lack of EB1 in *Leishmania major* has been noted before (Berriman et al., 2005) and, as in a previous study, we were able to validate the lack of XMAP215 using an iterative hidden Markov model (HMM)-based approach (Devaux et al., 2007). These data indicate that our approach can identify homologous sequences in multiple organisms and can also differentiate paralogous families.

Phylogenetic distribution of δ- and ε-tubulin

It has been demonstrated that δ- and ε-tubulin have a crucial centriolar role in *Chlamydomonas*, trypanosomes, humans and *Paramecium* (Chang and Stearns, 2000; Dupuis-Williams et al., 2002; Dutcher and Trabuco, 1998; Gadelha et al., 2006). These proteins are absent from non-ciliated species and also from *Drosophila melanogaster* and *C. elegans* (Chang and Stearns, 2000), both of which have cilia but build unusual centrioles (see below). Using our approach, we were able to unambiguously identify δ-tubulin and ε-tubulin homologues in 25 and 26 of the 29 ciliated species, respectively. As predicted, we did not detect homologues in any non-ciliated species included in the analysis (Fig. 1). Consistent with previous findings (Chang and Stearns, 2000), no homologues of either centriolar tubulin were found in *D. melanogaster* or *C. elegans* (see Delattre and Gonczy, 2004). *D. melanogaster* builds centrioles based on either doublet or triplet microtubules (depending on the cell type) (Callaini et al., 1997), whereas *C. elegans* centrioles are composed of singlet microtubules and lack the 'cartwheel' structure found at the proximal end of most centrioles (Perkins et al., 1986). Interestingly, the lack of both δ- and ε-tubulin genes in the *D. melanogaster* genome is a feature shared by two other dipteran genera – *Glossina*

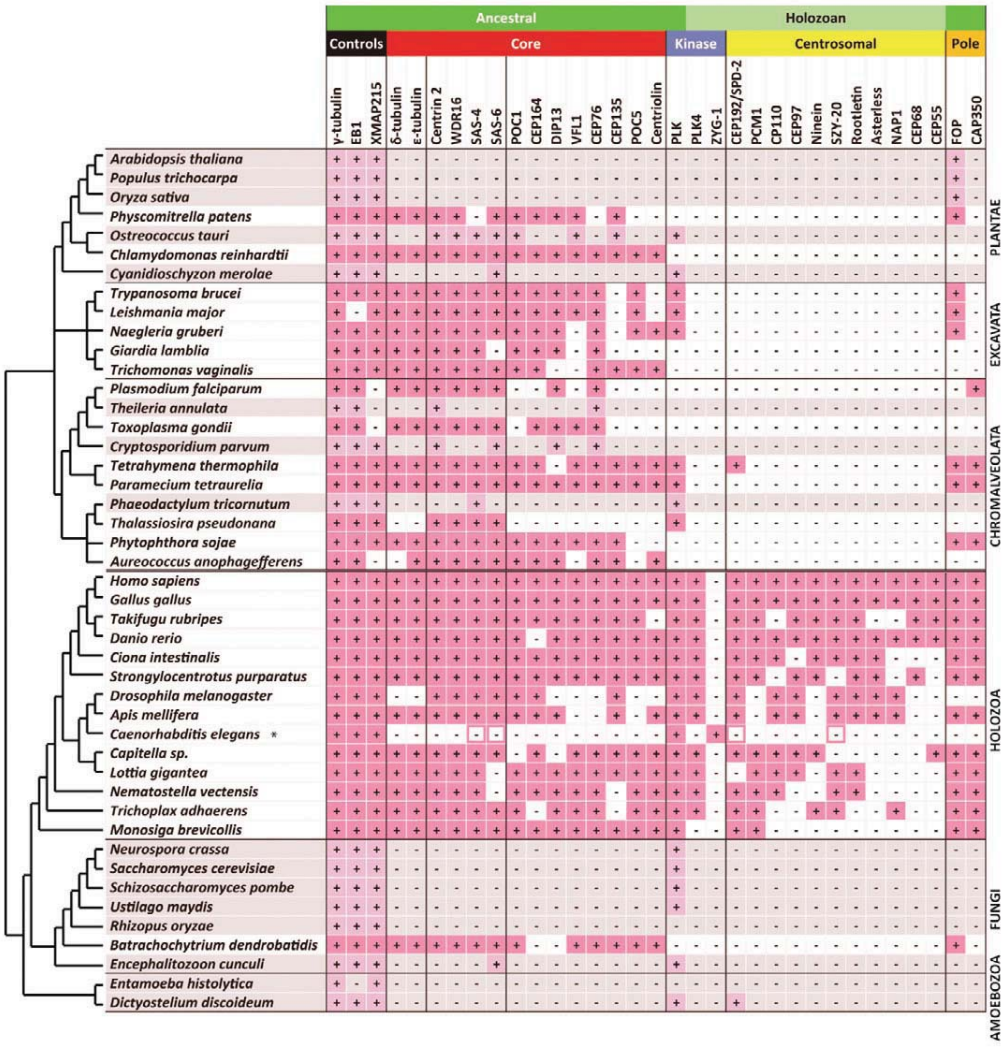

Fig. 1. Distribution of centriolar and centrosomal proteins among eukaryotes. Protein homologues were identified in 45 eukaryotic genomes, including 29 ciliated species and 16 non-ciliated species (grey). The presence of homologue(s) is indicated by a plus symbol (+). 'Core' proteins are conserved ancestral centriolar proteins. 'Centrosomal' proteins are associated with centrosomal functions. 'Pole' proteins might have fulfilled a function in the ancestral spindle pole. 'Controls' are proteins that are associated with general microtubule dynamics. 'Ancestral' proteins are present among extant eukaryotes. 'Holozoan' proteins have a restricted presence in Holozoa (Metazoa and *M. brevicollis*). The asterisk indicates sequence drift of core and centrosomal proteins in *C. elegans*; divergent homologues known in the literature but not identified by our approach are highlighted with a pink border.

and *Anopheles* – and also by the silkworm *Bombyx mori*. By contrast, the honeybee *Apis mellifera* (Fig. 1) and flour beetle *Tribolium castaneum* genomes contain both tubulins. These observations suggest that the loss of these tubulin forms is a specific feature of the Panorpoida (including Diptera and Lepidoptera), as opposed to being common to all insects. The distribution pattern of δ- and ε-tubulin is suggestive of a distinct functional module – in that the two proteins are almost always either absent from or present in a given organism. The presence of ε-tubulin but no identifiable δ-tubulin in the stramenopile alga *Aureococcus anophagefferens* might be an artefact of the incomplete status of the available genome sequence. However, along with *C. elegans* and Panorpoida, no evidence of either δ- or ε-tubulin was found in the ciliated diatom *Thalassiosira pseudonana*. The precise ultrastructure of the basal bodies formed in this species is unclear; however, other centric diatoms are known to produce basal bodies with only doublet microtubules (Jensen et al., 2003). These observations emphasise the association of δ- and ε-tubulin paralogues with a canonical triplet microtubule pathway for the formation of the centriole, as is seen from functional data on these proteins. However, the lack of δ- and ε-tubulin in dipteran genera shows that pathways for triplet formation have also evolved that are independent of these tubulins.

Ancestral centriolar core components

The ninefold triplet microtubule arrangement of centrioles is widely conserved among eukaryotes (for a review, see Beisson and Wright, 2003). However, it is not clear to what extent this ultrastructural consistency reflects the conservation of underlying molecular components. To investigate this question, we analysed the phylogenetic distribution of known centriolar proteins in our data set. This analysis identified a set of 14 proteins with proven centriolar localisation that are present in at least four major eukaryotic groups (Fig. 1). Given the current understanding of eukaryotic evolution, the most likely explanation for this pattern is that these 14 centriolar proteins were present in the ancestor of all extant eukaryotes (the cenancestor) and that this core set performs a widely conserved function. However, no single component of the set is ubiquitously conserved in organisms that possess centrioles or basal bodies. Furthermore, extant species vary considerably in which components of the set are present – indicating a surprising plasticity in the protein composition of centrioles.

In our analysis, four proteins (centrin 2, WDR16, SAS-4 and SAS-6) were found to be more consistently associated with ciliated species than ε-tubulin (Fig. 1). SAS-4 has been proposed to be involved in the attachment of microtubules to the central centriolar cylinder (Pelletier et al., 2006) and in the elongation of centriolar microtubules (Kohlmaier et al., 2009; Schmidt et al., 2009; Tang et al., 2009); SAS-6 has been implicated in cartwheel formation (Kilburn et al., 2007; Nakazawa et al., 2007; Rodrigues-Martins et al., 2007). Centrin 2 is a well-characterised centriolar component that is essential for centriole duplication (Geimer and Melkonian, 2005; Koblenz et al., 2003; Salisbury et al., 2002). Although the wider centrin family is involved in multiple cellular processes and is present in non-ciliated species, there is a clade termed CrCen-type centrin 2, which has a distribution restricted to ciliated species (Bornens and Azimzadeh, 2007). By contrast, WDR16 is a protein of unknown function associated with hydrocephalus in zebrafish (Hirschner et al., 2007). It is localised to the basal body, pro-basal body and, to a lesser extent, the flagellum of trypanosomes (Helen Farr and K.G., unpublished). Based on the observed distribution pattern, it is likely that WDR16 also plays a key role in basal-body and/or centriole function.

Interestingly, although the green alga *Ostreococcus tauri* is thought to be non-flagellate – and the whole-cell reconstruction of the vegetative stage is acentriolar (Henderson et al., 2007) – we found that 7 of the 14 core-set proteins are present in this species (i.e. more than in several organisms that definitively possess centrioles). Similarly, the stramenopile alga *A. anophagefferens* is also non-flagellate and acentriolar in the lifecycle stages thus far analysed (Sieburth et al., 1988), but possesses 11 of the 14 core centriolar proteins. Because of the presence of genes encoding components of intraflagellar transport (Woodland and Fry, 2008) and flagellar apparatus (Elias and Archibald, 2009), it has previously been suggested that *A. anophagefferens* might possess a flagellate stage similar to that seen in at least some other pelagophytes. On the basis of our observations here and the presence of genes encoding inner-arm dyneins (Wickstead and Gull, 2007), we predict that *O. tauri* also forms basal bodies and cilia at some point in its lifecycle – most likely in a yet to be observed gamete or zoospore.

Notably, none of the 14 core centriolar proteins could be identified in the predicted proteome of *C. elegans*. Clearly, comparative analyses cannot distinguish between proteins that have been lost entirely from an organism and those that have diverged in sequence to the extent that they are undetectable. Because SAS-4 and SAS-6 were originally identified in *C. elegans* (Dammermann et al., 2004; Kirkham et al., 2003; Leidel et al., 2005; Leidel and Gonczy, 2003), these two proteins at least are in the latter category. However, the sequences of SAS-4 and SAS-6 have changed more rapidly in *C. elegans* than in other lineages (supplementary material Fig. S2). This suggests that the unusual centrioles of *C. elegans* evolved in concert with extensive loss or divergence of the core centriolar components. Thus, *C. elegans* appears to represent the extremes of centriole divergence, without having lost the structure completely. A similar but less extreme process appears to have occurred in *Thalassiosira pseudonana*, in which we can identify only the four most highly conserved centriolar proteins (centrin 2, WDR16, SAS-4 and SAS-6). Such divergence must be considered when interpreting centriolar phenotypes or using particular organisms for comparative biology.

Centriole-associated kinases: origin and diversification

Kinase activity is crucial for the regulation of centriole duplication. The kinases ZYG-1 in *C. elegans*, SAK in *D. melanogaster* and polo-like kinase 4 (PLK4) in humans are all essential for centriole duplication (Bettencourt-Dias et al., 2005; Habedanck et al., 2005; O'Connell et al., 2001). Catalytically inactive mutants of PLK4 fail to induce centriole biogenesis (Habedanck et al., 2005) and cells in SAK mutant embryos lack centrioles (Bettencourt-Dias et al., 2005). It has been suggested that PLK4, SAK and ZYG-1 are orthologous (Bettencourt-Dias et al., 2005).

To resolve the distribution of and relationships between the centriole-associated kinases, we performed phylogenetic analysis of all PLKs, plus SAK and ZYG-1 homologues (supplementary material Fig. S3). Our phylogenetic inference unambiguously identifies a well-supported PLK clan in the majority of organisms in our analysis. This group includes PLK isoforms 1-4, where they exist. Within the PLK family, PLK4 and SAK form a clear subgroup and are orthologous, as expected. However, we find no evidence to support the grouping of ZYG-1 in the PLK4-SAK clan (supplementary material Fig. S3). Moreover, despite experimental

evidence suggesting that ZYG-1 has an analogous function to PLK4 (Bettencourt-Dias et al., 2005; Habedanck et al., 2005; O'Connell et al., 2001), sequence analysis does not place ZYG-1 within the PLK clan (note that *C. elegans* PLK1 sequences were readily identified). As ZYG-1 cannot be placed in any kinase family, it is unclear whether ZYG-1 is a PLK4 that has undergone rapid divergence or whether it is an entirely different kinase that has replaced PLK4 function. Regardless, the orphan nature of ZYG-1 is a further molecular demonstration of the unusual nature of *C. elegans* centrioles.

The pattern of PLK distribution shows that PLK was present in the cenancestor of eukaryotes, wherein it might have had a function that included initiation of centriole duplication. However, we show that, in common with much of the ancestral centriolar core, PLK has been lost multiple times. We found that neither PLK nor ZYG-1 was detectable in 9 of the 29 analysed ciliated species, suggesting either that centriolar duplication does not require kinase activity in these species or that other kinases fulfil that role.

Basal-body function is ancestral, but centrosomal components are not

In our analysis, we identified proteins that are found only in Holozoa (represented in our analysis by the metazoa and the choanoflagellate *Monosiga brevicollis*; Fig. 1). In general, these proteins are either associated with centrosomal functions or have been localised to the pericentriolar material within the centrosome. This restricted phylogenetic distribution has two alternative explanations: either many of the components of the animal centrosome were acquired only by the ancestor of the Holozoa or centrosomal components, in contrast to those of the basal body, are evolving at sufficient speed to render them undetectable in distantly related organisms. In keeping with the latter proposition, the proteins SPD-2 and SZY-20 – which were originally identified in *C. elegans* (Kemp et al., 2004; Pelletier et al., 2004; Song et al., 2008) – could not be detected in *C. elegans* by our approach when using canonical homologues from other Holozoa. Thus, it appears that the extreme divergence of centriolar proteins in *C. elegans* (see above) occurred concomitantly with the divergence of centrosomal components. However, unlike centriolar components, only 2 of the 13 centrosome-associated proteins analysed (FOP and CAP350) were detectable outside of the Holozoa (Fig. 1). The distribution of these two components does not correlate with organisms in which there is a centriole, which would be expected if these proteins function only in the centrosome. This implies that the animal centrosome is constructed from mainly holozoan-specific components.

The evolutionary relationship between the centriole and centrosomal material (with functions in the organisation of both cytoplasmic and spindle microtubules) is not as clear as might at first sight appear. One possibility is that a proto-centrosome with a role in microtubule organisation existed in an ancestral cell that also possessed separate basal bodies subtending cilia. Basal bodies became centrioles when they began 'piggy-backing' onto this proto-centrosome as a means of ensuring fidelity in the inheritance of cilia (Pickett-Heaps, 1971) (see also Beisson and Wright, 2003; Bornens and Azimzadeh, 2007). Alternatively, centrioles with a function in cell-cycle control were present before centrosomes and material associated with microtubule organisation, which can now be found in the centrosome, was accrued gradually by these stably inherited centrioles. Importantly, if the centrosome as an organelle already existed in the last common ancestor of eukaryotes, then all centrosomes are homologous. Conversely, if different material has been accumulated by centrioles in different lineages, then these structures are non-homologous. With the caveat noted above regarding rates of divergence, our finding that much of the animal centrosome is specific to Holozoa supports the latter evolutionary scenario and suggests that the animal centrosome is a holozoan innovation. This would imply that association of centrioles with spindle poles has arisen independently in more than one lineage (minimally, in the 'unikonts' and Chlorophyta) (Coss, 1974).

A sensory role for the ancestral cilium

Defects in centrioles and cilia cause a variety of human disorders, collectively known as ciliopathies (for a review, see Badano et al., 2006). To assess whether proteins associated with ciliopathies are conserved among eukaryotes, we investigated their phylogenetic distribution. The ciliopathy Bardet-Biedl syndrome (BBS) is linked to mutations in *BBS1* to *14* (see Jin and Nachury, 2009); BBS proteins 1, 2, 4, 5, 7, 8 and 9 act as a biochemical complex termed the 'BBSome' (Nachury et al., 2007). The BBSome complex is conserved in a modular fashion in that the seven proteins are generally present or absent as a group (Fig. 2) with BBS5 and BBS8 being the most widely conserved. On the basis of the phylogenetic distribution of this group, we propose that the cenancestor of eukaryotes possessed a BBSome.

The BBSome is proposed to play a role in transporting membrane proteins to sensory primary cilia, as opposed to motile cilia [for a review of primary cilia, see Singla and Reiter (Singla and Reiter, 2006)]. This proposal is supported by the fact that the complex is conserved in *C. elegans*, an organism that builds only immotile sensory primary cilia. The absence of the BBSome in four species that produce only motile cilia in gametes or zoospores – namely *Physcomitrella patens*, *Plasmodium falciparum*, *Thalassiosira pseudonana* and *Batrachochytrium dendrobatidis* (E. V. Armbrust, The life cycle of the centric diatom *Thalassiosira weissflogii*: control of gametogenesis and cell size. PhD Thesis, *Woods Hole Oceanographic Institution Massachusetts Institute of Technology*, 1990) (Berger et al., 2005; Merchant et al., 2007; Sinden et al., 1978) – further supports the role of the BBSome in sensory function and its dispensability for motility. In combination, these observations provide molecular evidence that the cenancestral cilium served a sensory function.

Another important ciliopathy, Meckel-Gruber syndrome (MKS), is characterised by mutations in *MKS1*, *3*, *4*, *5* and *6* (see Badano et al., 2006). Our data demonstrate that, as with the BBSome, MKS proteins were in the cenancestor of eukaryotes and their extant distribution correlates with the possession of cilia. However, BBSome and MKS proteins have distinct, albeit overlapping, phylogenetic distribution patterns (for example, *B. dendrobatidis* and *T. pseudonana* contain MKS but not BBS proteins). This observation suggests that these two ciliopathy-associated modules can function independently.

Correlation between ciliary eye evolution and ciliopathy-associated proteins

Many patients presenting with ciliopathies manifest the eye disease retinitis pigmentosa, because human eye development depends on ciliary function in photoreceptor cells. Animal photoreceptor cells can be classified as either rhabdomeric or ciliary, depending on how the membranes for photopigment storage are extended. In rhabdomeric photoreceptor cells, extension is achieved through

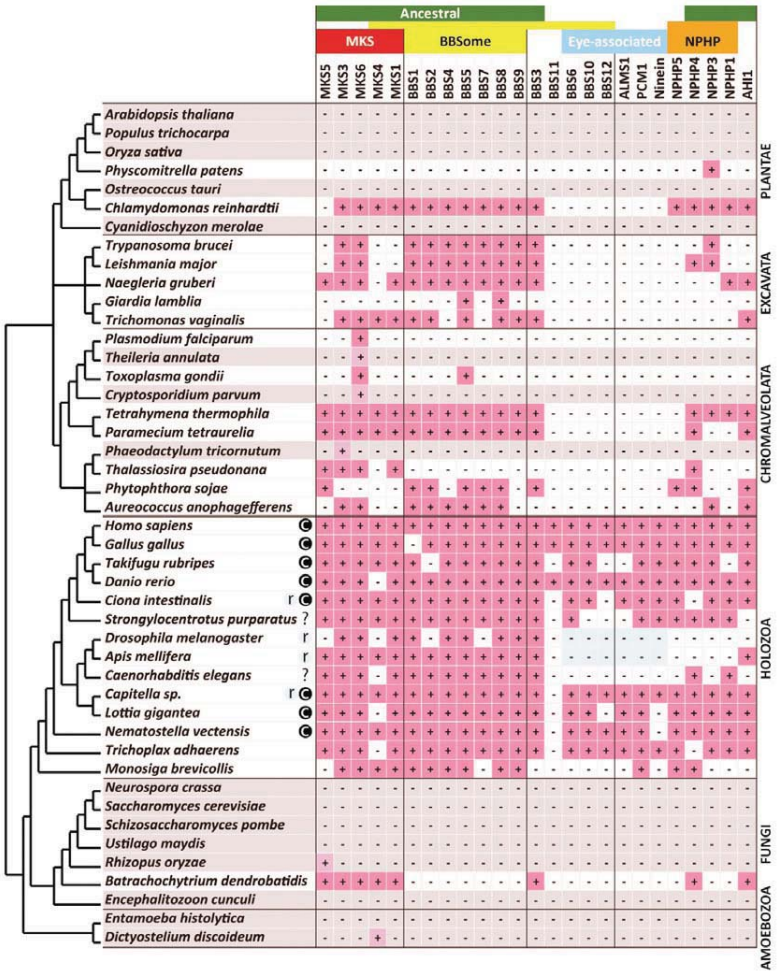

Fig. 2. Distribution of ciliopathy-associated proteins among eukaryotes. Protein homologues were identified in 45 eukaryotic genomes, including 29 ciliated species and 16 non-ciliated species (grey). The presence of homologue(s) is indicated by a plus symbol (+). The proteins are grouped according to the ciliopathy (MKS, BBS and NPHP) or/and ciliary photoreceptor association. 'Eye-associated' proteins show a distribution that correlates with ciliary 'c' photoreceptors. The light blue shade indicates the exclusive presence of rhabdomeric 'r' photoreceptors.

folding of the apical cell surface into actin-based microvilli, whereas in ciliary photoreceptor cells the ciliary membrane is folded (for reviews, see Arendt, 2003; Eakin, 1982). The ancestral proto-photoreceptor cell probably used the ciliary mechanism and possessed ciliary-specific opsins (for a review, see Shubin et al., 2009). It has been hypothesised that the last common ancestor of the Bilateria (animals excluding *Nematostella vectensis* and *Trichoplax adherens* in our analysis) had additionally acquired rhabdomeric photoreceptor cells and that loss of one or the other system has occurred in different lineages (see Arendt and Wittbrodt, 2001). Structural studies have shown that insects employ only rhabdomeric photoreceptor cells, whereas vertebrates and *Lottia gigantean* use only the ciliary system (Purschke et al., 2006). Both systems are still present in *Capitella* and *Ciona* (Purschke et al., 2006; Dilly, 1969). The phylogenetic distribution of rhabdomeric- and ciliary-specific opsins correlates with this structural analysis (Arendt et al., 2004). Proteins involved in ciliary photoreceptor development are therefore expected to have a specific pattern in our analysis: present in vertebrates, *C. intesinalis*, *S. purparatus*, *Capitella*, *L. gigantea*, *N. vectensis* and *T. adherens*, but absent in *D. melanogaster* and *Apis mellifera*.

Four out of twenty-three ciliopathy-associated proteins in our analysis – BBS6, BBS10, BBS12 and ALMS-1 (Fig. 2) – have a profile predictive of involvement in ciliary photoreceptor cells. In contrast to the BBSome, BBS6, BBS10 and BBS12 are predicted to be chaperonin-like proteins (Stoetzel et al., 2007) and none of the four are ancestral. Alongside these proteins, PCM1 and ninein also share the ciliary photoreceptor fingerprint. Interestingly, PCM1 is already functionally linked to ciliogenesis, because it interacts with BBS4 (Nachury et al., 2007). Our findings now predict an additional association between ninein and the eye. Nephronophthisis (NPHP) proteins 1, 3, 4 and 5 similarly display a paraphyletic profile for eye association in Metazoa, but these four proteins are also found outside this lineage, suggesting a more general function. The absence of any of these eye-associated proteins in the *C. elegans* genome also correlates with a lack of ciliary opsins (Satoh, 2006) and provides strong genomic data supporting the prediction that the photoreceptor spots in this species have a rhabdomeric-like structure (McLaren, 1976).

Conclusions

Our analyses provide molecular evidence to suggest that the cenancestor of eukaryotes possessed a centriole that had basal-body function, but no association with the centrosome. Moreover, this cenancestor also possessed the BBSome complex and hence was using flagella and cilia for both motility and sensory functions. The ancestral centriolar structure contained a cohort of proteins that are still present in the centrioles of most extant ciliated eukaryotes. Interestingly, the morphology of the centriole is surprisingly insensitive to multiple losses from this cohort, in that

gross changes in the ultrastructure of the centriole occur only when the majority of the cohort is lost or highly divergent, as demonstrated in the unusual centrioles of *C. elegans*. Similarly, kinases that are essential for the initiation of centriole assembly in some organisms are not ubiquitously conserved. Finally, in light of the evolutionary footprint of ciliary photoreceptor cells, we identify six proteins that we predict to function in ciliary eye cell development, but not in the eyes of insects. Collectively, these data provide a more coherent picture of the evolution of centriolar proteins.

Materials and Methods

Definition of data sets

An initial set of 53 proteins was selected on the basis of fulfilling one of two criteria: known localisation to the centriole or basal body and/or centrosome; or genetic evidence of involvement in cilia-associated pathologies. The sequences of three proteins involved in microtubule dynamics that are predicted to be widely distributed among eukaryotes – γ-tubulin, XMAP215/ch-TOG and EB1/Bim1p – were also included as controls. In all cases, query sequences were human homologues of the proteins, with the exception of *C. elegans* ZYG-1 (see Results and Discussion). A complete list of these proteins, with references, is given in supplementary material Table S2. These protein sequences were used to query the predicted proteomes of 45 eukaryotic organisms for which a complete or near-complete genome sequence is publicly available. These organisms were chosen to represent a wide evolutionary spread of extant eukaryotes with diverse microtubule biology. A list of genomic data set sources and versions used is provided in supplementary material Table S1.

Identification of homologous sets

During initial work, we found that reciprocal best BLAST approaches were generally too conservative when identifying orthologues, whereas simple BLAST searches (Altschul et al., 1990) were too noisy and unable to discriminate among paralogues. To overcome these problems, we used an approach based on clustering of proteins by BLASTp score (Wickstead and Gull, 2007). Briefly, a 'seed' set was generated for each query from a reciprocal best BLASTp search with an e-value threshold of $<10^{-5}$. A liberal set of putative homologues was then generated on the basis of all BLASTp hits to any seed sequence with an e-value $<10^{-2}$. Results from this search were then formed into clusters using a distance matrix derived from BLASTp scores, as described in (Wickstead and Gull, 2007), with the orthologous cluster being defined by eye (supplementary material Table S3). In the case of ambiguous clustering, sets were aligned, trimmed and then used in Bayesian and maximum likelihood phylogenetic inference (Guindon and Gascuel, 2003; Ronquist and Huelsenbeck, 2003). Parameters used during tree inference are given in the legends accompanying the respective figures.

Thanks to Monica Bettencourt-Dias (Instituto Gulbenkian de Ciência, Portugal) for useful discussions and sharing of prepublication data. We thank Helen Farr for communicating results on WDR16 before publication. We are grateful to Steven Kelly and Neil Portman for critical reading of the manuscript, and to Helen Dawe for information on ciliopathies. This work was funded by grants from the Wellcome Trust to K.G. and the Gatsby Charitable foundation to J.A.L. N.S. and M.E.H. are supported by graduate studentships from the EPA Trust and BBSRC, respectively. K.G. is a Wellcome Trust Principal Research Fellow. Deposited in PMC for release after 6 months.

Supplementary material available online at
http://jcs.biologists.org/cgi/content/full/123/9/1407/DC1

References

Altschul, S. F., Gish, W., Miller, W., Myers, E. W. and Lipman, D. J. (1990). Basic local alignment search tool. *J. Mol. Biol.* **215**, 403-410.

Arendt, D. (2003). Evolution of eyes and photoreceptor cell types. *Int. J. Dev. Biol.* **47**, 563-571.

Arendt, D. and Wittbrodt, J. (2001). Reconstructing the eyes of Urbilateria. *Philos. Trans. R. Soc. Lond. B. Biol. Sci.* **356**, 1545-1563.

Arendt, D., Tessmar-Raible, K., Snyman, H., Dorresteijn, A. W. and Wittbrodt, J. (2004). Ciliary photoreceptors with a vertebrate-type opsin in an invertebrate brain. *Science* **306**, 869-871.

Badano, J. L., Mitsuma, N., Beales, P. L. and Katsanis, N. (2006). The ciliopathies: an emerging class of human genetic disorders. *Annu. Rev. Genomics Hum. Genet.* **7**, 125-148.

Beisson, J. and Wright, M. (2003). Basal body/centriole assembly and continuity. *Curr. Opin. Cell Biol.* **15**, 96-104.

Berger, L., Hyatt, A. D., Speare, R. and Longcore, J. E. (2005). Life cycle stages of the amphibian chytrid *Batrachochytrium dendrobatidis*. *Dis. Aquat. Organ.* **68**, 51-63.

Berriman, M., Ghedin, E., Hertz-Fowler, C., Blandin, G., Renauld, H., Bartholomeu, D. C., Lennard, N. J., Caler, E., Hamlin, N. E., Haas, B. et al. (2005). The genome of the African trypanosome *Trypanosoma brucei*. *Science* **309**, 416-422.

Bettencourt-Dias, M., Rodrigues-Martins, A., Carpenter, L., Riparbelli, M., Lehmann, L., Gatt, M. K., Carmo, N., Balloux, F., Callaini, G. and Glover, D. M. (2005). SAK/PLK4 is required for centriole duplication and flagella development. *Curr. Biol.* **15**, 2199-2207.

Bornens, M. and Azimzadeh, J. (2007). Origin and evolution of the centrosome. In *Eukaryotic Membranes and Cytoskeleton: Origins and Evolution* (ed. G. Jékely), pp. 119-129. Austin, TX: Landes Bioscience.

Callaini, G., Whitfield, W. G. and Riparbelli, M. G. (1997). Centriole and centrosome dynamics during the embryonic cell cycles that follow the formation of the cellular blastoderm in *Drosophila*. *Exp. Cell Res.* **234**, 183-190.

Chang, P. and Stearns, T. (2000). Delta-tubulin and epsilon-tubulin: two new human centrosomal tubulins reveal new aspects of centrosome structure and function. *Nat. Cell Biol.* **2**, 30-35.

Coss, R. A. (1974). Mitosis in *Chlamydomonas reinhardtii* basal bodies and mitotic apparatus. *J. Cell Biol.* **63**, 325-329.

Dammermann, A., Muller-Reichert, T., Pelletier, L., Habermann, B., Desai, A. and Oegema, K. (2004). Centriole assembly requires both centriolar and pericentriolar material proteins. *Dev. Cell* **7**, 815-829.

Dawe, H. R., Farr, H. and Gull, K. (2007). Centriole/basal body morphogenesis and migration during ciliogenesis in animal cells. *J. Cell Sci.* **120**, 7-15.

Delattre, M. and Gonczy, P. (2004). The arithmetic of centrosome biogenesis. *J. Cell Sci.* **117**, 1619-1630.

Devaux, S., Kelly, S., Lecordier, L., Wickstead, B., Perez-Morga, D., Pays, E., Vanhamme, L. and Gull, K. (2007). Diversification of function by different isoforms of conventionally shared RNA polymerase subunits. *Mol. Biol. Cell* **18**, 1293-1301.

Dilly, P. N. (1969). Studies on the receptors in *Ciona intestinalis*. III. A second type of photoreceptor in tadpole larva of *Ciona intestinalis*. *Z. Zellforsch. Mikrosk. Anat.* **96**, 63-65.

Dupuis-Williams, P., Fleury-Aubusson, A., de Loubresse, N. G., Geoffroy, H., Vayssie, L., Galvani, A., Espigat, A. and Rossier, J. (2002). Functional role of epsilon-tubulin in the assembly of the centriolar microtubule scaffold. *J. Cell Biol.* **158**, 1183-1193.

Dutcher, S. K. and Trabuco, E. C. (1998). The *UNI3* gene is required for assembly of basal bodies of *Chlamydomonas* and encodes delta-tubulin, a new member of the tubulin superfamily. *Mol. Biol. Cell* **9**, 1293-1308.

Eakin, R. M. (1982). Morphology of invertebrate photoreceptors. *Methods Enzymol.* **81**, 17-25.

Elias, M. and Archibald, J. M. (2009). The RJL family of small GTPases is an ancient eukaryotic invention probably functionally associated with the flagellar apparatus. *Gene* **442**, 63-72.

Gadelha, C., Wickstead, B., McKean, P. G. and Gull, K. (2006). Basal body and flagellum mutants reveal a rotational constraint of the central pair microtubules in the axonemes of trypanosomes. *J. Cell Sci.* **119**, 2405-2413.

Geimer, S. and Melkonian, M. (2005). Centrin scaffold in *Chlamydomonas reinhardtii* revealed by immunoelectron microscopy. *Eukaryotic Cell* **4**, 1253-1263.

Guindon, S. and Gascuel, O. (2003). A simple, fast, and accurate algorithm to estimate large phylogenies by maximum likelihood. *Syst. Biol.* **52**, 696-704.

Habedanck, R., Stierhof, Y. D., Wilkinson, C. J. and Nigg, E. A. (2005). The Polo kinase Plk4 functions in centriole duplication. *Nat. Cell Biol.* **7**, 1140-1146.

Henderson, G. P., Gan, L. and Jensen, G. J. (2007). 3-D ultrastructure of *O. tauri*: electron cryotomography of an entire eukaryotic cell. *PLoS ONE* **2**, e749.

Hirschner, W., Pogoda, H. M., Kramer, C., Thiess, U., Hamprecht, B., Wiesmuller, K. H., Lautner, M. and Verleysdonk, S. (2007). Biosynthesis of Wdr16, a marker protein for kinocilia-bearing cells, starts at the time of kinocilia formation in rat, and wdr16 gene knockdown causes hydrocephalus in zebrafish. *J. Neurochem.* **101**, 274-288.

Jensen, K. G., Moestrup, O. and Schmid, A. M. M. (2003). Ultrastructure of the male gametes from two centric diatoms, *Chaetoceros laciniosus* and *Coscinodiscus wailesii* (*Bacillariophyceae*). *Phycologia* **42**, 98-105.

Jin, H. and Nachury, M. V. (2009). The BBSome. *Curr. Biol.* **19**, R472-R473.

Kemp, C. A., Kopish, K. R., Zipperlen, P., Ahringer, J. and O'Connell, K. F. (2004). Centrosome maturation and duplication in *C. elegans* require the coiled-coil protein SPD-2. *Dev. Cell* **6**, 511-523.

Kilburn, C. L., Pearson, C. G., Romijn, E. P., Meehl, J. B., Giddings, T. H., Jr, Culver, B. P., Yates, J. R., 3rd and Winey, M. (2007). New *Tetrahymena* basal body protein components identify basal body domain structure. *J. Cell Biol.* **178**, 905-912.

Kirkham, M., Muller-Reichert, T., Oegema, K., Grill, S. and Hyman, A. A. (2003). SAS-4 is a *C. elegans* centriolar protein that controls centrosome size. *Cell* **112**, 575-587.

Koblenz, B., Schoppmeier, J., Grunow, A. and Lechtreck, K. F. (2003). Centrin deficiency in Chlamydomonas causes defects in basal body replication, segregation and maturation. *J. Cell Sci.* **116**, 2635-2646.

Kohlmaier, G., Loncarek, J., Meng, X., McEwen, B. F., Mogensen, M. M., Spektor, A., Dynlacht, B. D., Khodjakov, A. and Gonczy, P. (2009). Overly long centrioles and defective cell division upon excess of the SAS-4-related protein CPAP. *Curr. Biol.* **19**, 1012-1018.

Leidel, S. and Gonczy, P. (2003). SAS-4 is essential for centrosome duplication in *C. elegans* and is recruited to daughter centrioles once per cell cycle. *Dev. Cell* **4**, 431-439.

Leidel, S., Delattre, M., Cerutti, L., Baumer, K. and Gonczy, P. (2005). SAS-6 defines a protein family required for centrosome duplication in *C. elegans* and in human cells. *Nat. Cell Biol.* **7**, 115-125.

McLaren, D. J. (1976). Nematode sense organs. *Adv. Parasitol.* **14**, 195-265.
Merchant, S. S., Prochnik, S. E., Vallon, O., Harris, E. H., Karpowicz, S. J., Witman, G. B., Terry, A., Salamov, A., Fritz-Laylin, L. K., Marechal-Drouard, L. et al. (2007). The *Chlamydomonas* genome reveals the evolution of key animal and plant functions. *Science* **318**, 245-250.
Nachury, M. V., Loktev, A. V., Zhang, Q., Westlake, C. J., Peranen, J., Merdes, A., Slusarski, D. C., Scheller, R. H., Bazan, J. F., Sheffield, V. C. et al. (2007). A core complex of BBS proteins cooperates with the GTPase Rab8 to promote ciliary membrane biogenesis. *Cell* **129**, 1201-1213.
Nakazawa, Y., Hiraki, M., Kamiya, R. and Hirono, M. (2007). SAS-6 is a cartwheel protein that establishes the 9-fold symmetry of the centriole. *Curr. Biol.* **17**, 2169-2174.
O'Connell, K. F., Caron, C., Kopish, K. R., Hurd, D. D., Kemphues, K. J., Li, Y. and White, J. G. (2001). The *C. elegans* zyg-1 gene encodes a regulator of centrosome duplication with distinct maternal and paternal roles in the embryo. *Cell* **105**, 547-558.
Pelletier, L., Ozlu, N., Hannak, E., Cowan, C., Habermann, B., Ruer, M., Muller-Reichert, T. and Hyman, A. A. (2004). The *Caenorhabditis elegans* centrosomal protein SPD-2 is required for both pericentriolar material recruitment and centriole duplication. *Curr. Biol.* **14**, 863-873.
Pelletier, L., O'Toole, E., Schwager, A., Hyman, A. A. and Muller-Reichert, T. (2006). Centriole assembly in *Caenorhabditis elegans*. *Nature* **444**, 619-623.
Perkins, L. A., Hedgecock, E. M., Thomson, J. N. and Culotti, J. G. (1986). Mutant sensory cilia in the nematode *Caenorhabditis elegans*. *Dev. Biol.* **117**, 456-487.
Pickett-Heaps, J. (1971). Autonomy of the centriole-fact or fallacy? *Cytobios* **3**, 205.
Purschke, G., Arendt, D., Hausen, H. and Muller, M. C. (2006). Photoreceptor cells and eyes in *Annelida*. *Arthropod. Struct. Dev.* **35**, 211-230.
Rodrigues-Martins, A., Bettencourt-Dias, M., Riparbelli, M., Ferreira, C., Ferreira, I., Callaini, G. and Glover, D. M. (2007). DSAS-6 organizes a tube-like centriole precursor, and its absence suggests modularity in centriole assembly. *Curr. Biol.* **17**, 1465-1472.
Ronquist, F. and Huelsenbeck, J. P. (2003). MrBayes **3**, Bayesian phylogenetic inference under mixed models. *Bioinformatics* **19**, 1572-1574.
Salisbury, J. L., Suino, K. M., Busby, R. and Springett, M. (2002). Centrin-2 is required for centriole duplication in mammalian cells. *Curr. Biol.* **12**, 1287-1292.
Satoh, G. (2006). Exploring developmental, functional, and evolutionary aspects of amphioxus sensory cells. *Int. J. Biol. Sci.* **2**, 142-148.
Schmidt, T. I., Kleylein-Sohn, J., Westendorf, J., Le Clech, M., Lavoie, S. B., Stierhof, Y. D. and Nigg, E. A. (2009). Control of centriole length by CPAP and CP110. *Curr. Biol.* **19**, 1005-1011.
Shubin, N., Tabin, C. and Carroll, S. (2009). Deep homology and the origins of evolutionary novelty. *Nature* **457**, 818-823.
Sieburth, J. M., Johnson, P. W. and Hargraves, P. E. (1988). Ultrastructure and ecology of *Aureococcus Anophagefferens* Gen-Et-Sp-Nov (*Chrysophyceae*) – the dominant picoplankter during a bloom in Narragansett Bay, Rhode-Island, Summer 1985. *J. Phycol.* **24**, 416-425.
Sinden, R. E., Canning, E. U., Bray, R. S. and Smalley, M. E. (1978). Gametocyte and gamete development in *Plasmodium falciparum*. *Proc. R. Soc. Lond. B. Biol. Sci.* **201**, 375-399.
Singla, V. and Reiter, J. F. (2006). The primary cilium as the cell's antenna: signaling at a sensory organelle. *Science* **313**, 629-633.
Song, M. H., Aravind, L., Muller-Reichert, T. and O'Connell, K. F. (2008). The conserved protein SZY-20 opposes the Plk4-related kinase ZYG-1 to limit centrosome size. *Dev. Cell* **15**, 901-912.
Stoetzel, C., Muller, J., Laurier, V., Davis, E. E., Zaghloul, N. A., Vicaire, S., Jacquelin, C., Plewniak, F., Leitch, C. C., Sarda, P. et al. (2007). Identification of a novel BBS gene (BBS12) highlights the major role of a vertebrate-specific branch of chaperonin-related proteins in Bardet-Biedl syndrome. *Am. J. Hum. Genet.* **80**, 1-11.
Tang, C. J., Fu, R. H., Wu, K. S., Hsu, W. B. and Tang, T. K. (2009). CPAP is a cell-cycle regulated protein that controls centriole length. *Nat. Cell Biol.* **11**, 825-831.
Wickstead, B. and Gull, K. (2007). Dyneins across eukaryotes: a comparative genomic analysis. *Traffic* **8**, 1708-1721.
Woodland, H. R. and Fry, A. M. (2008). Pix proteins and the evolution of centrioles. *PLoS ONE* **3**, e3778.

Journal of Cell Science

	ALMS1	AHI1	Asterless	BBS10	BBS11
Apis mellifera		GB12459-PA	GB11327-PA		
Arabidopsis thaliana					
Aureococcus anophagefferens		72559			
Batrachochytrium dendrobatidis		BDEG_04818			
Caenorhabditis elegans					
Capitella sp	229158	228034		193805	
Chlamydomonas reinhardtii v3.1		170267			
Chlamydomonas reinhardtii v2		178044			
Ciona intestinalis	ENSCINP00000013951 XP_002127193.1 ENSCINP00000021711	ENSCINP00000022494 ENSCINP00000022496 ENSCINP00000022495	XP_002122978.1 ENSCINP00000013334	XP_002125019.1	
Cryptosporidium parvum					
Cyanidioschyzon merolae					
Danio rerio	XP_690375.3 OTTDARP00000008743	NP_0010710291	XP_694227.3	NP_001082932.1 OTTDARP00000015588	NP_001107066.1
Dictyostelium discoideum					
Drosophila melanogaster			FBpp0078392		
Encephalitozoon cuniculi					
Entamoeba histolytica					
Gallus gallus	ENSGALP00000036306 ENSGALP00000036307 ENSGALP00000036308 XP_420887.2 ENSGALP00000025867 ENSGALP00000025793 XP_421818.2 ENSGALP00000015835	ENSGALP00000022567	XP_413819.2	ENSGALP00000016626 ENSGALP00000037679 XP_416107.2	ENSGALP00000011407
Giardia lamblia					
Homo sapiens	NP_055935.4 OTTHUMP00000070393 OTTHUMP00000070394 OTTHUMP00000070395 OTTHUMP00000020732 OTTHUMP00000020729 NP_001004298.2 OTTHUMP00000020731	NP_0011283041 OTTHUMP00000017263 NP_0601213 NP_0011283021 NP_0011283031 OTTHUMP00000017266 OTTHUMP00000017265	NP_055800.2 OTTHUMP00000176101	OTTHUMP00000168556 OTTHUMP00000190861	OTTHUMP00000022764 OTTHUMP00000022763
Leishmania major					
Lottia gigantea	231754	62094		169741	
Monosiga brevicollis					
Naegleria gruberi		73736			
Nematostella vectensis	246718	104652		240131	
Neurospora crassa					
Oryza sativa					
Ostreococcus tauri					

	ALMS1	AHI1	Asterless	BBS10	BBS11
Paramecium tetraurelia		GSPATP00023705001 GSPATP00036655001			
Phaedactylum tricornutum					
Physcomitrella patens					
Phytophthora sojae		143507			
Plasmodium falciparum					
Populus trichocarpa					
Rhizopus oryzae					
Saccharonyces cerevisiae					
Schizosacharomyces pombe					
Strongylocentrotus purparatus			GLEAN3_21838		
Takifugu rubripes		ENSTRUP00000035594 ENSTRUP00000020791 ENSTRUP00000020793 ENSTRUP00000020792 ENSTRUP00000020790		ENSTRUP00000003984	
Tetrahymena thermophila		54m00169			
Thalassiosira pseudonana					
Theileria anulata					
Toxoplasma gondii					
Trichoplax adherens	60736	58114		60786	
Trichomonas vaginalis		90380m00189 84684m00034 97465m00145			
Trypanosoma brucei					
Ustilago maydis					

	BBS12	BBS1	BBS2	BBS3	BBS4
Apis mellifera		GB15554-PA	GB16076-PA	GB13103-PA	XP_624286.2 GB15760-PA
Arabidopsis thaliana					
Aureococcus anophagefferens		24826	24976		1883
Batrachochytrium dendrobatidis				BDEG_08460	
Caenorhabditis elegans		CE25181	CE04433	CE00921	CE37774
Capitella sp	205266	108485	171644	143205 97109 202236	94608
Chlamydomonas reinhardtii v3.1		132537	126758 93657	24475	129948
Chlamydomonas reinhardtii v2		152526	159573	171782	
Ciona intestinalis		XP_002125520.1 ENSCINP00000012520	ENSCINP00000025380 ENSCINP00000013276 XP_002124766.1 ENSCINP00000025379	ENSCINP00000006473 ENSCINP00000009643	ENSCINP00000019082 XP_002125730.1
Cryptosporidium parvum					
Cyanidioschyzon merolae					
Danio rerio	XP_699172.3	NP_001091721.1	OTTDARP00000013101	OTTDARP00000019948 NP_001008733.1	XP_001920926.1 NP_001070934.1
Dictyostelium discoideum					
Drosophila melanogaster		FBpp0076621		FBpp0085718	FBpp0087297
Encephalitozoon cuniculi					
Entamoeba histolytica					
Gallus gallus	XP_420621.2 ENSGALP00000019293 ENSGALP00000036988		ENSGALP00000039092 ENSGALP00000004804 NP_001012795.1	XP_001236032.1	XP_413706.2 ENSGALP00000002771
Giardia lamblia					
Homo sapiens	OTTHUMP00000164085 OTTHUMP00000196371	OTTHUMP00000064293 OTTHUMP00000041483 OTTHUMP00000064288 OTTHUMP00000041484 OTTHUMP00000064289 OTTHUMP00000064284 OTTHUMP00000064292 OTTHUMP00000064291 OTTHUMP00000064285 OTTHUMP00000064290	OTTHUMP00000108453 OTTHUMP00000080176 OTTHUMP00000083205 OTTHUMP00000041825 OTTHUMP00000041826	OTTHUMP00000171958 OTTHUMP00000171957 OTTHUMP00000171956 OTTHUMP00000171960	OTTHUMP00000175949 OTTHUMP00000164777
Leishmania major		LmjF35.4180	LmjF30.0590	LmjF16.1380	LmjF36.2280
Lottia gigantea		115648	214128	204362	53377
Monosiga brevicollis		24309	22806		23427
Naegleria gruberi		65179	71257	44202 62886	28891
Nematostella vectensis	241874	186039	235159	216064	40410
Neurospora crassa					
Oryza sativa					
Ostreococcus tauri					

	BBS12	BBS1	BBS2	BBS3	BBS4
Paramecium tetraurelia		GSPATP00033252001	GSPATP00000964001	GSPATP00038302001 GSPATP00017502001	GSPATP00005292001
Phaedactylum tricornutum					
Physcomitrella patens					
Phytophthora sojae		136833	134838	109614	
Plasmodium falciparum					
Populus trichocarpa					
Rhizopus oryzae					
Saccharonyces cerevisiae					
Schizosacharomyces pombe					
Strongylocentrotus purparatus		GLEAN3_11446 XP_783764.2 XP_001176024.1	XP_001176955.1 XP_001176601.1 GLEAN3_00964 GLEAN3_06082 XP_001202157.1 XP_001187752.1 GLEAN3_27384	GLEAN3_17987 XP_796160.2 XP_001196617.1	GLEAN3_18697 XP_001202895.1 XP_786510.2
Takifugu rubripes		ENSTRUP00000010503 ENSTRUP00000010504		ENSTRUP00000008721 ENSTRUP00000008719 ENSTRUP00000008720 ENSTRUP00000044163 ENSTRUP00000044162	ENSTRUP00000042271 ENSTRUP00000042267 ENSTRUP00000042268 ENSTRUP00000042269 ENSTRUP00000042270
Tetrahymena thermophila		225.m00041	54.m00294	69.m00210	214.m00049
Thalassiosira pseudonana					
Theileria anulata					
Toxoplasma gondii					
Trichoplax adherens	54075	26650	29585	25605	18483
Trichomonas vaginalis		97190.m00036	93171.m00065	85228.m00099 89416.m00092 95645.m00121	
Trypanosoma brucei		Tb09.211.2080	Tb927.6.2020	Tb927.8.5060	Tb10.6k15.3940
Ustilago maydis					

	BBS5	BBS6	BBS7	BBS8	BBS9
Apis mellifera	GB17090-PA		GB18131-PA XP_395119.2	XP_001123116.1 GB10554-PA	GB12962-PA
Arabidopsis thaliana					
Aureococcus anophagefferens	72072		22539	54838 72299	
Batrachochytrium dendrobatidis					
Caenorhabditis elegans	CE01042		CE23024	CE31071	CE32166
Capitella sp	176376	214066	117810	163723	155802
Chlamydomonas reinhardtii v3.1	182299		190054	140113	101137
Chlamydomonas reinhardtii v2	161738		154949	171797	154402
Ciona intestinalis	ENSCINP00000005850 XP_002124803.1	XP_002129925.1	ENSCINP00000026073 ENSCINP00000008442 XP_002127808.1 ENSCINP00000008441	XP_002123464.1 ENSCINP00000019928 XP_002123334.1 XP_002123270.1 ENSCINP00000019927	XP_002125247.1
Cryptosporidium parvum					
Cyanidioschyzon merolae					
Danio rerio	NP_956593.1	NP_956459.1	NP_001070613.1	NP_001035399.1	XP_001921482.1
Dictyostelium discoideum					
Drosophila melanogaster	FBpp0078512			FBpp0077718	NP_611580.1
Encephalitozoon cuniculi					
Entamoeba histolytica					
Gallus gallus	ENSGALP00000015990	ENSGALP00000014647	ENSGALP00000019359	ENSGALP00000017328 XP_421311.1	XP_418843.2 ENSGALP00000019874 ENSGALP00000019873
Giardia lamblia	GL50803_8146			GL50803_8508	
Homo sapiens	OTTHUMP00000163062	OTTHUMP00000162353 OTTHUMP00000030274	OTTHUMP00000164091 NP_060660.2	NP_938052.1 OTTHUMP00000028245 NP_938051.1 NP_653197.2	NP_001028777.1 NP_940820.1 NP_001028776.1 OTTHUMP00000158833 OTTHUMP00000024560
Leishmania major	LmjF12.0680		LmjF29.0710	LmjF09.0440	LmjF32.1240
Lottia gigantea	207456	145572	223884	161371	222053 176459
Monosiga brevicollis	32801			32314	33174
Naegleria gruberi	34252		68114	80979	80972
Nematostella vectensis	164107	50325	148193 103100	159317 83222	10499 144317
Neurospora crassa					
Oryza sativa					
Ostreococcus tauri					

	BBS5	BBS6	BBS7	BBS8	BBS9
Paramecium tetraurelia	GSPATP00036912001 GSPATP00034169001		GSPATP00026091001	GSPATP00028481001	GSPATP00027545001
Phaedactylum tricornutum					
Physcomitrella patens					
Phytophthora sojae	109500		108146	109079	
Plasmodium falciparum					
Populus trichocarpa					
Rhizopus oryzae					
Saccharonyces cerevisiae					
Schizosacharomyces pombe					
Strongylocentrotus purparatus	GLEAN3_18028 GLEAN3_22767 XP_792212.1 XP_001202535.1	GLEAN3_24419 XP_786835.1 XP_001193589.1	XP_001203356.1 XP_001188908.1 GLEAN3_14001 XP_798575.2 XP_001191665.1 GLEAN3_05312 GLEAN3_23783 XP_790931.2 XP_001191706.1	XP_001198570.1 XP_001199780.1 GLEAN3_12560	GLEAN3_00493 XP_001190229.1 XP_001194456.1 XP_001201657.1 XP_793825.2
Takifugu rubripes	ENSTRUP00000045891	ENSTRUP00000000326 ENSTRUP00000000327	ENSTRUP00000018248	ENSTRUP00000046798 ENSTRUP00000046797 ENSTRUP00000046796	ENSTRUP00000000646 ENSTRUP00000000645
Tetrahymena thermophila	131.m00082		96.m00149	78.m00118	64.m00248
Thalassiosira pseudonana					
Theileria anulata					
Toxoplasma gondii	TGGT1_010150				
Trichoplax adherens	50116	53298	25051	49816	22294
Trichomonas vaginalis	90976.m00058			91962.m00087	89996.m00100
Trypanosoma brucei	Tb927.1.4140		Tb927.3.3640	Tb11.01.4290	Tb11.01.6070
Ustilago maydis					

	CEP135	Centrin	Centriolin	CEP164	CEP192
Apis mellifera	GB19598-PA XP_001121524.1 GB17790-PA	GB10266-PA XP_395906.2	XP_393975.3 GB18995-PA	GB16672-PA	GB11184-PA
Arabidopsis thaliana					
Aureococcus anophagefferens	68641	23303	38639	61427	
Batrachochytrium dendrobatidis	BDEG_01407	BDEG_08567	BDEG_01294		
Caenorhabditis elegans					
Capitella sp	173417	21986	114721 44232	100218	219671 211819
Chlamydomonas reinhardtii v3.1	166062	159554	172483	169222	
Chlamydomonas reinhardtii v2	168432	156177	164264	156609	
Ciona intestinalis	XP_002126689.1 ENSCINP00000021787 XP_002126770.1 ENSCINP00000010605	ENSCINP00000018417	XP_002119245.1 ENSCINP00000017781	XP_002121669.1	ENSCINP00000002349 XP_002122890.1 ENSCINP00000020451
Cryptosporidium parvum		cgd3_1270			
Cyanidioschyzon merolae					
Danio rerio	NP_001070757.1 OTTDARP00000011178	XP_001345066.1 XP_001922913.1	XP_001919236.1		XP_693893.3
Dictyostelium discoideum					DDB0218699
Drosophila melanogaster	FBpp0075391	FBpp0110460 FBpp0080611		FBpp0073951 FBpp0073952	FBpp0075122 FBpp0088671
Encephalitozoon cuniculi					
Entamoeba histolytica					
Gallus gallus	ENSGALP00000027006 XP_416892.2 ENSGALP00000036760 XP_420699.2 ENSGALP00000022332	XP_420280.1 ENSGALP00000012127 XP_420622.2 ENSGALP00000019297	XP_414814.1 ENSGALP00000007847 XP_415403.2 ENSGALP00000038078 ENSGALP00000038077 ENSGALP00000038081 ENSGALP00000038080	XP_417909.2 ENSGALP00000011817	ENSGALP00000022468
Giardia lamblia		GL50803_6744		GL50803_24423	
Homo sapiens	OTTHUMP00000161217 NP_079285.2	OTTHUMP00000071829 OTTHUMP00000162193 OTTHUMP00000026058	OTTHUMP00000022010 OTTHUMP00000158535 OTTHUMP00000022003 OTTHUMP00000022004	NP_055771.4	OTTHUMP00000071748 OTTHUMP00000071750 OTTHUMP00000071749 NP_115518.2 OTTHUMP00000071751
Leishmania major		LmjF07.0710		LmjF17.1140 LmjF28.2390 LmjF12.0510	
Lottia gigantea	213275 67690	218790	136351	105990	
Monosiga brevicollis	39071	19580	26670 37452	13726	11927
Naegleria gruberi		56351	77107	70383	
Nematostella vectensis		106028	91406	128876	225408 246496 219395
Neurospora crassa					
Oryza sativa					
Ostreococcus tauri	30149	28265			

	CEP135	Centrin	Centriolin	CEP164	CEP192
Paramecium tetraurelia	GSPATP00009438001 GSPATP00019908001	GSPATP00030725001 GSPATP00026291001	GSPATP00007697001 GSPATP00022750001	GSPATP00011678001 GSPATP00026805001 GSPATP00033074001 GSPATP00021670001	
Phaedactylum tricornutum					
Physcomitrella patens	69693	128401 87691 233973		232018	
Phytophthora sojae	133301	108216		132583 158245 143662	
Plasmodium falciparum		PFA0345w			
Populus trichocarpa					
Rhizopus oryzae					
Saccharonyces cerevisiae					
Schizosacharomyces pombe					
Strongylocentrotus purparatus	XP_792224.1 XP_001202035.1 XP_781904.2 XP_001189902.1	XP_794321.2 XP_001193391.1 XP_001177362.1 XP_001176455.1	XP_797673.1	XP_784792.2 XP_001189278.1	XP_001202129.1 XP_001187317.1 XP_790994.2 XP_001194286.1 GLEAN3_17452 XP_001181926.1 XP_001189923.1
Takifugu rubripes	ENSTRUP00000039917 ENSTRUP00000039916 ENSTRUP00000039921 ENSTRUP00000039918 ENSTRUP00000039919 ENSTRUP00000039920	ENSTRUP00000023721 ENSTRUP00000021965		ENSTRUP00000017587	ENSTRUP00000031444 ENSTRUP00000031445 ENSTRUP00000031443 ENSTRUP00000031442
Tetrahymena thermophila	399.m00011 260.m00025	41.m00190	54.m00206	214.m00046 94.m00127 16.m00389 7.m00305 13.m00328 57.m00243	72.m00131
Thalassiosira pseudonana		35423			
Theileria anulata		TA02500			
Toxoplasma gondii		TGVEG_004780 TGME49_047230 TGGT1_025770		TGME49_114360 TGVEG_099450	
Trichoplax adherens		25393	54619		57490 55530
Trichomonas vaginalis	80874.m00020 82538.m00086 83472.m00460	94232.m00202 80798.m00086 81190.m00171	93357.m00029	88914.m00133 92757.m00230 84963.m00116 90782.m00048 86088.m00555	
Trypanosoma brucei		Tb927.8.1080		Tb927.5.2440 Tb11.01.3520 Tb927.1.3560	
Ustilago maydis					

	CAP350	CEP55	CEP68	CEP76	CEP97
Apis mellifera	GB13282-PA XP_393557.3				GB17708-PA XP_001122173.1
Arabidopsis thaliana					
Aureococcus anophagefferens				456	
Batrachochytrium dendrobatidis				BDEG_07240	
Caenorhabditis elegans					
Capitella sp	226518 209677	223974		130762 151783	208434
Chlamydomonas reinhardtii v3.1					
Chlamydomonas reinhardtii v2				169826 170801	
Ciona intestinalis	ENSCINP00000002338 ENSCINP00000028718 XP_002123277.1 ENSCINP00000024075 ENSCINP00000002512 ENSCINP00000029651			XP_002130643.1 ENSCINP00000022633	
Cryptosporidium parvum				cgd5_780 cgd6_680 cgd7_3040	
Cyanidioschyzon merolae					
Danio rerio	XP_001343753.2 XP_001920199.1	OTTDARP00000022719 XP_692717.3	OTTDARP00000024180 NP_001074119.1 OTTDARP00000001702 XP_001919948.1	NP_001096589.1	NP_938185.1
Dictyostelium discoideum					
Drosophila melanogaster					FBpp0077192 FBpp0077193
Encephalitozoon cuniculi					
Entamoeba histolytica					
Gallus gallus	ENSGALP00000006296 XP_422260.2 ENSGALP00000002702	ENSGALP00000039000 XP_001231504.1 ENSGALP00000010710	ENSGALP00000014274 XP_419343.2 ENSGALP00000016220	XP_001231809.1 ENSGALP00000034644 ENSGALP00000022439 XP_001235558.1	XP_416617.2 ENSGALP00000024714
Giardia lamblia				GL50803_5672	
Homo sapiens	OTTHUMP00000033201 OTTHUMP00000033199 OTTHUMP00000033202 OTTHUMP00000033200 OTTHUMP00000192895 OTTHUMP00000033203	NP_060601.3 NP_001120654.1 OTTHUMP00000020117 OTTHUMP00000020118	OTTHUMP00000159934 OTTHUMP00000159935 OTTHUMP00000178791 OTTHUMP00000028233	OTTHUMP00000071724 OTTHUMP00000071719 OTTHUMP00000071721 OTTHUMP00000162484 OTTHUMP00000071720 OTTHUMP00000071722 OTTHUMP00000071723 OTTHUMP00000071718 NP_115645.3 OTTHUMP00000080445 OTTHUMP00000164678	OTTHUMP00000172078
Leishmania major				LmjF28.2090 LmjF05.1020	
Lottia gigantea	89468 135146 140328 56916			229828	210409
Monosiga brevicollis	28503			26831 32767	
Naegleria gruberi				31102	
Nematostella vectensis	215825 212801 87242 199442			219939	
Neurospora crassa					
Oryza sativa					
Ostreococcus tauri					

	CAP350	CEP55	CEP68	CEP76	CEP97
Paramecium tetraurelia	GSPATP00002266001 GSPATP00019107001			GSPATP00029653001 GSPATP00022693001 GSPATP00025665001 GSPATP00030898001	
Phaedactylum tricornutum					
Physcomitrella patens					
Phytophthora sojae	140128			142088	
Plasmodium falciparum	PFE0070w			PFF0185c PFL2110c	
Populus trichocarpa					
Rhizopus oryzae					
Saccharonyces cerevisiae					
Schizosacharomyces pombe					
Strongylocentrotus purparatus	GLEAN3_18326 XP_782826.2 XP_001188934.1		XP_800003.2 XP_001190247.1	XP_780096.2 XP_001184625.1	XP_001189892.1 XP_780440.2 XP_001194053.1 XP_780521.2 GLEAN3_21340
Takifugu rubripes	ENSTRUP00000024377 ENSTRUP00000024378 ENSTRUP00000024375 ENSTRUP00000024374 ENSTRUP00000024376	ENSTRUP00000027582 ENSTRUP00000027583 ENSTRUP00000027584 ENSTRUP00000027585 ENSTRUP00000027586	ENSTRUP00000001005	ENSTRUP00000030946	ENSTRUP00000031065 ENSTRUP00000031066 ENSTRUP00000031064 ENSTRUP00000031068 ENSTRUP00000031067 ENSTRUP00000031063
Tetrahymena thermophila	57.m00227			62.m00250	
Thalassiosira pseudonana					
Theileria anulata				TA11690 TA09225	
Toxoplasma gondii				TGVEG_067670 TGVEG_101860 TGME49_116730 TGME49_116720 TGGT1_094560 TGVEG_101850 TGME49_040910 TGVEG_090360 TGGT1_049850	
Trichoplax adherens	53203			18537 57170	
Trichomonas vaginalis				81869.m00193 87835.m00207 90175.m00081	
Trypanosoma brucei				Tb11.01.0600	
Ustilago maydis					

	CP110	DIP13	EB1	FOP	MKS1
Apis mellifera	GB18645-PA	GB13090-PA	XP_623370.1 GB19881-PA	XP_396617.3 GB18614-PA GB10545-PA	GB12794-PA XP_001120316.1
Arabidopsis thaliana			AT5G62500.1 AT3G47690.1 AT5G67270.1	AT3G55005.1 AT3G55000.1	
Aureococcus anophagefferens		55205	7035		
Batrachochytrium dendrobatidis			BDEG_07433	BDEG_02453	BDEG_00264
Caenorhabditis elegans			CE18982 CE26217 CE26218		CE41329 CE40712
Capitella sp	217735 195460		180168 226241	151396	157534
Chlamydomonas reinhardtii v3.1		131284	194209		20204
Chlamydomonas reinhardtii v2		159197	152507		169453
Ciona intestinalis	XP_002121364.1 ENSCINP00000011624	XP_002131700.1 ENSCINP00000024109 XP_002119469.1 ENSCINP00000029736	ENSCINP00000028931 ENSCINP00000028930 ENSCINP00000017486 ENSCINP00000028932 ENSCINP00000017488 XP_002127374.1	XP_002125932.1	ENSCINP00000003134 XP_002121395.1 ENSCINP00000025479 ENSCINP00000025478
Cryptosporidium parvum		cgd8_1690	cgd7_2370		
Cyanidioschyzon merolae			CMJ156C		
Danio rerio	XP_001345378.2	XP_689621.2	OTTDARP00000019628 NP_571461.1 NP_001018312.1 OTTDARP00000020723 OTTDARP00000022038 OTTDARP00000022037 OTTDARP00000020725 NP_956158.1 OTTDARP00000020724 NP_001103172.1 XP_001923886.1 NP_001002170.1 OTTDARP00000007138 OTTDARP00000024111	OTTDARP00000026261	OTTDARP00000018990 NP_001070841.1
Dictyostelium discoideum			DDB0191160		
Drosophila melanogaster	FBpp0077044 FBpp0100112		FBpp0076502 FBpp0071405 FBpp0079053 FBpp0085462 FBpp0089088 FBpp0085464 FBpp0085463 FBpp0085461 FBpp0112596 FBpp0112595		FBpp0073500
Encephalitozoon cuniculi			19068506 85691079		
Entamoeba histolytica					
Gallus gallus	ENSGALP00000039138 XP_414915.2 ENSGALP00000011207	ENSGALP00000011925 XP_418582.1 XP_001233637.1 XP_001233675.1	ENSGALP00000010754 ENSGALP00000035995 ENSGALP00000024507 NP_001026188.1	XP_419609.1 ENSGALP00000018610	XP_415705.2 ENSGALP00000000998 ENSGALP00000039895
Giardia lamblia		GL50803_16263	GL50803_14048		
Homo sapiens	NP_055526.3 OTTHUMP00000162162 OTTHUMP00000080381 OTTHUMP00000080380 OTTHUMP00000162163	OTTHUMP00000022691 OTTHUMP00000171223	OTTHUMP00000030608 OTTHUMP00000163373 OTTHUMP00000073450 OTTHUMP00000073451 OTTHUMP00000122582	OTTHUMP00000017612 OTTHUMP00000017613	OTTHUMP00000182058 OTTHUMP00000165111 OTTHUMP00000182059 OTTHUMP00000165109 OTTHUMP00000165110
Leishmania major		LmjF34.4540		LmjF33.0050	
Lottia gigantea	157573	214610	177133	236017 64934	228399
Monosiga brevicollis		10940	32858	22652	30962
Naegleria gruberi		71898	44546 65633	51775	29577
Nematostella vectensis	222993	90789	196354	233042	209121 248809
Neurospora crassa			NCU00243		
Oryza sativa			Os04g54940.1 Os10g35580.1	Os11g01170.1 Os12g01170.1	
Ostreococcus tauri			31915 5403		

	CP110	DIP13	EB1	FOP	MKS1
Paramecium tetraurelia		GSPATP00031715001 GSPATP00014975001	GSPATP00024775001 GSPATP00029347001 GSPATP00027278001 GSPATP00003968001 GSPATP00009957001 GSPATP00000446001 GSPATP00003747001 GSPATP00032765001 GSPATP00027670001 GSPATP00038011001 GSPATP00034868001	GSPATP00015241001 GSPATP00009206001 GSPATP00011360001 GSPATP00004410001 GSPATP00019104001 GSPATP00002270001 GSPATP00006720001	GSPATP00011904001
Phaedactylum tricornutum			54306		
Physcomitrella patens		65272 166011 172179	52398 114249 124399 124479 66459	167541	
Phytophthora sojae		108625	140534 108686	143118 134177	
Plasmodium falciparum		MAL13P1.331	PFC0305w		
Populus trichocarpa			661879 671317 208732 218504	563805 227781	
Rhizopus oryzae			RO3G_14394.1 RO3G_08998.1 RO3G_14395.1		
Saccharonyces cerevisiae			YER016W		
Schizosacharomyces pombe			SPAC18G6.15		
Strongylocentrotus purparatus		XP_791762.1 XP_001178037.1	XP_001185519.1 XP_001191889.1 XP_787950.1 GLEAN3_27631	XP_787100.2 XP_001176074.1	XP_787637.1 XP_001181959.1
Takifugu rubripes		ENSTRUP00000026152 ENSTRUP00000026239	ENSTRUP00000012966 ENSTRUP00000019118 ENSTRUP00000013241 ENSTRUP00000012594 ENSTRUP00000023374 ENSTRUP00000023373 ENSTRUP00000023372	ENSTRUP00000012779	ENSTRUP00000018719 ENSTRUP00000018717 ENSTRUP00000018718
Tetrahymena thermophila			8.m00318 73.m00186 229.m00036 58.m00179 10.m00342 78.m00136 77.m00205	69.m00270 105.m00161 6.m00534 61.m00222	89.m00156
Thalassiosira pseudonana			36137		5008
Theileria anulata			TA18025		
Toxoplasma gondii		TGGT1_096790 TGVEG_050430 TGGT1_054490 TGME49_095450	TGVEG_068550 TGME49_027650 TGGT1_083050		
Trichoplax adherens		24325	57922	56432	61316
Trichomonas vaginalis			93469.m00003 85241.m00262 89135.m00247 87955.m00265 85699.m00083		81238.m00180 85889.m00463
Trypanosoma brucei		Tb10.61.2720	Tb09.160.1440 Tb927.8.2890	Tb10.61.2870	
Ustilago maydis			UM05761.1		

	MKS3	MKS4	MKS5	MKS6	NAP1
Apis mellifera	GB12651-PA GB19576-PA GB14376-PA	GB18714-PA XP_001122136.1	GB18181-PA XP_001121635.1 GB18807-PA	GB16247-PA	GB30086-PA XP_624402.1 GB10082-PA
Arabidopsis thaliana					
Aureococcus anophagefferens	22040 61468			72175 72596	
Batrachochytrium dendrobatidis	BDEG_06113	BDEG_01167	BDEG_03262 BDEG_03261	BDEG_06092	
Caenorhabditis elegans	CE02726		CE25774 CE04269	CE06131	
Capitella sp	97867 105851	228963 217708	218340 228193	155172	
Chlamydomonas reinhardtii v3.1	168773	169091 9715		176993	
Chlamydomonas reinhardtii v2	160562 161322	163597		168825 171248	
Ciona intestinalis	ENSCINP00000025044 ENSCINP00000025047 ENSCINP00000009402 XP_002126630.1 ENSCINP00000025046	XP_002121281.1 ENSCINP00000026886 ENSCINP00000014504 ENSCINP00000014503 XP_002121206.1 ENSCINP00000026885 ENSCINP00000014500 XP_002124446.1	ENSCINP00000018342 XP_002121007.1 ENSCINP00000020603 ENSCINP00000018343 ENSCINP00000018339	ENSCINP00000006696 XP_002123322.1 ENSCINP00000006692 ENSCINP00000029710 XP_002125387.1	
Cryptosporidium parvum				cgd6_680 cgd7_3040	
Cyanidioschyzon merolae					
Danio rerio	XP_700974.3		XP_001922153.1 XP_001921881.1	XP_698801.3	XP_692550.3
Dictyostelium discoideum		DDB0191488			
Drosophila melanogaster	FBpp0112166			FBpp0086100 FBpp0086099	FBpp0083929
Encephalitozoon cuniculi					
Entamoeba histolytica					
Gallus gallus	ENSGALP00000025642 XP_418334.2	ENSGALP00000018199 XP_416130.2	ENSGALP00000012598 ENSGALP00000038922 ENSGALP00000005690 XP_001234248.1 XP_001236264.1	ENSGALP00000023382 ENSGALP00000023381 XP_420777.2 XP_001232304.1	XP_425750.2 ENSGALP00000002726 XP_417323.2
Giardia lamblia					
Homo sapiens	OTTHUMP00000177903 NP_001135773.1	OTTHUMP00000168670 NP_079390.3 OTTHUMP00000168672 OTTHUMP00000168671	NP_056087.2 OTTHUMP00000108509 OTTHUMP00000080888 OTTHUMP00000080887 OTTHUMP00000028336 NP_065099.3	OTTHUMP00000036196 OTTHUMP00000020166 NP_001073991.2 OTTHUMP00000036195 OTTHUMP00000036194 XP_001718184.1 XP_001717962.1 XP_001714415.1 XP_001725151.1 XP_001724777.1 XP_001718667.1 OTTHUMP00000020164	OTTHUMP00000196679 OTTHUMP00000061639 OTTHUMP00000061640 OTTHUMP00000196095 OTTHUMP00000030757 NP_001030595.1
Leishmania major	LmjF27.0020			LmjF01.0730	
Lottia gigantea	192673		184477	219375	
Monosiga brevicollis	38408	27498		25895 12869 26368	
Naegleria gruberi	62841		61544	77673	
Nematostella vectensis	120147	248638 20626 220337 223974 105650	50175	30054 145898 224689	
Neurospora crassa					
Oryza sativa					
Ostreococcus tauri					

	MKS3	MKS4	MKS5	MKS6	NAP1
Paramecium tetraurelia	GSPATP00015939001 GSPATP00005677001	GSPATP00005779001	GSPATP00016244001	GSPATP00007873001 GSPATP00025665001 GSPATP00030898001 GSPATP00025666001	
Phaedactylum tricornutum	48099				
Physcomitrella patens					
Phytophthora sojae			136855		
Plasmodium falciparum				PFF0185c PFL2110c	
Populus trichocarpa					
Rhizopus oryzae			RO3G_13248.1		
Saccharonyces cerevisiae					
Schizosacharomyces pombe					
Strongylocentrotus purparatus	XP_791033.1 XP_001199054.1	XP_001200309.1 XP_796292.2 XP_001189059.1 XP_799269.2 XP_796018.1 XP_001197771.1 XP_001185617.1 XP_001192113.1 XP_781881.2 XP_001194414.1 XP_798213.2 XP_001183119.1 XP_790657.1	XP_001198524.1 XP_792785.2 XP_790646.2 XP_001179958.1	XP_001203052.1 XP_781068.2 XP_001193651.1 XP_001193792.1	
Takifugu rubripes	ENSTRUP00000004863 ENSTRUP00000026816	ENSTRUP00000010885 ENSTRUP00000010884 ENSTRUP00000010882 ENSTRUP00000010883 ENSTRUP00000032490	ENSTRUP00000021978 ENSTRUP00000032778 ENSTRUP00000032777 ENSTRUP00000032779 ENSTRUP00000032781 ENSTRUP00000032780 ENSTRUP00000032782 ENSTRUP00000032783 ENSTRUP00000016611 ENSTRUP00000016606 ENSTRUP00000016607 ENSTRUP00000016605 ENSTRUP00000016609 ENSTRUP00000016608	ENSTRUP00000023018 ENSTRUP00000035842 ENSTRUP00000035843 ENSTRUP00000035844 ENSTRUP00000035841 ENSTRUP00000035845	
Tetrahymena thermophila	198.m00078 273.m00023	16.m00381 101.m00122	128.m00081	36.m00254 62.m00250	
Thalassiosira pseudonana	6924		4971	6295	
Theileria anulata				TA11690 TA09225	
Toxoplasma gondii				TGVEG_024920 TGME49_030660 TGGT1_117190 TGGT1_049850 TGVEG_090360 TGME49_040910	
Trichoplax adherens	55538		51343	28071	55968
Trichomonas vaginalis	81244.m00185 86322.m00058 93588.m00120 90756.m00173 86498.m00447 80754.m00134	102888.m00005 93784.m00040		97465.m00138 96723.m00091 95634.m00071 88273.m00365	
Trypanosoma brucei	Tb927.5.3540			Tb09.160.3240	
Ustilago maydis					

	Ninein	NPHP1	NPHP3	NPHP4	NPHP5
Apis mellifera					
Arabidopsis thaliana					
Aureococcus anophagefferens			72389		
Batrachochytrium dendrobatidis				BDEG_06365	
Caenorhabditis elegans		CE16278		CE38409	
Capitella sp	201605	203909 141498 121714 120958	219276 186605	223925	168052
Chlamydomonas reinhardtii v3.1		191079	194130	32880	
Chlamydomonas reinhardtii v2		157551		164333	155819
Ciona intestinalis	XP_002120842.1	XP_002127999.1	ENSCINP00000029018 XP_002123449.1 ENSCINP00000009831 ENSCINP00000029015 NP_001071784.1 ENSCINP00000007133		ENSCINP00000024112 ENSCINP00000014179 XP_002131862.1
Cryptosporidium parvum					
Cyanidioschyzon merolae					
Danio rerio	XP_700610.3 XP_001922227.1 XP_001335233.2 XP_001332720.1 XP_690418.3	NP_001070638.1	XP_691073.2	OTTDARP00000011238 XP_001921573.1 OTTDARP00000017142 NP_001124247.1 OTTDARP00000017097 OTTDARP00000017143	NP_001008622.1 NP_001104719.1
Dictyostelium discoideum					
Drosophila melanogaster					
Encephalitozoon cuniculi					
Entamoeba histolytica					
Gallus gallus	XP_426482.2 ENSGALP00000020163	ENSGALP00000013332 XP_419298.2	XP_418790.2 ENSGALP00000019105	ENSGALP00000001428	ENSGALP00000019025 ENSGALP00000024116
Giardia lamblia					
Homo sapiens	NP_891989.2 OTTHUMP00000195019 NP_065972.3 NP_891991.1 NP_057434.3 OTTHUMP00000195018 OTTHUMP00000195017 OTTHUMP00000195016 OTTHUMP00000195510 OTTHUMP00000195014 OTTHUMP00000043419	NP_001121651.1 NP_001121650.1 OTTHUMP00000161841 OTTHUMP00000161840	OTTHUMP00000172836 OTTHUMP00000172842 OTTHUMP00000172838 OTTHUMP00000172839 OTTHUMP00000172837 OTTHUMP00000172835	OTTHUMP00000000745 NP_055917.1	OTTHUMP00000172423 OTTHUMP00000158861 OTTHUMP00000172420 OTTHUMP00000172425 OTTHUMP00000172422 OTTHUMP00000172421 OTTHUMP00000172424
Leishmania major			LmjF34.3490	LmjF25.2000	
Lottia gigantea		232470	126945	125375	185823
Monosiga brevicollis				8015	37188
Naegleria gruberi		71176			
Nematostella vectensis		217835	244876	242529	158806
Neurospora crassa					
Oryza sativa					
Ostreococcus tauri					

	Ninein	NPHP1	NPHP3	NPHP4	NPHP5
Paramecium tetraurelia				GSPATP00008603001 GSPATP00000785001 GSPATP00010871001 GSPATP00005471001	
Phaedactylum tricornutum					
Physcomitrella patens			135076		
Phytophthora sojae				140465	158462
Plasmodium falciparum					
Populus trichocarpa					
Rhizopus oryzae					
Saccharonyces cerevisiae					
Schizosacharomyces pombe					
Strongylocentrotus purparatus	XP_788604.2 XP_001179087.1	XP_782288.2 XP_001185182.1	XP_001203493.1 XP_795144.2 GLEAN3_22587	XP_797126.1 XP_001203768.1 XP_793289.1 XP_001195422.1	XP_001192289.1 XP_782682.2 XP_001199176.1 XP_782804.2
Takifugu rubripes	ENSTRUP00000021428 ENSTRUP00000021430 ENSTRUP00000021429 ENSTRUP00000021427 ENSTRUP00000014916 ENSTRUP00000014915 ENSTRUP00000014914		ENSTRUP00000045676 ENSTRUP00000045677 ENSTRUP00000045678	ENSTRUP00000045307	ENSTRUP00000023183 ENSTRUP00000023182
Tetrahymena thermophila		96.m00096	7.m00547 31.m00371	95.m00130 12.m00312	
Thalassiosira pseudonana				3508	
Theileria anulata					
Toxoplasma gondii					
Trichoplax adherens	52869	54526	22397 54460		53628
Trichomonas vaginalis					
Trypanosoma brucei			Tb927.4.1280		
Ustilago maydis					

	PCM1	PLK4	PLK	POC1	POC5
Apis mellifera		XP_623133.2 GB15315-PA	GB10053-PA	GB15587-PA XP_624420.1	
Arabidopsis thaliana					
Aureococcus anophagefferens				27325	
Batrachochytrium dendrobatidis				BDEG_01586	BDEG_05569 BDEG_06763 BDEG_03888
Caenorhabditis elegans			CE22877 CE26649 CE30602		
Capitella sp	228845	221177	72562 160517		224814
Chlamydomonas reinhardtii v3.1				112249	144089 9798
Chlamydomonas reinhardtii v2				162499	155108
Ciona intestinalis	XP_002127807.1	ENSCINP00000026188 XP_002125497.1 ENSCINP00000026189 ENSCINP00000004628	ENSCINP00000015359 XP_002121371.1 ENSCINP00000007493 ENSCINP00000007506 ENSCINP00000007522	XP_002127877.1 ENSCINP00000018966	XP_002130350.1 ENSCINP00000006751
Cryptosporidium parvum					
Cyanidioschyzon merolae			CME146C		
Danio rerio	OTTDARP00000019790 NP_001108595.1	NP_001112364.1	OTTDARP00000020344 NP_958465.1 NP_001092715.1 XP_001919481.1 OTTDARP00000019795 NP_001003890.3	OTTDARP00000022008 NP_956412.1 NP_998214.1	OTTDARP00000018901
Dictyostelium discoideum			DDB0216332		
Drosophila melanogaster		FBpp0078042		FBpp0075597	
Encephalitozoon cuniculi			19068465 85690997		
Entamoeba histolytica					
Gallus gallus	ENSGALP00000031473 ENSGALP00000022090 ENSGALP00000036784	ENSGALP00000016553	ENSGALP00000023702 XP_424739.2 NP_001025810.1	NP_001006232.1 ENSGALP00000018266 XP_414244.1 ENSGALP00000002194	XP_424797.2 ENSGALP00000024081
Giardia lamblia				GL50803_33762	
Homo sapiens	OTTHUMP00000177082 OTTHUMP00000177087 OTTHUMP00000177083 OTTHUMP00000096525 NP_006188.3 OTTHUMP00000177086 OTTHUMP00000177084 OTTHUMP00000177085	OTTHUMP00000164423	OTTHUMP00000010159 OTTHUMP00000122549 OTTHUMP00000122462 OTTHUMP00000081380	OTTHUMP00000168680 OTTHUMP00000168681 OTTHUMP00000171441 OTTHUMP00000171439 NP_056241.2	NP_001092741.1 NP_689621.2
Leishmania major			LmjF17.0790	LmjF34.0470	LmjF36.2690
Lottia gigantea	153121 176986	111275 111267	223730	223819	174270
Monosiga brevicollis	33155		39338	14637	37735
Naegleria gruberi			63986 53552	33676 3161	73050
Nematostella vectensis	202784 228836	246408	128941 230033	162437	246342 246343
Neurospora crassa			NCU09258		
Oryza sativa					
Ostreococcus tauri			32134	3915	

	PCM1	PLK4	PLK	POC1	POC5
Paramecium tetraurelia			GSPATP00018143001 GSPATP00025198001 GSPATP00009060001 GSPATP00031090001 GSPATP00028443001 GSPATP00026684001 GSPATP00036333001 GSPATP00022475001 GSPATP00009588001 GSPATP00006256001 GSPATP00039351001	GSPATP00016878001 GSPATP00013588001 GSPATP00005111001 GSPATP00027105001	GSPATP00030131001 GSPATP00029936001
Phaedactylum tricornutum			10628		
Physcomitrella patens				133767	
Phytophthora sojae				139367	
Plasmodium falciparum					
Populus trichocarpa					
Rhizopus oryzae					
Saccharonyces cerevisiae			YMR001C		
Schizosacharomyces pombe			SPAC23C11.16		
Strongylocentrotus purparatus	XP_786223.2 XP_001188717.1	GLEAN3_16352 XP_001184023.1 XP_001192451.1	GLEAN3_00468 GLEAN3_17949	XP_797493.2	XP_797483.2 XP_001186713.1
Takifugu rubripes	NP_001027776.1 ENSTRUP00000040906 ENSTRUP00000040912	ENSTRUP00000018584 ENSTRUP00000018583	ENSTRUP00000003764 ENSTRUP00000003763 ENSTRUP00000033671 ENSTRUP00000033670 ENSTRUP00000033668 ENSTRUP00000033669 ENSTRUP00000037778 ENSTRUP00000037777	ENSTRUP00000043776 ENSTRUP00000043775 ENSTRUP00000043770 ENSTRUP00000043774 ENSTRUP00000043772 ENSTRUP00000043771 ENSTRUP00000043773 ENSTRUP00000019669 ENSTRUP00000019672 ENSTRUP00000019671 ENSTRUP00000019670 ENSTRUP00000019675 ENSTRUP00000019668 ENSTRUP00000019673	ENSTRUP00000017168 ENSTRUP00000017169 ENSTRUP00000017170
Tetrahymena thermophila			56.m00207 220.m00040 392.m00011 15.m00540	318.m00023	5.m00513
Thalassiosira pseudonana			33979		
Theileria anulata					
Toxoplasma gondii					
Trichoplax adherens	62202	30306	50801	51125	60303
Trichomonas vaginalis				82686.m00037 84958.m00099 93446.m00217	87526.m00089
Trypanosoma brucei			Tb927.7.6310	Tb10.70.4780	Tb10.6k15.3050
Ustilago maydis			UM03234.1		

	Rootletin	SAS-4	SAS-6	SZY-20	Delta-tubulin
Apis mellifera	GB30086-PA GB10082-PA XP_624402.1	GB11770-PA XP_396122.3	GB15158-PA XP_395972.3	GB11242-PA	GB16674-PA XP_001122683.1
Arabidopsis thaliana					
Aureococcus anophagefferens		15226	72351		
Batrachochytrium dendrobatidis		BDEG_06323	BDEG_07637		BDEG_02728
Caenorhabditis elegans					
Capitella sp		148844 226664	198072		136680 159439
Chlamydomonas reinhardtii v3.1		142043	136677 176336		136082
Chlamydomonas reinhardtii v2		152791 162786 171974	158310 157385		164724
Ciona intestinalis	ENSCINP00000016483 ENSCINP00000016482 XP_002119303.1 ENSCINP00000016484	XP_002123980.1 ENSCINP00000000162	ENSCINP00000018623 XP_002128064.1	XP_002119900.1 ENSCINP00000021131	XP_002121850.1 NP_001027643.1
Cryptosporidium parvum			cgd4_2610 cgd8_490		
Cyanidioschyzon merolae			CMB012C CMX010C		
Danio rerio	XP_692550.3 XP_688293.3 XP_001922586.1	OTTDARP00000026300 XP_697409.3	XP_001335692.2 NP_998603.1 OTTDARP00000009325	OTTDARP00000022968	NP_001002093.1 OTTDARP00000024251
Dictyostelium discoideum					
Drosophila melanogaster	FBpp0083929 FBpp0083930	FBpp0081088	FBpp0084912	FBpp0079057 FBpp0079058	
Encephalitozoon cuniculi			19068525 85691117		
Entamoeba histolytica					
Gallus gallus	XP_425750.2 ENSGALP00000005940 ENSGALP00000002726 XP_417323.2	ENSGALP00000027641 ENSGALP00000018491 XP_419608.2 XP_417152.2 ENSGALP00000027640	NP_001026444.1 ENSGALP00000008489	ENSGALP00000005915	ENSGALP00000008290
Giardia lamblia		GL50803_13352			GL50803_5462
Homo sapiens	OTTHUMP00000196095 NP_001030595.1 OTTHUMP00000030757 OTTHUMP00000196679 OTTHUMP00000061639 OTTHUMP00000002222 OTTHUMP00000002223 XP_001732878.1	OTTHUMP00000018137 OTTHUMP00000018138 OTTHUMP00000174371 OTTHUMP00000174372 OTTHUMP00000067368 NP_004601.3 OTTHUMP00000017628	OTTHUMP00000012455	OTTHUMP00000002235 NP_056424.1 XP_932280.1 XP_943492.1 XP_001714740.1	OTTHUMP00000182090 OTTHUMP00000182091 OTTHUMP00000182092
Leishmania major		LmjF13.1590	LmjF35.4280		LmjF36.4990
Lottia gigantea	169115 133011	103874 174618		234409	126843 225368
Monosiga brevicollis		27468	29189		33187
Naegleria gruberi		61107	68996		65724 69007
Nematostella vectensis	232574 165346	104524 26007 90077		244736	82063 209136
Neurospora crassa					
Oryza sativa					
Ostreococcus tauri		11326	30207		

	Rootletin	SAS-4	SAS-6	SZY-20	Delta-tubulin
Paramecium tetraurelia		GSPATP00017531001 GSPATP00004155001 GSPATP00010124001 GSPATP00002681001 GSPATP00004862001 GSPATP00003188001	GSPATP00032784001 GSPATP00027645001 GSPATP00020097001 GSPATP00019787001 GSPATP00009285001 GSPATP00024268001 GSPATP00005603001 GSPATP00008149001 GSPATP00011824001		GSPATP00003638001 GSPATP00005791001
Phaedactylum tricornutum		45511			
Physcomitrella patens			66367		66250
Phytophthora sojae		129996 108440	128318 143809		158567
Plasmodium falciparum		PF14_0558	PFF0375c MAL13P1.85		PFI1635w
Populus trichocarpa					
Rhizopus oryzae					
Saccharonyces cerevisiae					
Schizosacharomyces pombe					
Strongylocentrotus purparatus	XP_001193842.1 XP_001199206.1 XP_001200030.1 XP_001180033.1 XP_001187086.1 XP_786339.2 XP_001199159.1 XP_794353.2	XP_001201907.1 XP_796778.2 XP_001201804.1 XP_796764.2	XP_791931.2 XP_001176207.1 XP_784418.2 XP_001185553.1		GLEAN3_04266
Takifugu rubripes	ENSTRUP00000026159 ENSTRUP00000026160	ENSTRUP00000039772 ENSTRUP00000039773 ENSTRUP00000039774	ENSTRUP00000015629 ENSTRUP00000015630	ENSTRUP00000027083 ENSTRUP00000027084 ENSTRUP00000015723 ENSTRUP00000015724 ENSTRUP00000015725	ENSTRUP00000012851 ENSTRUP00000012850
Tetrahymena thermophila		16.m00410 40.m00264	15.m00309 101.m00122 113.m00089 10.m00435 41.m00222		24.m00232 34.m00277
Thalassiosira pseudonana		10156	23096		
Theileria anulata					
Toxoplasma gondii		TGME49_058710 TGVEG_075750 TGGT1_011480	TGGT1_040920 TGVEG_107890 TGME49_106430 TGME49_101420 TGGT1_059860		TGME49_007600 TGVEG_040680 TGGT1_020490
Trichoplax adherens		28606 55968	51343	57681	54235 28772
Trichomonas vaginalis		83057.m00080 83007.m00259 92349.m00199 85746.m00238 80829.m00091 86485.m00546	94652.m00132 86581.m00019 136524.m00028		87205.m00083
Trypanosoma brucei		Tb11.02.3880 Tb11.02.0810	Tb10.6k15.2630 Tb09.211.1930 Tb927.8.4950		Tb11.01.2695
Ustilago maydis					

	Epsilon-tubulin	Gamma-tubulin	VFL1	WDR16	XMAP215
Apis mellifera	XP_394700.3 GB15835-PA	XP_394981.3 GB18755-PA		GB13234-PA	GB30364-PA GB10660-PA XP_392874.3
Arabidopsis thaliana		AT3G61650.1 AT5G05620.1			AT2G35630.1
Aureococcus anophagefferens	2189	23795		21121 28848	
Batrachochytrium dendrobatidis	BDEG_05632 BDEG_08433	BDEG_04849	BDEG_07084	BDEG_06826	BDEG_04589
Caenorhabditis elegans		CE00224			CE41405 CE20707 CE20858 CE28252
Capitella sp	218781 89314	174186	212152	218269 229244	154948
Chlamydomonas reinhardtii v3.1	188195	188933		150613 128114	175143
Chlamydomonas reinhardtii v2	165702	158831	155034	159155 168135	156582
Ciona intestinalis	ENSCINP00000002530 XP_002128990.1	XP_002129233.1	XP_002122133.1 ENSCINP00000025492	ENSCINP00000011660 XP_002124411.1 ENSCINP00000011659	ENSCINP00000015586 ENSCINP00000026759 ENSCINP00000015576 ENSCINP00000015580
Cryptosporidium parvum		cgd7_1980			cgd5_1680
Cyanidioschyzon merolae		CMN304C			CMO196C
Danio rerio	OTTDARP00000003871 NP_957279.1 OTTDARP00000003844	NP_957202.1	XP_690381.2	OTTDARP00000015128 NP_001018475.1	NP_001032756.1
Dictyostelium discoideum		DDB0185068			DDB0168274 DDB0232951
Drosophila melanogaster		FBpp0077326 FBpp0080769		FBpp0076646	FBpp0082678
Encephalitozoon cuniculi		19173393 19170982 51701890			19069715 19074990
Entamoeba histolytica		55.m00198 307.m00057			62.m00181
Gallus gallus	ENSGALP00000024172	XP_418146.2 ENSGALP00000004979	ENSGALP00000025453 XP_418316.2	ENSGALP00000001912	ENSGALP00000013536 XP_001233233.1
Giardia lamblia	GL50803_6336	GL50803_114218		GL50803_15218	GL50803_96399 GL50803_91480
Homo sapiens	OTTHUMP00000017033 OTTHUMP00000017035 OTTHUMP00000017034	OTTHUMP00000181220 OTTHUMP00000181218	OTTHUMP00000177815 NP_001070969.1	NP_001074025.1 OTTHUMP00000182860 OTTHUMP00000196460 OTTHUMP00000182859	OTTHUMP00000081795 OTTHUMP00000081794 OTTHUMP00000081793
Leishmania major	LmjF21.1010	LmjF25.0960	LmjF25.0880	LmjF28.1110	LmjF30.1760
Lottia gigantea	224456	237817	65544	105926	228176
Monosiga brevicollis	29416	21602	22748	17788	32952
Naegleria gruberi	44774	56069		59637	62456 49612
Nematostella vectensis	89613	173802	123151	84810	183698
Neurospora crassa		NCU03954			NCU04535
Oryza sativa		Os05g06450.2 Os05g06450.1			Os01g60050.1 Os01g60040.2 Os01g60040.1
Ostreococcus tauri		25029	37183	18472	20299

	Epsilon-tubulin	Gamma-tubulin	VFL1	WDR16	XMAP215
Paramecium tetraurelia	GSPATP00038073001	GSPATP00017668001 GSPATP00001868001	GSPATP00020493001	GSPATP00027925001 GSPATP00027924001 GSPATP00031525001 GSPATP00013985001 GSPATP00025338001 GSPATP00039722001 GSPATP00027926001	GSPATP00035152001 GSPATP00032050001 GSPATP00034778001 GSPATP00032198001 GSPATP00003603001 GSPATP00000281001 GSPATP00008659001 GSPATP00000836001
Phaedactylum tricornutum		44225			47936
Physcomitrella patens	99422	170153 170860	80573	102190	166936 106216
Phytophthora sojae	118214	109415	136445	137588	156611
Plasmodium falciparum	PF14_0725	PF08_0125		MAL13P1.245	
Populus trichocarpa		755367 572355			727336 550419
Rhizopus oryzae		RO3G_11100.1			RO3G_09527.1 RO3G_06225.1
Saccharonyces cerevisiae		YLR212C			YLR045C
Schizosacharomyces pombe		SPBC32F12.04			SPCC736.14 SPCC895.07
Strongylocentrotus purparatus	GLEAN3_13393 GLEAN3_02663 XP_781720.2 XP_001182983.1 GLEAN3_12141 XP_783098.2 XP_001183033.1	NP_999657.1 GLEAN3_20943	XP_001185066.1 XP_793924.1	XP_787783.1 XP_001176293.1 XP_001199653.1 XP_001183767.1	XP_001199992.1 XP_798563.2 GLEAN3_15952 XP_001182362.1 XP_001183804.1 XP_001199963.1 XP_001188972.1 XP_790495.2 XP_001188266.1
Takifugu rubripes	ENSTRUP00000012199	ENSTRUP00000037747	ENSTRUP00000007528 ENSTRUP00000007527 ENSTRUP00000007529	ENSTRUP00000033492	ENSTRUP00000039530 ENSTRUP00000039528 ENSTRUP00000039529
Tetrahymena thermophila	8.m00446	5.m00548	83.m00211	231.m00034	85.m00176 1.m00993 49.m00230
Thalassiosira pseudonana		29237		260819	7217
Theileria anulata		TA03470			
Toxoplasma gondii	TGGT1_000470 TGME49_075870 TGVEG_055390	TGVEG_067890 TGME49_026870 TGGT1_082260	TGVEG_028740 TGGT1_104540 TGME49_078010	TGGT1_011670 TGVEG_075940 TGME49_058530	
Trichoplax adherens	50572	49610	52611	53754	51833
Trichomonas vaginalis	82471.m00124	83992.m00196 93106.m00014		81295.m00071	105221.m00002 88808.m00117 83992.m00172
Trypanosoma brucei	Tb10.70.6950 Tb11.0530	Tb927.3.910	Tb11.03.0280	Tb11.02.5550	Tb927.6.3090
Ustilago maydis		UM03803.1			UM06328.1

	ZYG1
Apis mellifera	
Arabidopsis thaliana	
Aureococcus anophagefferens	
Batrachochytrium dendrobatidis	
Caenorhabditis elegans	CE28571
Capitella sp	
Chlamydomonas reinhardtii v3.1	
Chlamydomonas reinhardtii v2	
Ciona intestinalis	
Cryptosporidium parvum	
Cyanidioschyzon merolae	
Danio rerio	
Dictyostelium discoideum	
Drosophila melanogaster	
Encephalitozoon cuniculi	
Entamoeba histolytica	
Gallus gallus	
Giardia lamblia	
Homo sapiens	
Leishmania major	
Lottia gigantea	
Monosiga brevicollis	
Naegleria gruberi	
Nematostella vectensis	
Neurospora crassa	
Oryza sativa	
Ostreococcus tauri	

	ZYG1
Paramecium tetraurelia	
Phaedactylum tricornutum	
Physcomitrella patens	
Phytophthora sojae	
Plasmodium falciparum	
Populus trichocarpa	
Rhizopus oryzae	
Saccharonyces cerevisiae	
Schizosacharomyces pombe	
Strongylocentrotus purparatus	
Takifugu rubripes	
Tetrahymena thermophila	
Thalassiosira pseudonana	
Theileria anulata	
Toxoplasma gondii	
Trichoplax adherens	
Trichomonas vaginalis	
Trypanosoma brucei	
Ustilago maydis	